Final Report

East Texas and Western Louisiana Coastal Erosion Study

Robert A. Morton, William A. White, and James C. Gibeaut
Assisted by Sigrid Clift, Ed Garner, Ted Angle, and Tucker Hentz

Prepared for the U.S. Department of Interior
U.S. Geological Survey

Cooperative Agreement No. 14-08-0001-A0912

Bureau of Economic Geology
Noel Tyler, Director
The University of Texas at Austin
Austin, Texas 78713-8924

September 1996

CONTENTS

Addenda

Report Organization

The following report serves two purposes. It presents the major project objectives and achievements by the Bureau of Economic Geology during the fifth year of the cooperative program (FY 95-96), and it summarizes the results of the entire five-year study of coastal erosion and wetlands loss along the southeastern Texas coast. The report covers activities between June 28, 1991, and August 31, 1996. Major accomplishments are reported for each work element and task presented in the 5-year work plan of the cooperative agreement. Documents summarizing the major accomplishments and containing the important data sets and scientific conclusions are included as Addenda 1-11.

Work Element 1: Coastal Erosion Analysis

The southeastern Texas Gulf shoreline includes the entire spectrum of morphogenetic shore types: transgressive and regressive beaches and barriers as well as deltaic headlands. These features both control and respond to shoreline changes on variable time scales. A principal reason for studying the dynamics and permanent changes of these landforms is to understand the temporal and spatial time scales of movement that are important for coastal planning and resource management.

Stated goals for work element 1 were to (1) establish a computerized database of historical shoreline positions (1882-1982), (2) update the database using the most recent shoreline information (1990's), (3) analyze historical trends of shoreline movement in the context of the regional geologic framework and human modifications, (4) synthesize the physical and habitat characteristics of different shoreline types, (5) establish a network of field monitoring sites for surveying coastal changes, and (6) prepare documents of shoreline change suitable for coastal planning and resource management.

Task 1: Shoreline Mapping Dynamics of the Gulf beaches as well as other coastal features in southeastern Texas were analyzed using standard mapping techniques employing the latest concepts and available equipment. Standard historical monitoring procedures included selecting shoreline features such as the berm crest, the dense vegetation line, or land/water interface in wetlands to directly detect coastal change. These boundaries were identified and mapped on low-altitude vertical aerial photographs, the boundaries were optically transferred to stable bases having common map scales, and the boundaries were then digitized, manipulated, and stored in a computer system (ARC-INFO). Magnitudes and rates of coastal change were quantified at sites that were predetermined on the basis of uniform spacing along the coast or site specific selection.

The quantitative data summarizing shoreline movement were then presented in tabular and/or graphical form and analyzed statistically to establish significant trends for the most recent monitoring period and for the entire period of record (1800s to 1990s).

We also examined relationships between rates of fluvial sedimentation, rates of wetland loss, and accelerated rates of relative sea-level rise resulting from human-induced subsidence and faulting along the southeastern Texas coast. Wetland loss in the vicinity of major oil and gas fields were analyzed. Marshes that have been converted to open water along active faults were identified and mapped to determine the extent of losses. Synthesis of data on wetland losses along the southeastern Texas coast shows that more than 11,700 ha of vegetated wetlands have been replaced by shallow subaqueous flats and open water. Salt, brackish, and fresh marshes and fluvial woodlands have been affected. Major losses have occurred in fluvial-deltaic areas along the Neches and Trinity rivers. Although many processes or activities may contribute to wetland loss, human-induced subsidence resulting from production of hydrocarbons and associated formation water is a major process affecting wetlands along the southeastern Texas coast.

Task 2: Geomorphic Characterization. A complementary task to shoreline mapping involves the establishment and repeated occupation of beach profile sites. These sites are typically concentrated on the Gulf shoreline where changes are rapid and the potential loss of property is greatest. The BEG annually conducts beach surveys at approximately 10 profile stations in the study area, most of them located on Bolivar Peninsula, the West Beach of Galveston Island, and on Follets Island. Most of these stations were established and have been monitored since Hurricane Alicia in 1983. The field data provide ground-truth for the aerial photographic interpretations, provide a basis for evaluating seasonal fluctuations in shoreline position compared to long-term trends, and they provide a means of quantifying volumetric changes and time-averaged sediment transport estimates for the beach and nearshore zone.

This task also provided data on the physical characteristics and natural habitats of the various shoreline types in the context of shoreline stability. The morphodynamic analyses synthesized data and observations made as a result of the shoreline change analysis (retreat/advance) and field surveys (beach width, beach slope, beach composition, dune development, artificial stabilization, beach use).

SIGNIFICANT RESULTS. In year 5 we completed a report that summarizes shoreline movement along the southeastern Texas coast between 1974 and 1996 (**Addendum 1**). The report, entitled "Gulf shoreline movement between Sabine Pass and the Brazos River, Texas - 1974-1996", also served as the basis for calculating the average annual erosion rates and predicting the position of the shoreline 60 years into the future. The latter work in Galveston and Brazoria

Counties, is being conducted for the Texas General Land Office and the Federal Emergency Management Agency. During year 5 we also completed an analysis of wetland changes in the lower Neches river valley. The site is being considered for restoration of lost wetlands due to submergence. A report of that site investigation is included in **Addendum 10**. The wetlands work was done in cooperation with the Texas Parks and Wildlife Department.

We adapted GPS technology and were pioneers in the use of GPS kinematic surveys for delineation of shorelines and beaches. A paper was published that compares conventional and GPS beach surveys and provides a description of the new techniques developed by the Bureau of Economic Geology in cooperation with the University of Texas Applied Research Laboratory (Morton, R. A., Leach, M. P., Paine, J. G., and Cardoza, M. A., 1993, Monitoring beach changes using GPS surveying techniques: Journal of Coastal Research, v. 9, p. 702-720). Also during the five-year project we conducted low-altitude aerial video surveys in cooperation with the Louisiana Geological Survey and mapped shoreline types for the Gulf shore and the interior bays (Westphal, K. A., Penland, S., Seal, R. W., and Morton, R. A., 1992, Aerial videotape survey of coastal Texas and Louisiana: Center for Coastal, Energy, and Environmental Resources, Louisiana State University, Coastal Geology Map Series No. 13, 210p).

The video surveys were subsequently used as a primary basis for mapping shoreline types and employing the environmental sensitivity index (ESI) that is used for oil spill response and contingency planning. Shores of the entire study area were mapped at 1:24,000, digitized, and entered as layers in ARC/INFO (**Addendum 9**). The shoreline type work was done in cooperation with Research Planning Inc. under sponsorship of the Texas General Land Office and NOAA.

We completed 10 reports pertaining to work element 1 (**Addendum 7**). Two reports summarize and illustrate significant wetland losses associated with oil and gas production (White, W. A., and Tremblay, T. A., 1995, Submergence of wetlands as a result of human-induced subsidence and faulting along the upper Texas Gulf coast: Journal of Coastal Research, v. 11 p. 788-807; White, W. A., and Morton, R. A., in press, Wetland losses related to fault movement and hydrocarbon production, southeastern Texas coast: Journal of Coastal Research). The reports conclude that most of these losses are caused by faults that were activated as a result of large-volume production of subsurface fluids (oil, gas, and formation water).

A major accomplishment during the project was completion of an electronic data base of historical shoreline positions, monitoring transects, and other layers in ARC-INFO (**Addendum 9**) that permit rapid analyses of shoreline movement. The digitized shorelines span the time interval from the mid 1860s to 1996. Electronic results of this effort have been used by universities and by State and Federal agencies in a variety of applications (see Task 6). Also our GPS beach surveys

and field observations were used by the Texas General Land Office to help establish the dune protection line in Galveston County.

Work Element 2: Regional Geologic Framework

The primary goals of Work Element 2 were to: (1) determine the geologic origin and evolution of the principal coastal subenvironments in southeastern Texas, (2) investigate the shallow subsurface structure especially as it relates to subsidence and land loss, (3) establish a chronostratigraphic framework for the coastal systems and construct relative sea-level curves for the reconstruction of Holocene coastal evolution, (4) determine the nearshore bathymetric changes since the 1800s, (5) relate the bathymetric changes to nearby shoreline changes, and (6) prepare an atlas of bathymetric changes. The first three goals were achieved, whereas the goals related to bathymetric analysis were not achieved because the project was redirected. Bathymetric surveys in Louisiana proved to be costly and time consuming, and some of the results involving comparisons with older (1800s) data were uncertain since surveying datums and methods of conducting surveys have changed. Therefore we did not undertake tasks dealing with bathymetric changes.

Task 1: Stratigraphic Analysis The study area encompasses a chenier plain, two deltaic headlands, two progradational barriers, a retrogradational barrier, four tidal inlets, associated lagoons and estuaries, and the inner continental shelf. Work conducted on all of these features prior to our study concentrated mainly on the surficial morphology, areal extent, composition, and textural changes of the features. A few features (the chenier plain and Galveston Island) have been age dated, but little work had been done on short-term sea-level fluctuations and coastal response during the Holocene, changes in sediment supply and coastal processes during the past few thousand years and, more importantly, changes in sediment supply and coastal processes on a historical time scale. When combined with the shoreline change analyses, results of these investigations now provide a basis for predicting future magnitudes and rates of land loss.

Vibracores, faunal assemblages, isotopic dates, and seismic surveys were used to investigate the late Quaternary and Holocene stratigraphy of the study area. These data were used to construct cross sections illustrating the various coastal and non-marine facies and to construct a relative sea-level curve for the late Holocene and Modern time periods.

We also used commercial structure maps and releveling surveys to independently evaluate shallow fault activity and related subsidence. Preliminary investigations indicate that subsidence is aggravated by both shallow and deep subsurface fluid withdrawal.

SIGNIFICANT RESULTS. During year 5, we collected, prepared, photographed and described 11 vibracores from Galveston Island, Bolivar Peninsula, and the mainland on the north side of East Bay that separates Bolivar Peninsula from the mainland. The cores were taken to investigate the origin and timing of unusually high ridges that occupy the landward parts of the barrier islands. The vibracore descriptions and geographic locations are presented in **Addendum 3** and **Addendum 4**, respectively.

During the five-year investigation we acquired foundation boring descriptions and constructed cross sections that traversed the southeastern Texas coastal plain rivers. Long topographic profiles were prepared for the Sabine, Neches and Trinity rivers showing the elevations and gradients of the Beaumont surface, Deweyville terraces, and modern floodplain. We also collected 15 deep hollow-stem auger cores between High Island and the Neches River Valley, 7 vibracores from the McFaddin National Wildlife Refuge, 30 vibracores from Sabine Lake, 32 vibracores from Sabine and Heald Banks in the Gulf of Mexico, 6 vibracores from the inner continental shelf in the Gulf of Mexico, and 11 vibracores from Galveston Island and Bolivar Peninsula. We also jointly collected numerous trackline miles of high-resolution seismic profiles from Sabine Lake, the inner continental shelf, and over Sabine Bank in the Gulf of Mexico.

Twenty two samples from 11 coastal plain and Sabine Lake cores were obtained for radiocarbon analyses. Materials sampled are whole valves and shell fragments (*Rangia*, *Crassostrea*, *Mulinea*, *Anadara*), peat, wood, and organic clay. The samples, which represent a wide range of environments including oyster reef, bayhead delta, shoreface, beach ridge, transgressive marsh, fluvial sand, and floodbasin swamp, were submitted to the University of Texas at Austin Radiocarbon Laboratory for analysis.

Seismic profiles, deep and shallow cores, foraminifera data, and ^{14}C ages are being used to begin a systematic stratigraphic analysis of the Sabine Lake-Sabine Bank region. Preliminary interpretations of depositional environments were made on the basis of detailed descriptions and stratigraphic cross sections prepared for the interfluve, chenier plain, and incised valley areas.

Dr. Martin Lagoe, deceased micropaleontologist with the Department of Geological Sciences the University of Texas at Austin, and Laura Stewart, one of his graduate students, completed the analyses of foraminifera from onshore cores CE-2, CE-4, CE-6, CE-7, CE-10, and CE-13 to help with the interpretation of depositional environments represented by homogeneous muds. Species identification and abundance were plotted against depth to establish changes in paleosalinity of coastal waters and the types of geological setting represented by the examined samples. Preliminary results indicate that the interfluve sediments (CE-2, CE-4, CE-6) are mostly barren of forams. It is uncertain whether the absence of forams is related to the original depositional environment or diagenetic reactions since deposition. Agglutinated species are also largely absent from other samples and the reason for this is probably related to dissolution at depth. Discussions

with Dr. Eric Collins (Dave Scott post-doctoral researcher at Dalhousie Univ.) indicated that drying of the cores may have resulted in loss of the forams, but our examination of wet cores from Sabine Lake also showed that agglutinated forams were not preserved below about 2m. Results of the foram study have been accepted for publication (Stewart, L. B., Morton, R. A., and Lagoe, M. B., 1996, Holocene development of the southeastern Texas coast, Sabine Lake area, from foraminiferal biofacies: Transactions Gulf Coast Association of Geological Societies, in press). This paper examines climatic changes and evolution of the coastal system by interpreting the record of foraminifera contained in the sediments.

Four other papers dealing with the regional geologic framework of the southeastern Texas coastal plain and shelf have been published or accepted for publication and a fifth is in preparation (**Addendum 7**). One paper (Paine, J. G., Morton, R. A., and Garner, L. E., in press, Site dependency of shallow seismic data quality in saturated, unconsolidated coastal sediments: Journal of Coastal Research) investigated the use of onshore high-resolution seismic techniques for stratigraphic interpretation of the late Quaternary coastal plain sediments. Two papers (Blum, M. D., Morton, R. A., and Durbin, J. E., 1995, "Deweyville" terraces and deposits of the Texas Gulf Coastal Plain: Transactions Gulf Coast Association of Geological Societies, v. 45, p. 53-60; Morton, R. A., Blum, M. D., and White, W. A., 1996, Valley fills of incised coastal plain rivers, southeastern Texas: Transactions Gulf Coast Association of Geological Societies, in press) have focused on the fluvial responses to changing sea levels and sediment loads as conditioned by changing climate between the glacial and interglacial periods. Another paper (**Addendum 2**) describes the geologic history of Holocene sediments of Sabine Lake and the Sabine delta and human modifications to the rivers and estuary that have occurred since the late 1800s.

Work Element 3: Coastal Processes

Understanding physical processes operating today that shape the coast is the key to understanding coastal erosion and predicting future coastal changes. Therefore, work element 3 involved numerous tasks that quantified basin energy, sediment motion, and the forcing functions that drive the coastal system. The objectives of this work element were to evaluate the magnitudes and rates of the relative rise in sea level during geological and historical time, to provide a basis for assessing wave and current energy as well as sediment transport, to assess climatic and meteorological influences on coastal processes, to evaluate the impacts of storms on shoreline stability and instantaneous erosion potential, and to begin quantifying the coastal sediment budget.

Task 1: Relative Sea Level Rise and Subsidence Sea level is perhaps the single most important variable with regard to coastal erosion and planning for future development of the coast.

Historical data indicate that average sea level in the Gulf of Mexico fluctuates over short periods of time but is steadily increasing over longer time periods. The implications of this phenomenon are well known and include inundation of low-lying areas as well as retreat of the shoreline. In the western Gulf Coast basin, the relative rise in sea level is primarily a result of subsidence that in some areas is augmented by fluid production.

An analysis of relative sea level involved acquiring tidal data at selected gauges with long-term records and releveling surveys from the National Oceanic and Atmospheric Administration (NOAA). Aerial photographs were also used to evaluate submergence in some low-lying interior areas where uplands are converted to wetlands and where wetlands are converted to open water in the absence of waves and currents.

Task 2: Sediment Transport. Quantifying sediment transport along a shoreline of variable composition is one of the most difficult tasks included in this proposal. The initial quantification depended on seasonal beach and nearshore profiles as a first approximation of time-averaged sediment transport.

We also conducted two high-precision kinematic GPS surveys at Galveston Island State Park to improve data collection techniques and to document actual beach changes. Preliminary results of the post-processed data indicate substantial changes in beach width and elevation attributed to transfer of sand from the forebeach to the backbeach probably as a result of beach cleaning operations routinely conducted after accumulations of *Sargassum* (seaweed) wash ashore.

Task 3: Sediment Budget. This task evaluated the primary sediment sources (updrift erosion and fluvial sediment supply) and the principal sediment sinks (beach accretion, onshore washover, dune construction, and offshore deposition) along the southeastern Texas coast. Some additional sediment losses occur at tidal inlets and some unknown quantity is trapped in the deep-draft navigation channels.

Task 4: Climatic and Meteorological Impacts The impacts of weather and climate on coastal processes were examined by using historical records (droughts and floods, wind patterns), aerial photographs, and by making field observations. Of particular interest are high- and intermediate-frequency events that cause subtle changes in water level, interfere with accurate shoreline mapping, and influence sediment transport near the beach. The results of this task were combined with those of work element 1

Task 5: Storm Impacts This task involved the reconstruction of storm impacts from historical records and the development of methods to predict the response of each shoreline type to storms

having variable characteristics. Materials available for this effort included aerial photographs taken immediately after Hurricanes Carla (1961), Allen (1980), Alicia (1983), and Gilbert (1988). Field surveys were conducted to locate erosional escarpments for some of the most severe storms in areas where the shoreline is relatively stable. We also planned to monitor beach profiles before and after a major storm to provide a quantitative measure of beach changes and to calculate mass transfer of sediments. However, a major storm did not impact the area during the five-year study so completion of the latter part of the task was not possible.

SIGNIFICANT RESULTS. We analyzed beach and offshore surveys along the northeastern end of Galveston Island encompassing the beach nourishment project in front of the seawall. These profiles were merged with additional offshore surveys conducted by T. L. James Co., the dredging contractor for the beach nourishment project. We also interpreted the textural data for 70 sediment samples collected along the profiles and in the borrow site as part of their beach nourishment project. Because the beach and offshore profiling was conducted before the dredging and pumping operations, the profiles and textural data provide pre-project baseline data. Those data sets are now being used by Texas A&M University-Galveston for comparison with their post-project monitoring results.

We obtained the wave refraction model RCPWAVE provided by the U.S. Army Corps of Engineer's Coastal Engineering Research Center. A rectilinear bathymetric grid was constructed covering the study area from East Matagorda Bay to Sabine Pass. Grid cells measure 500 m alongshore and 125 m normal to shore forming a grid with 600 by 800 cells. A report summarizing results of the wave refraction analysis are presented in **Addendum 5**. Results show constructive wave interference that is controlled by regional bathymetry and correlates well with the average long-term erosion rates on adjacent beaches.

Subregional analyses of nearshore sediment transport, changes in beach sediment volume, meteorological impacts on physical processes, and storm impacts on morphology and sediment budget are contained in two published reports (Morton, R. A., Paine, J. G., and Gibeaut, J. C., 1994, Stages and durations of post-storm beach recovery, southeastern Texas Coast: Journal of Coastal Research, v. 10, p. 884-908; Morton, R. A., Gibeaut, J. C., and Paine, J. G., 1995, Meso-scale transfer of sand during and after storms: implications for prediction of shoreline movement: Marine Geology, v. 126, p. 161-179). One paper dealing with the relative rise in sea level and its influence on the rate of wetland loss has been accepted for publication (White, W. A., and Morton, R. A., in press, Wetland losses related to fault movement and hydrocarbon production, southeastern Texas coast: Journal of Coastal Research); another paper that also examines sea level rise and sediment supply is in preparation (**Addendum 2**).

Work Element 4: Prediction of Future Coastal Response

One of the principal purposes of conducting the five-year study was to develop models that are capable of predicting coastal responses within reasonable temporal and spatial limits. Those limits correspond to the range of coastal changes documented from the geological and historical records of the area. Current time-averaged linear methods of estimating future rates of shoreline movement are inappropriate for future predictions of shoreline position that magnify the inherent errors by an order of magnitude or as much as 60 times in the case of coastal construction setback lines and flood hazard zones.

The goals of work element 4 were to (1) improve rate of change estimations of shoreline movement and land loss, (2) integrate chronostratigraphic and lithostratigraphic data into a geologic framework, (3) develop conceptual models that synthesize coastal changes on both geological and historical time scales, and (4) develop quantitative models that predict shoreline changes and coastal inundation.

Task 1: Mathematical Analysis of Rates of Change The purpose of this task was to explore emerging mathematical theories such as nonlinear dynamics and fractal geometry as possible techniques for analyzing time-series data including shoreline changes. Our efforts emphasized incorporation of appropriate statistical techniques to adequately address the problems of nonlinear and nonuniform shoreline movement, trend reversal, and short-term variability that increase the margin of error in quantitative analyses. Most of the effort was directed toward task 2 that resulted in development of a predictive model of shoreline positions.

Task 2: Development of Predictive Models Predictive models of coastal erosion and inundation require the best available projections of global warming and the local relative rise in sea level. This task utilized all of the data generated during the project and it represents a major synthesis of results. The synthesis phase also provided responses to questions and requests for assistance from technical consultants, coastal planners, developers, and resource managers regarding nearshore dynamics, anticipated future changes in the coastal environments, and projected position of the shoreline.

SIGNIFICANT RESULTS. The Shoreline Shape and Projection Program (SSAP) was developed to aid in analyzing changes in past shoreline positions and determining future shoreline positions. The program projects future shoreline positions based on established statistical methods that compute shoreline rates-of-change and a new method that involves comparing the shape of the

projected shoreline with the expected shape. SSAP is written in FORTRAN for the Windows operating environment and is designed to easily accept historical shoreline data from a Geographic Information System (GIS) and to return projected shorelines to the GIS. A report providing detailed explanations of the methodology and test results is presented in **Addendum 6**.

The empirical analytical and predictive capabilities of SSAP form the basis for estimating the position of future shorelines and flood hazard zones along the southeastern Texas coast. This work serves as the foundation for State coastal zone management and Federal flood hazard delineation conducted by the Federal Emergency Management Agency.

Work Element 5: Sand Resources Investigations

Work element 5 addressed a current Gulf-wide need for sand resources that could be used to nourish and replenish recreational beaches that have been degraded as a result of coastal erosion. Principal objectives of the work element were to (1) locate sand deposits that could be used for beach restoration, (2) evaluate the physical characteristics of the sand deposits (size, water depth, overburden thickness), (3) characterize the sedimentological attributes of the deposits and compare them with composition of eroding beaches, (4) prepare maps showing the locations of the deposits with respect to eroding beaches. This work was done in cooperation with the US Department of Interior, Minerals Management Service.

SIGNIFICANT RESULTS. High-resolution seismic surveys were used initially to evaluate the potential sand deposits. After these data were interpreted, vibracores were taken to determine the lateral extent and thickness of the overburden. Standard sedimentological laboratory procedures were used to determine the composition, textures, and sorting of the sand deposits. We processed and described 32 vibracores collected from the Sabine Bank-Heald Bank region and completed textural analyses for selected samples from the vibracores. Core profiles for each of the 32 cores were prepared from visual descriptions and the sediment textures, and cross-sections of Heald and Sabine Banks were constructed from the core profiles.

Work Element 6: Technology Transfer

Task 1: Geographic Information System We used ARC-INFO, a standard geographic information system, to store digitized data such as topographic base maps, shorelines, and wetland boundaries (**Addendum 9**). In addition, an electronic database was established to preserve information sources (aerial photographs, maps, tide gauge records, leveling surveys, seismic

surveys, vibracores) as well as significant data (areal changes, volumetric changes, beach profiles, sediment textures).

Task 2: Dissemination of Data and Results During the fifth year of the project, two papers were presented at a conference on Sabine Lake sponsored by State, Federal, and local agencies. The extended abstracts published in the conference proceedings are included as **Addendum 10**.

The five-year program resulted in numerous reports, maps, and other products that have been or will be jointly published by the BEG and USGS in refereed journals (**Addendum 7**). Progress reports during the course of the study took the form of oral presentations at informal meetings between the BEG and USGS, at technical meetings and conferences, and at information transfer meetings sponsored by State and Federal agencies. We also responded to numerous requests for data generated by the project. The most significant requests are listed in **Addendum 11**.

SIGNIFICANT RESULTS. An invited symposium on coastal research was held at the 1996 South-central Section Meeting of the Geological Society of America. The meeting, which was held in Austin Texas, showcased the USGS-BEG-LSU coastal cooperative research program.

Electronic files (ARC-INFO) containing all the shoreline positions for the southeastern Texas coast were transferred to the Minerals Management Service at the request of Melanie Stright, for an archaeological investigation. We also transferred ARC-INFO electronic files of shorelines of Galveston Island to a graduate student at Texas A&M University College Station. ARC/INFO electronic files of shorelines of South Padre Island, North Padre Island, and Mustang Island were transferred to Texas A&M University Corpus Christi, Conrad Blucher Institute. Reprints of BEG articles documenting large-scale sedimentological and morphological changes in coastal environments related to hurricanes were sent to Chris Barton of the USGS in St. Petersburg.

We also submitted for inclusion on a CD-ROM all the important data sets, manuscripts, and GIS files that were generated by the project. The files and folders transferred electronically are listed in **Addendum 9**.

Addendum 1

Gulf Shoreline Movement between Sabine Pass and the Brazos River, Texas: 1974 to 1996

GULF SHORELINE MOVEMENT BETWEEN SABINE PASS AND THE BRAZOS RIVER, TEXAS: 1974 TO 1996

Robert A. Morton
Assisted by Sigrid Clift, Ted Angle, and Erika Boghici

INTRODUCTION

Regional studies of shoreline movement are now regarded as important sources of data for policy decisions because State and Federal agencies rely on average rates of shoreline movement and projected future shoreline positions for regulatory purposes. These coastal investigations that at one time were considered merely academic exercises now serve as a primary technical basis for decisions made by coastal planners and managers of natural resources located near the shore.

The use of shoreline data to establish construction setback lines or to delineate flood hazard zones creates a high standard that can only be met by achieving highly accurate results when recent short-term changes in shoreline position are examined. The keys to improved accuracy and reliability of predictions are (1) understanding the conditions that control beach morphology, (2) documenting short-term variability in shoreline position at representative sites, and (3) reducing the errors that are inherent in mapping and analyzing changes in shoreline positions (Morton, 1991).

Increased public demand for quantitative shoreline data and predictions of future shoreline positions that are both reliable and current have altered the ways coastal scientists collect and analyze shoreline data. Field monitoring of beaches for twenty years or mapping shorelines on sets of aerial photographs to distinguish long-term shoreline movement from short-term fluctuations is no longer an option in some regions because decisions to develop valuable coastal property are being made rapidly. Now coastal scientist must utilize rapid, highly accurate methods that minimize the errors of mapping and processing data.

The Bureau of Economic Geology has met the challenge of accurately mapping shoreline movement by improving the methods of data collection and analysis. The most common shoreline proxy derived from aerial photographs is the high water line separating the wet beach from the dry beach. However, more than two decades of beach surveys and field observations have demonstrated clearly that the high water line mapped on aerial photographs is dynamic and therefore is a less reliable indicator of shoreline position than the berm crest, base of the dune, vegetation line, or other beach feature

(fig. 1) that is either unaffected or only nominally altered by short-term changes in water levels. Furthermore, development of relatively low-cost, accurate Global Positioning Systems (GPS) now permit direct correlation between mapped shorelines and field observations of the mapped features instead of relying on interpretations from aerial photographs (Morton et al., 1993).

The principal objective of this study was to document recent shoreline movement along the southeastern Texas coast (Jefferson, Chambers, Galveston, and Brazoria Counties) between Sabine Pass and the mouth of the Brazos River (fig. 2) using shoreline positions that were mapped from aerial photographs taken in 1974, 1982, and 1990, and from field surveys conducted in 1996. Secondary objectives were (1) to document the different types of shoreline features present along the coast, and (2) to relate beach morphology and shoreline movement to the regional geologic framework.

SHORELINE MONITORING FEATURES

Shoreline movement is documented by identifying and monitoring the positions of beach features that are leading indicators of beach movement. This means that the monitored feature should respond to changes in environmental conditions but it should not be so sensitive to fluctuations in local conditions that it gives spurious results if monitored in the field or from aerial photographs. Typical morphological features on the Gulf beach between Sabine Pass and the Brazos River are the berm crest, erosional scarp, vegetation line, and crest of the washover terrace (figs. 1 and 3). In the absence of a more reliable morphological feature, the high water line or wet-beach/dry-beach line may be used as the shoreline proxy. Shoreline positions may also be defined by hard structures or other artificial features that largely determine the inland extent of high water. Shoreline monitoring features used in this study serve the same purpose as the shoreline erosion features defined by the Federal Emergency Management Agency (FEMA).

Berm Crest

The berm crest (fig. 1a) is the morphological feature that separates the steeper forebeach from the gentler sloping backbeach. It is a depositional feature when constructed by runup of normal waves (generally summer conditions) and a destructional feature when eroded by waves at abnormally high water levels (generally winter conditions). The berm crest may be entirely eroded by high storm waves, transforming the beach into a broad, featureless surface that slopes seaward uniformly.

On some beaches there are two berm crests; a high crest and a low crest (fig. 1a). Multiple berm crests are constructed by erosion of the backbeach and subsequent deposition on the forebeach by onshore migration of a sand bar and runup by low waves. Eventually the low berm will increase its height and merge with the high berm or the cycles of erosion and partial recovery will be repeated. Where there are multiple berm crests, the highest, most landward crest is used as the shoreline monitoring feature because it is more stable and responds to events of lower frequency than the lower berm crest. Laterally along the beach, the berm crest may become steeper and change to a mid-beach erosional scarp (fig. 1c) or it may flatten, become indistinct, and grade into a concave beach profile without a berm crest (fig. 1e).

Erosional Scarp

Erosional scarps are destructional features that are located in the mid-beach or form an abrupt break in slope at the landward limit of the backbeach (fig. 1c). Backbeach scarps normally represent the long-term beach morphology and they typically coincide with the vegetation line (fig. 1c). In contrast, mid-beach scarps are ephemeral features that are excavated during a rapid rise in water level when waves approach the shore at a high angle and generate strong alongshore currents, or a mid-beach scarp may be constructed when the beach is oversteepened such as after a beach nourishment project. Backbeach scarps typically grade into low dunes or washover terraces (fig. 1b), whereas mid-beach scarps generally pass laterally into high berm crests (fig. 1a).

Vegetation Line

On beaches and in wetlands, the vegetation line (fig. 1a, 1c, 1d, 1e) is a biological indicator of the limits of regular flooding by high water and therefore it represents a nearly ideal indicator of shoreline movement. Because the vegetation line is controlled by backbeach flooding, elevations of the vegetation line are consistently about 5 to 6 ft above sea level along sand beaches of the southeastern Texas coast (fig. 3). Plants that colonize the dunes and backbeaches can tolerate salt spray but they cannot survive if their roots are submerged for prolonged periods. The vegetation line can be a more reliable indicator of long-term shoreline movement than the high water line because it is not affected by short-term variations in water level.

Two factors prevent the vegetation line from being an ideal mapping boundary. First, the vegetation line is a biological feature that responds to environmental conditions that

are different from oceanic conditions that control beach morphology and position. For long periods (decades) the vegetation line will naturally reflect beach movement, but the vegetation line on sandy beaches can move independent of and in directions opposite to those of the beach for short periods (Morton, 1975). Second, the vegetation line is not always a distinct, easily identifiable feature. On many stable or accreting sand beaches, there are two vegetation boundaries that can be mapped; a line of dense vegetation that spreads continuously inland, and a line of sparse vegetation adjacent to the bare backbeach (Morton, 1975). The line of dense vegetation marks the most stable position beyond which the beach typically is unaffected by most storm surges. The zone of sparse vegetation consists of low mounds or dunes that have accumulated since the last major storm but have not coalesced to form a more continuous ridge of vegetated dunes.

The vegetation line is also subject to either deliberate or unintentional manipulation and artificial stabilization. In general, the vegetation line is natural between Sabine Pass and High Island (fig. 2). However, southwest of High Island, position of the vegetation line is controlled largely by property owners or beach scraping activities. Property owners erect sand fences, plant dunes grasses, and engage in other activities that tend to encourage the accumulation of sand and seaward advancement of the vegetation line. Rubble-cored sand mounds have been constructed in some developed areas to serve as wave protection and to dispose of debris created by Hurricane Alicia in 1983. Artificial dunes have also been created by the counties in conjunction with beach raking and scraping. Beach cleaning inadvertently mixes some sand with the beach debris. To keep the sand on the beach, piles of sand and trash are pushed into the backbeach where they become vegetated and act as low dunes. Along some beach segments, the piles of sand and debris form a zone 115 ft wide, which represents an artificial advancement of the vegetation line. Because manipulation of the vegetation line is prevalent along the southeastern Texas beaches, an ordinal ranking was developed to classify the extent of backbeach modification on the basis of field observations (Table 1).

In wetlands, such as salt-water marshes, the vegetation line is typically lower in elevation and seaward of the high water line because the wetland plants require frequent flooding to survive. Despite this discrepancy between the shoreline and the high water line, the marsh vegetation line is a good indicator of shoreline movement. Between High Island and the Brazos River, the marsh vegetation line forms the shore only for a short segment of Bolivar Flats, just north of the north jetty at Bolivar Roads. Nevertheless, for eroding marshes (fig. 1d), the marsh vegetation line is a good indicator of shoreline position and it was used to delineate the shore west of the Sabine Pass jetties.

Crest of Washover Terrace

Washover terraces (fig. 1b) are deposited where beaches are highly erosional and adjacent ground elevations are lower than the highest storm surges. The terraces are composed of sand with high concentrations of shell and rock fragments (Morton, 1975). The crest of the washover terrace forms the highest beach elevation and is the best indicator of shoreline movement for these types of beaches. Terrace crests can pass laterally into backbeach erosional scarps (higher elevations) or marshes (lower elevations). During storm washover, beach sand and shell are transferred onshore burying adjacent marsh or upland vegetation and concealing the vegetation line until vegetation either grows through the washover deposit or new vegetation colonizes the washover surface.

High Water Line

Some eroding sandy beaches exhibit a concave upward profile that lacks a distinct berm crest (fig. 1e). On these beaches the vegetation line and the high water line are two potential indicators of shoreline movement.

The high water line is also commonly used on aerial photographs as the shoreline proxy because it is easily identified (Stafford, 1971; Morton, 1979, 1991; Dolan and Hayden, 1983; Leatherman, 1983). The high water line observed in the field and on aerial photographs has been described (incorrectly) as closely approximating the position of mean high water (McBeth, 1956; Shalowitz, 1964; Stafford, 1971). However, field surveys clearly show that the position of the high water line is a function of beach morphology, water level, and wave characteristics immediately preceding the field observation. Furthermore, the wet-beach/dry-beach boundary seldom coincides with the berm crest (even when one is present) or with the mean high water line, which is a surveyed boundary. Most of the time the high water line is seaward of the berm crest but it can also be landward of the berm crest when slowly rising water floods the backbeach (spring tides) without completely eroding the berm.

The high water line was mapped on the aerial photographs taken in 1974, 1982, and 1990. It was not mapped during the 1996 field surveys.

Coastal Structures

On some developed beaches of the southeastern Texas coast, the most prominent shoreline features are coastal structures erected parallel to the shore (fig. 1f). Such structures include bulkheads, seawalls, and revetments that are designed to protect the adjacent upland property from flooding by high water and erosion by storm waves. Coastal structures have variable lengths parallel to the beach. Some structures are extremely long, such as the 10 mile-long Galveston sea wall, whereas others may extend only the width of a single lot (75 to 100 ft). Because coastal structures are products of human intervention, they have discrete lateral limits and can be adjacent to any other type of shoreline or shoreline feature.

Coastal structures such as seawalls and bulkheads do not always indicate that the beach is eroding and they are commonly constructed on stable or accreting beaches to prevent storms from damaging upland property. In these situations, the coastal structure is landward of the shoreline feature that should be used for monitoring beach movement. On retreating beaches, coastal structures form the shore and coincide with the landward limit of annual flooding by high water. Where beaches are highly erosional, coastal structures may fail physically and the shore will continue to retreat, thus establishing a new shoreline feature or another coastal structure position for monitoring.

BEACH MORPHOLOGY

Proper selection of a shoreline monitoring feature that tracks long-term shoreline movement partly depends on understanding the factors that control beach morphology at different time scales. Shoreline stability is ultimately controlled by the regional geologic framework, which includes the bedrock or late Quaternary deposits and coastal processes. Where tidal range and wave climate are essentially constant, such as along the southeastern Texas coast, alongshore variations in beach morphology (fig. 3) are related to the interaction of several factors including beach composition, substrate composition, direction and volume of sediment transport, beach stability, adjacent elevations, and strength of the highest storm waves. Beach morphology is an integrated response to these variables, which themselves are interactive and not totally independent. For example, beach morphology is closely linked to pairs of physical variables such as (1) beach and substrate composition, (2) volume of sediment transport and beach stability, and (3) adjacent elevations and storm wave heights.

Beach and Substrate Composition

The relationship between beach morphology and sediment textures is well known. Gravel beaches are generally steep and devoid of dunes, whereas fine sand beaches typically have low slopes and well-developed dunes. Beach morphology is also related to underlying sediments because they are a source of some beach material and they can control beach shape if the substrates are either immobile (bedrock or cemented sediments) or resistant to wave and current erosion (stiff mud).

The Gulf shore between Sabine Pass and the Brazos River can be divided into four morpho-compositional sections that are related to the regional coastal depositional systems (Fisher et al., 1973). The eastern section is the chenier plain, which is characterized by a broad salt marsh with muddy substrate (fig. 3a). The salt marsh formed Gulfward of an arcuate series of beach ridges that converge about 11 km west of Sabine Pass. Beaches of this section are narrow and steep, and composed of mud or a thin veneer of sand and shell over mud. The next morpho-compositional section, which extends from the beach-ridge complex to Rollover Pass, consists of a headland that is composed of late Pleistocene fluvial-deltaic deposits (McGowen et al., 1977). These mud-rich deposits are the source of abundant rock fragments, caliche nodules, and estuarine shells (*Rangia* and *Crassostrea*) that constitute the gravel concentrated on the beach between Sea Rim State Park and High Island (fig. 2). Beaches that coincide with the Pleistocene headland (fig. 3b) are narrow, relatively steep, and covered by shell pads that migrate along the beach depending on wave heights and sediment transport directions. Forebeaches are steep and high berm crests are well defined where thick shell pads are present. An exception to this morphology is the moderately wide sand beach with low dunes that is located in the vicinity of Sea Rim State Park. Apparently the beach sand is locally derived from the underlying Pleistocene river deposits that are exposed farther inland on the coastal plain (Morton, 1975).

A transitional morpho-compositional section between the Pleistocene headland and barrier island (Bolivar Peninsula) is located between Rollover Pass and Caplen (fig. 2). This segment of Bolivar Peninsula is narrow and overlies Holocene muddy estuarine deposits that contain oyster shells that constitute the gravel component commonly found on the beach.

The western morpho-compositional section is the broad, sand-rich barriers (Bolivar Peninsula, Galveston Island, Follets Island) that extend from Caplen to Freeport (fig. 2). Within this section, Gulf beaches are sandy and moderately wide, and the undeveloped backbeaches grade into low, densely vegetated dunes (fig. 3f) or an erosional scarp (fig.

3e). Beach morphologies from Freeport to the Brazos River (new Brazos delta) are similar in that Gulf beaches are sandy, and the undeveloped backbeaches grade into low, densely vegetated dunes (fig. 3f) or an erosional scarp (fig. 3e). However beaches tend to be relatively narrow southwest of Freeport.

Sediment Supply and Beach Stability

There is a direct correlation between volume of sediment transported along a coastal compartment and stability of the adjacent beaches. Where sediment supply is abundant relative to wave energy, the beaches advance; conversely, where sediment supply is low, the beaches typically retreat. Sediment supply is also related to transport directions. Sand eroded at one site is transported by longshore currents and deposited at another downdrift or offshore site.

The Gulf shore between Sabine Pass and the Brazos River corresponds to three coastal compartments. The jetties at Bolivar Roads and at Freeport (fig. 2) form the boundaries of the middle compartment. No rivers empty into the first two compartments, and the only sediment available for beach construction is either sand and shell eroded from the substrates or suspended sediment transported around the jetties and deposited in the wave shadow zone immediately west of the jetties. Although the flow of longshore currents throughout the year is bidirectional, net flow is to the southwest under the influence of east and southeast winds.

Where sediment supply is negligible or low, such as between Sabine Pass and High Island and on Bolivar Peninsula east of Caplen, the narrow steep beaches are generally retreating. Conversely, where sediment supply is moderate or high, such as on Bolivar Peninsula west of Caplen, on East Beach and central Galveston Island, and on Follets Island, relatively flat sand beaches are slowly retreating or advancing.

Adjacent Elevations and Storm-Wave Heights

The relationship between wave heights in the Gulf of Mexico and elevations of adjacent land largely determines if erosion or deposition occurs during high water events. Where waves are higher than the adjacent land, the land is inundated, overwashed, and possibly buried by washover deposits. Conversely, where storm waves are lower than the adjacent land, the backbeach-dune area is eroded by high water and scarps typically form in the dunes or barrier flat.

Between Sabine Pass and Caplen (fig. 2), storm waves regularly flood the adjacent land and deposit washover terraces of sand and shell. The marshes near Sabine Pass and the upland east of High Island are flooded several times each year when water levels are abnormally high. Frequent upland flooding coupled with long-term erosion have destroyed Highway 87 between Sea Rim and High Island. Within this flood prone segment, only the low dunes at Sea Rim State Park prevent annual flooding. Thickest washover deposits are preserved near Caplen where sediments deposited by Hurricanes Carla (1961) and Alicia (1983) are about 4 ft thick. Age of the thickest washover deposit (Carla) is inferred by the presence of concrete slabs and a TV antenna at the base of the deposit (fig. 4). Storm waves currently do not exceed the land elevation, therefore the washover deposits are exposed in a high scarp. Southwest of Caplen where the beach is sandy and wide, storm waves seldom overtop the dunes, which are about 10 ft high.

Dunes on East Beach of Galveston Island are also high enough to prevent washover by most storm waves except where the dunes have been removed at the parks and for beach parking. The lack of well-developed dunes on West Beach of Galveston Island makes it vulnerable to overwash as shown by the extensive flooding and washover deposition associated with Hurricane Alicia (Morton and Paine, 1985). Only the dunes northeast of Sea Isle are high enough to prevent inundation by most hurricanes. Dunes on Follets Island, Quintana Beach, and Bryan Beach are generally narrow and low, and adjacent land elevations are incapable of preventing overwash by even moderate storms.

MAPPED SHORELINE POSITIONS

Field Surveys

Classification and Distribution of Shoreline Features

Before the field survey was conducted, an ordinal ranking of shoreline features was prepared based on the variability in shoreline types (figs. 1 and 5) observed along the southeastern Texas coast (Morton, 1975; Morton and White, 1995). The ordinal ranking emphasizes stable beach features that are sensitive to long-term movement in beach position but are not appreciably altered by human activities. The ranking, which follows, provided the basis for selecting a shoreline proxy that was practical, repeatable, and relatively stable: (1) berm crest, (2) crest of washover terrace, (3) base of erosional escarpment, (4) vegetation line, (5) high water line, (6) artificial shore.

Just west of Sabine Pass the vegetation line forms the Gulf shore (fig. 5), which is irregular in planform and characterized by salt marsh with a muddy substrate. This short (0.7 mi) shoreline segment was surveyed on foot because the soft mud and high grass prevented progress of the all terrain vehicles. The marsh grades westward into a sand and shell washover terrace overlying marsh mud that extends westward for about 7.2 mi. Morphology of the washover terrace is disrupted locally and the shoreline is offset by a partially destroyed rock and concrete groin and failed wooden bulkhead backfilled by construction debris. These structures are known locally as the Hatfield structures. The washover terrace grades into a low erosional escarpment about 2 mi east of Sea Rim State Park. The low scarp becomes indistinct southwestward, and passes into a wide sandy beach with low, vegetated (enhanced) dunes and berm crest that forms the shore of Sea Rim State Park. About 6 mi southwest of Sea Rim, beach morphology changes and the berm crest grades into a low erosional escarpment and washover terrace where Highway 87 has been destroyed. The beach is a thin veneer of sand with abundant shells and rock fragments that overlies mud (McGowen et al., 1977). Widespread blocks of road pavement and other rubble on the beach prevented surveying the base of the scarp, therefore the shoreline feature of this 9.8 mi long beach segment is the edge of the unpaved road, which is essentially equivalent to the seaward edge of the scarp.

About 7.2 mi east of High Island, scarp (road) elevation decreases and the shore is the seaward edge of broken pavement or the equivalent high-water-line transition into a beach morphology characterized by a double berm crest. For this 15 mi long beach segment, which extends to Rollover Pass (fig. 2), either the upper berm crest or the trough between the high and low berms was surveyed as the shore. Southwest of Rollover Pass, an erosional scarp forms the shore except where the shoreline is locally altered by hard structures such as concrete and rock revetments. The protective structures typically are only one or two lots wide, but they protrude so far toward the water that they frequently block lateral movement along the beach. Maximum elevation of the erosional scarp (3 m) is near Caplen (fig. 2).

Southwest of Caplen, scarp elevation is lower and the scarp passes into a wide sand and shelly sand beach with low dunes and a berm crest that forms the shore. This beach morphology characterizes the Gulf shore to the southwestern end of Bolivar Peninsula where the normal berm crest passes into broad sand flats that are a depositional continuation of the beach. A high berm crest and the vegetation line were surveyed as the shoreline feature from the northeastern boundary of the Bolivar Flats Bird Refuge to the marsh shore at the Bolivar Roads jetty.

The high berm crest also was surveyed as the shoreline feature on East Beach of Galveston Island between the south jetty and the rock groin at 10th Street. The 1996 shoreline was not surveyed where the shore is formed by the Galveston seawall (transects 4-12, fig. 2). The reasons a survey was not conducted along the seawall are: (1) the groins break up the shore into a series of individual compartments, each with slightly different responses to wave energy and currents, (2) the high rock groins represent physical barriers that are difficult to traverse in a vehicle, (3) because the wall is so massive and nearly indestructible, future shoreline positions will not be farther landward than the wall, (4) the seawall beach from 10th street to 61st street was artificially nourished in the spring of 1995 and comparison of the 1996 shoreline with pre-nourishment shorelines would appear as recent beach advancement, and (5) the shoreline was near the wall before it was nourished.

On West Beach, a prominent erosional scarp forms the shore between the southwestern end of the seawall and Galveston Island State Park. At the State Park, the beach widens and the upper berm crest is the shoreline feature that was mapped to near the Bay Harbor subdivision (fig. 2). There beach morphology changes and an erosional scarp forms the shore. The scarp is continuous to just northeast of San Luis Pass where it is locally buried by recent accumulation of sand. At San Luis Pass the beach merges into a broad sand flat that has low, sparsely vegetated dunes. Along this short beach segment, both the vegetation line and the berm crest were mapped as shoreline features.

The high berm crest was the mapped shoreline feature in Brazoria County with the following exceptions. On the northeastern end of Follets Island, several houses and associated bulkheads form the shore and southwest of the bulkheads an erosional scarp forms the shore. For the remainder of Follets Island, at Surfside, along Quintana Beach, and along the Brazos delta, the berm crest forms the shore.

Global Positioning System

The 1996 shoreline feature between Sabine Pass and the Brazos River was surveyed using a dual antenna real-time differential GPS system (Trimble Pathfinder and Omnistar DGPS) mounted on a four-wheel drive all terrain vehicle (fig. 6). The DGPS equipment provided positions accurate to within 3 to 6 ft compared to shoreline positions derived from aerial photographs, which are only accurate to about 25 ft (Morton, 1991). During kinematic beach surveys, horizontal positions (UTM WGS-84) were collected at a 1 sec sampling rate, which translates to an average spacing of approximately 15 ft at high speed and 10 ft at low speed. Static positions were recorded for 5 minutes at the beginning and

at the end of each beach segment (data file). Beach segments were limited in length by natural features, such as large drainage channels, or physical barriers, such as cables or revetments across the beach, that prevented continuous lateral movement. Within a beach segment, way points were recorded to mark the positions of prominent (reference) features (drainage channels, houses on the beach) or the locations where the surveyed shoreline feature changed from one type to another. Most of the way points were photographed and field notes were recorded for future reference.

The raw GPS data were converted to State Plane, South-central Zone, NAD 27 datum, survey feet. Several files were collected in a non-differential mode when the Omnistar receiver was unable to provide corrected positions. These files were corrected in post-processing using differential corrections from the Texas Department of Transportation HARN station in Houston, Texas. The converted files of shoreline segments were merged, creating a single, continuous coverage for the 1996 shoreline.

Beach Profiles

Beach profiles from Sabine Pass to Bolivar Roads have been surveyed intermittently since 1974, whereas profiles on West Beach of Galveston Island and the northeastern end of Follets Island have been surveyed continuously since 1983 (Morton et al., 1994, 1995). Most of the original profile markers east of High Island have been destroyed by erosion and several of those west of Caplen have been destroyed by beach-front construction. Markers have been reestablished at those sites where monitoring has been continuous.

Alongshore variability in beach morphology is illustrated by representative profiles at selected sites from each of the morpho-compositional sections (fig. 3). The shapes of the profiles, particularly the width and steepness of the backbeach, are indicators of long-term beach stability.

Most of the beach profiles on West Beach document shoreline retreat. Profiles exhibiting the most retreat are just east of San Luis Pass near transect 29 and just southwest of the seawall near transect 14. Profiles exhibiting the least retreat are at Galveston Island State Park near transect 19, and at Jamaica Beach near transect 21. Beach profiles on West Beach showing shoreline advancement are east of Sea Isle near transect 24 and at San Luis Pass near transect 31.

The temporal variability in beach morphology at a particular site and the evolution of beach shape from one type to another is documented by comparing sequential profiles surveyed over a period of several years. The morphological evolution of beach profiles reflects changes in beach shape that are primarily responses to changes in sand supply

(figs. 7 and 8). On Follets Island, alongshore transport of sand and subsequent beach deposition during a 10-year period produced a change in beach shape from an erosional scarp to a wide sandy beach with low dunes (fig. 7). Conversely, erosion of sand on Galveston Island just downdrift of the seawall during an 8-year period transformed a wide sandy beach with low dunes into a steep, narrow concave beach with no dunes and an erosional scarp (fig. 8). The composite beach profiles illustrate how beach morphologies rapidly evolve depending on a surplus or deficit in sediment budget.

Geographic Information System (GIS)

Recent shoreline movement between Sabine Pass and the Brazos River was documented using ARC-INFO by comparing shoreline positions in June 1974 and either February 1996 (Sabine to Bolivar) or May 1996 (Galveston to Brazos River). The 1974 shoreline was mapped on aerial photographs and optically transferred to a 1:24,000 U.S.G.S. topographic base map (Morton, 1975). Later, the 1974 shoreline and shore-normal transects used for data reduction (fig. 2) were digitized and entered into the BEG ARC-INFO GIS. The 1996 shoreline was derived from a real-time differential GPS survey as described above. Distances between the 1974 and 1996 shorelines were measured at each transect, rates of change were calculated for the 21.7 or 21.9 year period, and a table was generated summarizing the trends (- retreat, + advance), magnitudes, and rates of shoreline movement (Tables 2-4).

ANALYSIS OF NET SHORELINE MOVEMENT 1974-1996

Shoreline Features

Beaches and bluffs are dynamic coastal features that are constantly changing shape and position in response to waves and water levels of the adjacent water body. Therefore, accurate depiction of shoreline movement relies on the accuracy of each shoreline position and consistency among shorelines incorporated into the shoreline change analysis. Consistency involves using the same shoreline feature and mapping criteria for each time period, whereas reliability refers to how accurately the shoreline feature represents long-term shoreline movement.

Ever since the concept of monitoring the shoreline from aerial photographs was first proposed, there has been an ongoing debate regarding the most appropriate proxy for shoreline position along coasts where beach morphologies are diverse. The wet beach/dry

beach boundary, which is also referred to as the high water line, is widely accepted as the reference feature for mapping shorelines (Stafford, 1971; Morton, 1979, 1991; Dolan and Hayden, 1983; Leatherman, 1983) despite the fact that the high water line is also an unstable feature that moves frequently throughout the year. For most shores, the stability of shoreline features increases landward and the frequency of movement of a shoreline feature increases seaward. Consequently the vegetation line, crest of washover terrace, erosional scarp, or bluff toe are more stable than the berm crest, and the berm crest is more stable than the high water line. However, defining the shoreline as the erosional scarp, vegetation line, or crest of the washover terrace instead of the high water line or berm crest may result in a landward shift of the mapped shoreline feature and an apparent change in the rate of movement for the period that includes the redefined shoreline. The magnitude of the discrepancy and apparent shift in shoreline position attributed to redefinition is the ground distance between the newly defined and previously defined features.

In the Gulf coast region, aerial photographic missions are commonly flown in the winter after a cold front passes the coast because then the atmosphere is clear and there are no clouds to block the view of the camera. Preceding passage of a cold front is also the time when low barometric pressure and strong onshore winds typically cause abnormally high water and flooding of the backbeach. Under these conditions the high water line depicted on aerial photographs corresponds to the vegetation line, erosional scarp, or other backbeach feature regardless of whether the forebeach morphology is characterized by a convex profile with a berm crest or a concave profile without a berm crest. Beach observations during the past 25 years clearly demonstrate that (1) the high water line responds to high frequency events and therefore does not have any particular physical significance regarding long-term shoreline movement and (2) the lateral mobility of the high water line results in noisy data sets and may be responsible for apparent cycles of shoreline advance and retreat that are only a function of sequential differences in water levels and not actual changes in beach sediment volume.

Spatial Analysis

Sabine Pass to Bolivar Roads - Shoreline movement from Sabine Pass to Bolivar Roads between 1974 and 1996 (Table 2) describes an alongshore pattern similar to the one established by previous analyses (Morton, 1975). Shoreline recession was recorded at 51 of the 62 transects, indicating that about 82% of the shore was retreating, whereas only about 18% of the shore was stable or advancing (fig. 9). The summary data (Table 2) help

identify four shoreline segments based on the most recent trend of shoreline movement, two segments where the shoreline is receding and two where the shoreline is stable or advancing.

From the south jetty at Sabine Pass to just east of Sea Rim State Park (transects 1-8) the shoreline retreated as much as 32 ft/yr (Table 2). This erosional segment of the Gulf shore is characterized by salt marshes or muddy beaches overlain by a washover terrace composed of sand and shell. The crest of the washover terrace or the seaward edge of the marsh vegetation is the shoreline feature mapped for this segment (fig. 5). Although cloud cover on the 1974 photographs prevents quantifying shoreline movement at transects 1-4, field observations clearly show that the beach along this segment is eroding rapidly. Minor erosion recorded at transect 8 (Table 2) is an artifact of sand trapped by a rubble groin and bulkhead (Hatfield structures). These structures drastically altered local shoreline orientation causing accretion northeast of the groin and accelerating erosion at the southwest end of the bulkhead. If the groin had not been constructed, then the shoreline retreat rate at transect 8 probably would have been about 15-20 ft/yr.

Destroyed houses and an erosional scarp at transect 9 indicate that the shoreline is actually retreating although advancement is indicated in Table 2. The apparent advancement in shoreline position at transect 9 may be an artifact of comparing shoreline positions digitized from topographic maps and surveyed with DGPS. Considering the positions of beach houses relative to the Gulf shore in 1982 and in 1996, the rate of shoreline retreat between the Hatfield bulkhead and transect 9 was probably about 10 ft/yr.

The shoreline advanced at transects 10-15 (fig. 9), which includes Sea Rim State Park. The beach of this segment is relatively wide, exhibits low vegetated dunes, and is composed of sand over mud. The berm crest is the shoreline feature mapped for this segment. Except for anomalous rapid advancement at transects 10 and 11, rates of shoreline advancement averaged about 2 to 4 ft/yr (Table 2). This shoreline advancement probably is related to a local supply of sand from underlying Pleistocene sand-rich fluvial sediments, the arcuate change in shoreline orientation (Morton, 1975), and the recent release of beach sand that had previously been impounded by the Hatfield structures. In 1991, the top part of the groin was removed, lowering its elevation to about average water level in the Gulf of Mexico. At that time beach sand and shell released from the groin began migrating southwest under the influence of longshore currents and nourishing downdrift beaches.

From transects 15 through 58, the entire Gulf shoreline retreated (fig. 9). Shoreline recession was highest, more than 10 ft/yr, between transects 18 and 32 (Table 2), which

includes the beach segment where Highway 87 has been destroyed by erosion. This beach segment is characterized by a narrow, relatively steep beach and washover terrace composed of sand and shell and underlain by mud. The crest of the washover terrace or edge of the destroyed road is the shoreline feature for this beach segment. Recession rates were relatively low near and southwest of High Island (transects 37-42) where the berm crest is the mapped shoreline feature. This moderately wide sand beach with artificial dunes is partly nourished by sand eroded from beaches to the northeast. The erosion rate at transect 42 (Table 2) is anomalous low as a result of sand trapped by pilings at a nearby fishing pier that acts as a permeable groin.

Near Rollover Pass (transects 43-46), rates of shoreline recession averaged about 5 ft/yr. This segment of the Gulf shore is characterized by a relatively steep narrow sand beach and washover terrace without dunes, or a low (< 5 ft) erosional scarp. The high berm crest or erosional scarp is the shoreline feature mapped for this segment (fig. 5). Slightly higher rates of erosion for this beach segment compared to those to the northeast are partly attributable to sand losses from the littoral system. Some sand migrating along the beach is transported through Rollover Pass into East Bay where it is deposited as a flood-tidal delta. This deposit has increased the shoaling rates in the Gulf Intracoastal Waterway.

Recession rates are moderately low (4-6 ft/yr) along Bolivar Peninsula southwest of Caplen (Table 2, transects 47-58). There the beach is sandy, relatively wide, and low vegetated dunes have formed. Because the beach is relatively wide, the berm crest is the shoreline feature mapped for this segment (fig. 9).

From transect 59 to the north jetty at Bolivar Roads, the Gulf shoreline is advancing (fig. 9) in response to the sand supplied by updrift erosion and alongshore transport. The berm crest is the shoreline feature mapped for this segment, which is characterized by a wide sand beach. Rates of shoreline advancement systematically increase to the southwest from a few feet per year to more than 17 ft/yr (Table 2). Rapid deposition near the north jetty caused continued expansion of a broad sand flat (Bolivar Flats), which is a designated sanctuary for nesting and migrating birds.

Galveston Island - Almost the entire Gulf shore of Galveston Island experienced net retreat between 1974 and 1996 (Table 3, fig. 9). Exceptions to this general statement were beaches at the extreme northeastern and southwestern ends of the island, where the shoreline advanced, and along the Galveston seawall where a beach nourishment project in 1995 stabilized the shore between 10th Street and 61st Street. Average annual rates of shoreline retreat were lowest on East Beach and highest on West Beach between the

seawall and Galveston Island State Park (transect 19, fig. 2). Retreat rates were moderate for the remainder of West Beach to San Luis Pass.

East Beach (transects 1-4) is characterized by a wide sand beach with a well defined berm crest that is frequently modified by beach scraping to remove trash and debris that floats in from the Gulf. Sand trapped by the counter current between the seawall and the jetties has kept the beach relatively stable since the mid 50s (Appendix B). This explains the net shoreline advance at transects 1 and 2 and the generally low average annual retreat rates of less than 3 ft/yr at transects 3 and 4 (Table 3).

On West Beach, average annual rates of shoreline retreat were 10 to 14 ft/yr from the end of the seawall to Galveston Island State Park (Table 3, fig. 9). The beach, which is narrow and steep at the seawall, gradually widens to the southwest. Except for a few rubble revetments and bulkheads in Spanish Grant and Bermuda Beach, the shoreline erosion feature for this beach segment is the erosional scarp that is generally well exposed. Recent beach scraping and placement of sand mounds in the backbeach obscures the scarp in some places. Despite the beach maintenance activities, the scarp persists throughout this reach and an indicator of frequent backbeach flooding and scour by waves. From Galveston Island State Park (transect 19) to Bay Harbor (transect 27), the undeveloped beach is wider, the dunes are 5 to 12 ft high, and the shoreline erosion feature is the berm crest. For this beach segment, average annual retreat rates are 5 to 8 ft/yr (Table 3). Southwest of Bay Harbor (transects 28-30) the beach progressively narrows and steepens, and the shoreline erosion feature is an erosional scarp. Average annual retreat rates for this segment of narrow beach range from 7 to 16 ft/yr (Table 3). Near San Luis Pass (transect 31), the erosional scarp grades southwestward into low, sparsely vegetated dunes and the beach widens into a broad sand flat. For this beach segment the shoreline advanced seaward nearly 500 ft between 1974 and 1996. The sand flat is part of the tidal inlet system at San Luis Pass that gains and loses sand volume as the channel and adjacent shoals shift position. Marginal sand flats of tidal inlets are notoriously unstable; consequently shoreline movement on the flats is rapid and typically covers large distances.

San Luis Pass to the Brazos River - An analysis of shoreline movement from San Luis Pass to the Brazos River between 1974 and 1996 (Table 4) reveals some trends that are similar and some trends that are different from those established by prior surveys (Morton and Pieper, 1975). Shoreline movement along the northeastern half of Follets Island was characterized by alternating zones of net retreat and net advance (Table 4). Greatest net changes occurred on the northeastern end of the island (transect 1) where the beach

retreated about 890 ft at an average annual rate of 40 ft/yr. Near transect 1, along the southern margin of San Luis Pass, the shore rapidly changes from a wide sand beach with berm crest to a narrow beach with erosional scarp that abuts several bulkheads at the Treasure Island subdivision. These bulkheads became the shoreline feature after Hurricane Alicia removed the broad sand flat that previously formed the shore. The beach is relatively narrow and an erosional scarp is present just southwest of the bulkheads indicating recent beach retreat, possibly related to the bulkheads interfering with the littoral system. Some of the beach and shoreface sand eroded near transect 1 during Hurricane Alicia, has been deposited near transect 3 (fig. 8), which explains the relatively rapid advance of the shore at that location. This recent accumulation of beach sand also has been documented with beach profiles since 1983 (Morton et al., 1995).

From central Follets Island to Surfside (transects 8-15), the beach is moderately wide and the berm crest is the shoreline erosion feature (fig. 5). Along this beach segment, the shoreline advanced slightly or was relatively stable between 1974 and 1996 (Table 4, fig. 9) despite lowering of the beach 1 to 1.5 ft and inland transport of sand by Hurricane Gilbert in 1988. Slight net advancement of the beach at transect 15 (Table 4) is related to dredged material placed on the beach in conjunction with relocation of the jetties and widening the ship channel at the entrance to Freeport Harbor. This undesigned beach replenishment project was conducted by the Corps of Engineers in October, 1991.

The beach at Quintana southwest of the Freeport jetty is narrow and the beach locally widens at the mouth of the Brazos River. Essentially all of the shore on Quintana Beach and Bryan Beach (transects 16-21) experienced net retreat except at the mouth of the Brazos River (transect 22) where net advance was recorded (Table 4, fig. 9). Greatest retreat occurred at transects 19-21 where the Bryan Beach side of the Brazos delta has been reworked by oceans waves and currents. Along this beach segment, a well defined erosional scarp reflects the trend in shoreline movement except near the mouth of the river were the scarp merges with low vegetated dunes that are adjacent to a broad sand flat characterized by sand ridges and swales containing water. This beach topography in 1996 indicates relatively recent accumulation of sand at the river mouth where the beach was formerly retreating. Sand was deposited at the river mouth after several major floods on the Brazos River built a broad mouth bar that was later reworked and welded to the former shore.

Temporal Analysis

Recent accelerations and decelerations in shoreline movement and changes in the trend of net advancement or retreat can be evaluated by comparing shoreline changes at each transect during the last two twenty-year periods. Twenty-year monitoring periods are considered to be long enough so that the long-term trend is accurately reflected in the changes in shoreline position. Comparing shoreline trends and rates of change from 1955-56 to 1974 (Morton, 1974; Morton 1975; Morton and Pieper, 1975) and from 1974 to 1996 (Tables 2-4) reveals the following conditions that are illustrated in Appendices A, B, and C.

Sabine Pass to Bolivar Roads - Northeast of transect 7, the marsh shoreline continuously retreated and the retreat rate accelerated (Appendix A) to more than 20 ft/yr. This rapid retreat rate is probably not related to mapping the washover crest instead of the high water line because inspection of the 1974 shoreline indicates that the high water line and the washover crest are essentially identical along this segment of steep narrow beach. Retreat rates actually decreased locally at transect 8 (Appendix A) as a result of the coastal structures (groin and bulkhead) that were erected and then partly removed. This human interference with the littoral system caused shoreline advancement between 1974 and 1982, and retreat from 1982 to 1996. At transects 9 and 10, the shoreline retreated until 1974 when it began to advance. In the vicinity of Sea Rim State Park (Appendix A, transects 11-15), the trend in shoreline movement changed from retreat to advance, partly in response to sand liberated from the coastal structures at transect 8, and then retreat. Most of these transects recorded net retreat since 1956. Southwest of Sea Rim at transects 16-31, the shoreline remained relatively stable or retreated slightly between 1956 and 1982, then shoreline retreat generally accelerated between 1982 and 1996. Accelerated retreat rates for this shoreline segment are probably both real and apparent. The beach retreated more rapidly after the Texas Department of Transportation attempted to stop erosion by constructing breakwaters out of steel guard rails. The retreat rates may also be slightly exaggerated because the crest of the washover terrace (edge of Highway 87) was mapped as the shoreline feature instead of the high water line.

Addition of a 1990 shoreline position helps delineate shoreline movement for the remaining transects from High Island to Bolivar Roads (fig. 2, Appendix A). Shoreline movement at transects 32-35 was similar to trends at nearby transects to the northeast. The shore was generally stable or retreating slowly from 1956 to 1982 and then retreat accelerated from 1990 to 1996. Shoreline movement was cyclical at transects 36 to 58. The shoreline retreated between 1956 and 1974, advanced from 1974 to 1990, and then

retreated between 1990 and 1996. The overall trend since the 1950s has been net retreat. At transects 59 and 60, shoreline movement was also cyclical with recent retreat; however, the overall trend since the 1950s has been net advance. At transects 61 and 62, the most recent trend of shoreline stability between 1990 and 1996 suggests a reduction in the rate of advancement that had been recorded previously (Appendix A).

Galveston Island - Since 1956, the beach at transects 1 and 2 generally has either remained stable of advanced slightly (Appendix B). Although some sand continues to accumulate south of the south jetty, rates of advancement greatly declined after the beach reached an equilibrium position in the mid 1950s. The beach at transect 3 also has been relatively stable, despite short-term cycles of shoreline advance and retreat. Shoreline movement also has been cyclical at transect 4, but the overall trend has been net retreat (Appendix B).

On West Beach, shoreline movement since 1956 has been variable, but net retreat has been the predominant trend at transects 13-18, 22-25, and 28-30. Net shoreline retreat has also been the predominant trend at transects 19-21 and 26-27 even though the most recent change in shoreline position was minor advancement (Appendix B). This apparent reversal in trend may be an artifact of using the berm crest modified by beach scraping as the erosion feature rather than the vegetation line.

At San Luis Pass (transect 31), actual trends of shoreline movement reversed following Hurricane Alicia in 1983 (Appendix B). The shore, which had been rapidly retreating, began advancing as the shoal and tidal flat on the eastern side of San Luis Pass began to accumulate sand (Morton et al., 1995).

San Luis Pass to the Brazos River - The beach between San Luis Pass and the Brazos river has undergone net retreat at all transects since 1956; however, there have been more recent changes in shoreline movement that are significant. Between 1956 and 1996, the major trends of shoreline movement reversed at transects 1 and 2 (Appendix C). Retreating beaches advanced between 1956 and 1974 and then later began retreating again. These large-scale trend reversals involving hundreds of feet of shoreline movement are attributed to dynamics of tidal inlets and the large volumes of beach and shoreface sediment that get redistributed periodically by storms. The trend of shoreline movement also reversed at transect 3, but the beach is still advancing slightly and has not retreated since 1974.

Anomalous shoreline advance between 1982 and 1991 was followed by either retreat or stability at transects 4 through 22 (Appendix C). Since 1982, short-term net advance

was recorded at transects 4, 8-17, and 22, whereas short-term net retreat was recorded at transects 5-7 and 18-21. On Follets Island and at Surfside (transects 4-15), the trend toward greater shoreline stability began about 1974 (Appendix C). Short-term reversing cycles of advance and retreat are difficult to interpret and essentially impossible to predict with available data and available quantitative methods of analysis. If the short-term variability in shoreline position is minor (less than 100 ft) then the oscillations tend to indicate either stable or slowly changing long-term conditions.

SUMMARY

Alongshore variations in beach morphology of the southeastern Texas coast are controlled by beach composition, substrate composition, sand transport volume, adjacent elevations, and storm wave height. Decadal variations in beach morphology at a site are related to changes in sand transport; consequently beach morphology and beach composition are also strongly correlated with beach stability.

Shoreline features used to depict shoreline position for the southeastern Texas coast are the vegetation line, berm crest, erosional scarp, and crest of washover terrace. These shoreline proxies have predictable morphologies, occupy predictable positions on the beach, and spatial changes in their positions reflect long-term stability of the beach. Five linked beach morphologies and shoreline stability pairs are recognized within the study area. They are wide backbeach with distinct berm crest (stable or advancing sand beach), concave beach or scour trough (slowly retreating sand beach), erosional scarp (moderately to rapidly retreating sand beach), crest of washover terrace (rapidly retreating sandy shell veneer over mud), and seaward edge of *Spartina alterniflora* (retreating muddy marsh shore).

Although the high water line (wet beach/dry beach line) was used in prior studies as the shoreline proxy, it is not recommended for future analyses of shoreline movement. This change in shoreline mapping strategy is justified because the high water line occupies a wide range of seasonal positions related to fluctuations in water level, it does not conform to a particular geomorphic feature on the beach, and it is less diagnostic of long term shoreline movement than the other shoreline features.

Between Sabine Pass and the Brazos River, regional patterns of shoreline advancement and retreat generally were similar during the past twenty years as they were during previous monitoring periods. Most of the developed beach segments continue to retreat. There were, however, some local differences in the trend of shoreline movement or the rates of movement. For example, shoreline retreat accelerated between Sea Rim

State Park and High Island where State Highway 87 was destroyed. Shoreline retreat also was more noticeable between Rollover Pass and Caplen on Bolivar Peninsula. Some beach segments of Follets Island either advanced or retreated more slowly after 1983 when strong alongshore currents during Hurricane Alicia transported sand from San Luis Pass to the southwest, where it has nourished beaches northeast of Freeport. Also, the beach is slightly wider at Surfside after dredged material was placed on the beach as part of widening and deepening the ship channel and harbor entrance to Freeport.

ACKNOWLEDGMENTS

This work was supported by the U.S. Geological Survey Coastal Geology Program and the Texas General Land Office Coastal Division. We gratefully acknowledge the cooperation of the Region 1 Oil Spill Division of the Texas General Land Office for providing the all terrain vehicles used to conduct the 1996 GPS shoreline surveys.

REFERENCES

Dolan, R. and Hayden, B., 1983, Patterns and prediction of shoreline change, *in* Komar, P. D., ed., Handbook of coastal processes and erosion. CRC Press, Inc., Boca Raton, FL, p. 123-149.

Fisher, W. L., Brown, L. F., McGowen, J. H., and Groat, C. G., 1973, Environmental geologic atlas of the Texas coastal zone, Beaumont-Port Arthur area: The University of Texas at Austin, Bureau of Economic Geology, 93 p.

Leatherman, S., 1983, Shoreline mapping: a comparison of techniques. Shore and Beach, 51: 28-33.

McBeth, F. H., 1956, A method of shoreline delineation: Photogrammetric Engineering, v. 22, p. 400-405.

McGowen, J. H., Garner, L. E., and Wilkinson, B. H., 1977, The Gulf shoreline of Texas: Processes, characteristics and factors in use: University of Texas at Austin, Bureau of Economic Geology, Geological Circular 77-3, 27 p.

Morton, R. A., 1974, Shoreline changes on Galveston Island: The University of Texas at Austin, Bureau of Economic Geology, Geological Circular 74-2, 34 p.

Morton, R. A., 1975, Shoreline changes between Sabine Pass and Bolivar Roads: University of Texas at Austin, Bureau of Economic Geology, Geological Circular 75-6, 43 p.

Morton, R. A., 1979, Temporal and spatial variations in shoreline changes, Texas Coast. Journal of Sedimentary Petrology, v. 49, p. 1101-1111.

Morton, R. A., 1991, Accurate shoreline mapping: past, present, and future: American Society of Civil Engineers, Coastal Sediments '91, v. 1, p. 997-1010.

Morton, R. A., Leach, M. P., Paine, J. G., and Cardoza, M. A., 1993, Monitoring beach changes using GPS surveying techniques: Journal of Coastal Research, v. 9, p. 702-720.

Morton, R. A., Gibeaut, J. C., and Paine, J. G., 1995, Meso-scale transfer of sand during and after storms: implications for prediction of shoreline movement: Marine Geology, v. 126, p. 161-179.

Morton, R. A., and Paine, J. G., 1985, Beach and vegetation-line changes at Galveston Island, Texas: erosion, deposition, and recovery from Hurricane Alicia: The University of Texas at Austin, Bureau of Economic Geology, Geological Circular 85-5, 39 p.

Morton, R. A., and Pieper, M. J., 1975, Shoreline changes in the vicinity of the Brazos River delta: The University of Texas at Austin, Bureau of Economic Geology, Geological Circular 75-4, 47 p.

Morton, R. A., and White, W. A., 1995, Shoreline types of the upper Texas Coast: Sabine-Galveston-Freeport-Sargent Areas: University of Texas at Austin, Bureau of Economic Geology, contract report prepared for the Texas Natural Resources Inventory Program, Interagency Contract IAC 94-0198, 40 p.

Morton, R. A., White, W. A., Gibeaut, J. C., Gutierrez, R., and Paine, J. G., 1994, East Texas and Western Louisiana Coastal Erosion Study Annual Report, Year 3: The University of Texas at Austin, Bureau of Economic Geology, contract report prepared for the U.S. Department of Interior, Geological Survey Contract No. 14-08-0001-A0912, variously paginated.

Shalowitz, A. L., 1964, Shore and sea boundaries: U.S. Department of Commerce Publ. 10-1, v. 2, 749p.

Stafford, D. B., 1971. An aerial photographic technique for beach erosion surveys in North Carolina. Technical Memorandum 36, Coastal Engineering Research Center, 115 p.

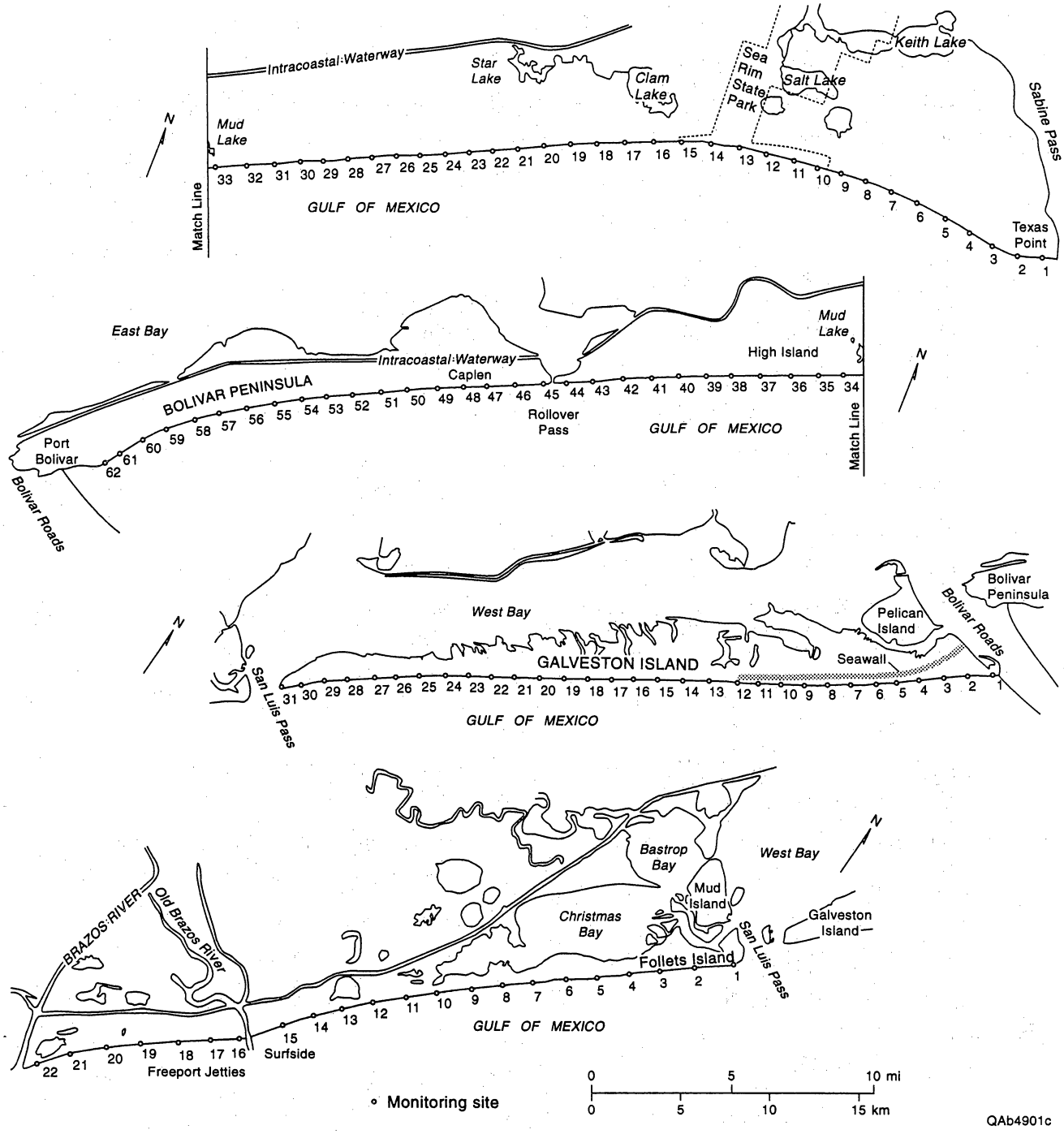

Figure 1. Geographic localities and locations of shore-normal transects used to analyze recent movement of the Gulf shore between Sabine Pass and the Brazos River.

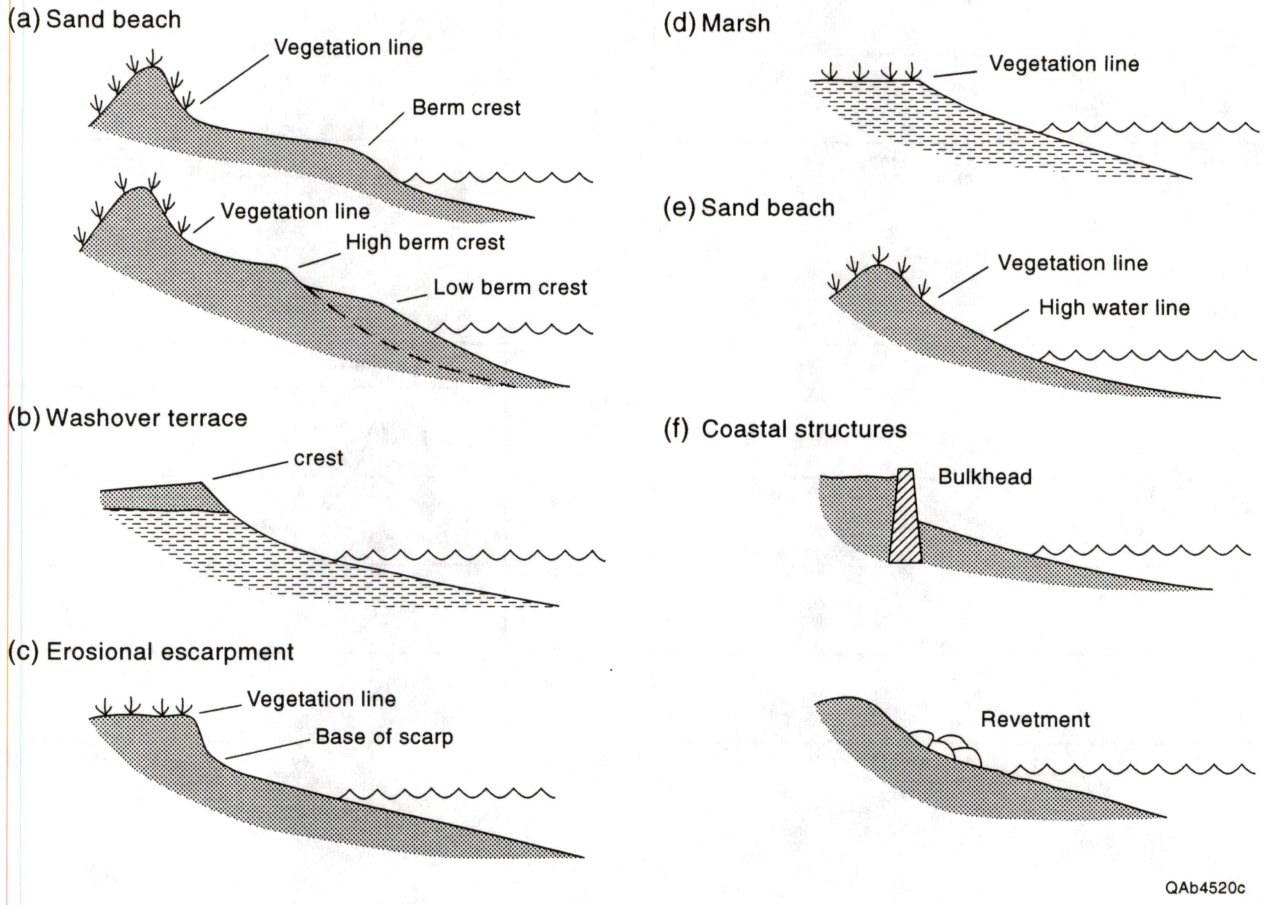

Figure 2. Generalized beach profiles illustrating typical beach morphologies and associated shoreline features observed in the study area. The profiles represent (a) sand beach with single and multiple berm crests, (b) sandy washover terrace overlying mud beach, (c) erosional scarp, (d) marsh vegetation line, (e) concave erosional sand beach without berm crest, and (f) common small-scale coastal structures.

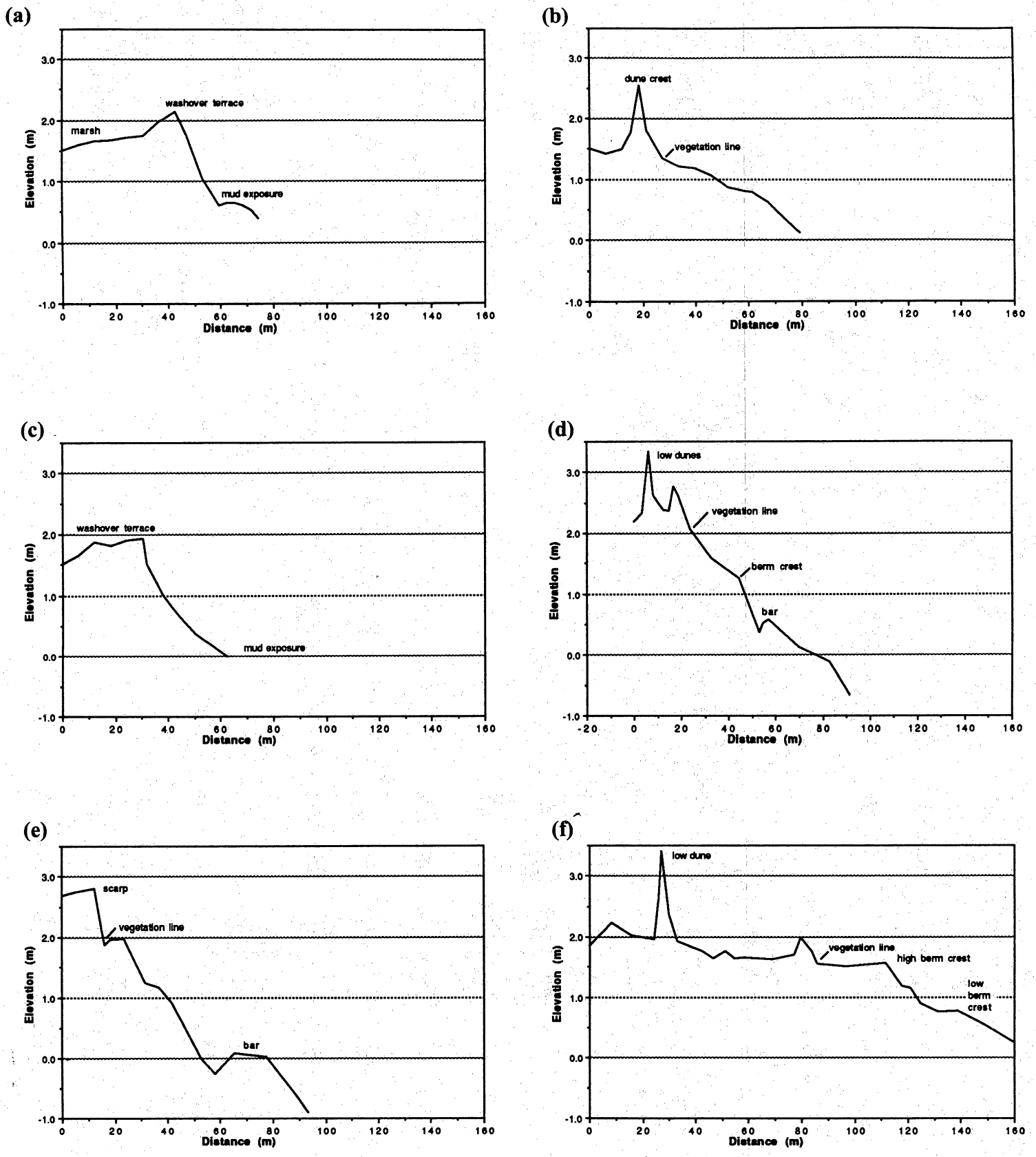

Figure 3. Surveyed profiles selected from the four morpho-compositional beach sections representing (a) washover terrace and marsh (mud) substrate west of Sabine Pass, (b) sand beach with low dunes near Sea Rim State Park, (c) washover terrace with mud substrate along Highway 87 east of High Island, (d) narrow sand beach with artificial dunes west of High Island, (e) steep sand beach and erosional scarp west of Rollover Pass, and (f) wide sand beach with low dunes on the southwestern end of Bolivar Peninsula.

Figure 4. Washover sand and shell deposited by Hurricanes Carla (1961), and exposed by erosion of a scarp. Large concrete slab is at the base of the washover deposit. Location is near transect 47 between Caplen and Rollover Pass (fig. 1).

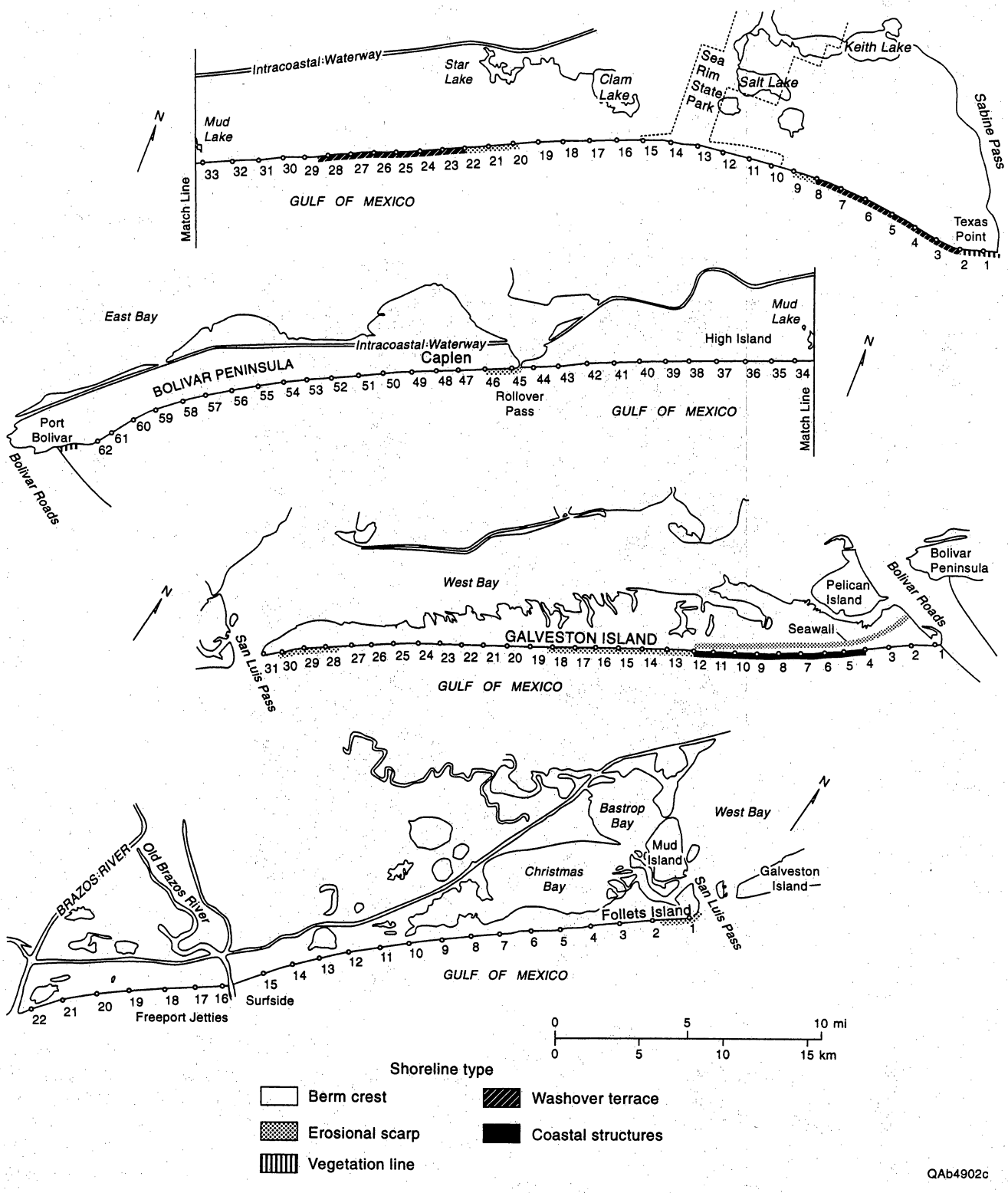

Figure 5. Distribution of shoreline types between Sabine Pass and the Brazos River.

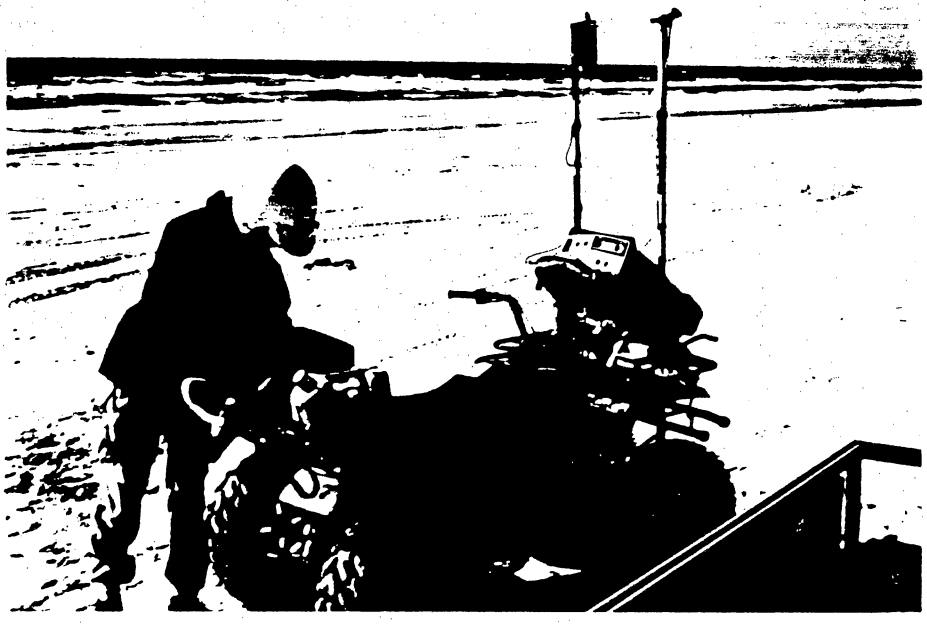

Figure 6. Real-time differential GPS equipment mounted on a four-wheel drive all terrain vehicle.

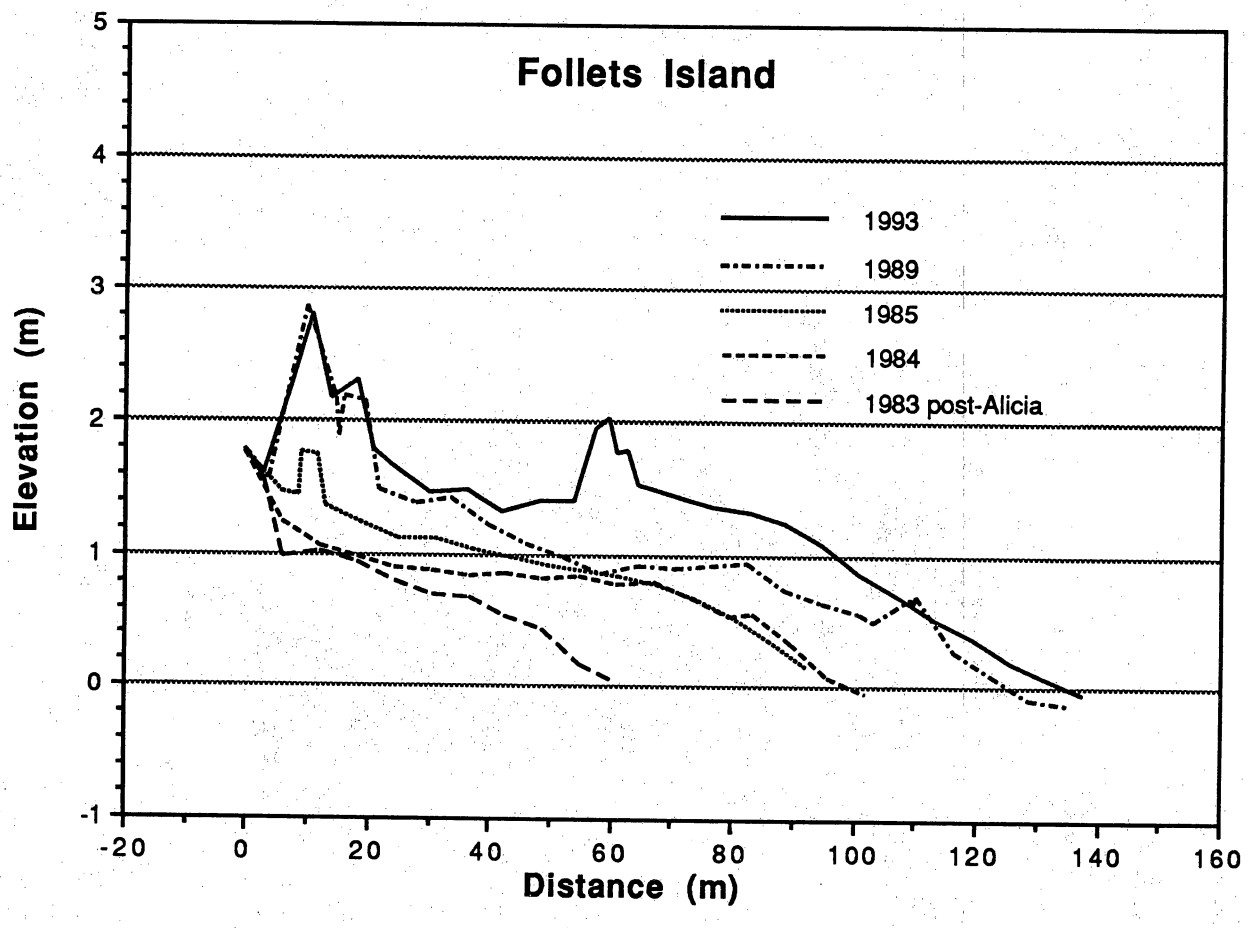

Figure 7. Ten-year evolution of an advancing beach profile, Follets Island near transect 3.

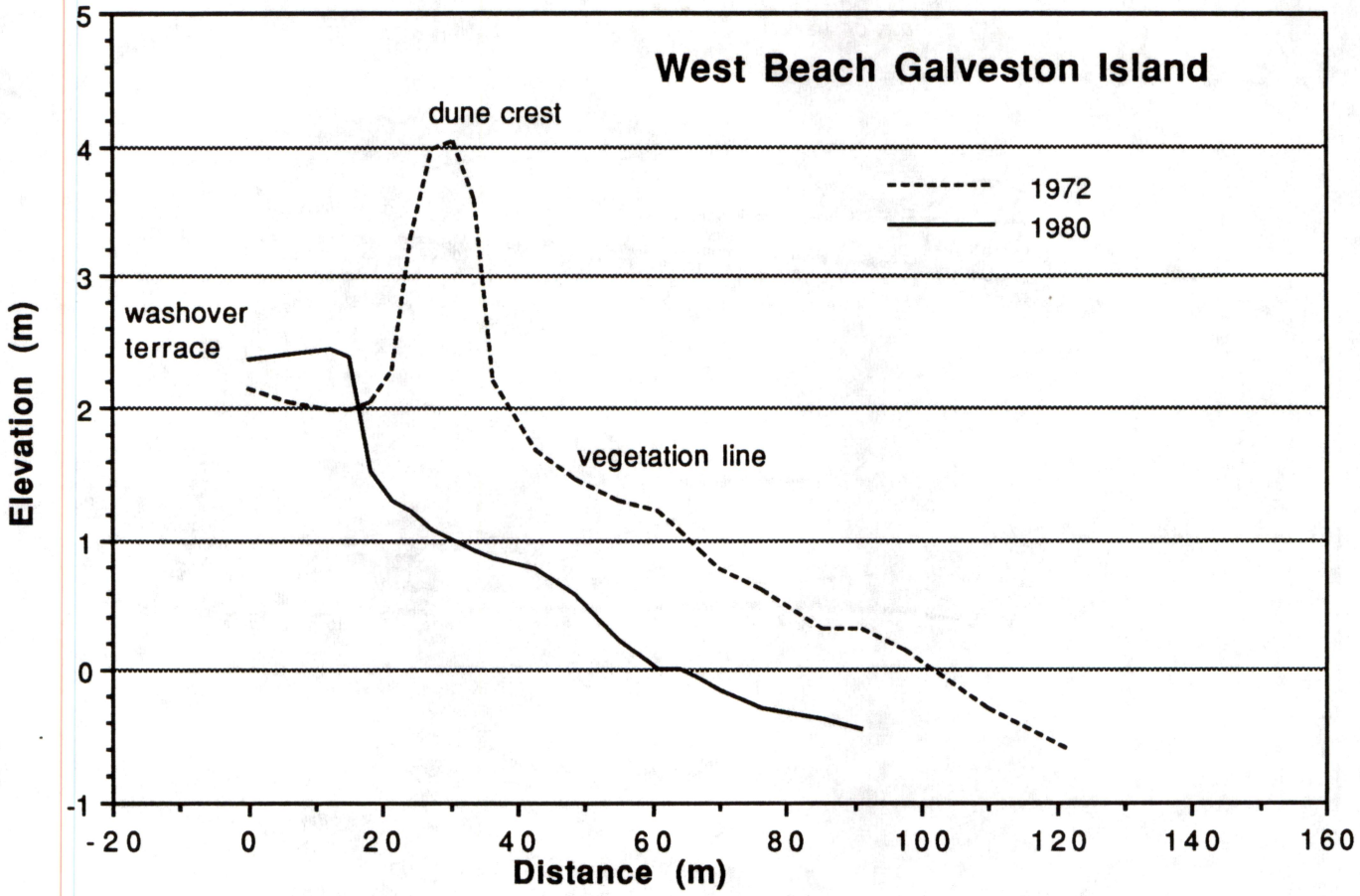

Figure 8. Eight-year evolution of a retreating beach profile, Galveston Island near transect 13.

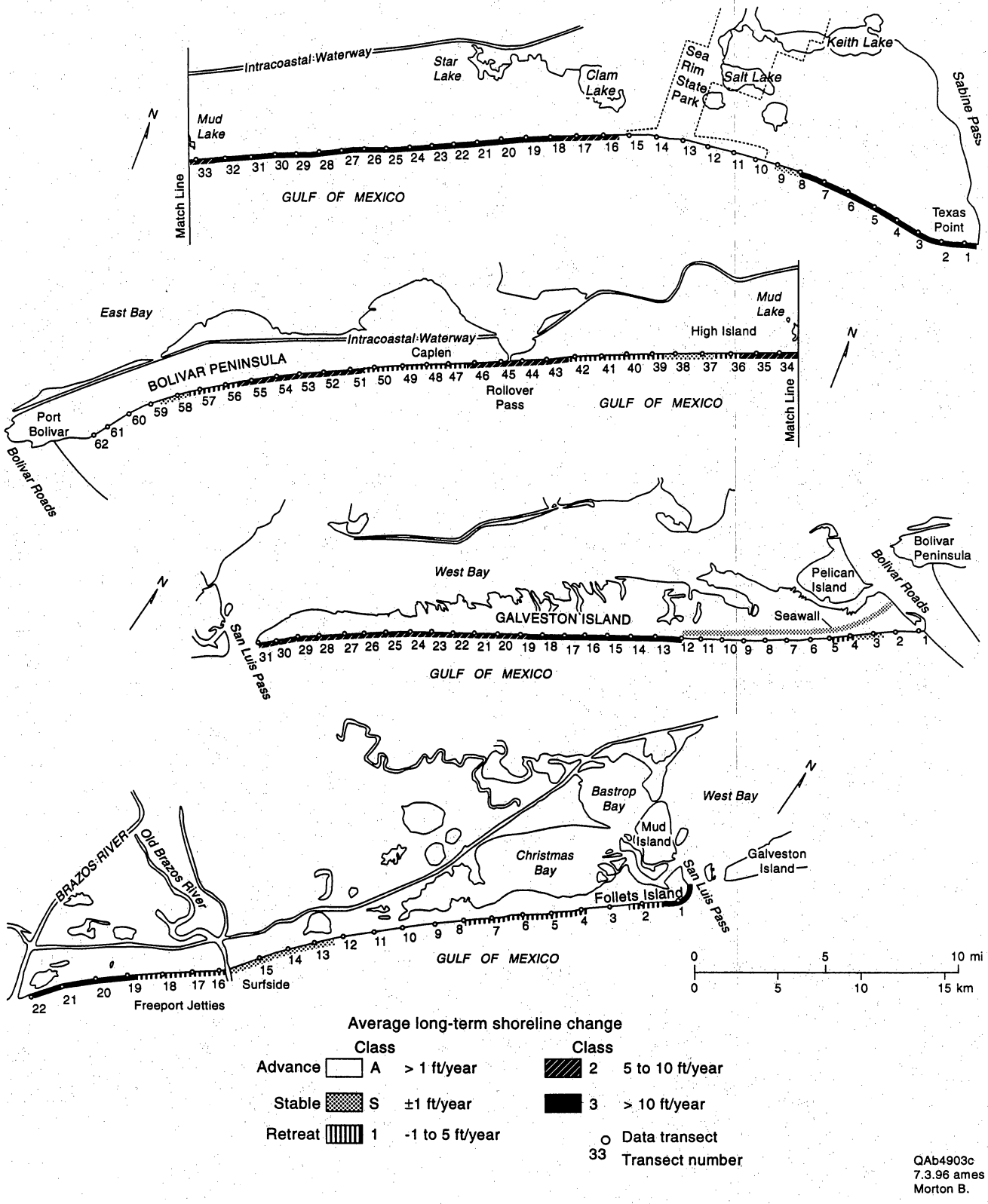

Figure 9. Summary diagram illustrating recent (1974-1996) shoreline movement between Sabine Pass and the Brazos River.

Table 1. Index of human impact on dunes and beach vegetation of the southeastern Texas coast.

Index	Description
0	No visible impact of beach scraping or evidence of backbeach dumping. Dune morphologies and plant communities are natural. Essentially no modification of beach and dune profile.
1	Low, small-volume mounds of sand containing some minor beach trash such as *Sargassum*. Trash represents less than 20% of mound volume. Altered zone is narrow relative to the entire beach width.
2	Low, small-volume mounds of sand and some minor beach trash such as *Sargassum* and small pieces of wood. Trash represents less than 33% of mound volume. Altered zone is narrow relative to the entire beach width.
3	Moderately large mounds of sand at least 3 ft high. Mounds composed of approximately 33% trash including moderately large pieces of wood or other debris. Several rows (2-3) of modified dunes or sand mounds. Altered zone is moderately wide relative to the entire beach width.
4	Moderately large mounds of sand greater than 3 ft high. Mounds composed of more than 33% trash. Multiple rows of modified dunes or sand mounds forming moderately wide zone relative to the entire beach width. Modified area may include bypass zone(s) representing former backbeach road(s).
5	Large mounds of sand up to 6 ft high. Mounds composed of as much as 50% trash containing large logs, cut wood, tires, appliances, and concrete or other rubble. Multiple rows of modified dunes or sand mounds forming wide zone relative to the entire beach width. Modified area may include bypass zone(s) representing former backbeach road(s).

Table 2. Net shoreline changes between Sabine Pass and Bolivar Roads, 1974-1996. Locations of transects shown on fig. 2. Plus sign indicates shoreline advance, minus sign indicates shoreline retreat.

Transect	Net Change (ft)	Average Rate (ft/yr)	Transect	Net Change (ft)	Average Rate (ft/yr)
5	-700	-32.3	34	-183	-8.4
6	-639	-29.5	35	-197	-9.1
7	-466	-21.5	36	-83	-3.8
8	-5	-0.2	37	-18	-0.8
9	73	3.4	38	-5	-0.2
10	251	11.6	39	-39	-1.8
11	261	12.0	40	-42	-1.9
12	48	2.2	41	-28	-1.3
13	82	3.8	42	-8	-0.4
14	94	4.4	43	-110	-5.1
15	44	2.0	44	-99	-4.6
16	-116	-5.3	45	-122	-5.6
17	-201	-9.3	46	-138	-6.3
18	-265	-12.2	47	-90	-4.2
19	-257	-11.8	48	-109	-5.0
20	-248	-11.4	49	-105	-4.8
21	-263	-12.1	50	-50	-2.3
22	-308	-14.2	51	-131	-6.0
23	-376	-17.3	52	-77	-3.5
24	-339	-15.6	53	-140	-6.5
25	-294	-13.5	54	-167	-7.7
26	-313	-14.4	55	-108	-5.0
27	-337	-15.5	56	-57	-2.6
28	-288	-13.3	57	-116	-5.4
29	-253	-11.6	58	-16	-0.7
30	-247	-11.4	59	28	1.3
31	-240	-11.0	60	49	2.2
32	-245	-11.3	61	142	6.5
33	-211	-9.7	62	379	17.5

Table 3. Net shoreline changes along Galveston Island, 1974-1996. Locations of transects shown on fig 2. Plus sign indicates shoreline advance, minus sign indicates shoreline retreat.

Transect	Net Change (ft)	Average Rate (ft/yr)	Transect	Net Change (ft)	Average Rate (ft/yr)
1	+353	+16.1	20	-171	-7.8
2	+116	+5.3	21	-178	-8.0
3	-12	-0.6	22	-149	-6.7
4	-52	-2.4	23	-137	-6.1
13	-313	-14.3	24	-152	-6.8
14	-303	-13.8	25	-105	-4.7
15	-260	-11.9	26	-112	-4.9
16	-286	-13.1	27	-138	-5.9
17	-273	-12.5	28	-154	-6.9
18	-225	-10.3	29	-217	-9.7
19	-159	-7.2	30	-346	-15.8
			31	+501	+22.9

Table 4. Net shoreline changes from San Luis Pass to the Brazos River, 1974-1996. Locations of transects shown on fig. 2. Plus sign indicates shoreline advance, minus sign indicates shoreline retreat.

Transect	Net Change (ft)	Average Rate (ft/yr)	Transect	Net Change (ft)	Average Rate (ft/yr)
1	-892	-40.7	12	+79	+3.8
2	-66	-3.0	13	+16	+0.9
3	+292	+13.3	14	+4	+0.4
4	+69	+3.1	15	+27	+1.5
5	-39	-1.8	16	-27	-1.2
6	-56	-2.6	17	-25	-1.0
7	-34	-1.6	18	-112	-5.0
8	+57	+2.6	19	-302	-13.6
9	+86	+3.9	20	-289	-13.0
10	+81	+3.7	21	-243	-10.9
11	+30	+1.4	22	+78	+3.8

APPENDIX A

SHORELINE HISTORY PLOTS:

SABINE PASS TO BOLIVAR ROADS

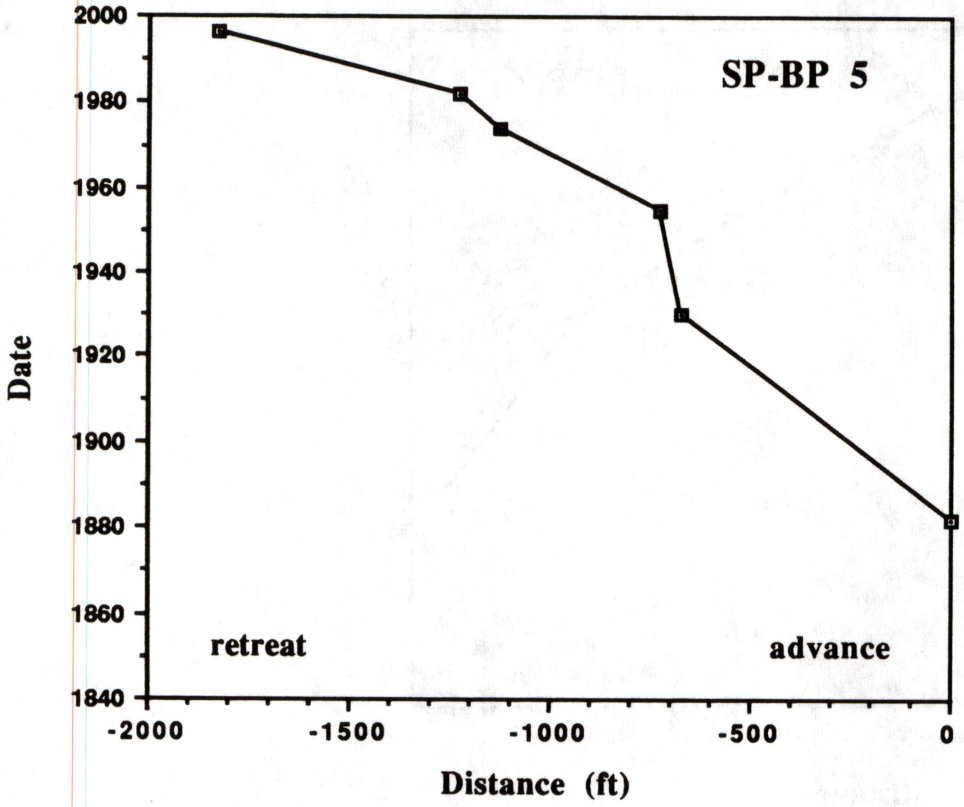
SP-BP 5
Date
2000
1980
1960
1940
1920
1900
1880
1860
1840
retreat
advance
-2000
-1500
-1000
-500
0
Distance (ft)

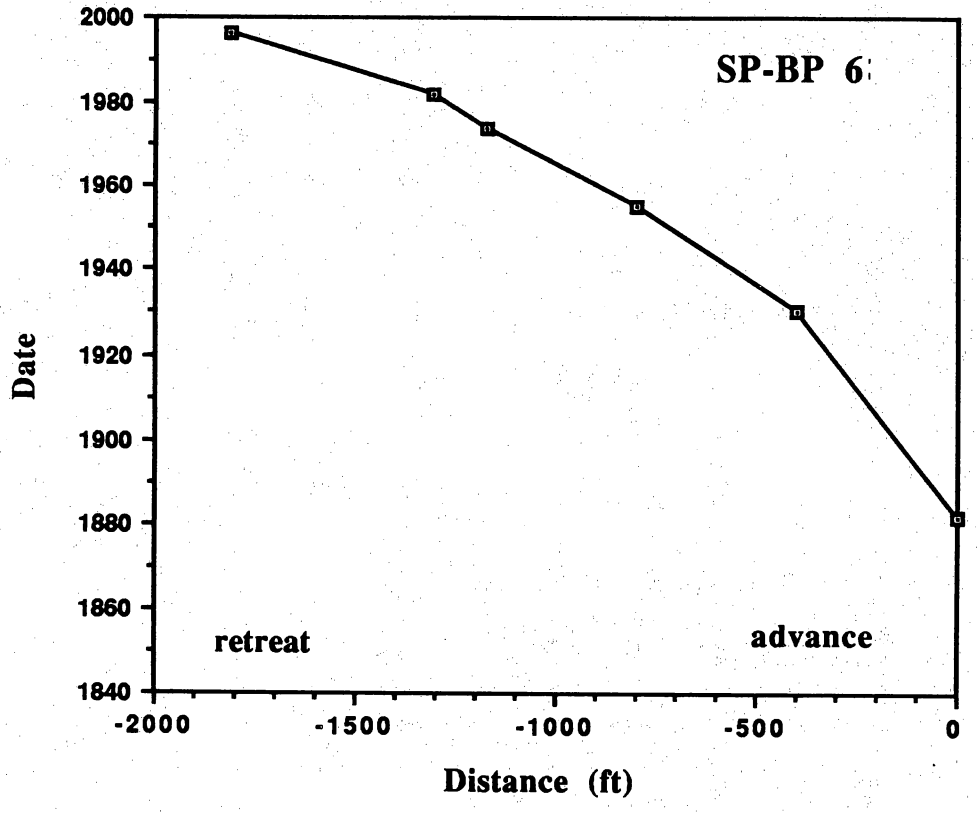
SP-BP 6
2000
1980
1960
1940
1920
1900
1880
1860
1840
Date
retreat
advance
-2000
-1500
-1000
-500
0
Distance (ft)

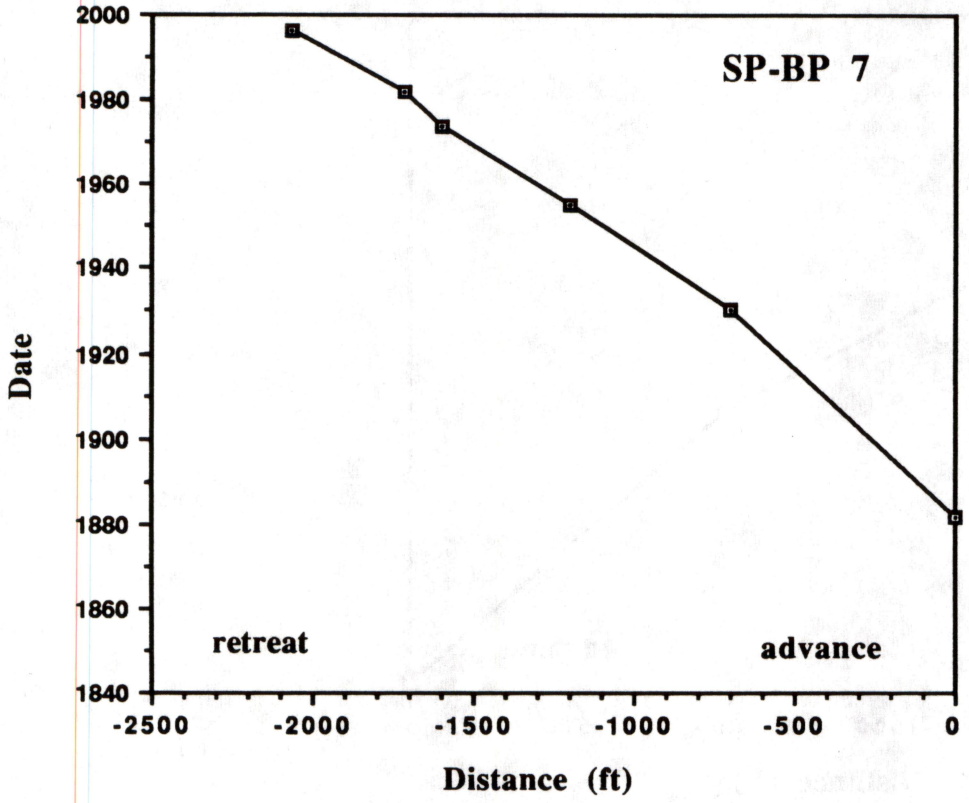
SP-BP 7
Date
2000
1980
1960
1940
1920
1900
1880
1860
1840
retreat
advance
-2500
-2000
-1500
-1000
-500
0
Distance (ft)

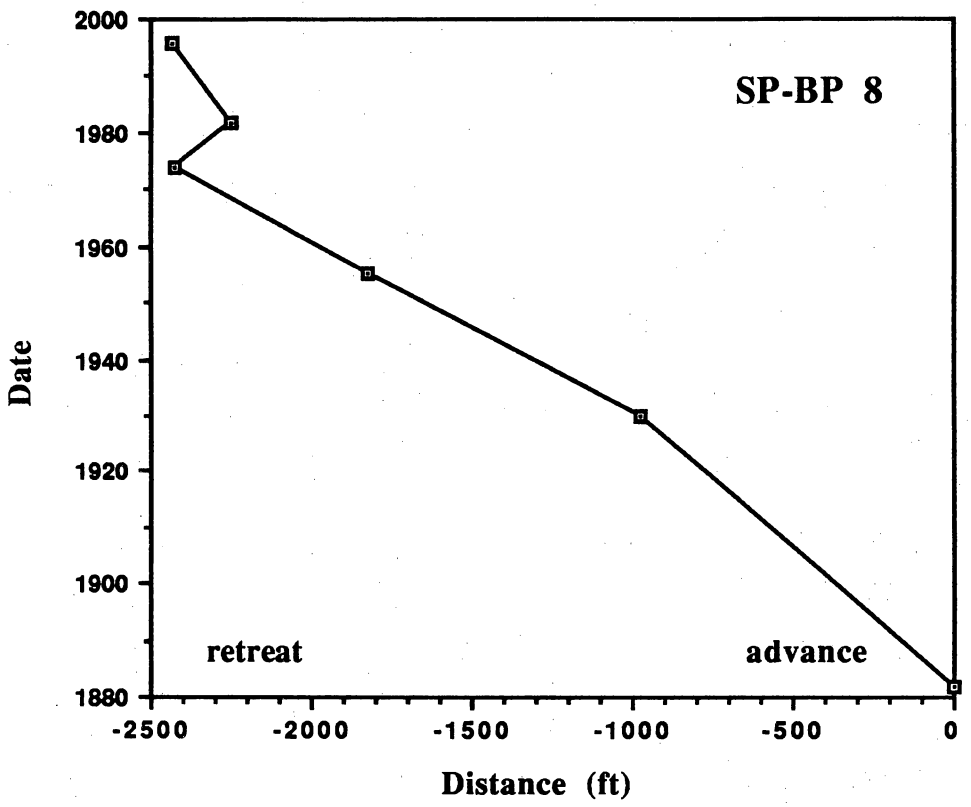
SP-BP 8
2000
1980
1960
1940
1920
1900
1880
Date
retreat
advance
-2500
-2000
-1500
-1000
-500
0
Distance (ft)

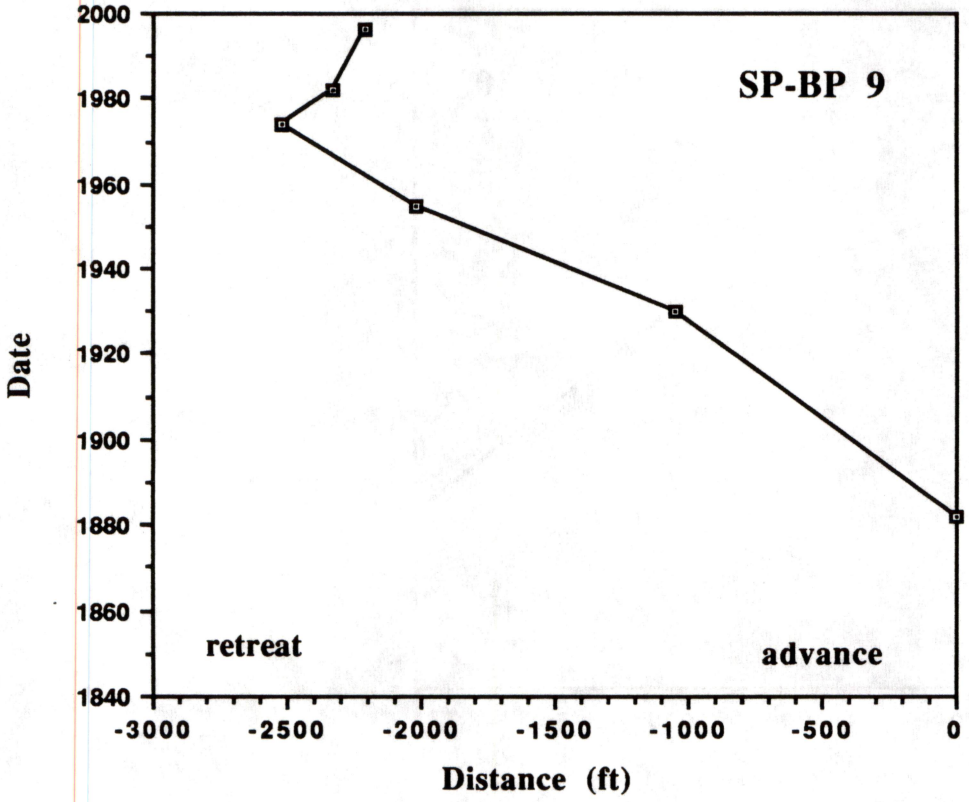
SP-BP 9
Date
2000
1980
1960
1940
1920
1900
1880
1860
1840
retreat
advance
-3000
-2500
-2000
-1500
-1000
-500
0
Distance (ft)

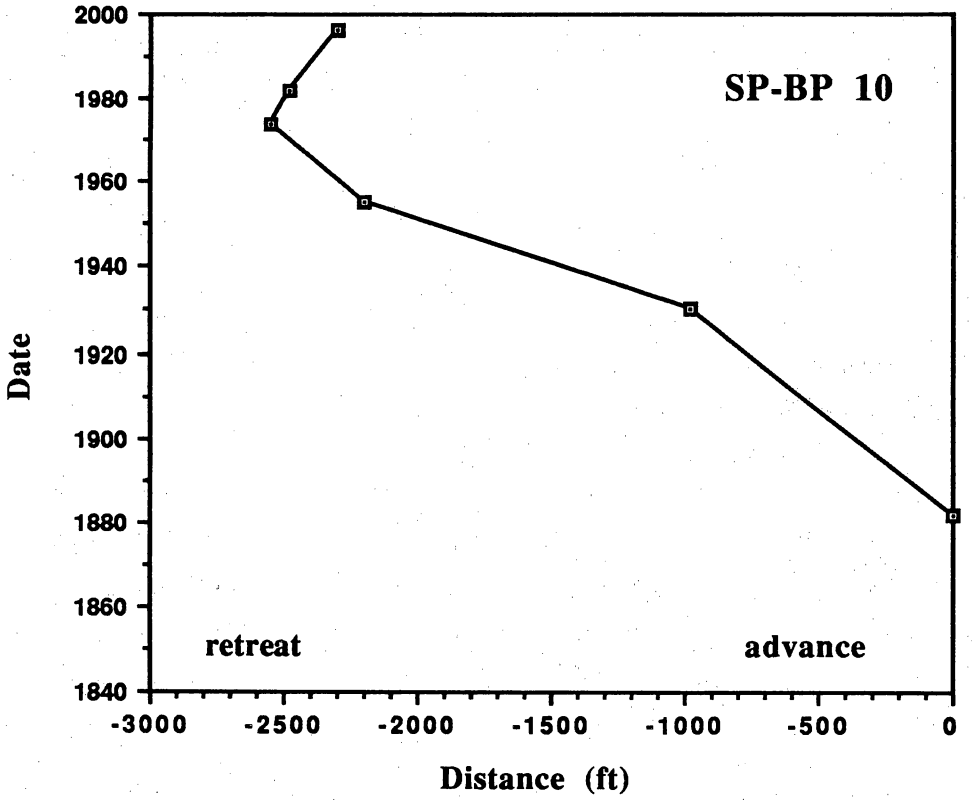
SP-BP 10
Date
2000
1980
1960
1940
1920
1900
1880
1860
1840
retreat
advance
-3000
-2500
-2000
-1500
-1000
-500
0
Distance (ft)

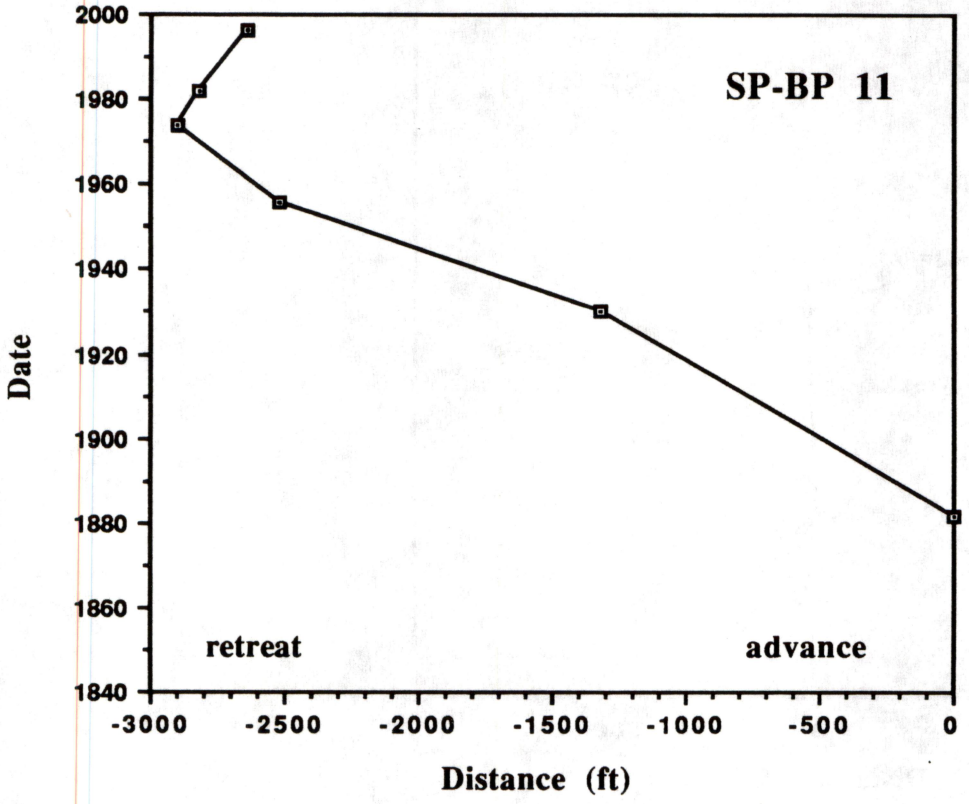
SP-BP 11
Date
2000
1980
1960
1940
1920
1900
1880
1860
1840
retreat
advance
-3000
-2500
-2000
-1500
-1000
-500
0
Distance (ft)

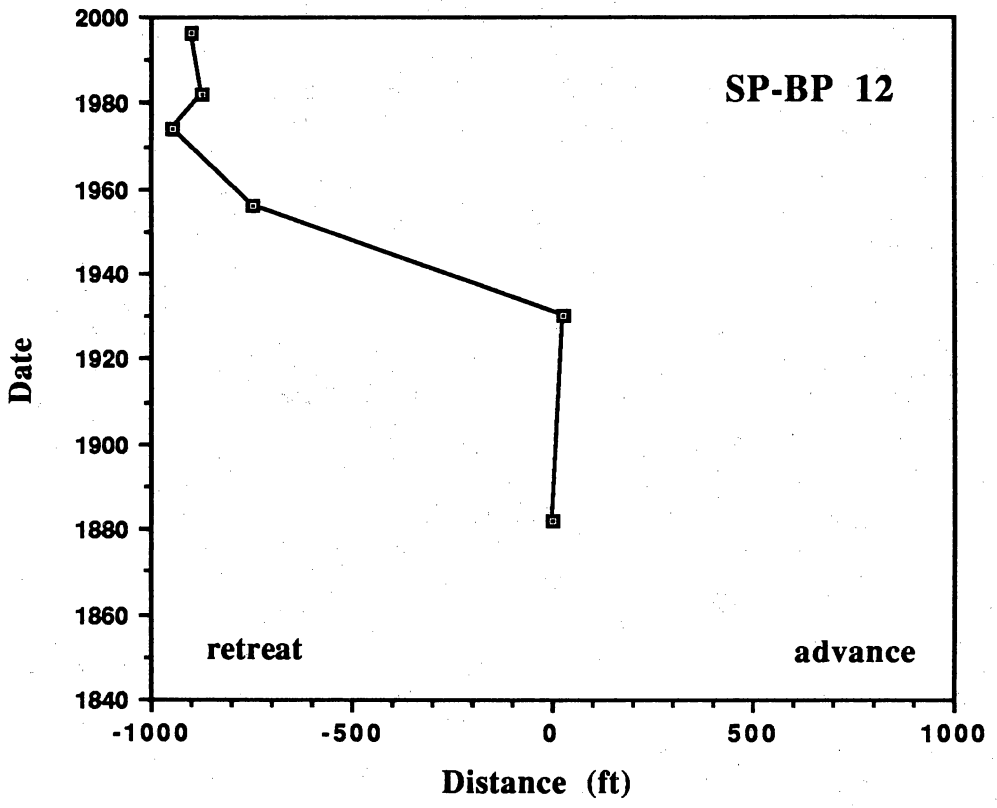
SP-BP 12
Date
2000
1980
1960
1940
1920
1900
1880
1860
1840
retreat
advance
-1000
-500
0
500
1000
Distance (ft)

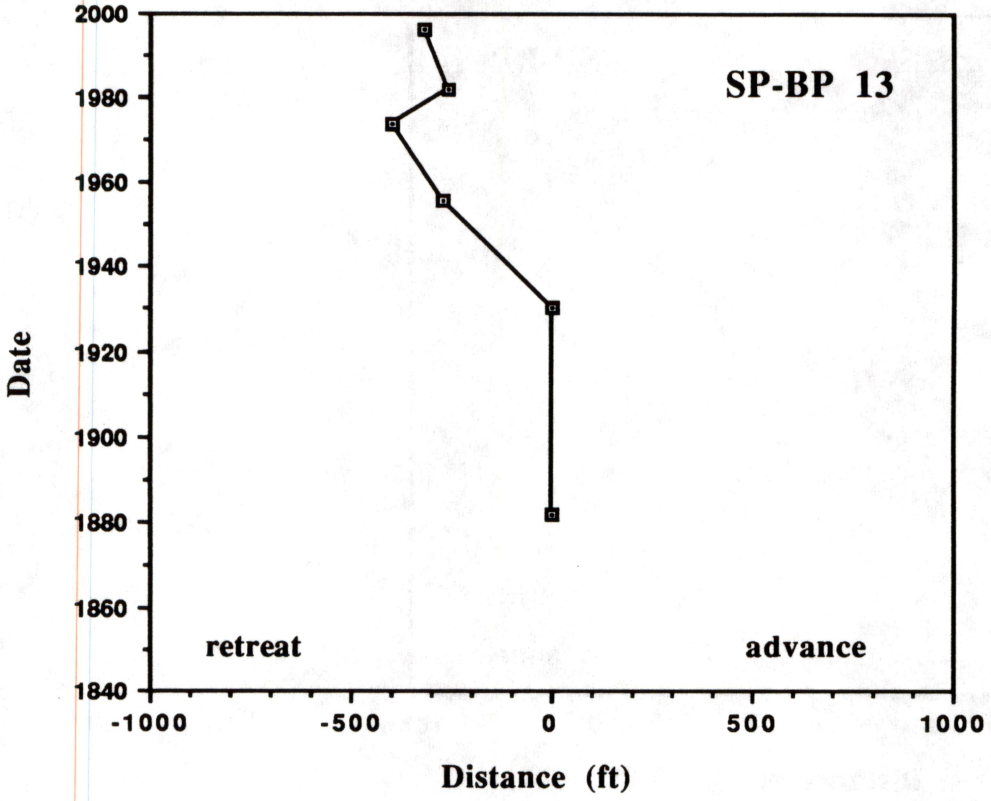
SP-BP 13
Date
2000
1980
1960
1940
1920
1900
1880
1860
1840
retreat
advance
-1000
-500
0
500
1000
Distance (ft)

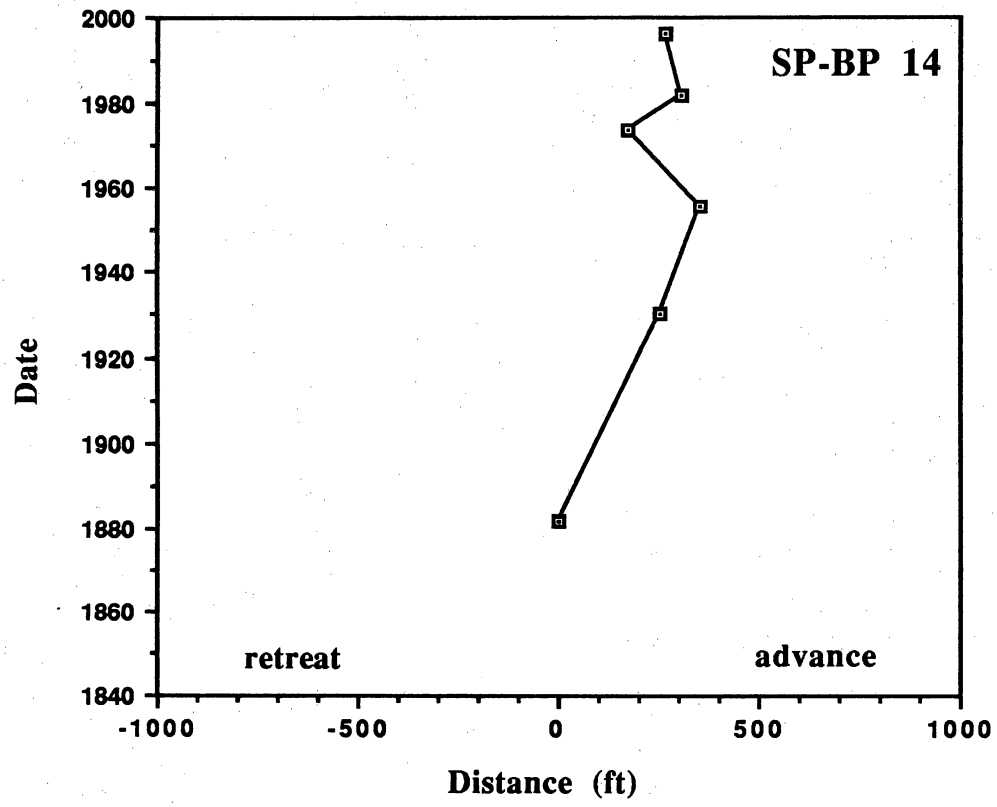
SP-BP 14
Date
2000
1980
1960
1940
1920
1900
1880
1860
1840
retreat
advance
-1000
-500
0
500
1000
Distance (ft)

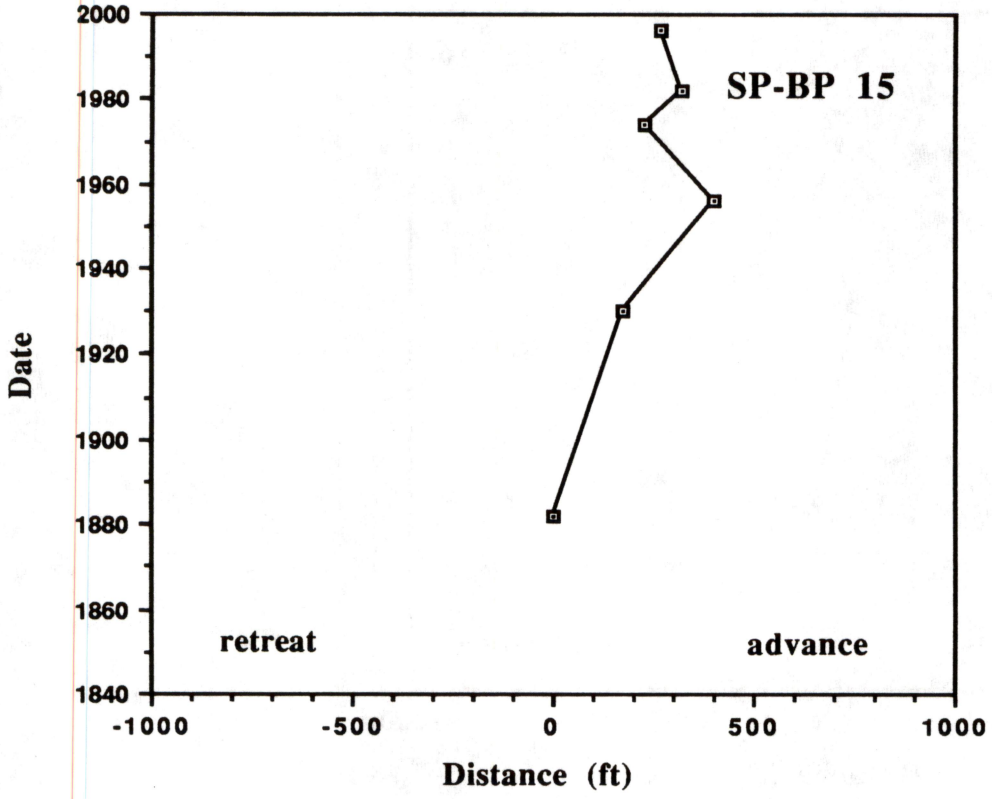
SP-BP 15
Date
2000
1980
1960
1940
1920
1900
1880
1860
1840
retreat
advance
-1000
-500
0
500
1000
Distance (ft)

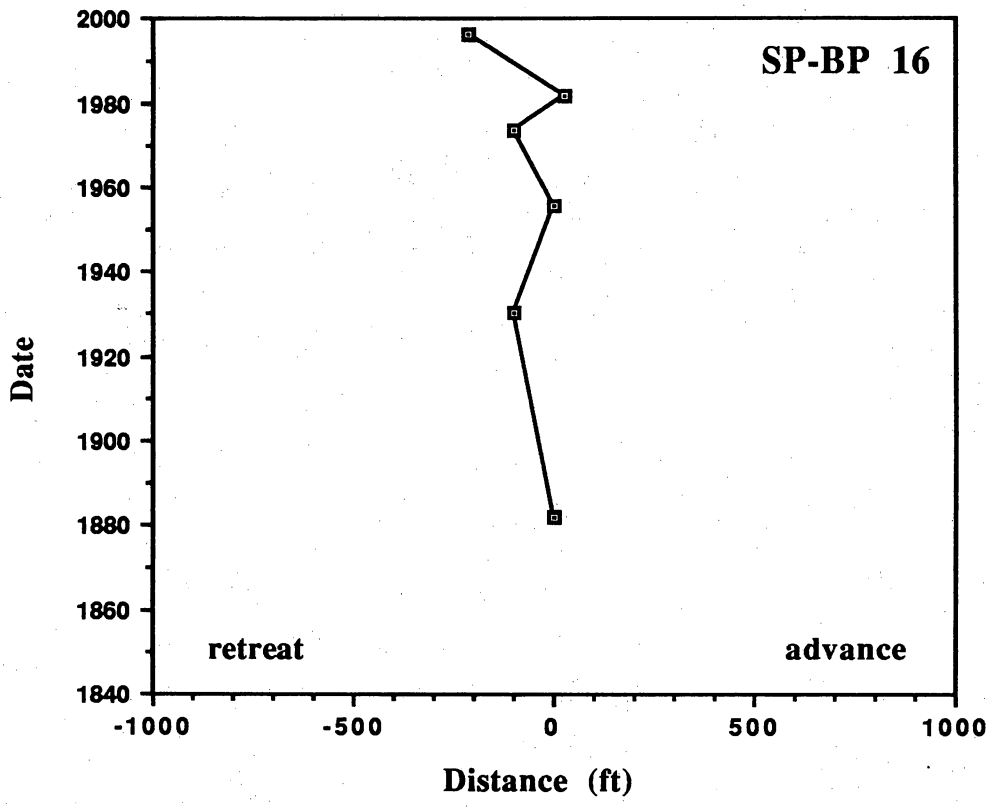
SP-BP 16
Date
2000
1980
1960
1940
1920
1900
1880
1860
1840
retreat
advance
-1000
-500
0
500
1000
Distance (ft)

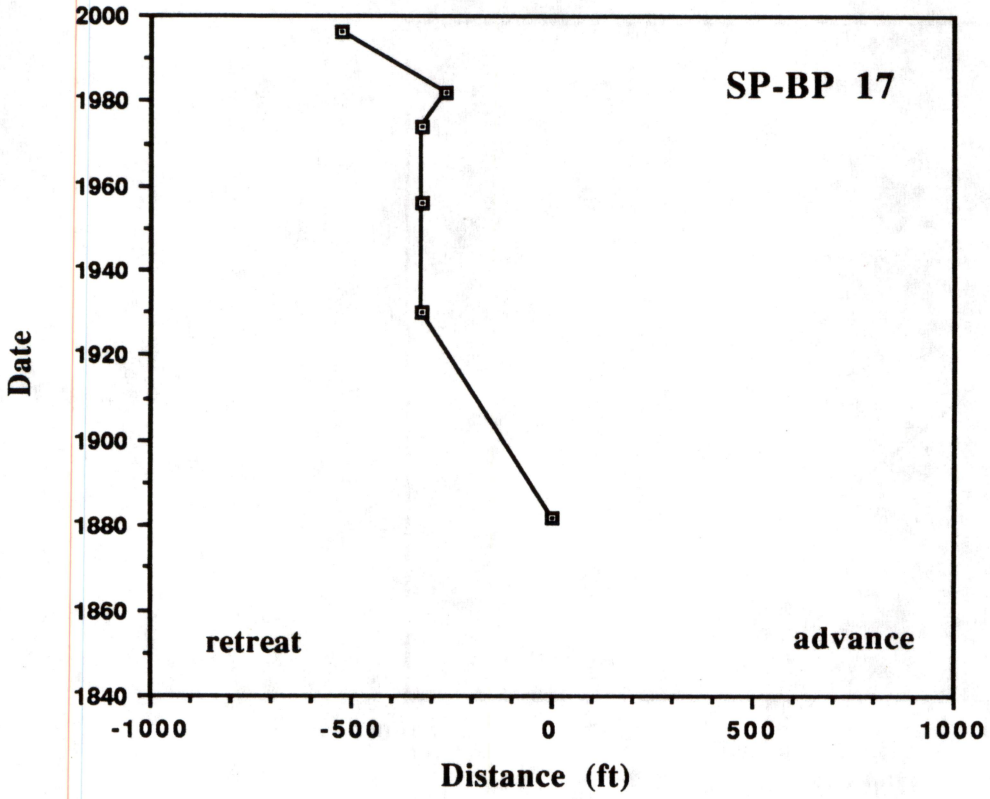
SP-BP 17
Date
2000
1980
1960
1940
1920
1900
1880
1860
1840
retreat
advance
-1000
-500
0
500
1000
Distance (ft)

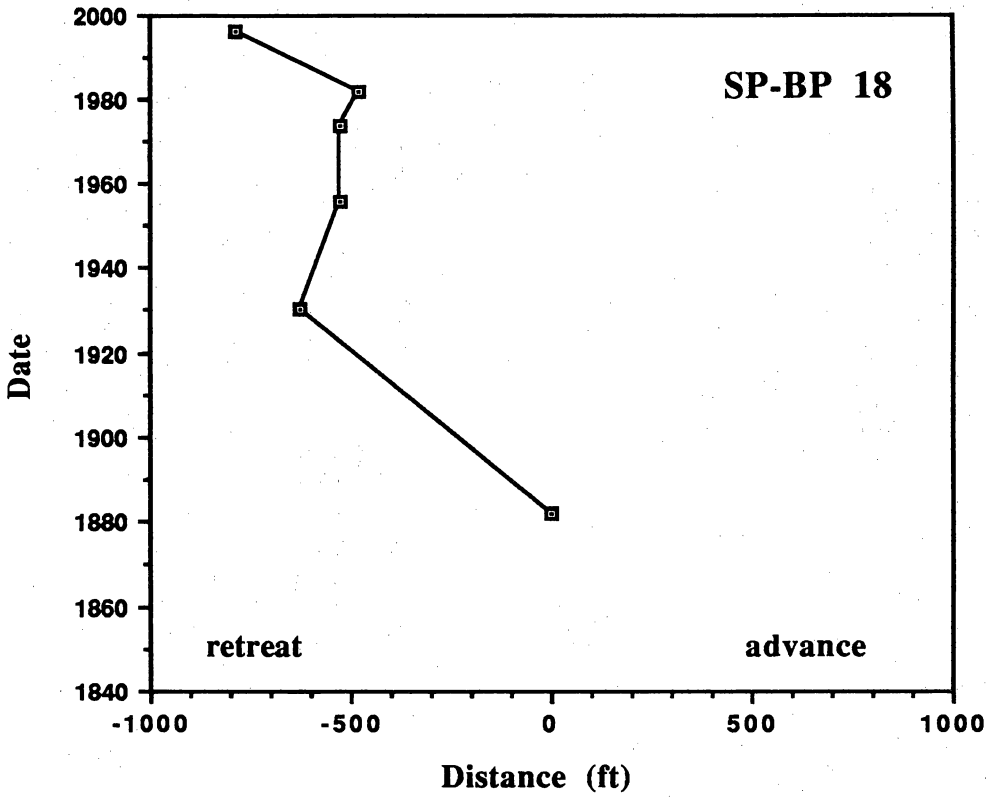
SP-BP 18
Date
2000
1980
1960
1940
1920
1900
1880
1860
1840
retreat
advance
-1000
-500
0
500
1000
Distance (ft)

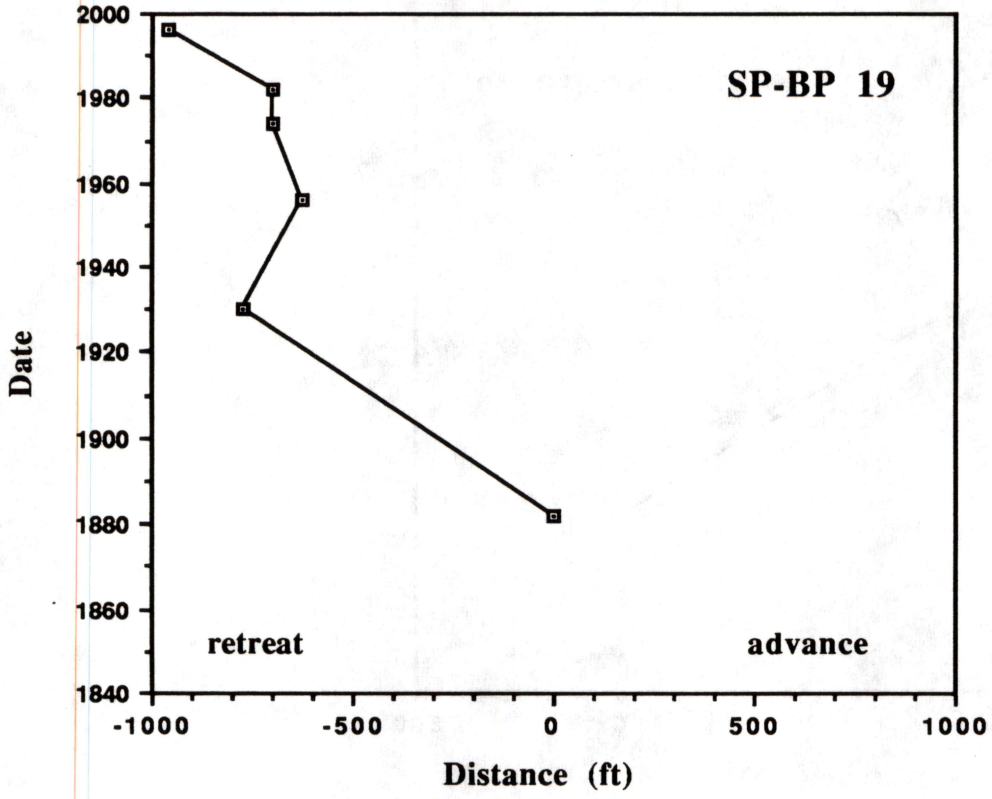
SP-BP 19
Date
2000
1980
1960
1940
1920
1900
1880
1860
1840
retreat
advance
-1000
-500
0
500
1000
Distance (ft)

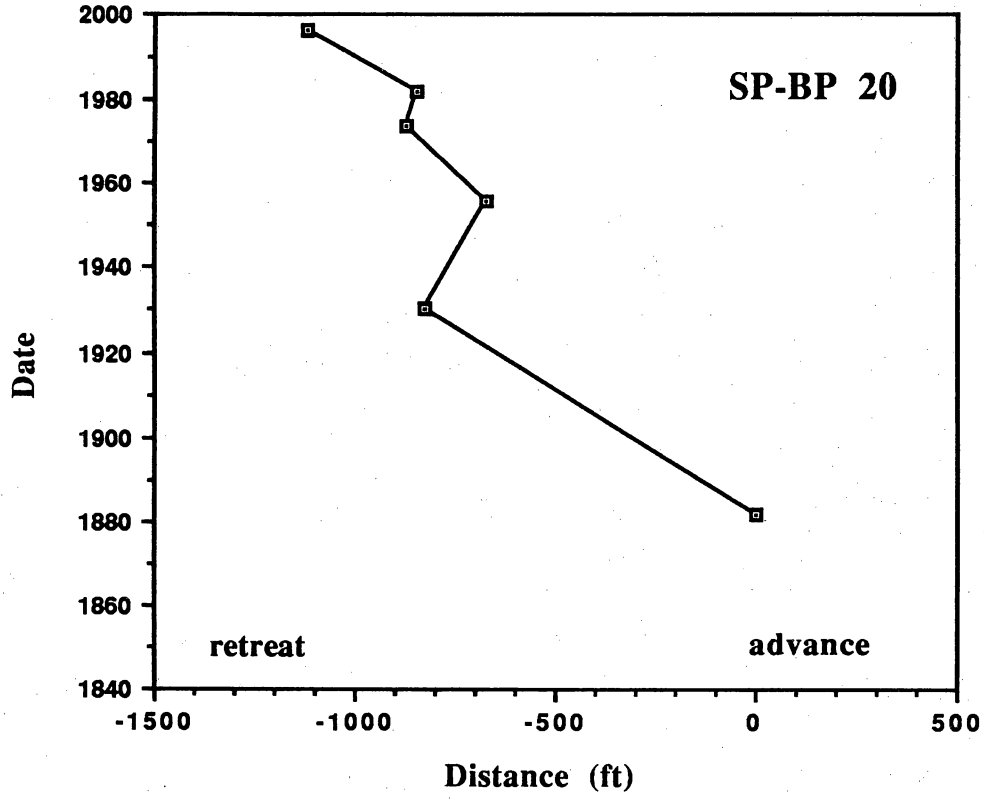
SP-BP 20
Date
2000
1980
1960
1940
1920
1900
1880
1860
1840
retreat
advance
-1500
-1000
-500
0
500
Distance (ft)

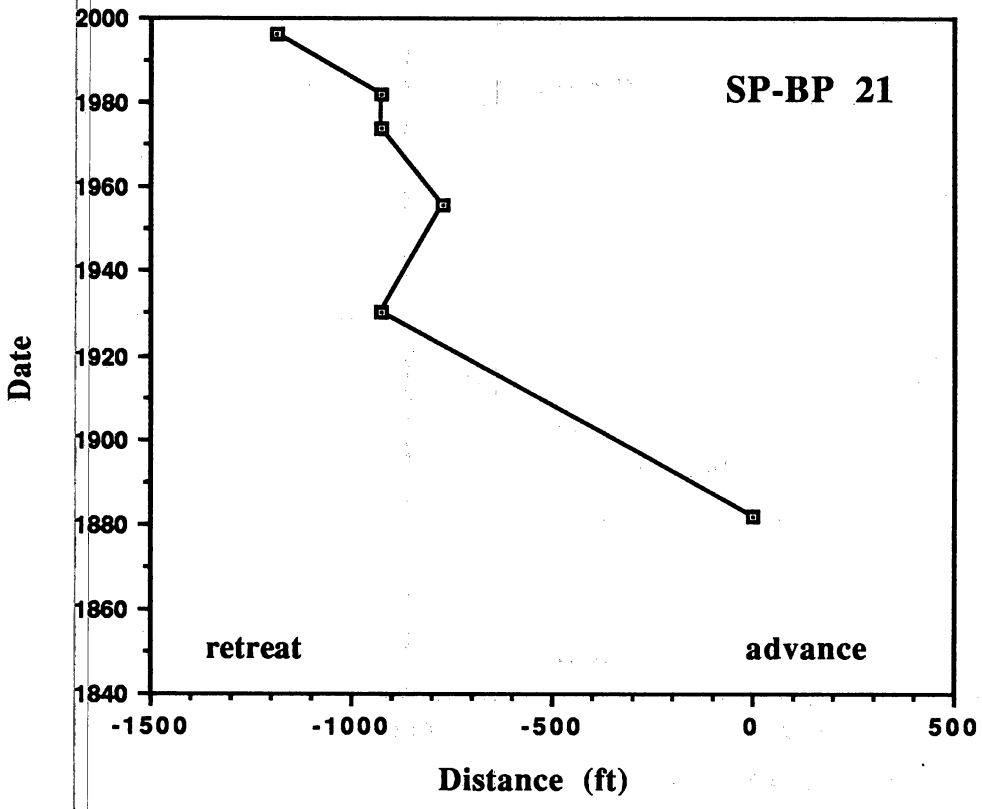
SP-BP 21
Date
2000
1980
1960
1940
1920
1900
1880
1860
1840
retreat
advance
-1500
-1000
-500
0
500
Distance (ft)

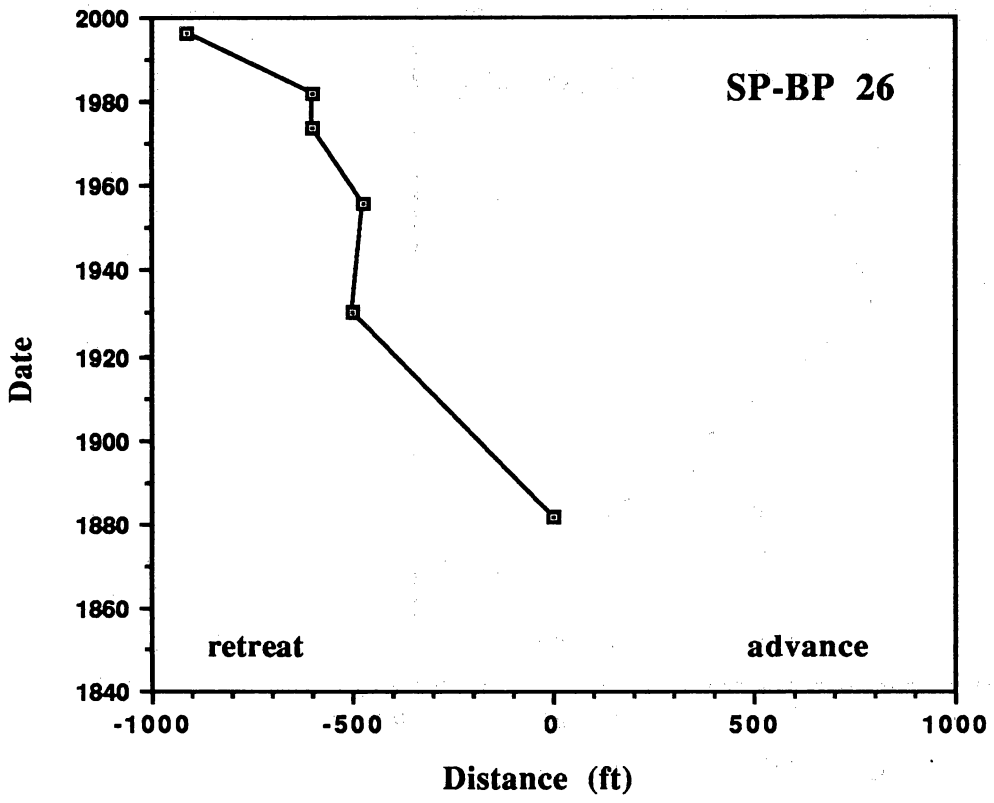
SP-BP 26
Date
2000
1980
1960
1940
1920
1900
1880
1860
1840
retreat
advance
-1000
-500
0
500
1000
Distance (ft)

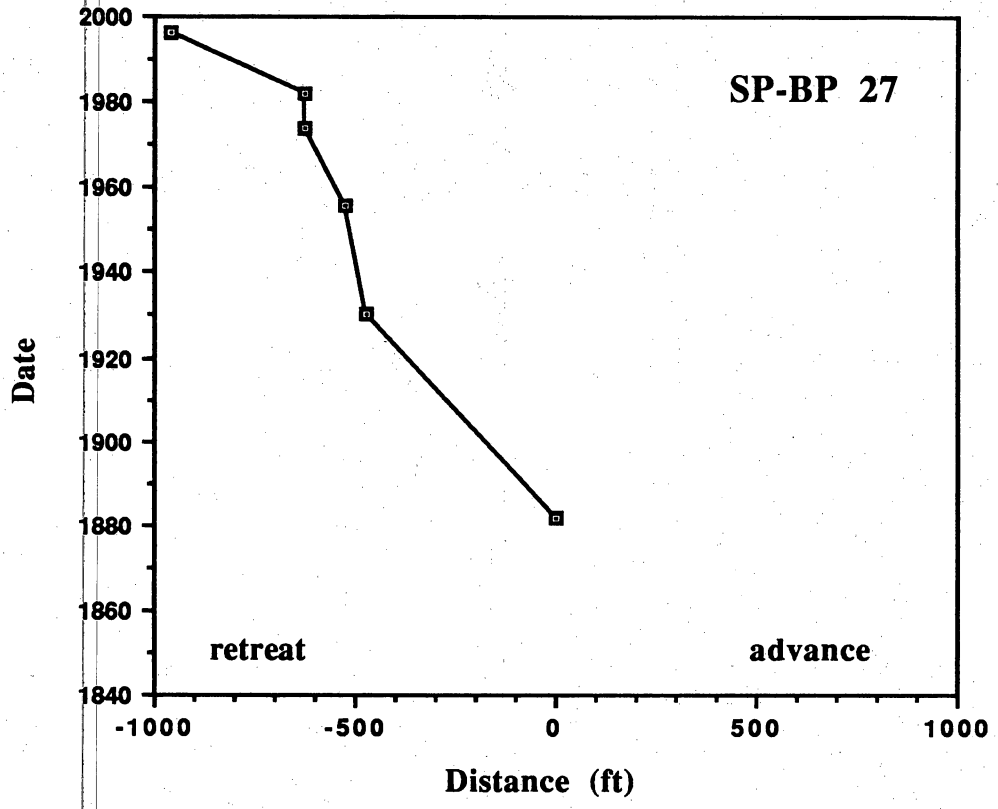
SP-BP 27
Date
2000
1980
1960
1940
1920
1900
1880
1860
1840
retreat
advance
-1000
-500
0
500
1000
Distance (ft)

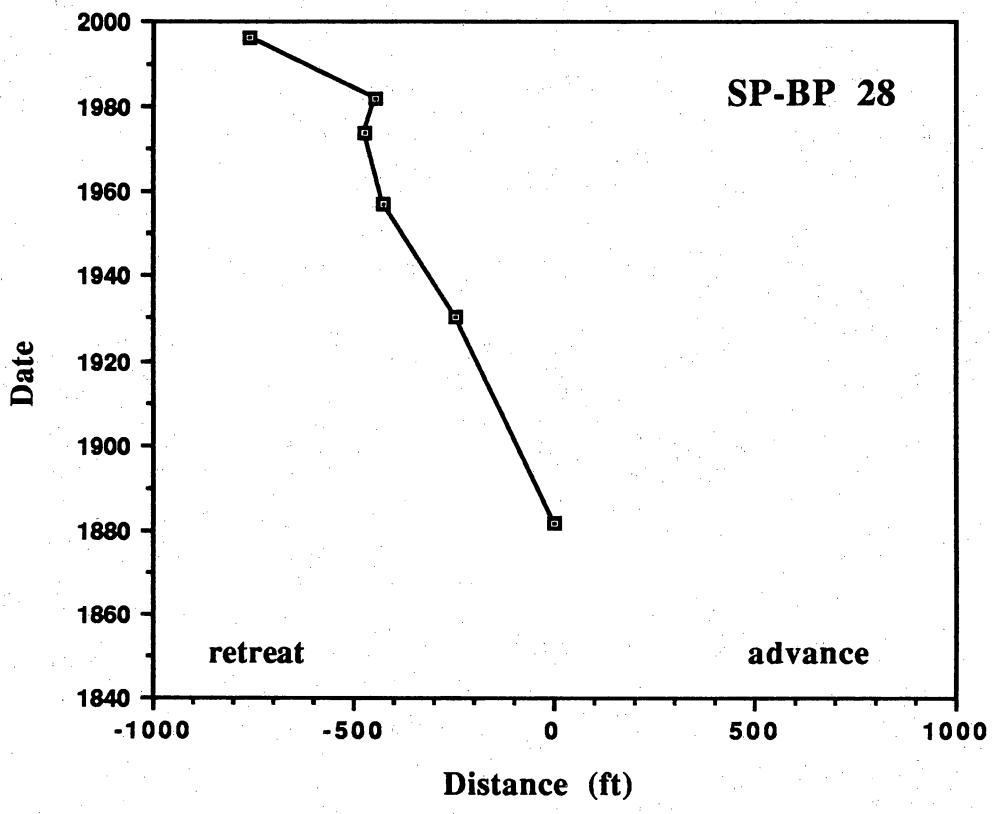
SP-BP 28
Date
2000
1980
1960
1940
1920
1900
1880
1860
1840
retreat
advance
-1000
-500
0
500
1000
Distance (ft)

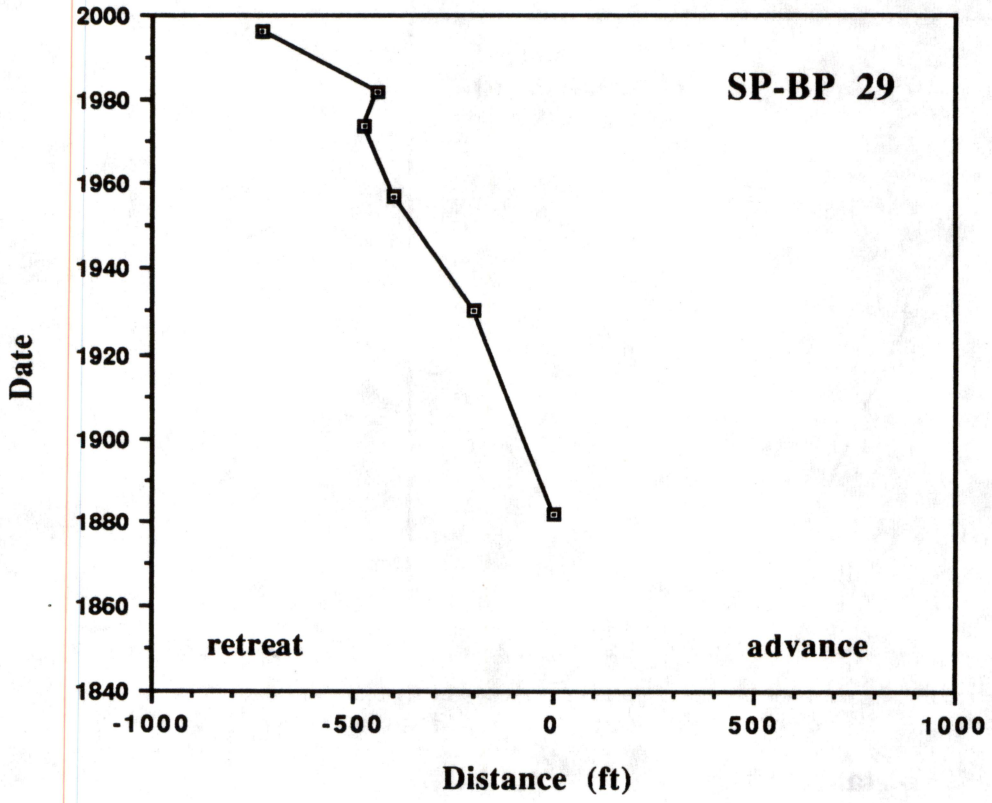
SP-BP 29
Date
2000
1980
1960
1940
1920
1900
1880
1860
1840
retreat
advance
-1000
-500
0
500
1000
Distance (ft)

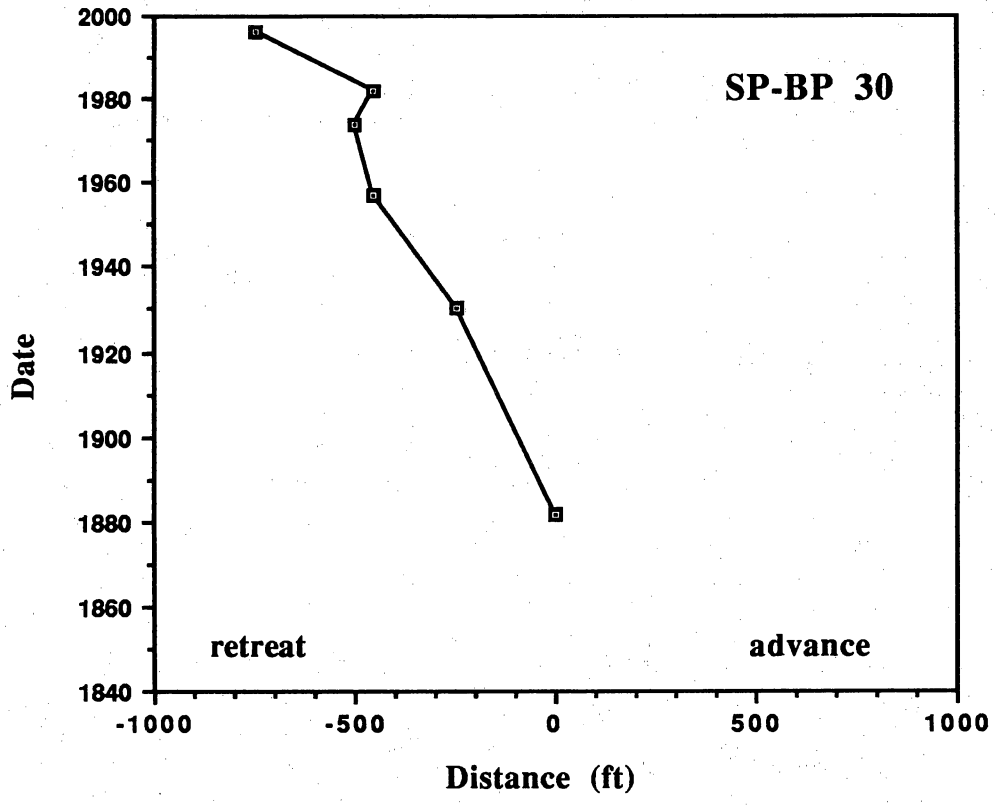
SP-BP 30
Date
2000
1980
1960
1940
1920
1900
1880
1860
1840
retreat
advance
-1000
-500
0
500
1000
Distance (ft)

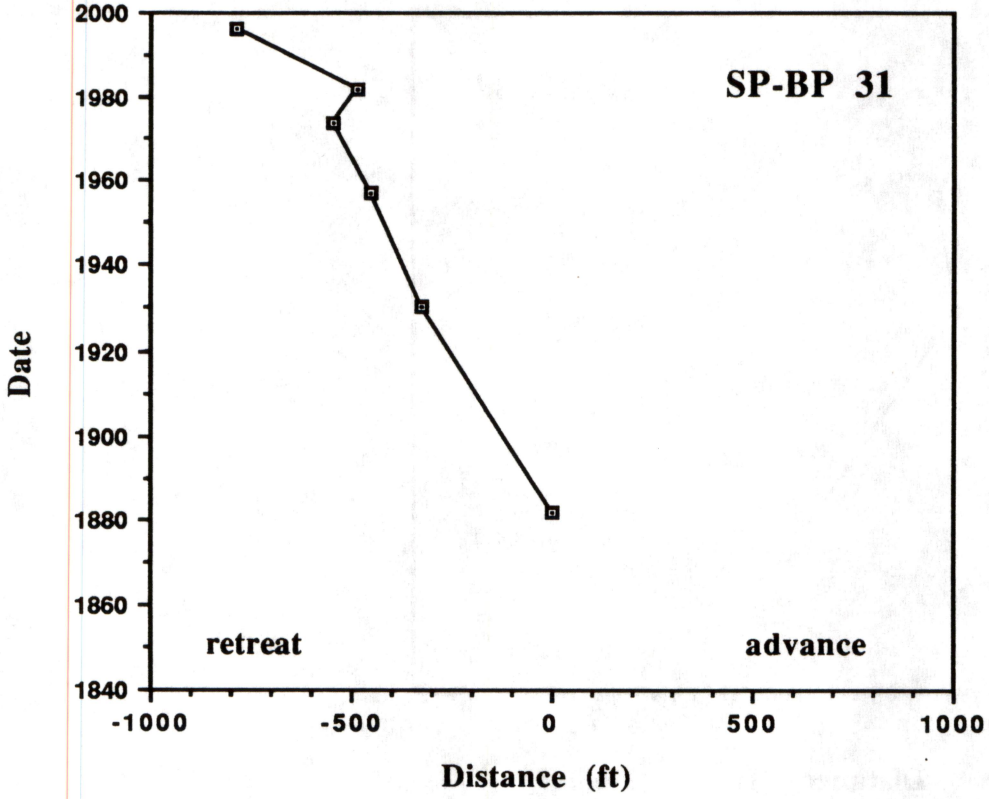
SP-BP 31
Date
2000
1980
1960
1940
1920
1900
1880
1860
1840
retreat
advance
-1000
-500
0
500
1000
Distance (ft)

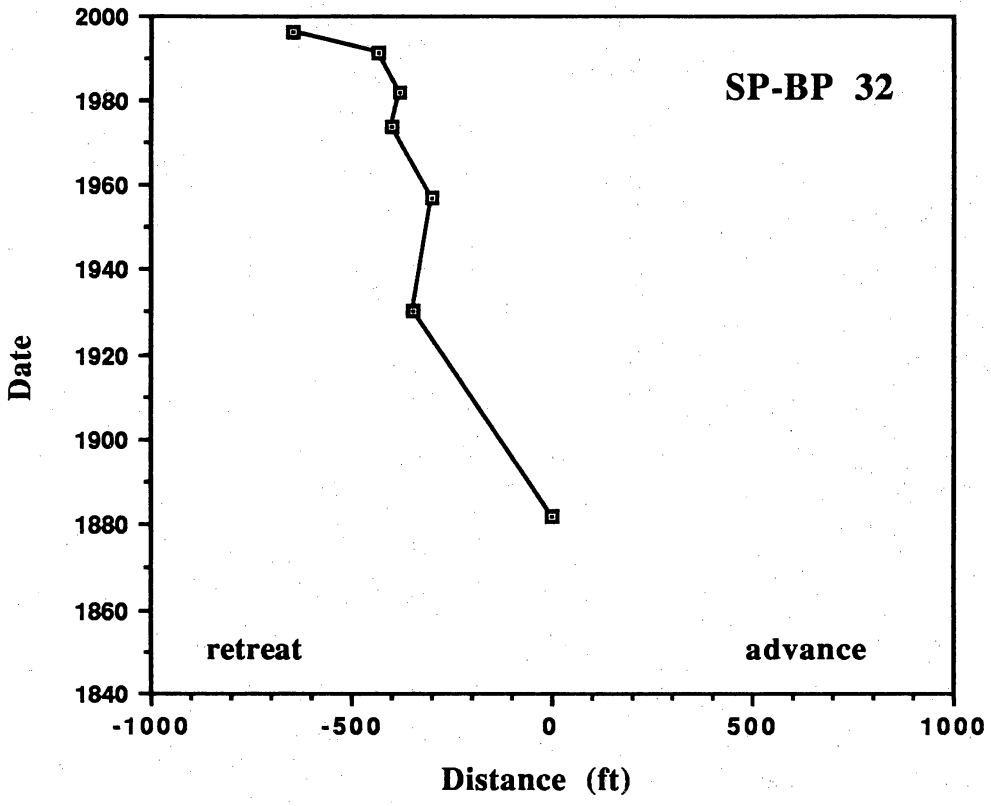
SP-BP 32
Date
2000
1980
1960
1940
1920
1900
1880
1860
1840
retreat
advance
-1000
-500
0
500
1000
Distance (ft)

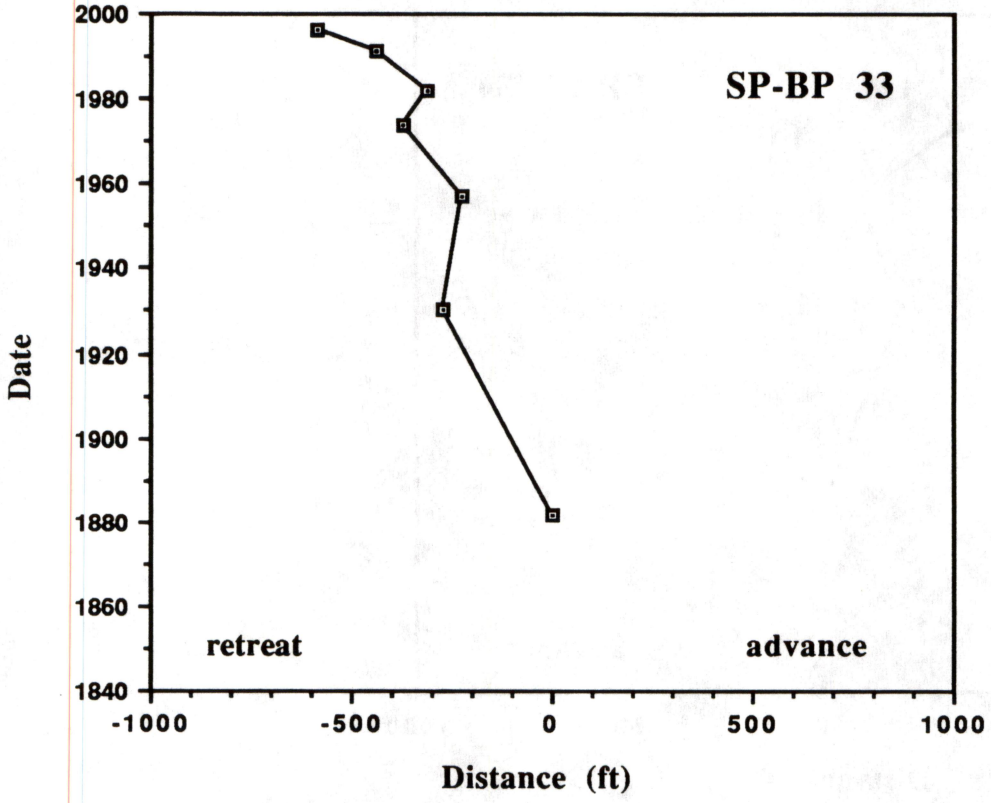
SP-BP 33
Date
2000
1980
1960
1940
1920
1900
1880
1860
1840
retreat
advance
-1000
-500
0
500
1000
Distance (ft)

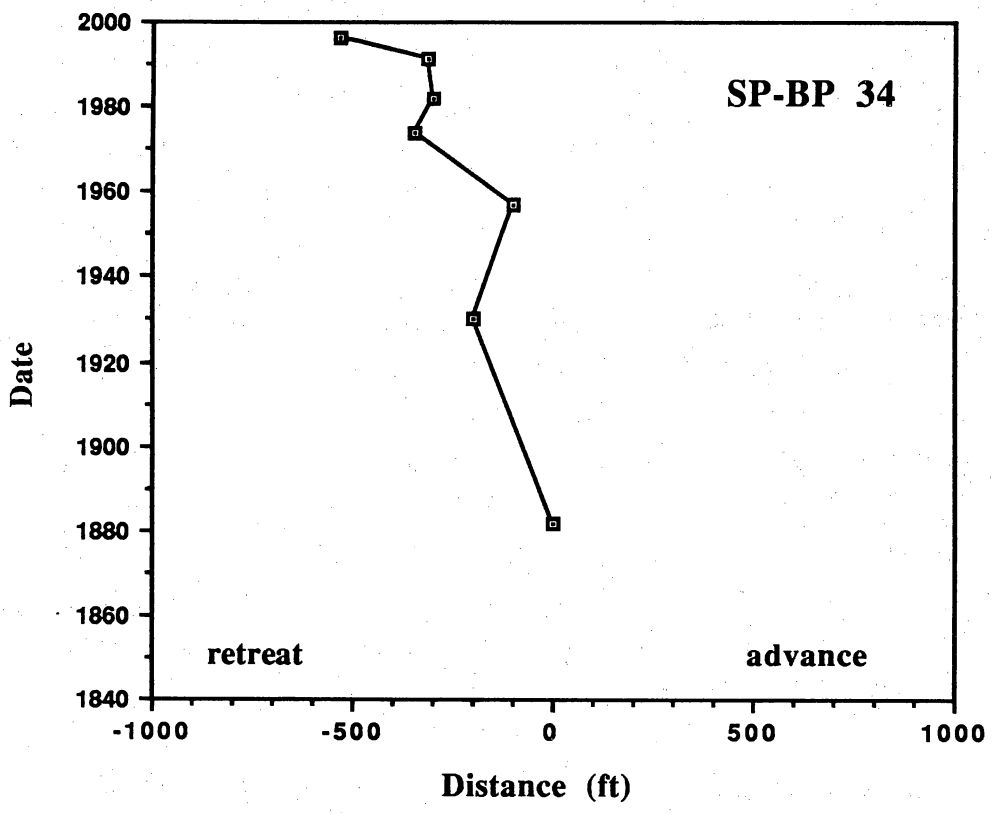
SP-BP 34
Date
2000
1980
1960
1940
1920
1900
1880
1860
1840
retreat
advance
-1000
-500
0
500
1000
Distance (ft)

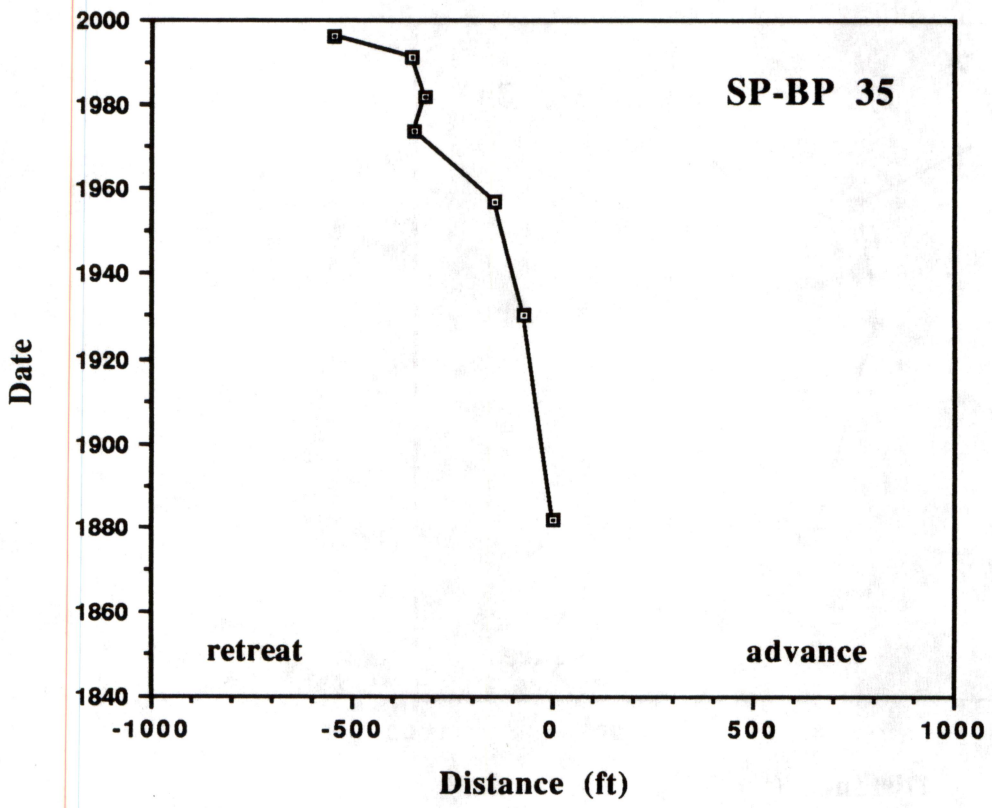
SP-BP 35
Date
2000
1980
1960
1940
1920
1900
1880
1860
1840
retreat
advance
-1000
-500
0
500
1000
Distance (ft)

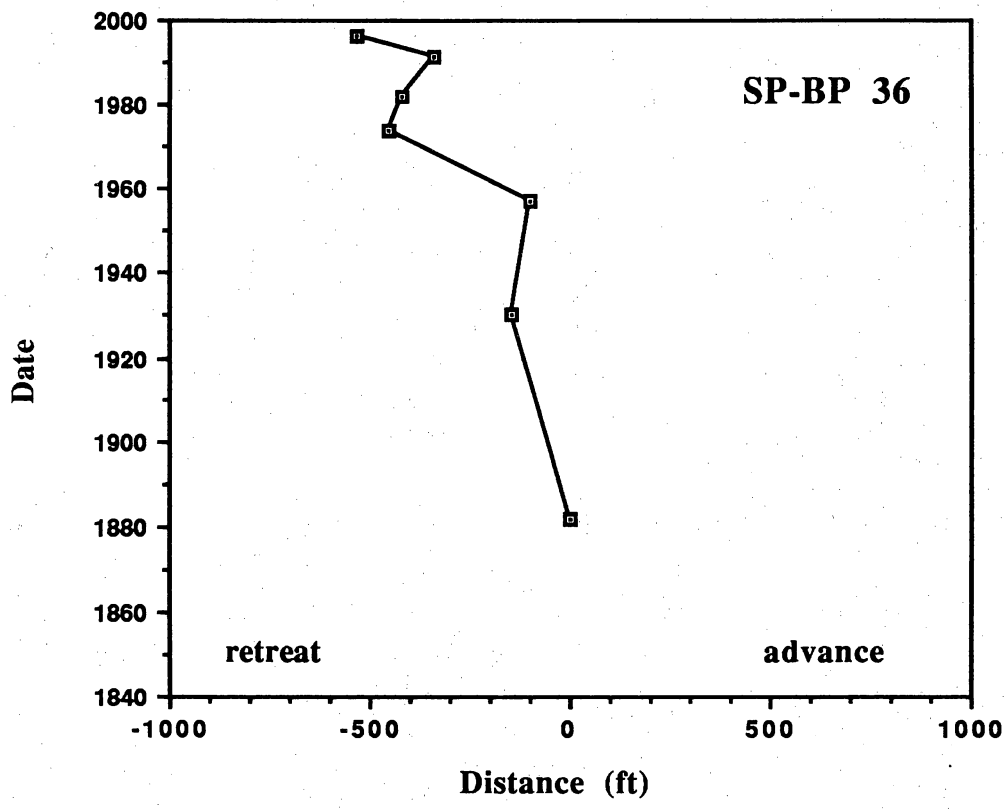
SP-BP 36
Date
2000
1980
1960
1940
1920
1900
1880
1860
1840
retreat
advance
-1000
-500
0
500
1000
Distance (ft)

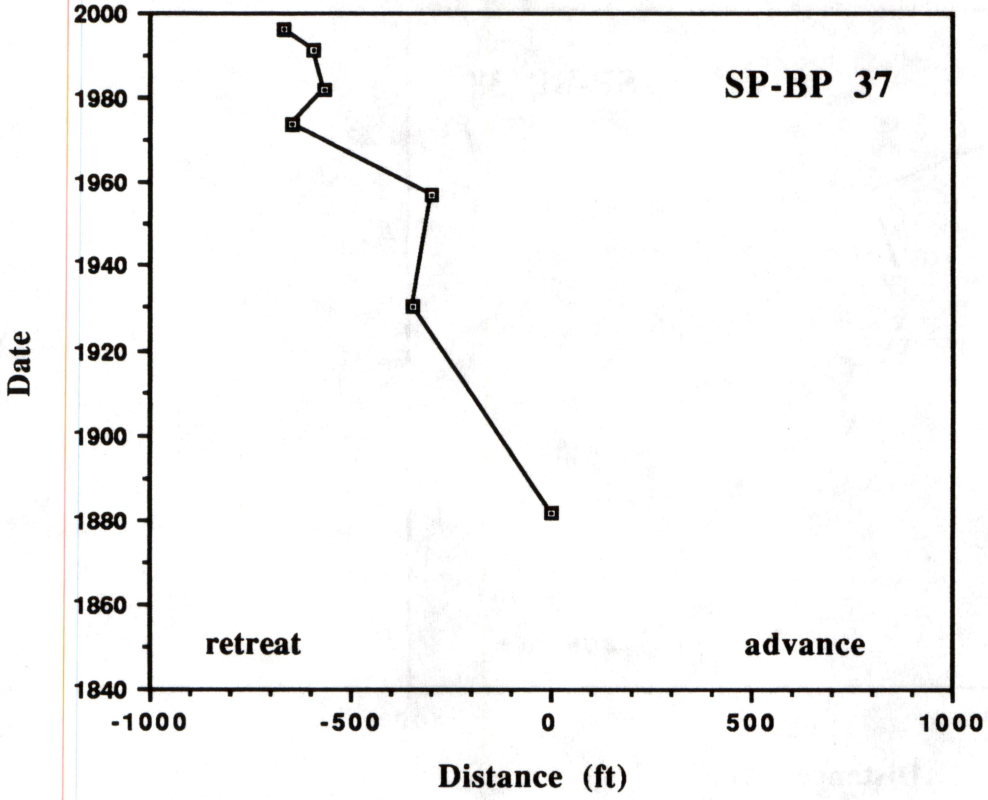
SP-BP 37
Date
2000
1980
1960
1940
1920
1900
1880
1860
1840
retreat
advance
-1000
-500
0
500
1000
Distance (ft)

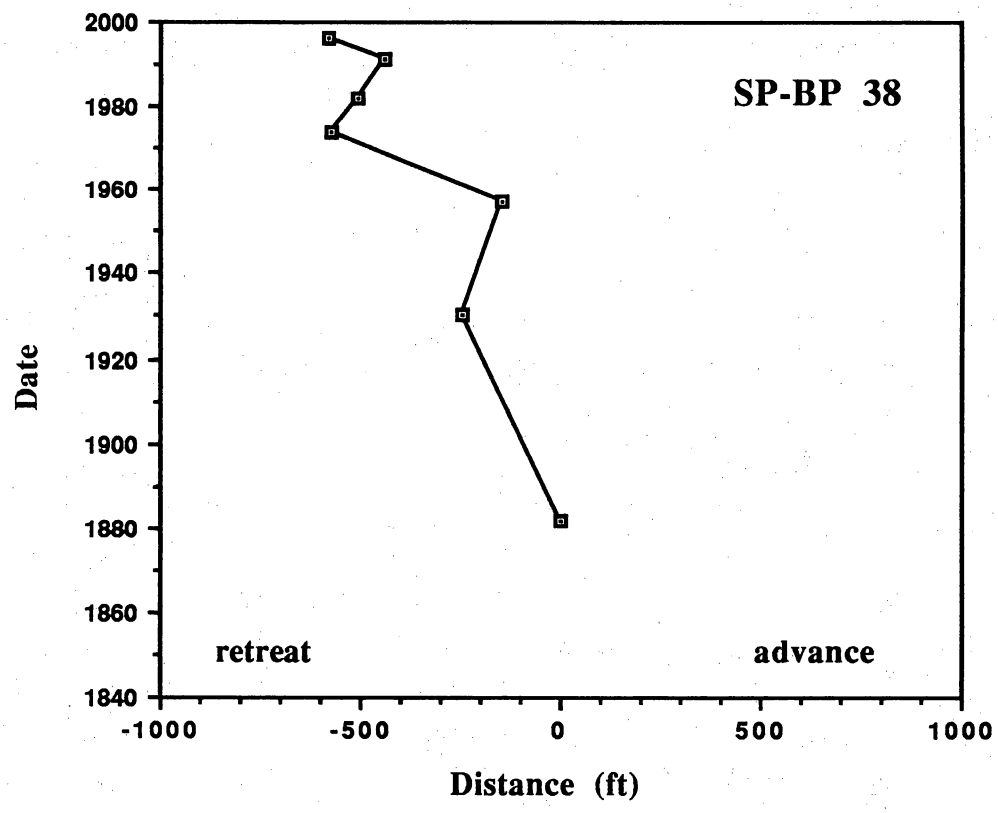
SP-BP 38
Date
2000
1980
1960
1940
1920
1900
1880
1860
1840
retreat
advance
-1000
-500
0
500
1000
Distance (ft)

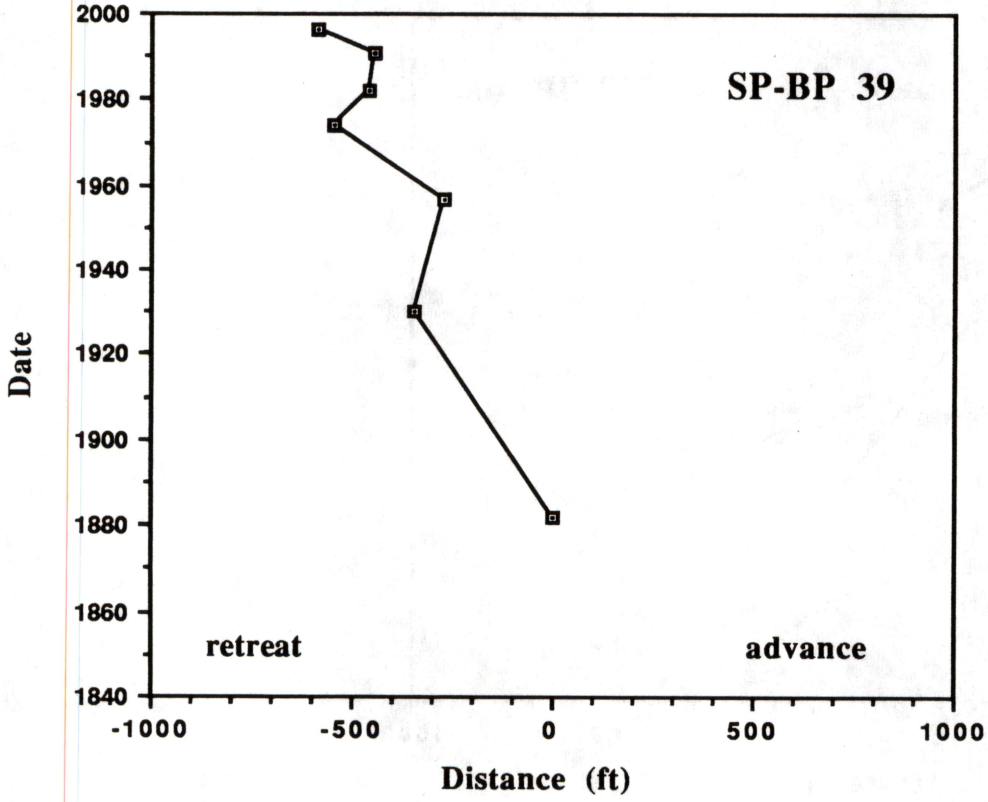
SP-BP 39
Date
2000
1980
1960
1940
1920
1900
1880
1860
1840
retreat
advance
-1000
-500
0
500
1000
Distance (ft)

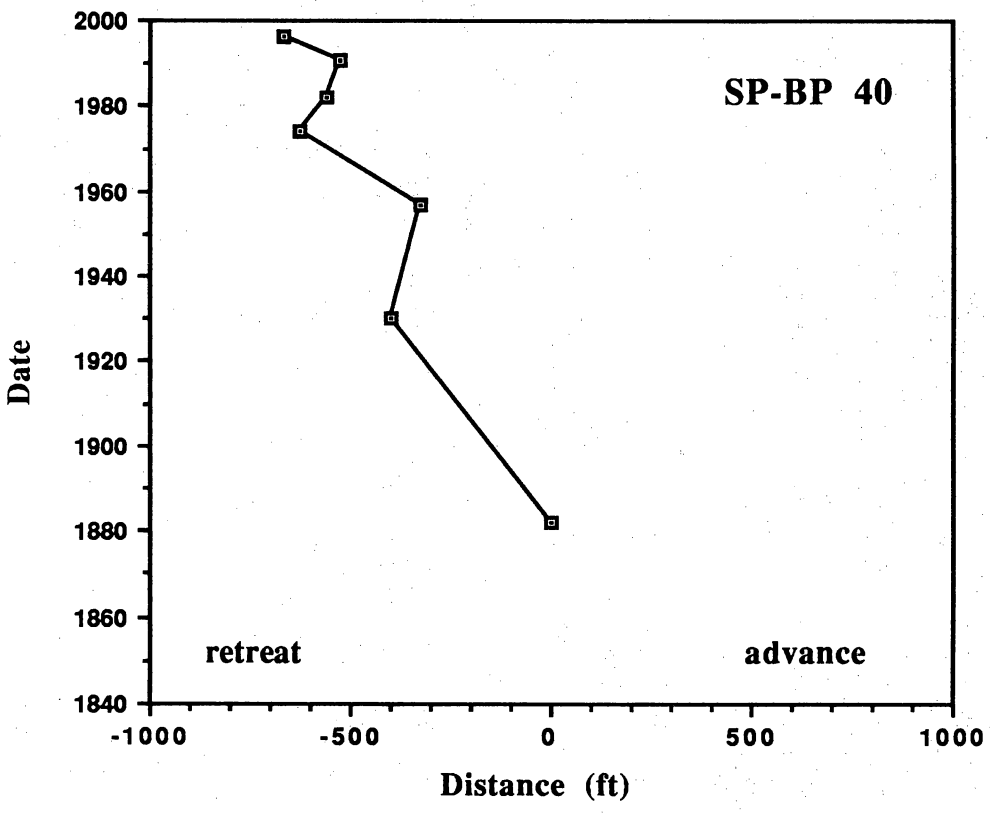
SP-BP 40
Date
2000
1980
1960
1940
1920
1900
1880
1860
1840
retreat
advance
-1000
-500
0
500
1000
Distance (ft)

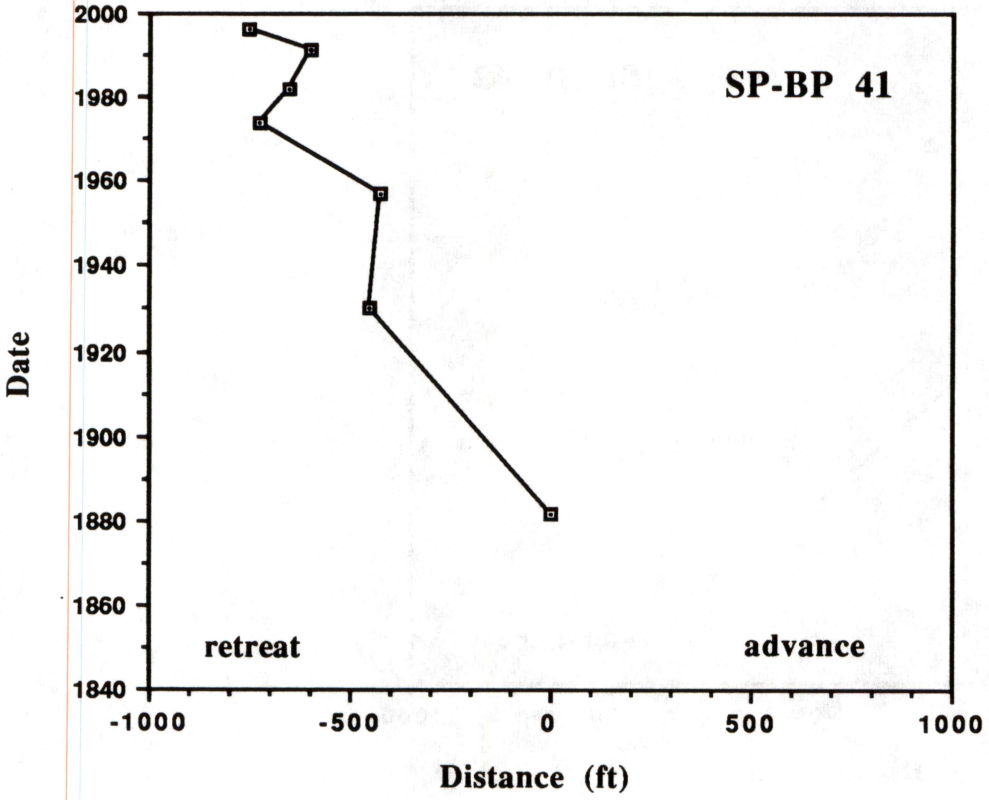
SP-BP 41
Date
2000
1980
1960
1940
1920
1900
1880
1860
1840
retreat
advance
-1000
-500
0
500
1000
Distance (ft)

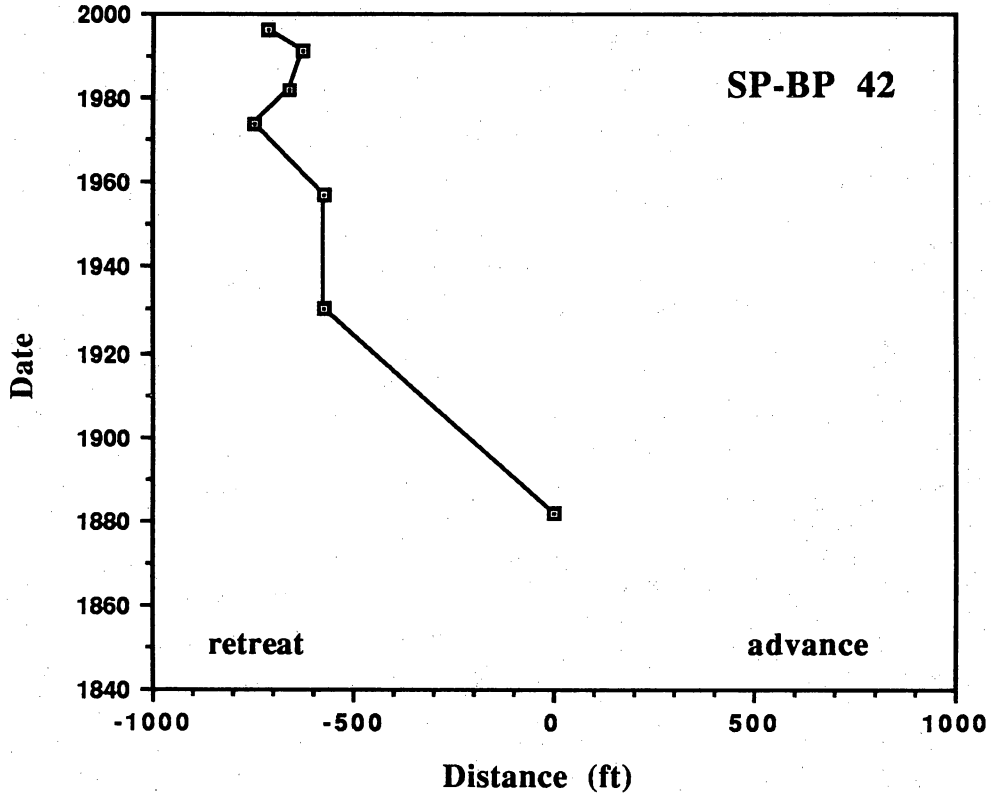
SP-BP 42
Date
2000
1980
1960
1940
1920
1900
1880
1860
1840
retreat
advance
-1000
-500
0
500
1000
Distance (ft)

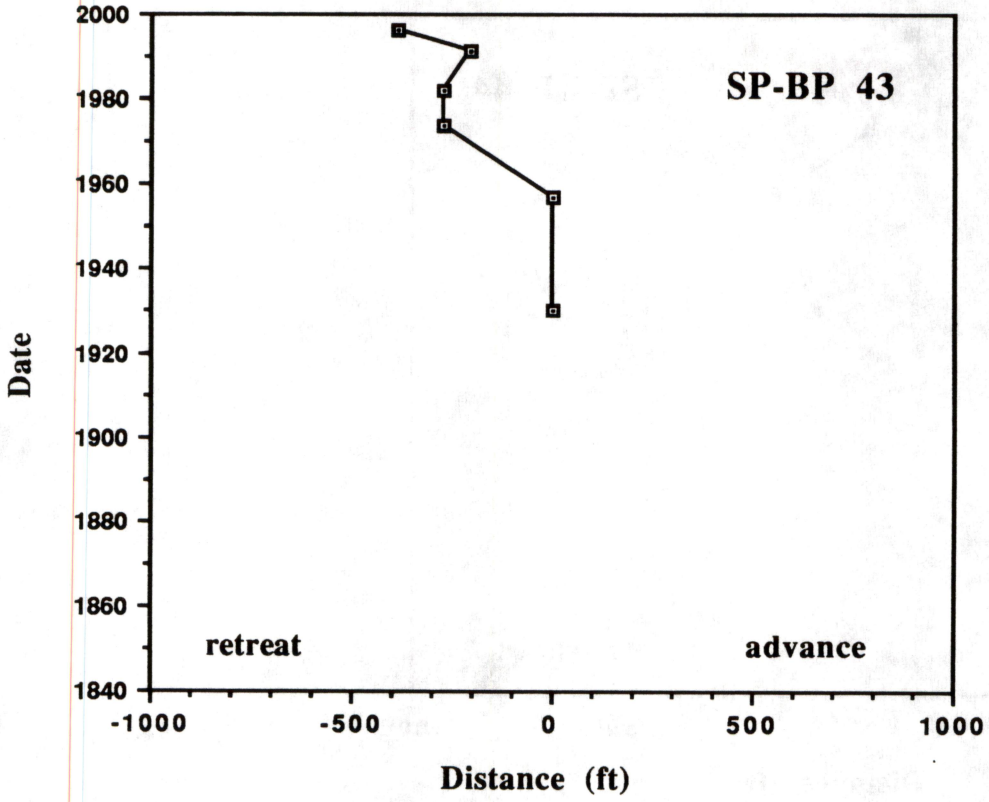
SP-BP 43
Date
2000
1980
1960
1940
1920
1900
1880
1860
1840
retreat
advance
-1000
-500
0
500
1000
Distance (ft)

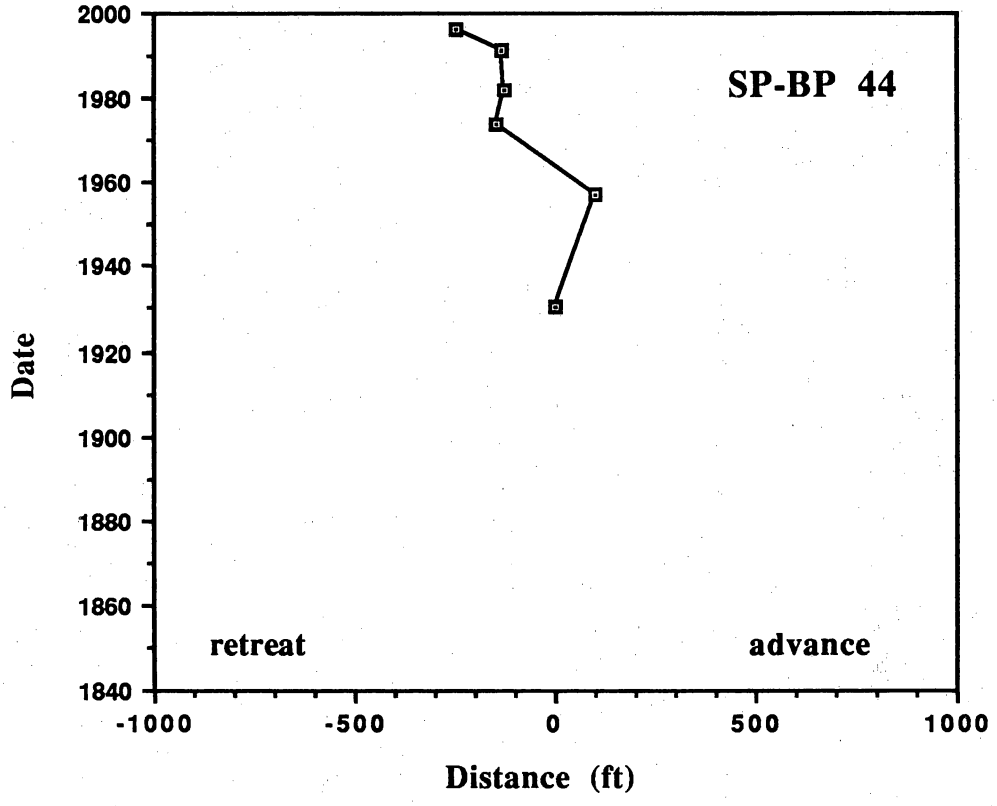
SP-BP 44
Date
2000
1980
1960
1940
1920
1900
1880
1860
1840
retreat
advance
-1000
-500
0
500
1000
Distance (ft)

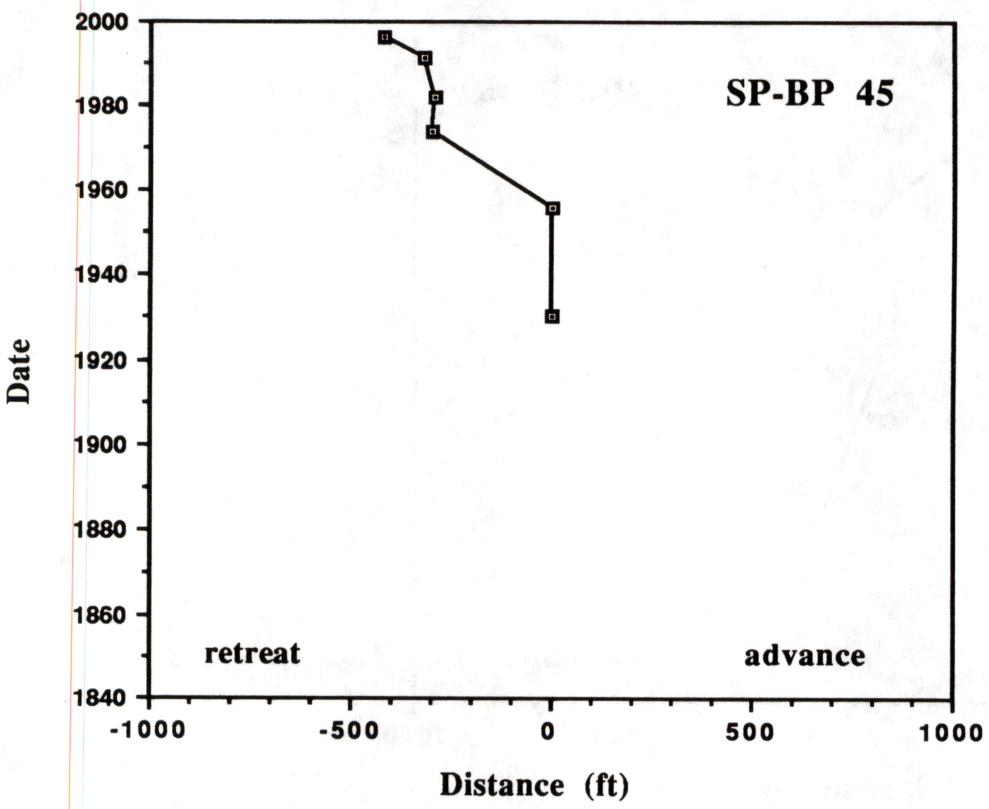
SP-BP 45
Date
2000
1980
1960
1940
1920
1900
1880
1860
1840
retreat
advance
-1000
-500
0
500
1000
Distance (ft)

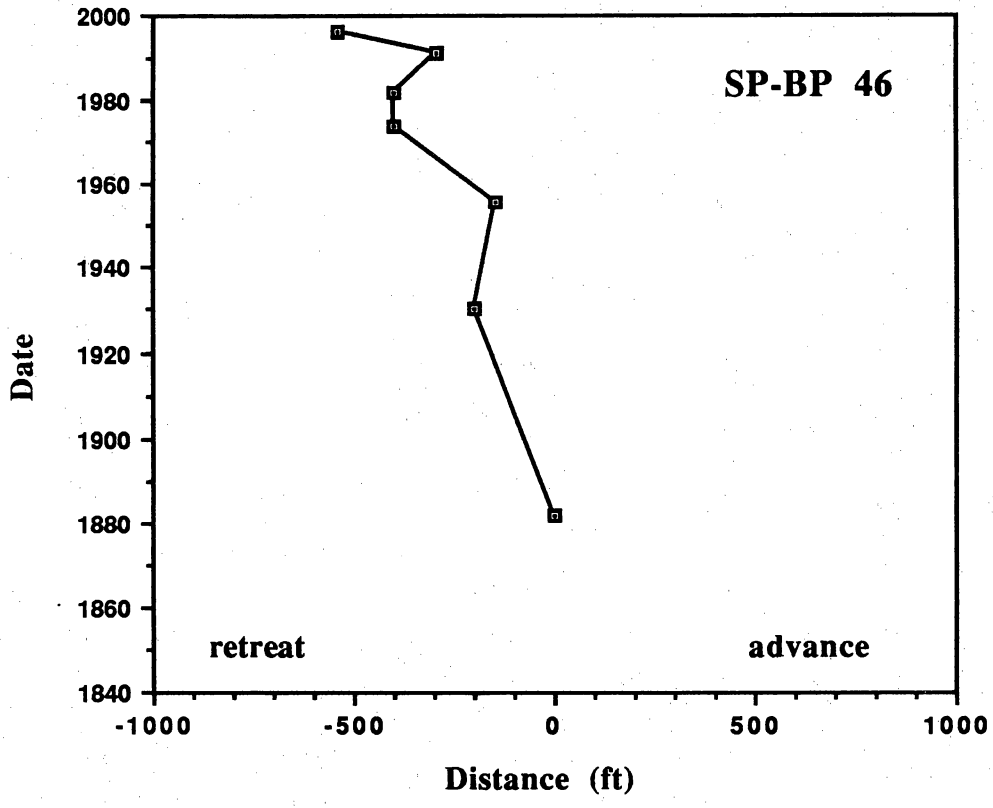
SP-BP 46
Date
2000
1980
1960
1940
1920
1900
1880
1860
1840
retreat
advance
-1000
-500
0
500
1000
Distance (ft)

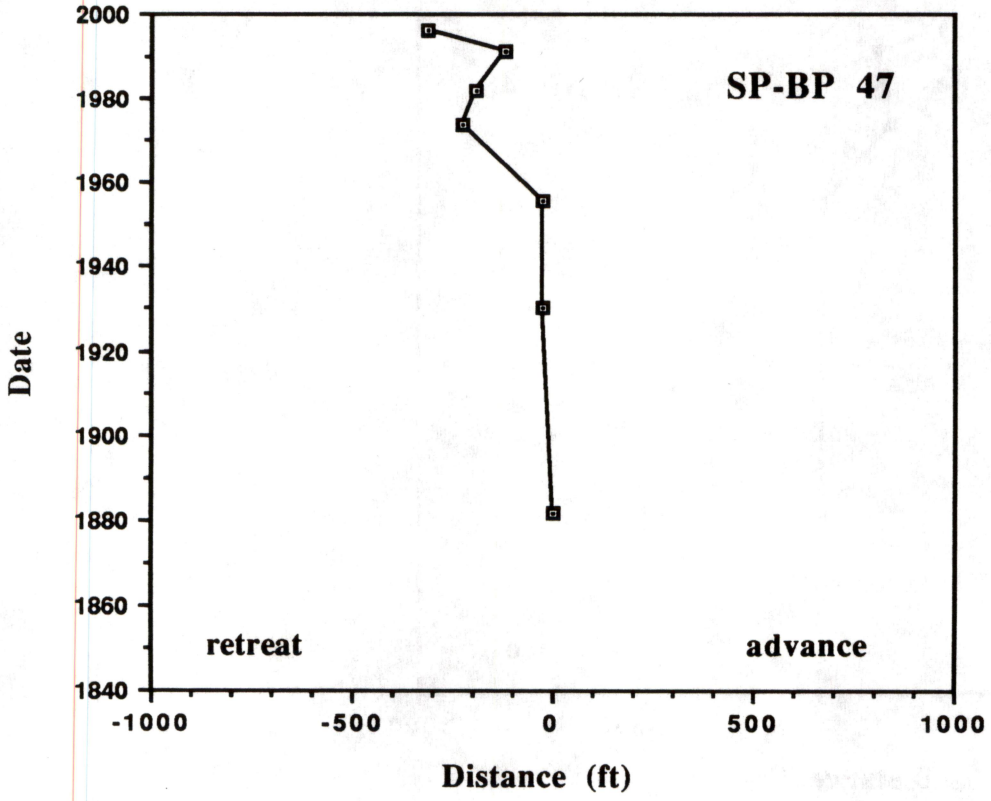
SP-BP 47
Date
2000
1980
1960
1940
1920
1900
1880
1860
1840
retreat
advance
-1000
-500
0
500
1000
Distance (ft)

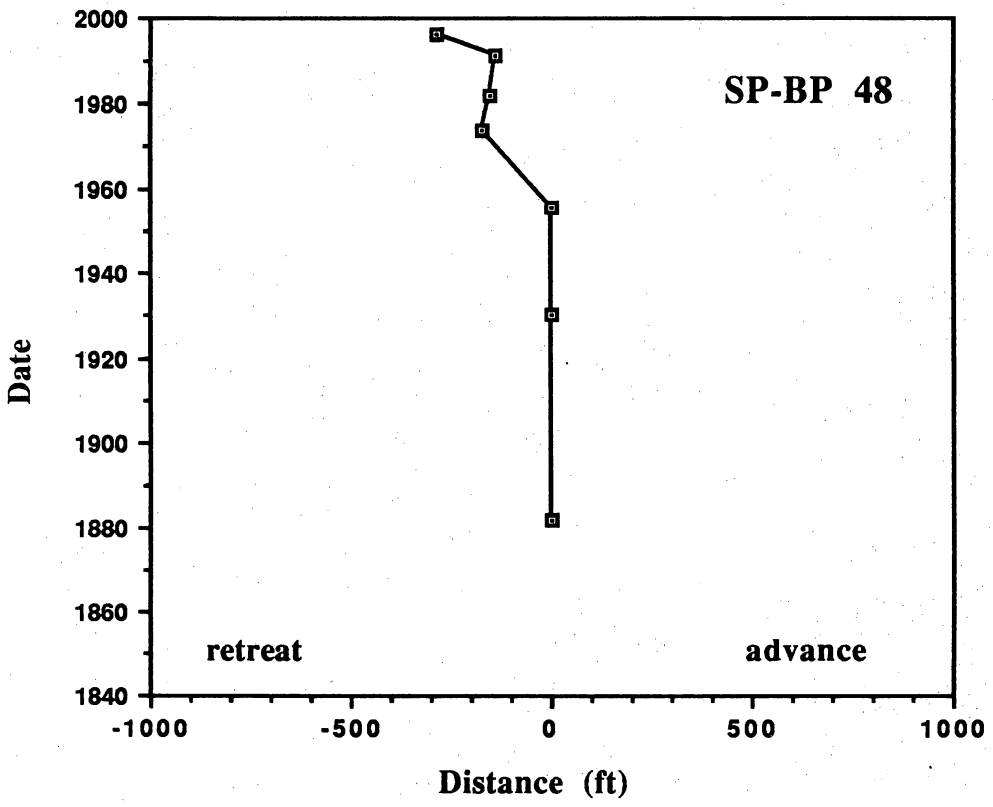
SP-BP 48
Date
2000
1980
1960
1940
1920
1900
1880
1860
1840
retreat
advance
-1000
-500
0
500
1000
Distance (ft)

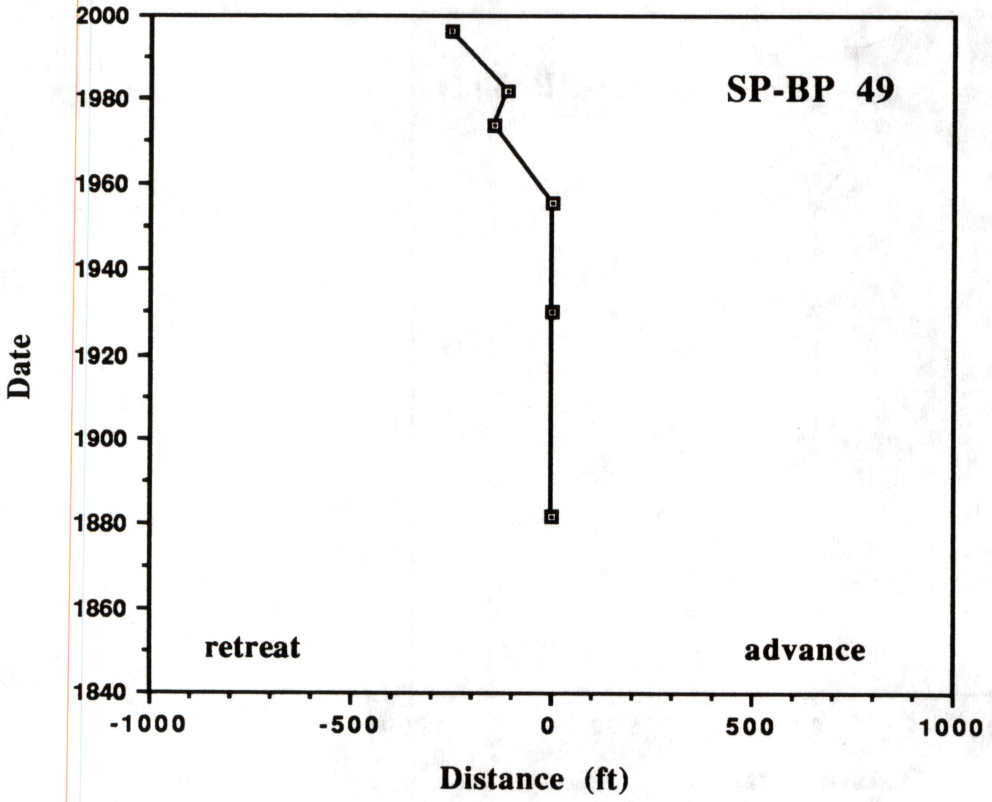
SP-BP 49
Date
2000
1980
1960
1940
1920
1900
1880
1860
1840
retreat
advance
-1000
-500
0
500
1000
Distance (ft)

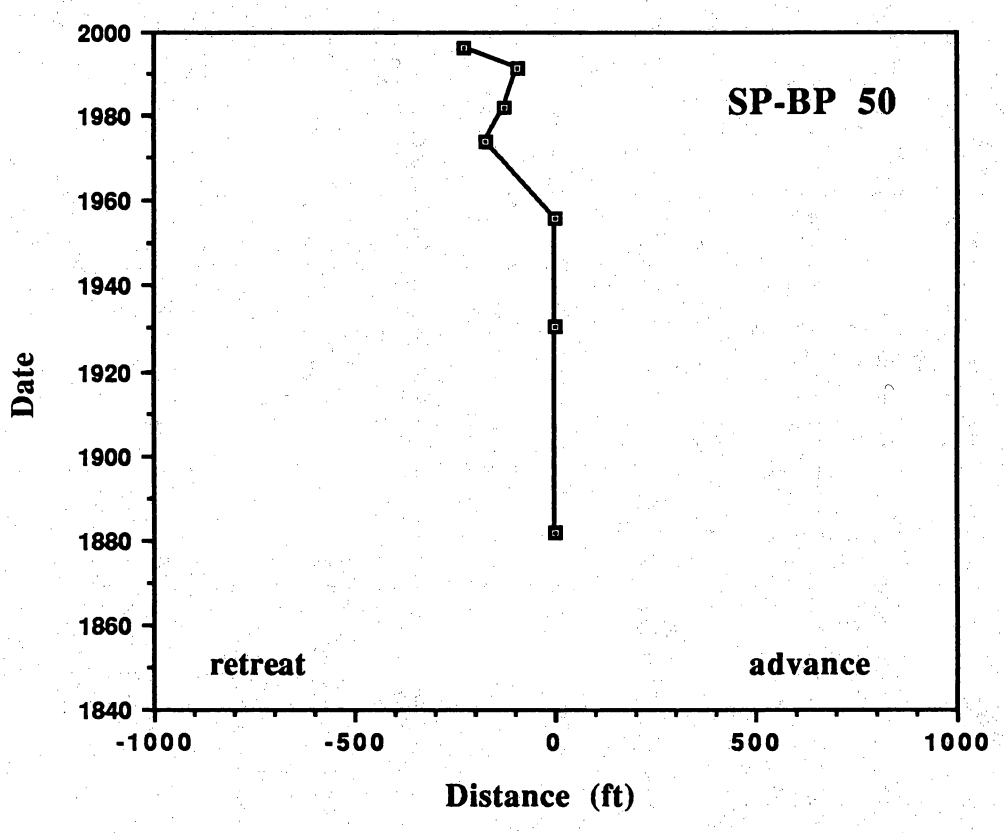
SP-BP 50
Date
2000
1980
1960
1940
1920
1900
1880
1860
1840
retreat
advance
-1000
-500
0
500
1000
Distance (ft)

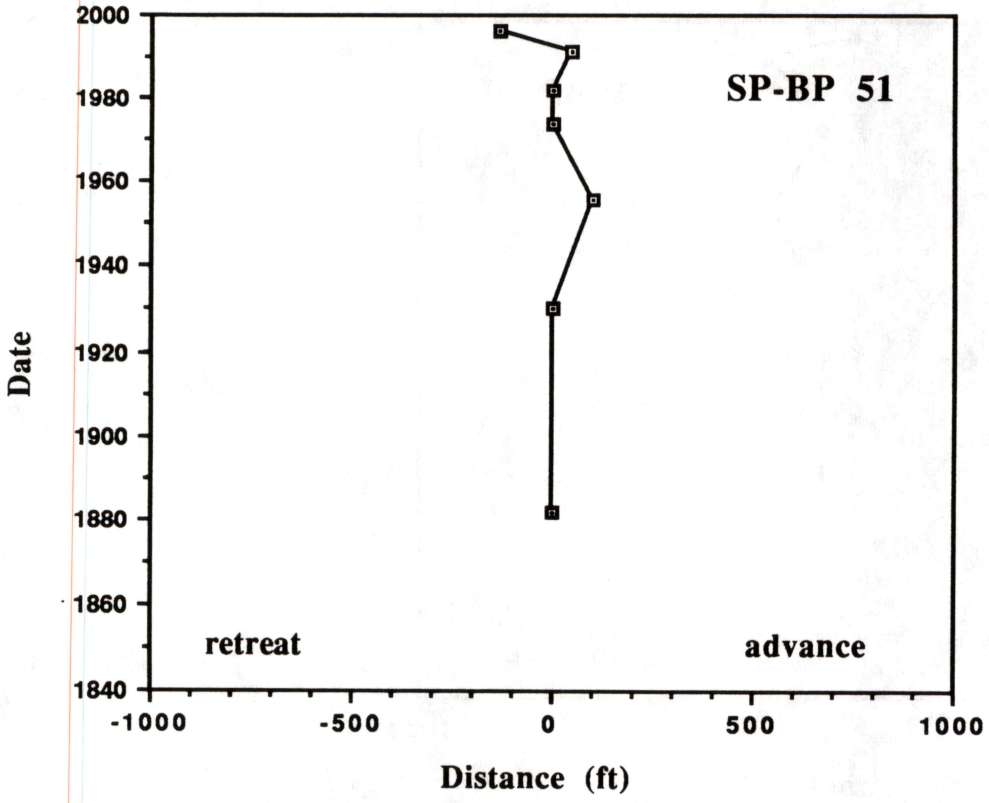
SP-BP 51
Date
2000
1980
1960
1940
1920
1900
1880
1860
1840
retreat
advance
-1000
-500
0
500
1000
Distance (ft)

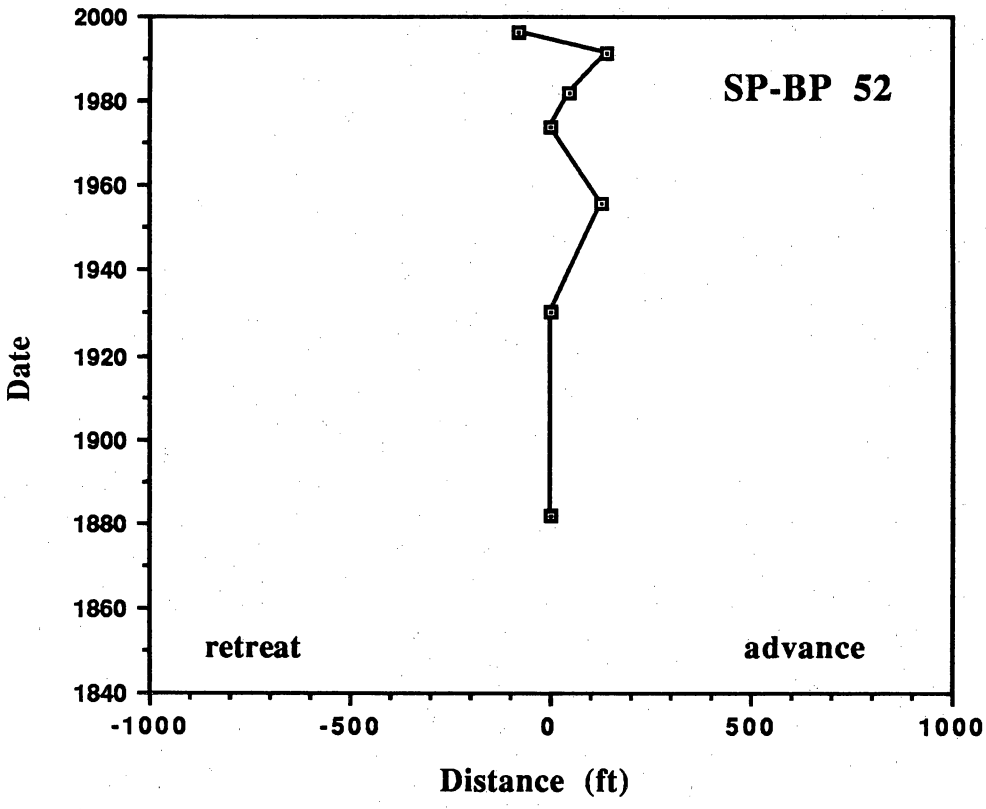
SP-BP 52
Date
2000
1980
1960
1940
1920
1900
1880
1860
1840
retreat
advance
-1000
-500
0
500
1000
Distance (ft)

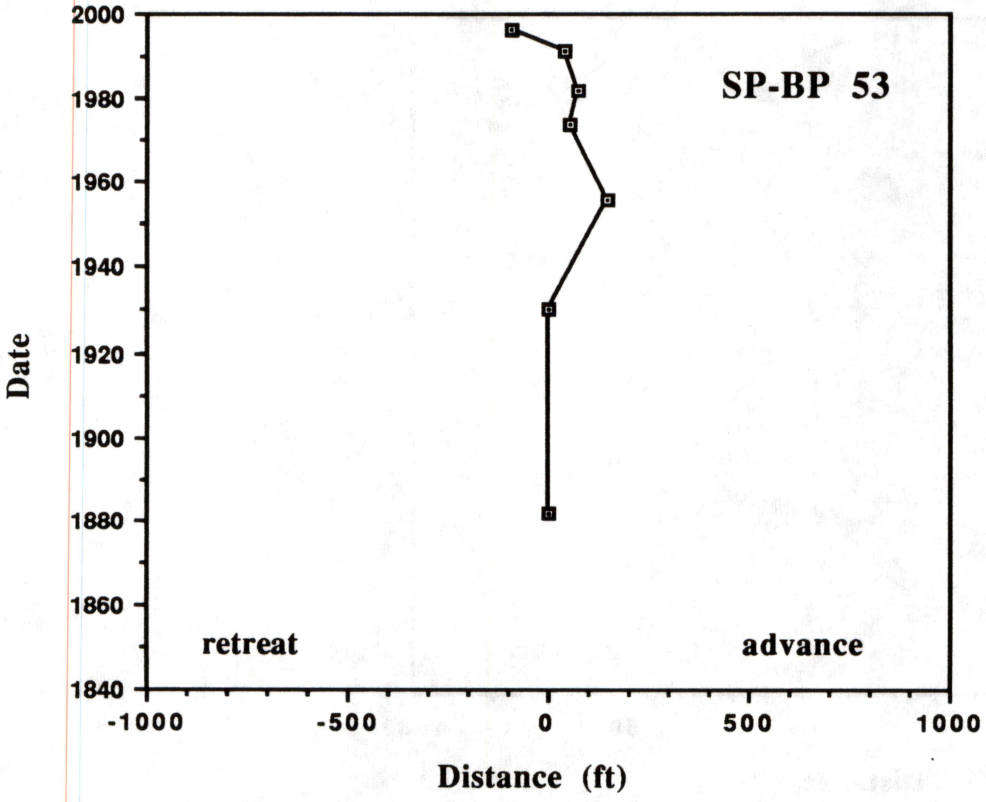
SP-BP 53
Date
2000
1980
1960
1940
1920
1900
1880
1860
1840
retreat
advance
-1000
-500
0
500
1000
Distance (ft)

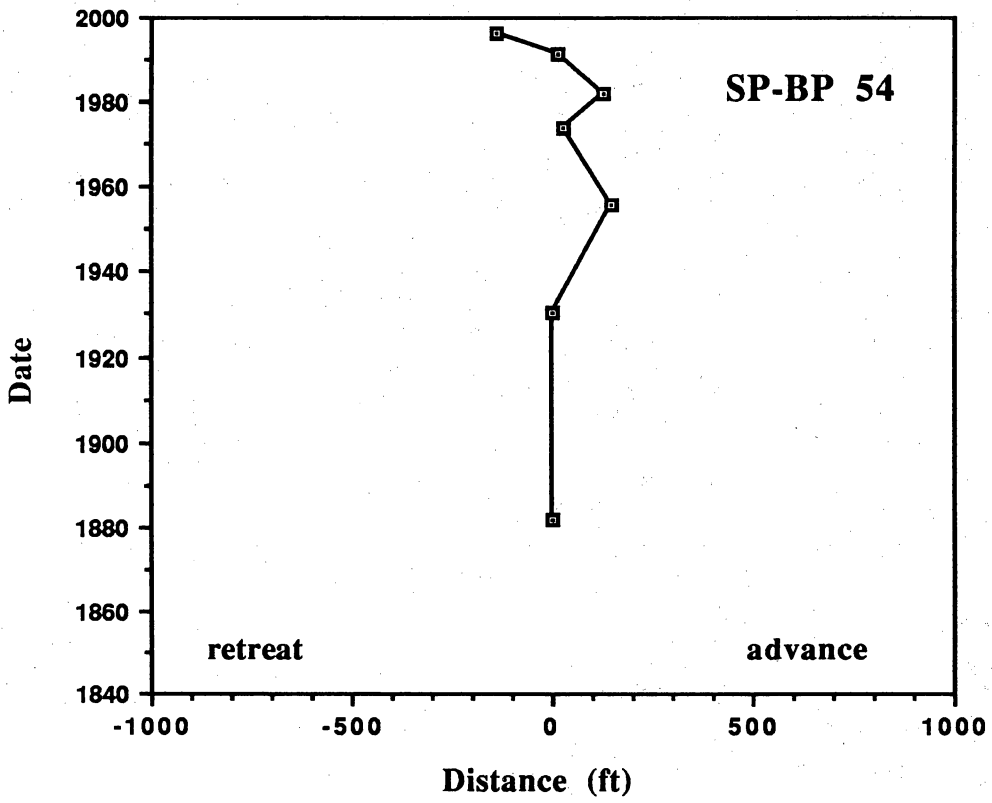
SP-BP 54
Date
2000
1980
1960
1940
1920
1900
1880
1860
1840
retreat
advance
-1000
-500
0
500
1000
Distance (ft)

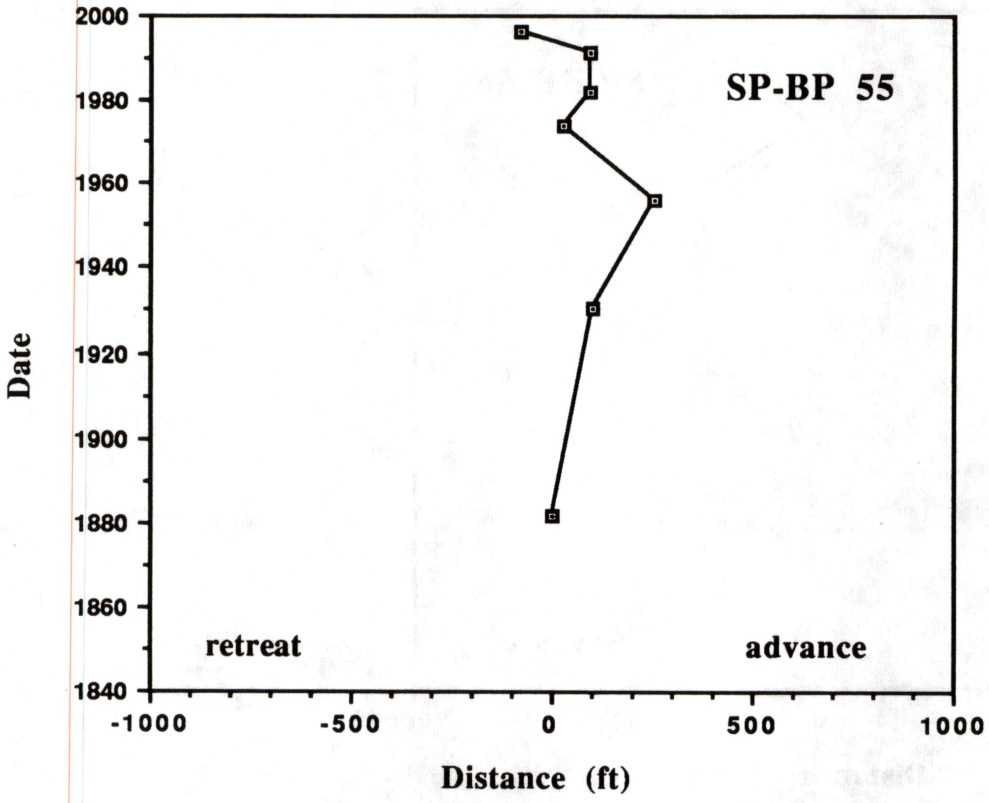
SP-BP 55
Date
2000
1980
1960
1940
1920
1900
1880
1860
1840
retreat
advance
-1000
-500
0
500
1000
Distance (ft)

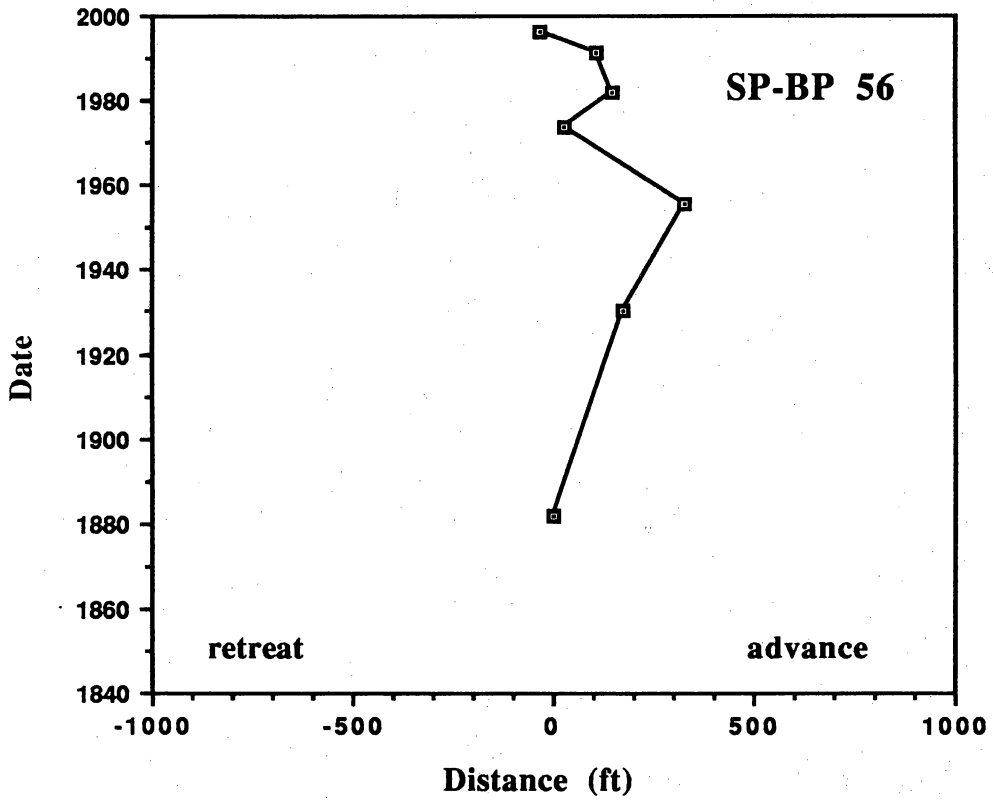
SP-BP 56
Date
2000
1980
1960
1940
1920
1900
1880
1860
1840
retreat
advance
-1000
-500
0
500
1000
Distance (ft)

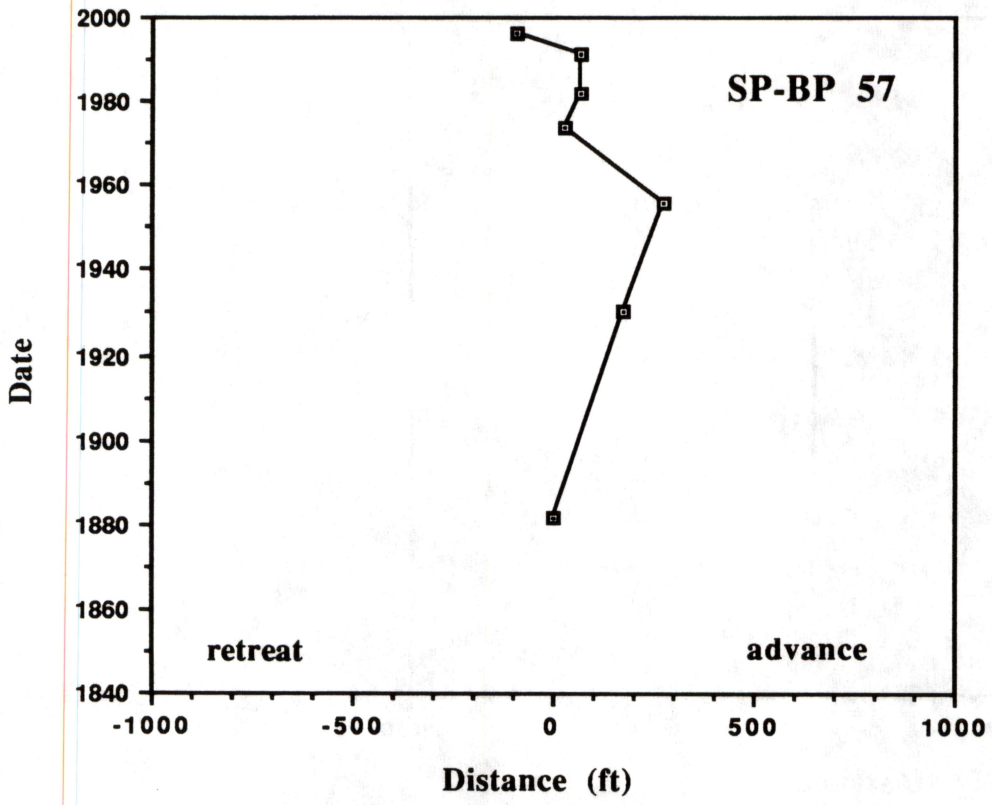
SP-BP 57
Date
2000
1980
1960
1940
1920
1900
1880
1860
1840
retreat
advance
-1000
-500
0
500
1000
Distance (ft)

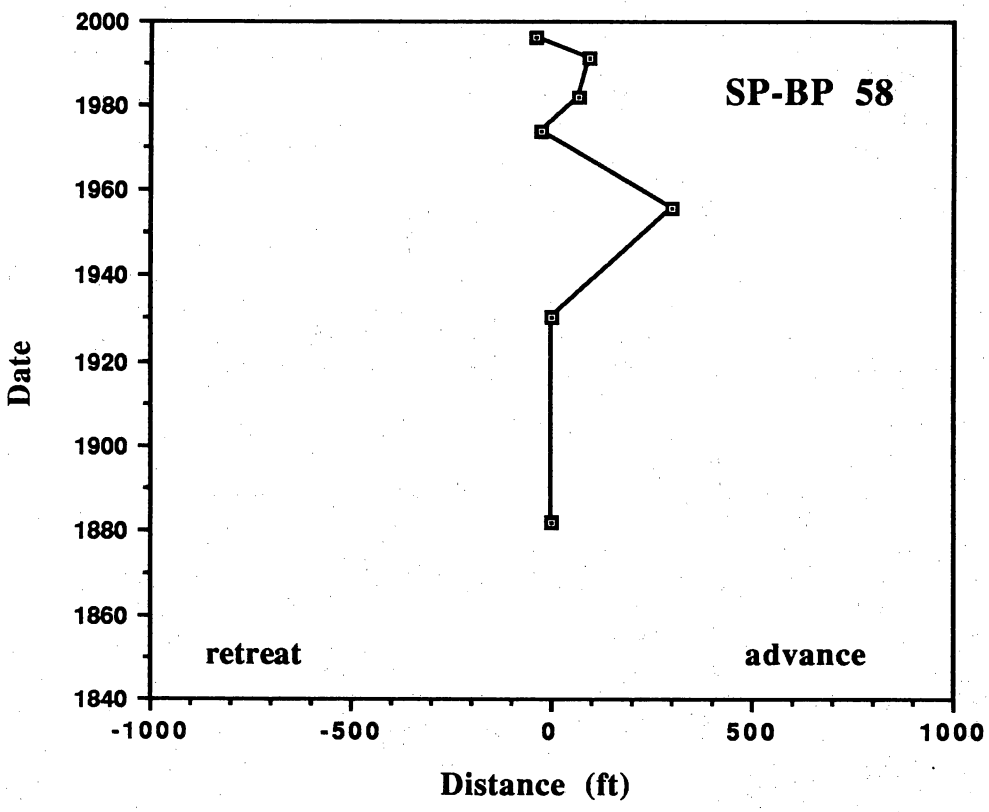
SP-BP 58
Date
2000
1980
1960
1940
1920
1900
1880
1860
1840
retreat
advance
-1000
-500
0
500
1000
Distance (ft)

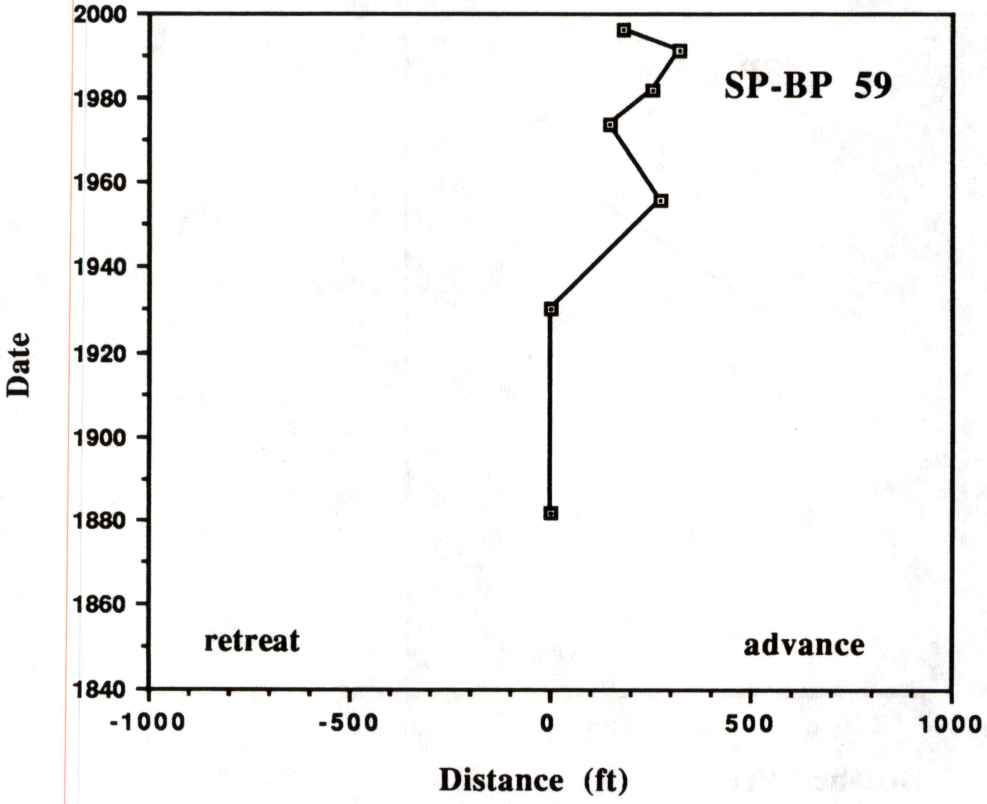
SP-BP 59
Date
2000
1980
1960
1940
1920
1900
1880
1860
1840
retreat
advance
-1000
-500
0
500
1000
Distance (ft)

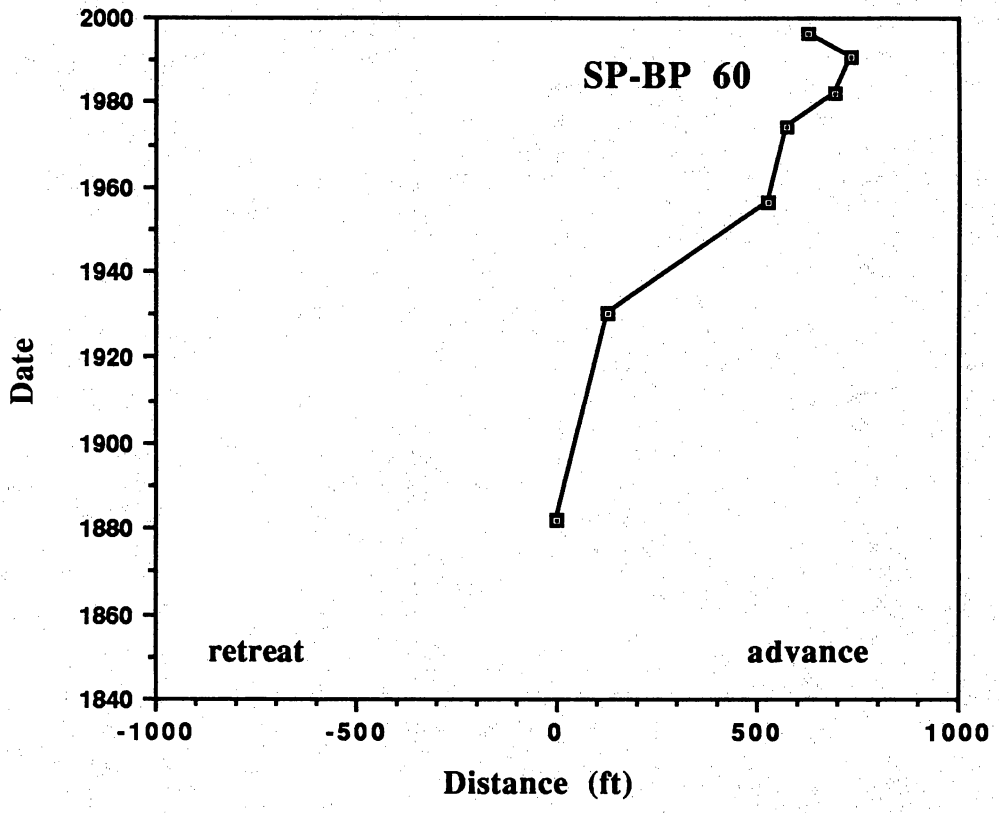
SP-BP 60
Date
2000
1980
1960
1940
1920
1900
1880
1860
1840
retreat
advance
-1000
-500
0
500
1000
Distance (ft)

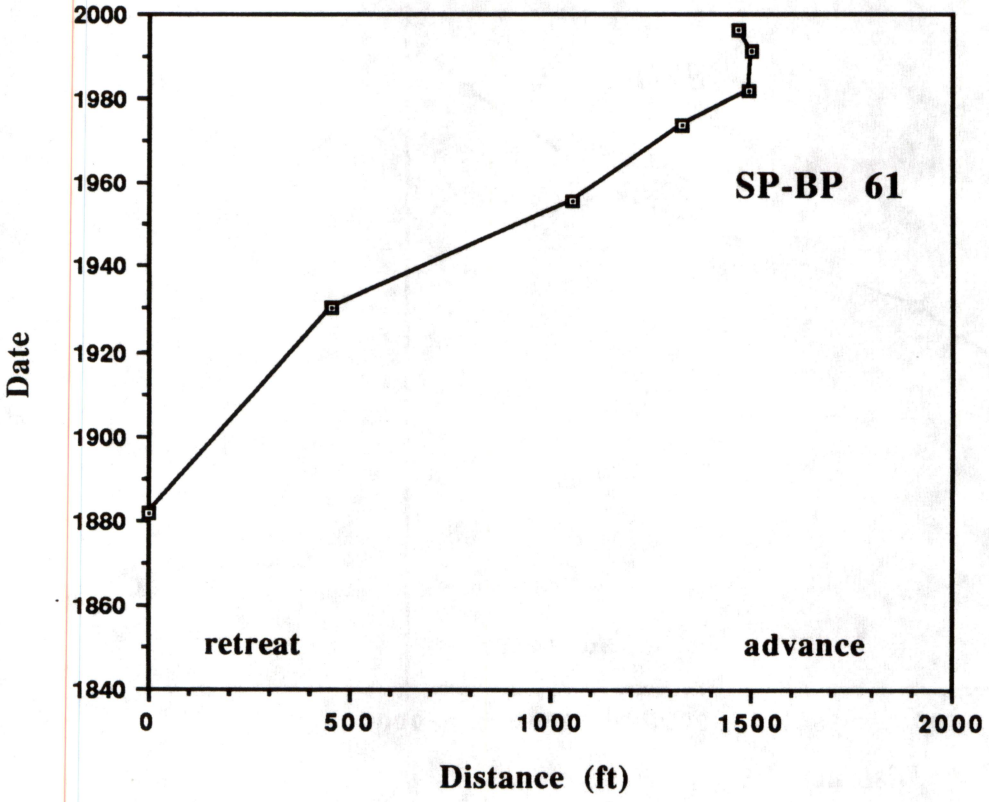
2000
1980
1960
1940
1920
1900
1880
1860
1840
Date
SP-BP 61
retreat
advance
0
500
1000
1500
2000
Distance (ft)

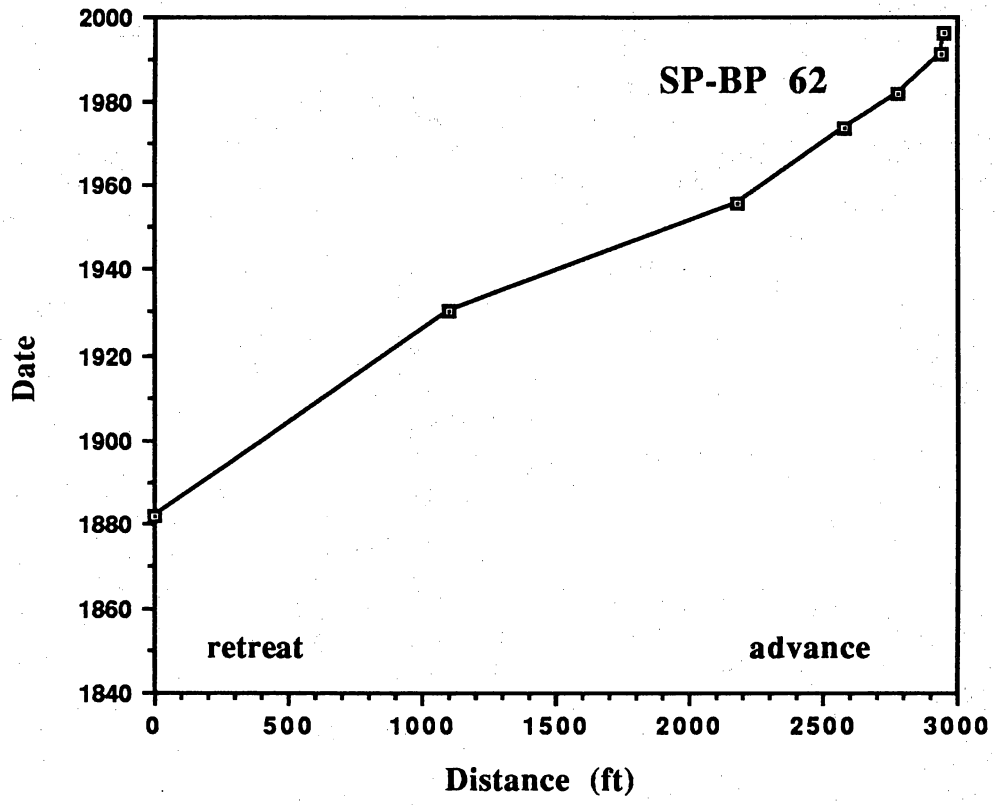
SP-BP 62
Date
2000
1980
1960
1940
1920
1900
1880
1860
1840
retreat
advance
0
500
1000
1500
2000
2500
3000
Distance (ft)

APPENDIX B

SHORELINE HISTORY PLOTS:

BOLIVAR ROADS TO SAN LUIS PASS
(GALVESTON ISLAND)

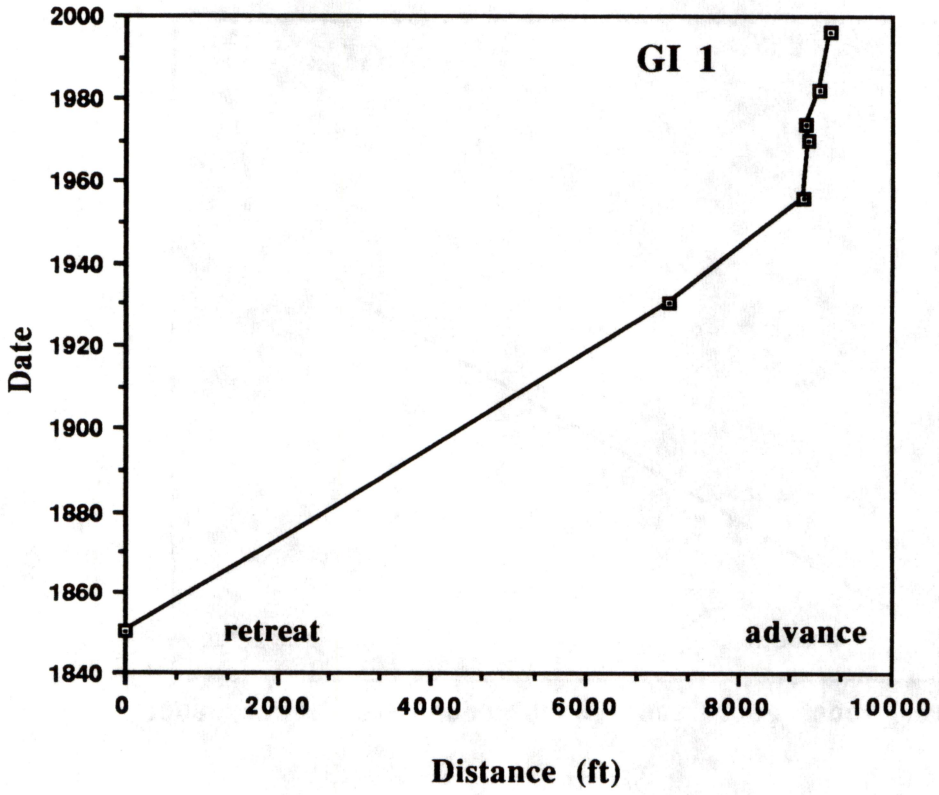
GI 1
2000
1980
1960
1940
1920
1900
1880
1860
1840
Date
retreat
advance
0
2000
4000
6000
8000
10000
Distance (ft)

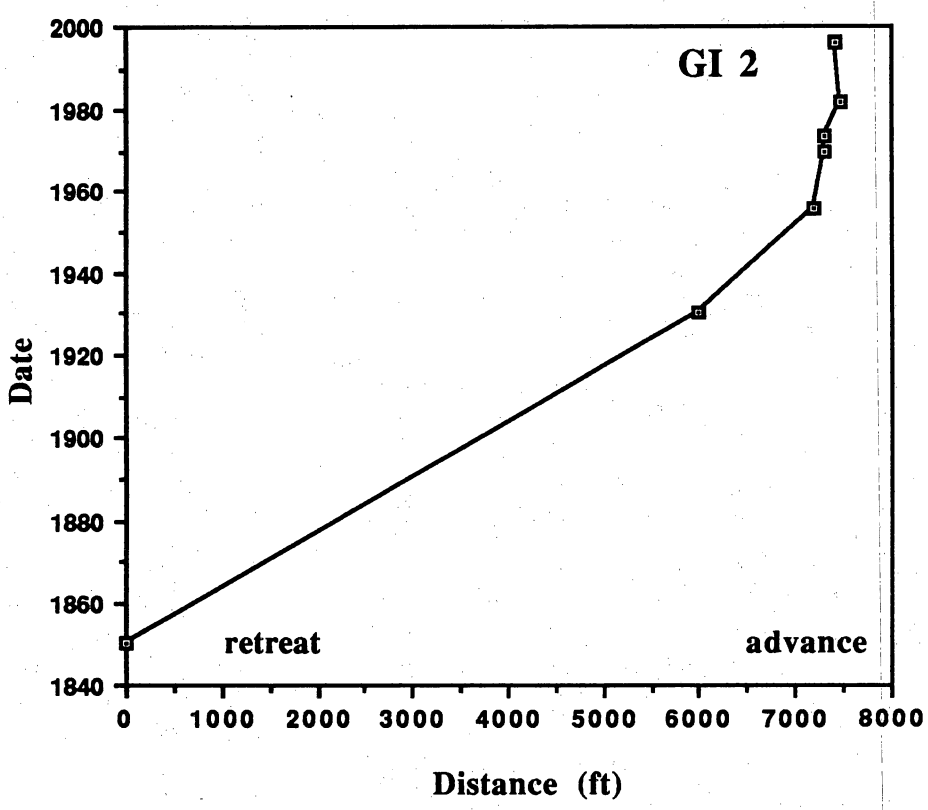
GI 2
2000
1980
1960
1940
1920
1900
1880
1860
1840
Date
retreat
advance
0
1000
2000
3000
4000
5000
6000
7000
8000
Distance (ft)

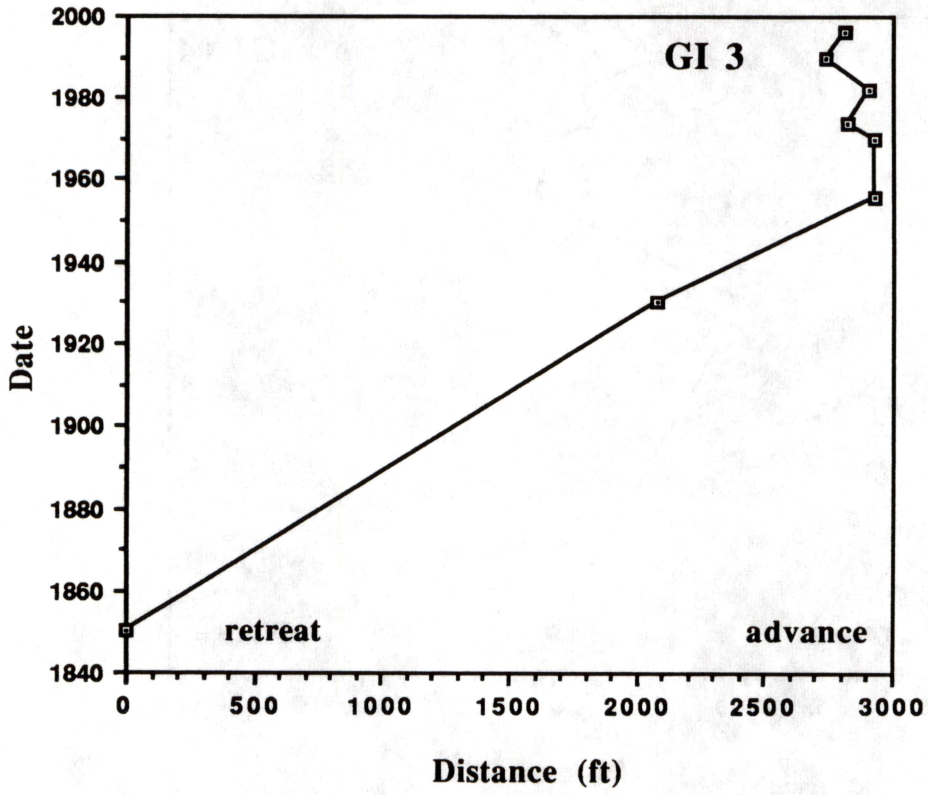
GI 3
2000
1980
1960
1940
1920
1900
1880
1860
1840
Date
retreat
advance
0
500
1000
1500
2000
2500
3000
Distance (ft)

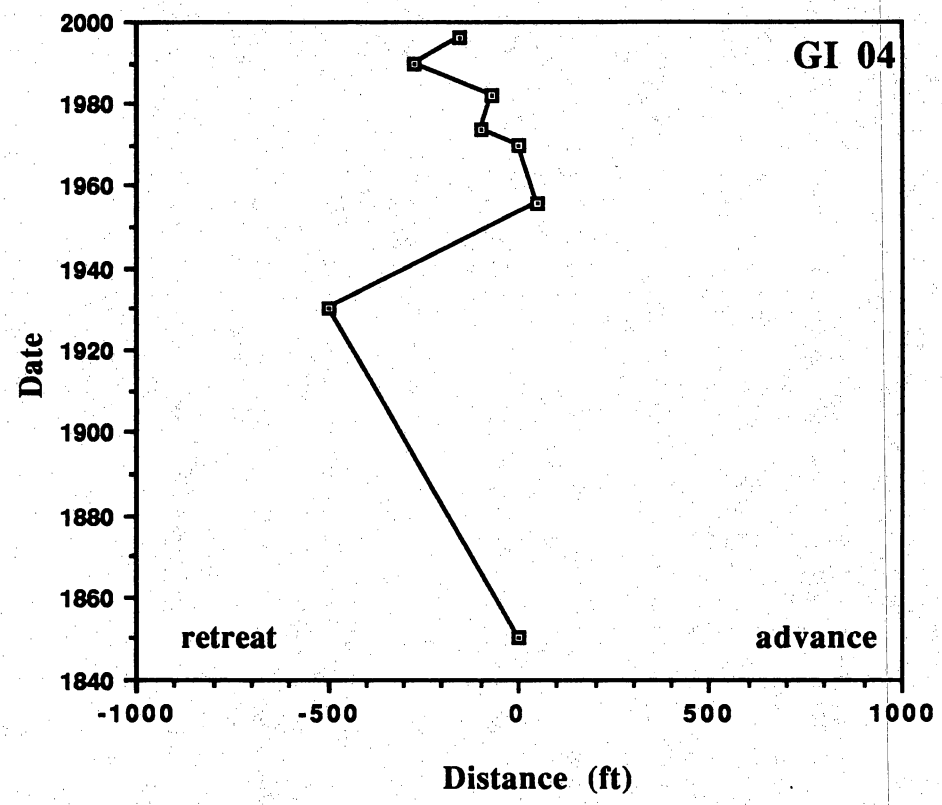
GI 04
2000
1980
1960
1940
1920
1900
1880
1860
1840
Date
retreat
advance
-1000
-500
0
500
1000
Distance (ft)

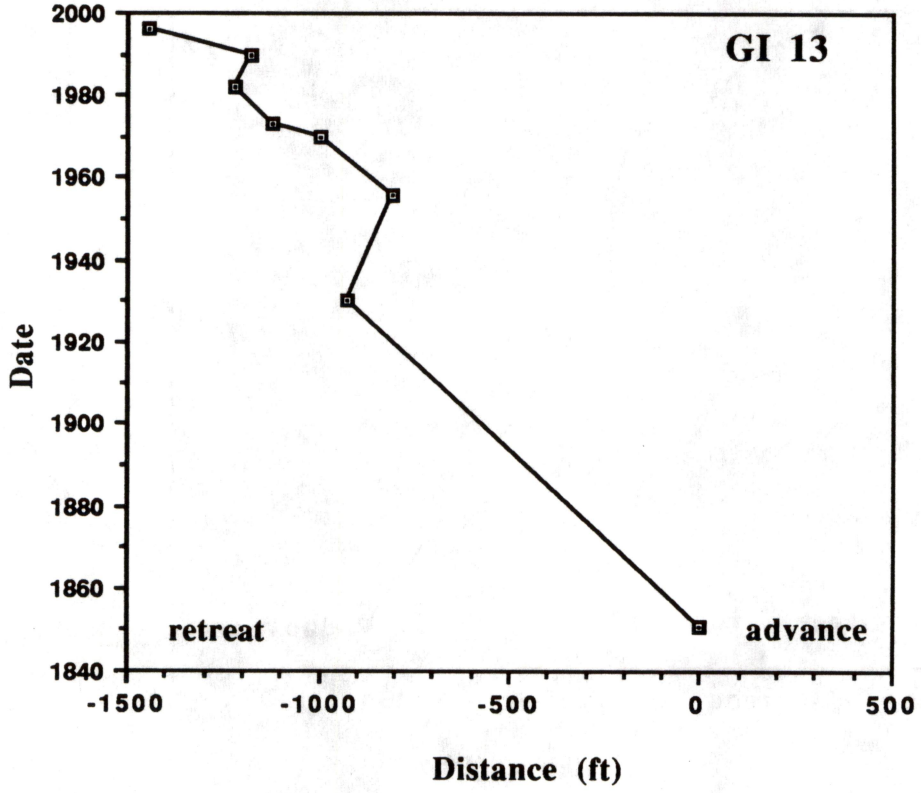
GI 13
2000
1980
1960
1940
1920
1900
1880
1860
1840
Date
retreat
advance
-1500
-1000
-500
0
500
Distance (ft)

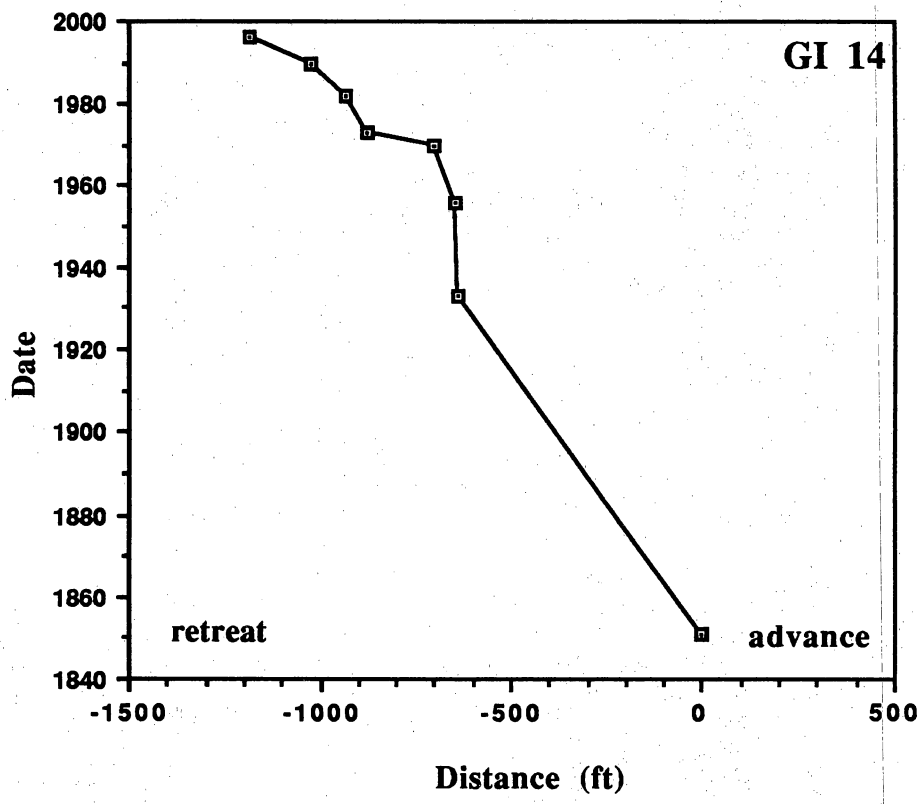
GI 14
2000
1980
1960
1940
1920
1900
1880
1860
1840
Date
retreat
advance
-1500
-1000
-500
0
500
Distance (ft)

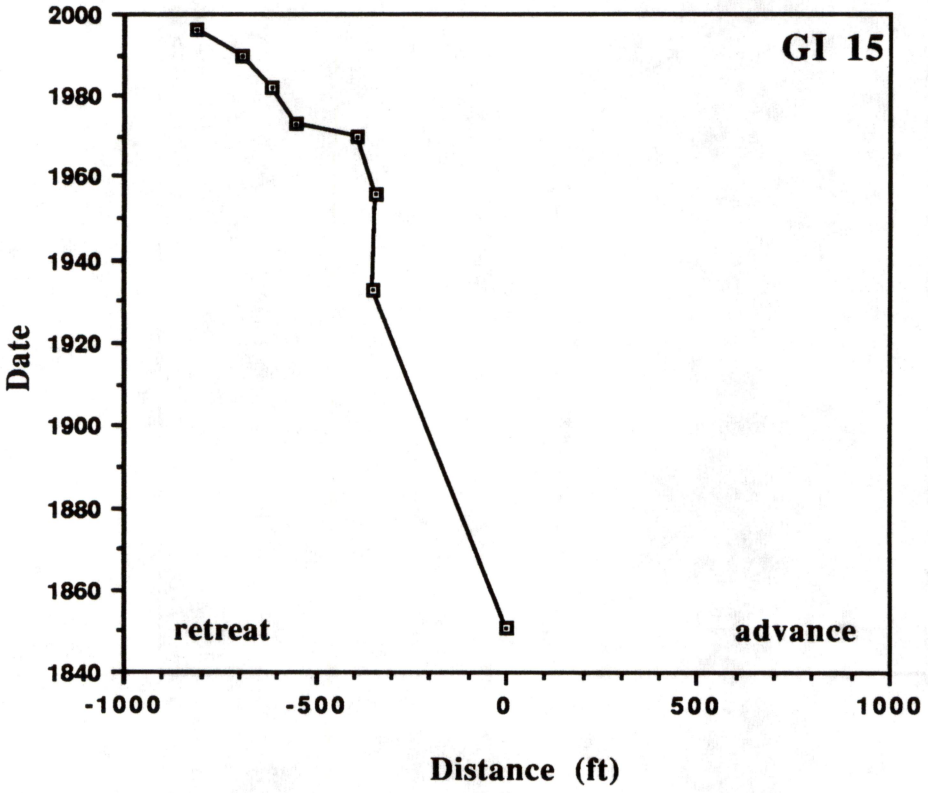
GI 15
2000
1980
1960
1940
1920
1900
1880
1860
1840
Date
retreat
advance
-1000
-500
0
500
1000
Distance (ft)

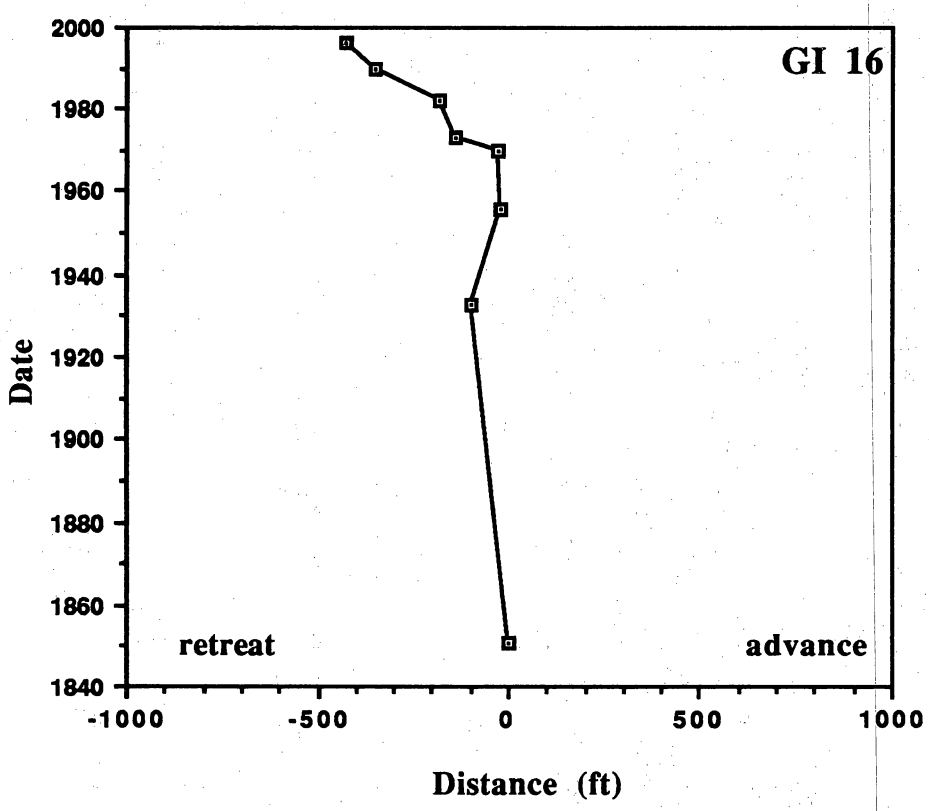
GI 16
2000
1980
1960
1940
1920
1900
1880
1860
1840
Date
retreat
advance
-1000
-500
0
500
1000
Distance (ft)

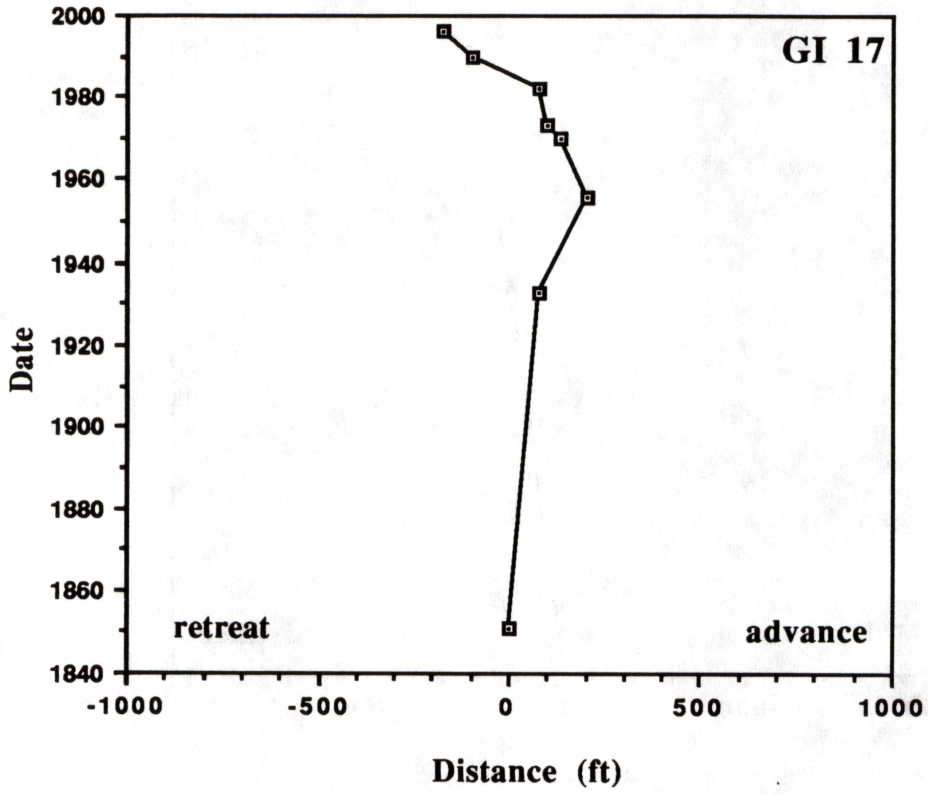
GI 17
2000
1980
1960
1940
1920
1900
1880
1860
1840
Date
retreat
advance
-1000
-500
0
500
1000
Distance (ft)

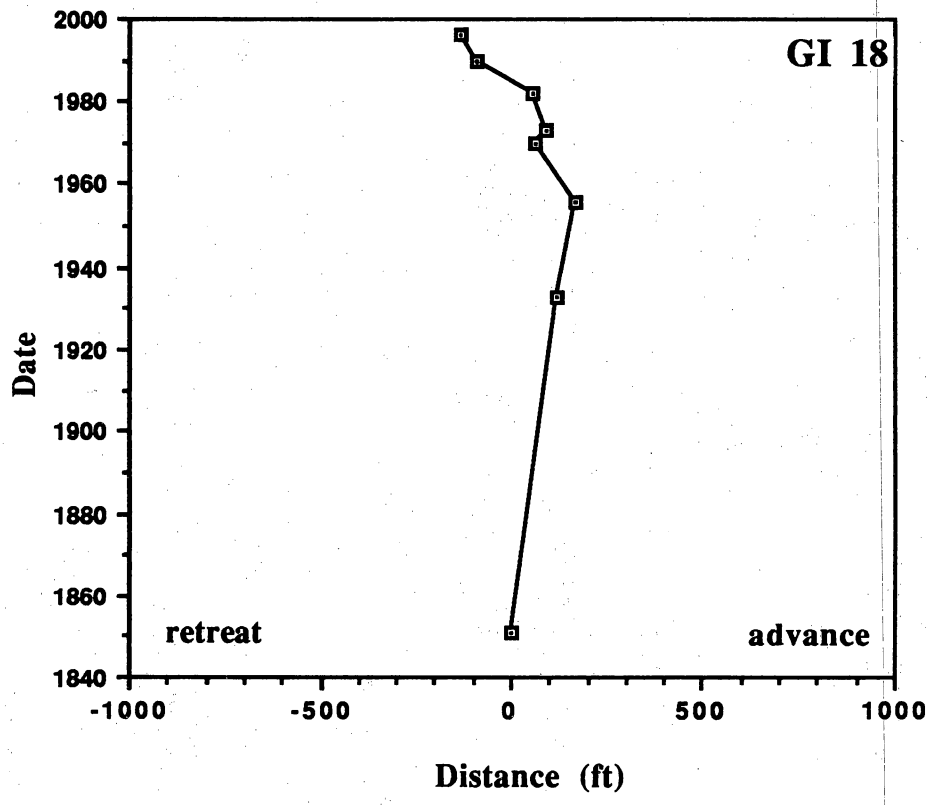
GI 18
2000
1980
1960
1940
1920
1900
1880
1860
1840
Date
retreat
advance
-1000
-500
0
500
1000
Distance (ft)

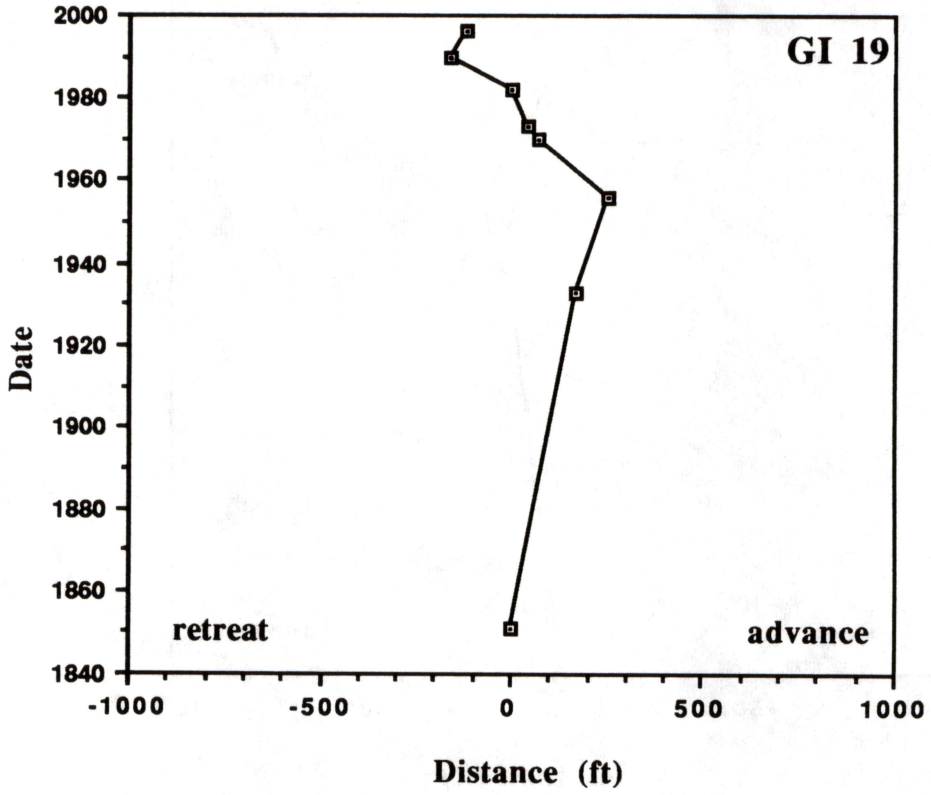
GI 19
2000
1980
1960
1940
1920
1900
1880
1860
1840
Date
retreat
advance
-1000
-500
0
500
1000
Distance (ft)

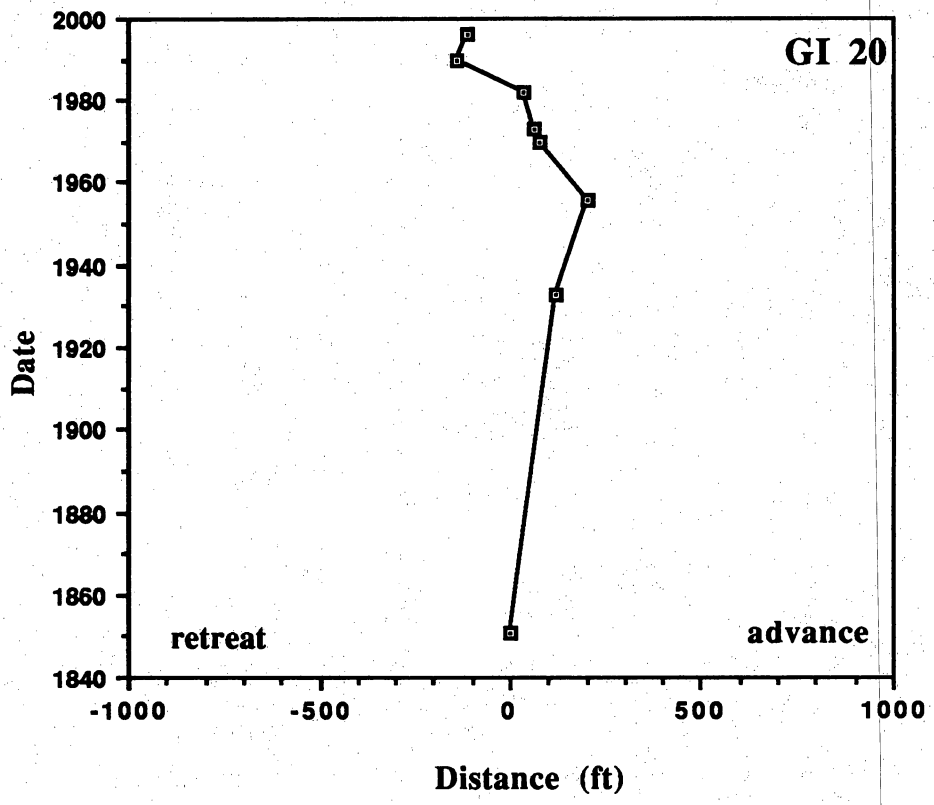
GI 20
2000
1980
1960
1940
1920
1900
1880
1860
1840
Date
retreat
advance
-1000
-500
0
500
1000
Distance (ft)

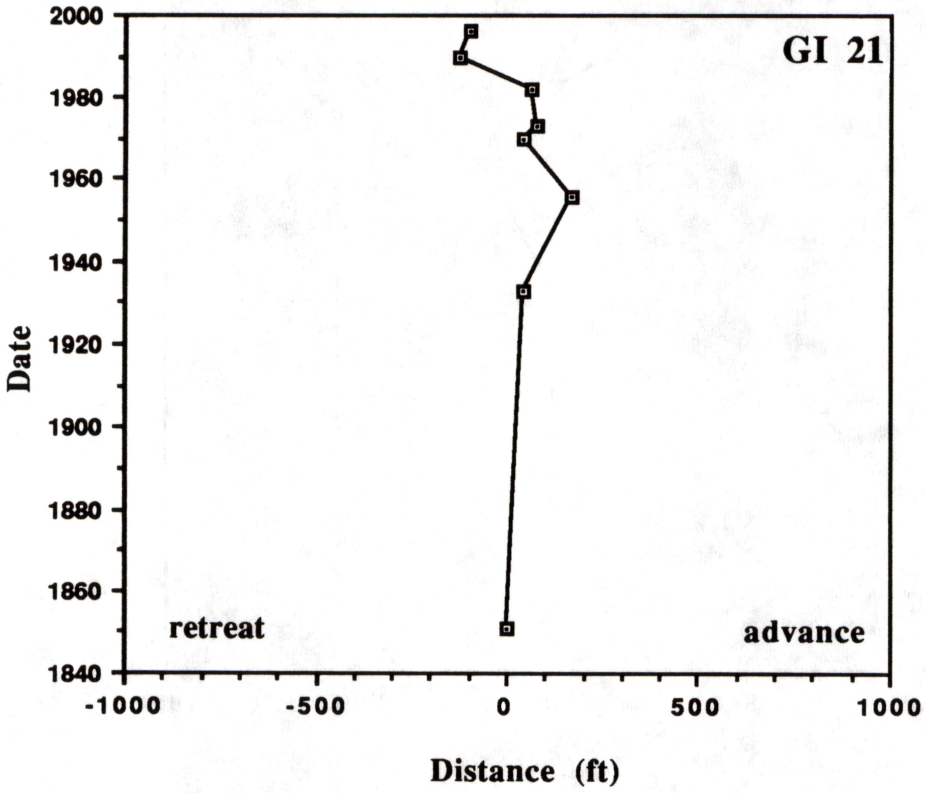
GI 21
2000
1980
1960
1940
1920
1900
1880
1860
1840
Date
retreat
advance
-1000
-500
0
500
1000
Distance (ft)

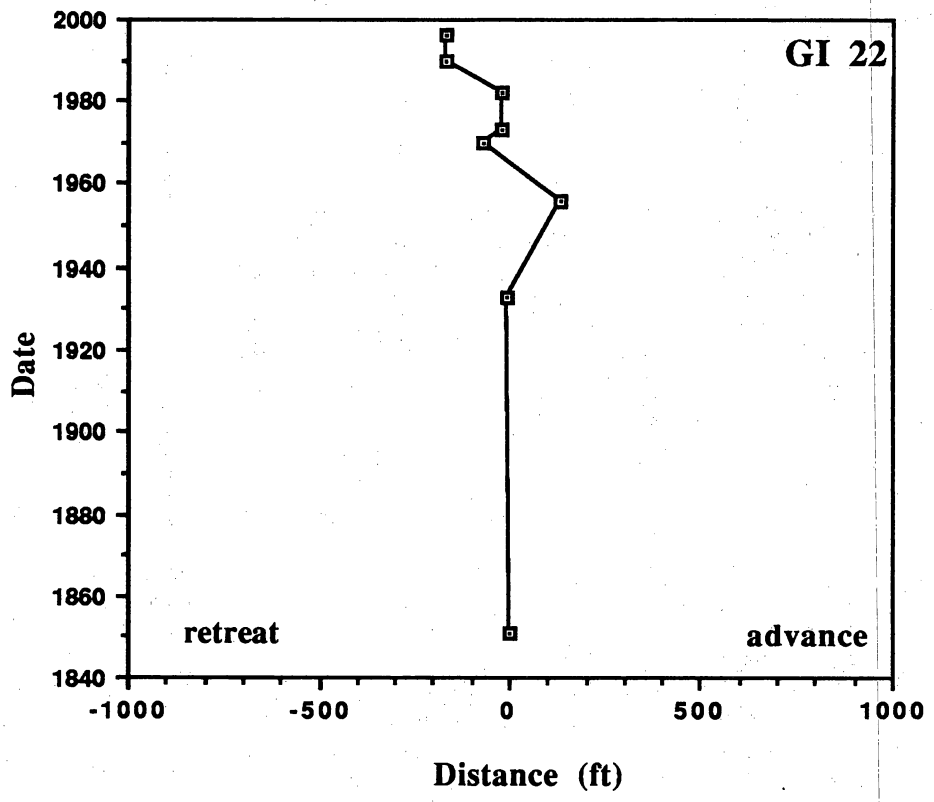
GI 22
2000
1980
1960
1940
1920
1900
1880
1860
1840
Date
retreat
advance
-1000
-500
0
500
1000
Distance (ft)

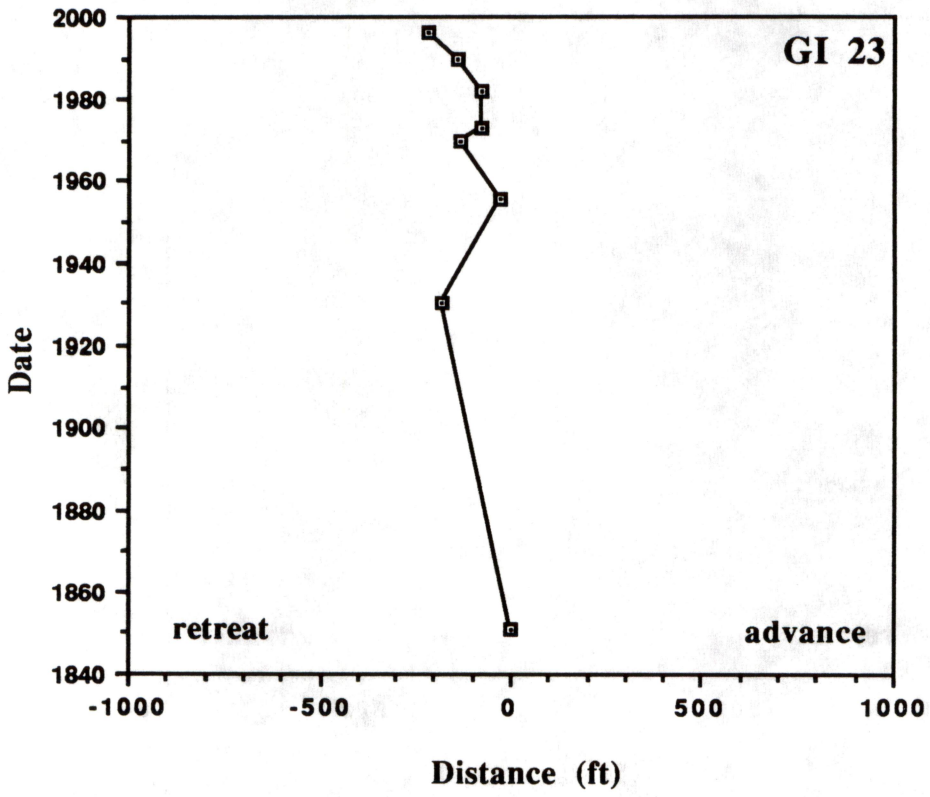
GI 23
Date
2000
1980
1960
1940
1920
1900
1880
1860
1840
retreat
advance
-1000
-500
0
500
1000
Distance (ft)

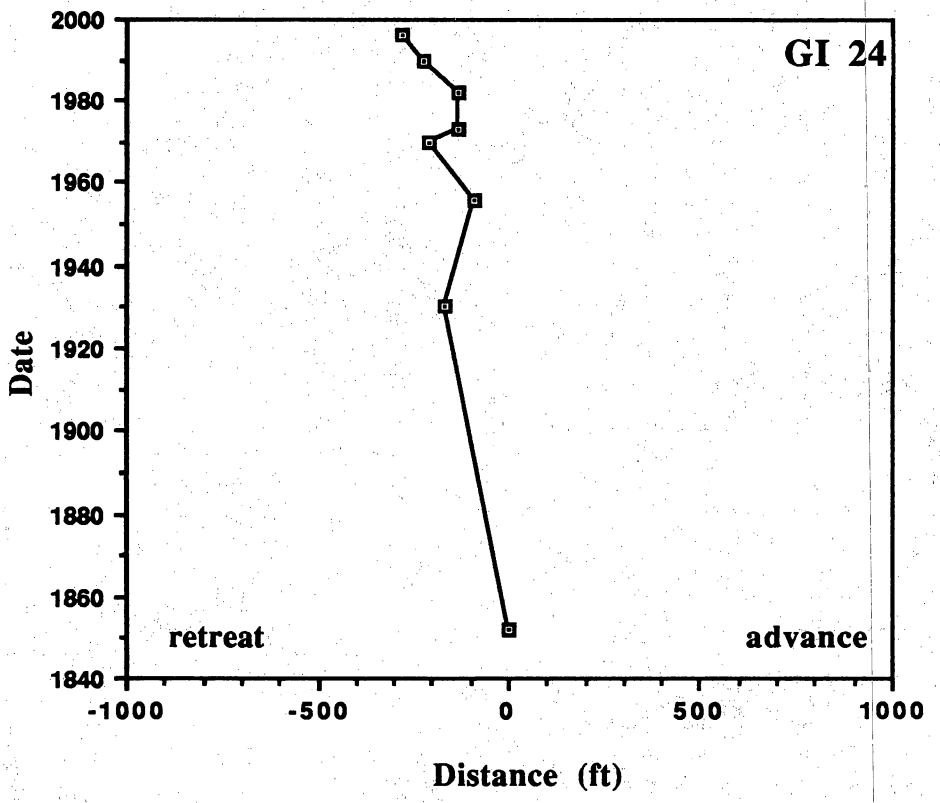
GI 24
2000
1980
1960
1940
1920
1900
1880
1860
1840
Date
retreat
advance
-1000
-500
0
500
1000
Distance (ft)

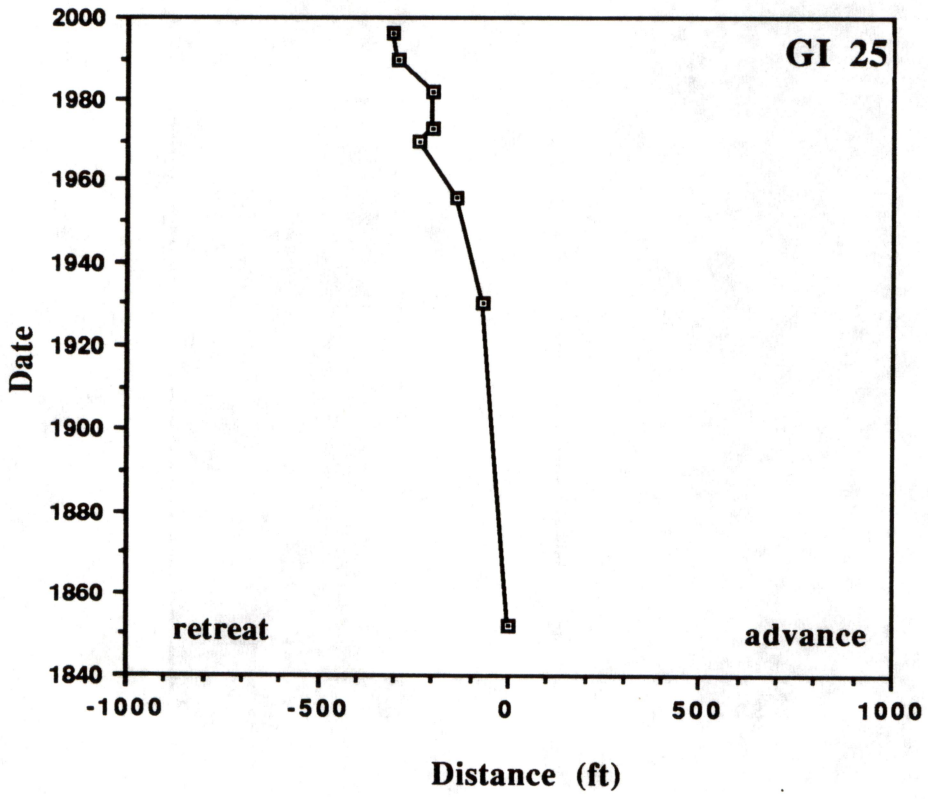
GI 25
2000
1980
1960
1940
1920
1900
1880
1860
1840
Date
retreat
advance
-1000
-500
0
500
1000
Distance (ft)

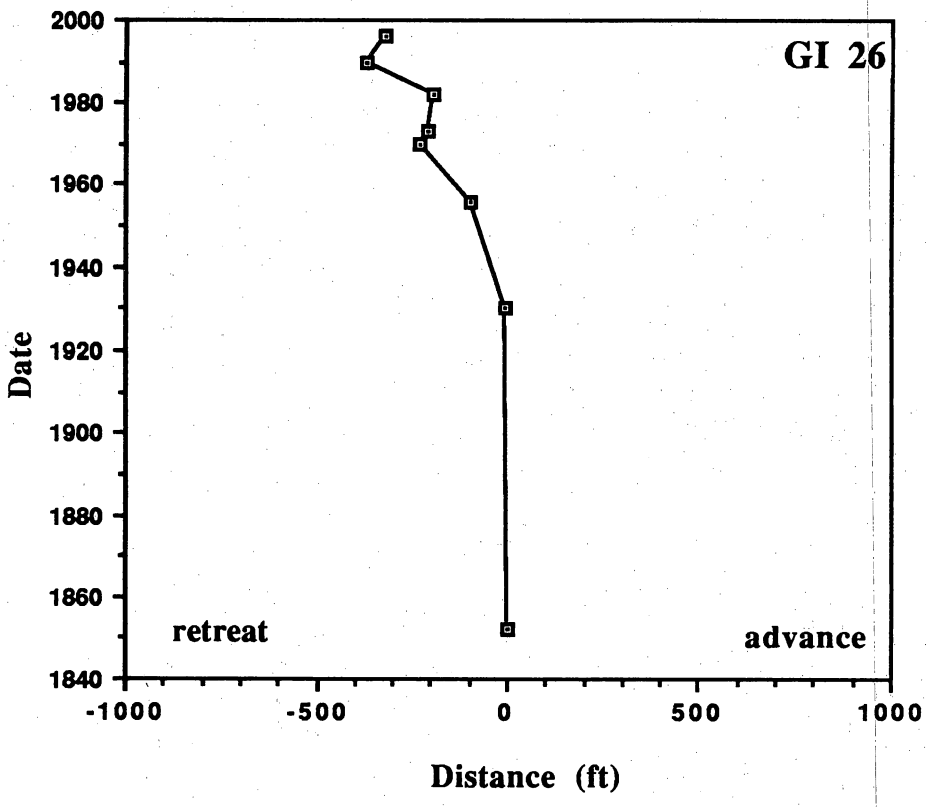
GI 26
2000
1980
1960
1940
1920
1900
1880
1860
1840
Date
retreat
advance
-1000
-500
0
500
1000
Distance (ft)

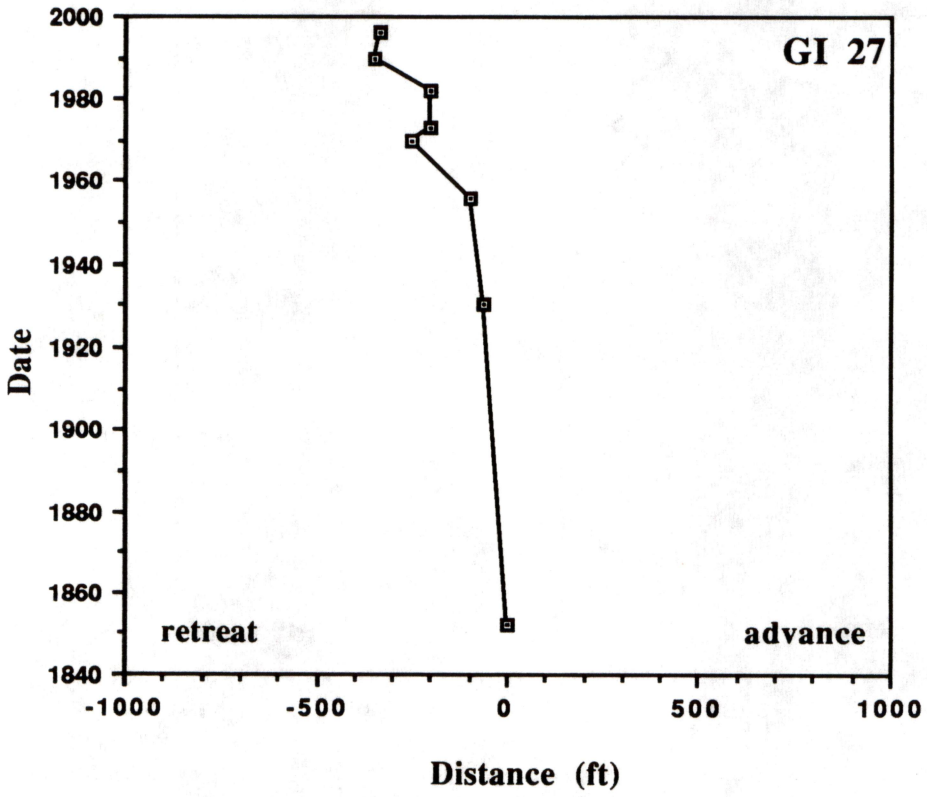
GI 27
2000
1980
1960
1940
1920
1900
1880
1860
1840
Date
retreat
advance
-1000
-500
0
500
1000
Distance (ft)

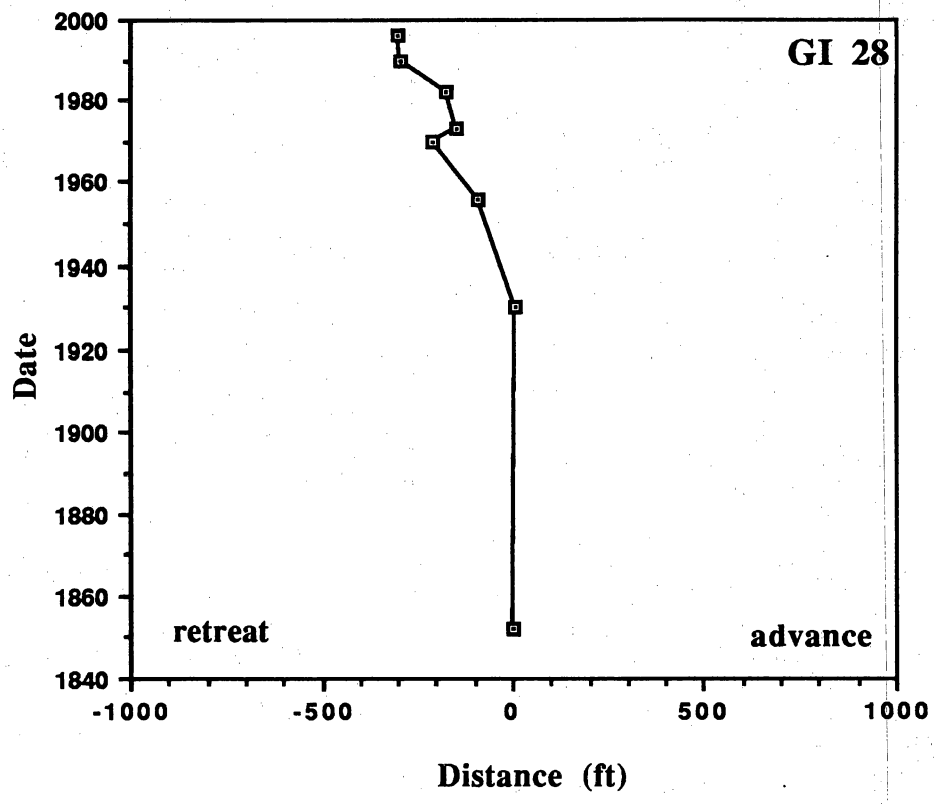
GI 28
2000
1980
1960
1940
1920
1900
1880
1860
1840
Date
retreat
advance
-1000
-500
0
500
1000
Distance (ft)

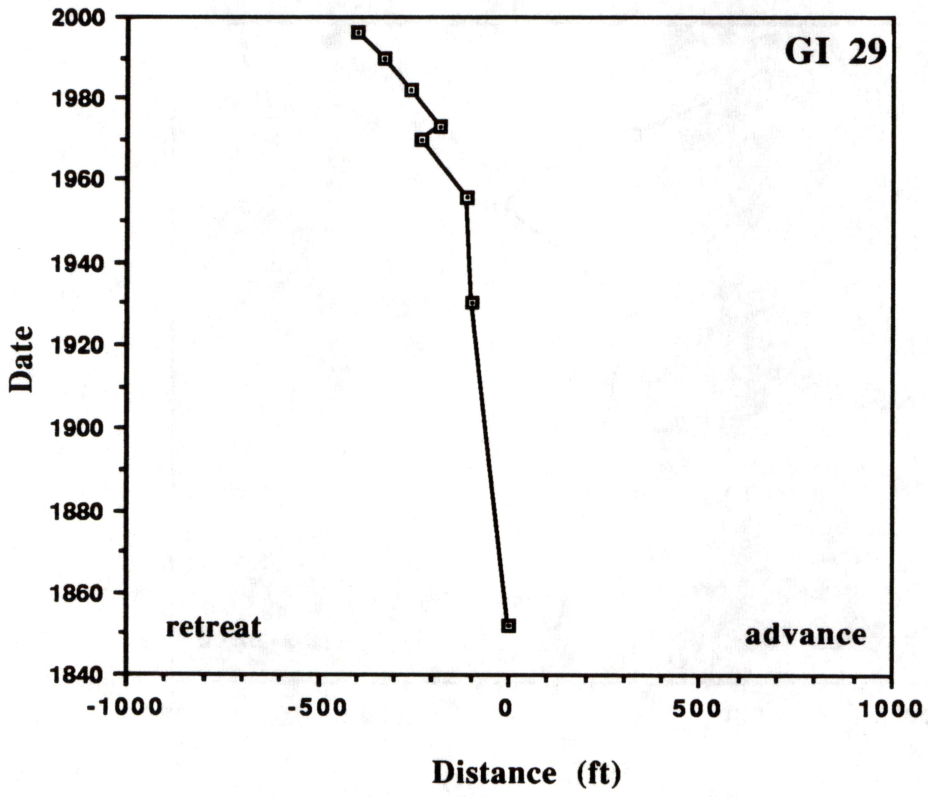
GI 29
2000
1980
1960
1940
1920
1900
1880
1860
1840
Date
retreat
advance
-1000
-500
0
500
1000
Distance (ft)

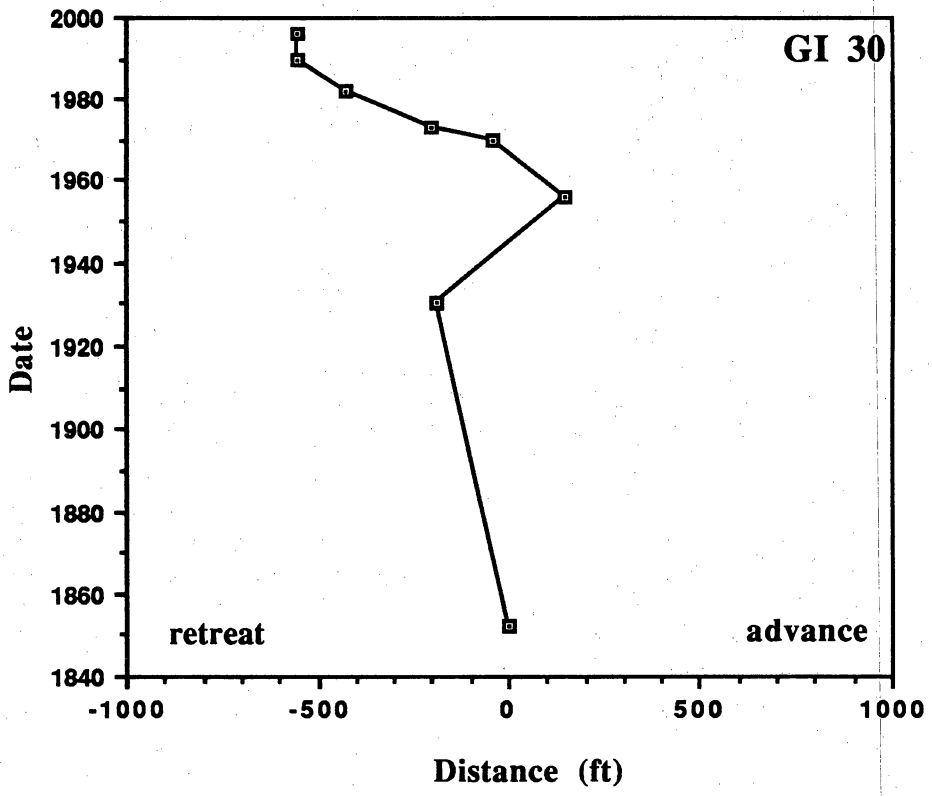
GI 30
2000
1980
1960
1940
1920
1900
1880
1860
1840
Date
retreat
advance
-1000
-500
0
500
1000
Distance (ft)

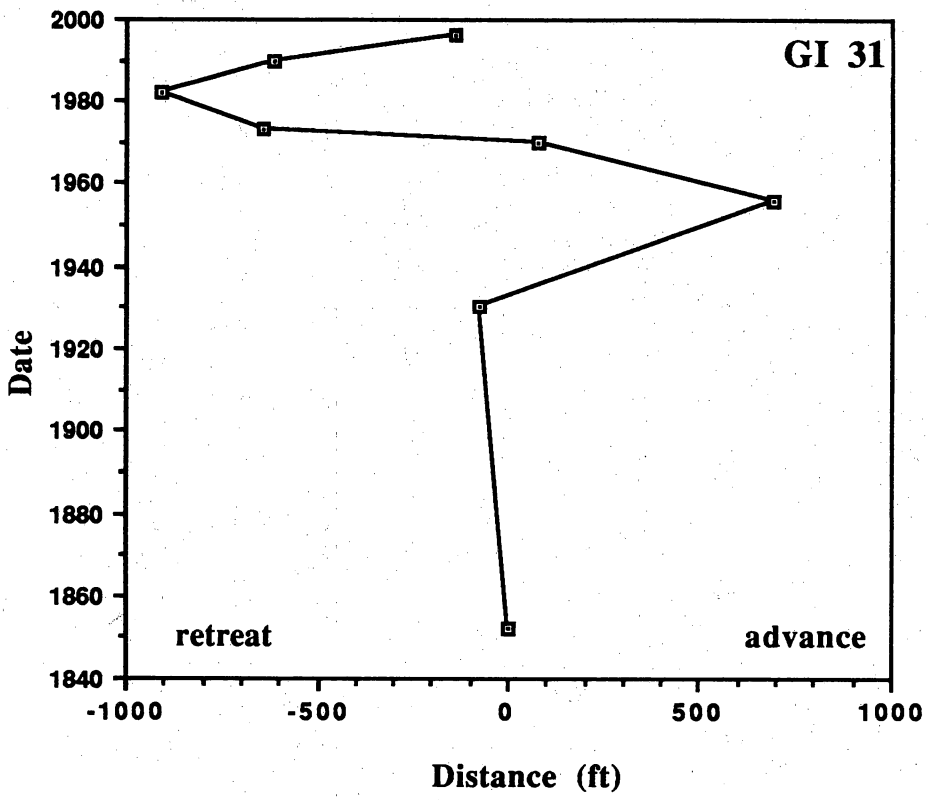
GI 31
2000
1980
1960
1940
1920
1900
1880
1860
1840
Date
retreat
advance
-1000
-500
0
500
1000
Distance (ft)

APPENDIX C

SHORELINE HISTORY PLOTS:

SAN LUIS PASS TO THE BRAZOS RIVER

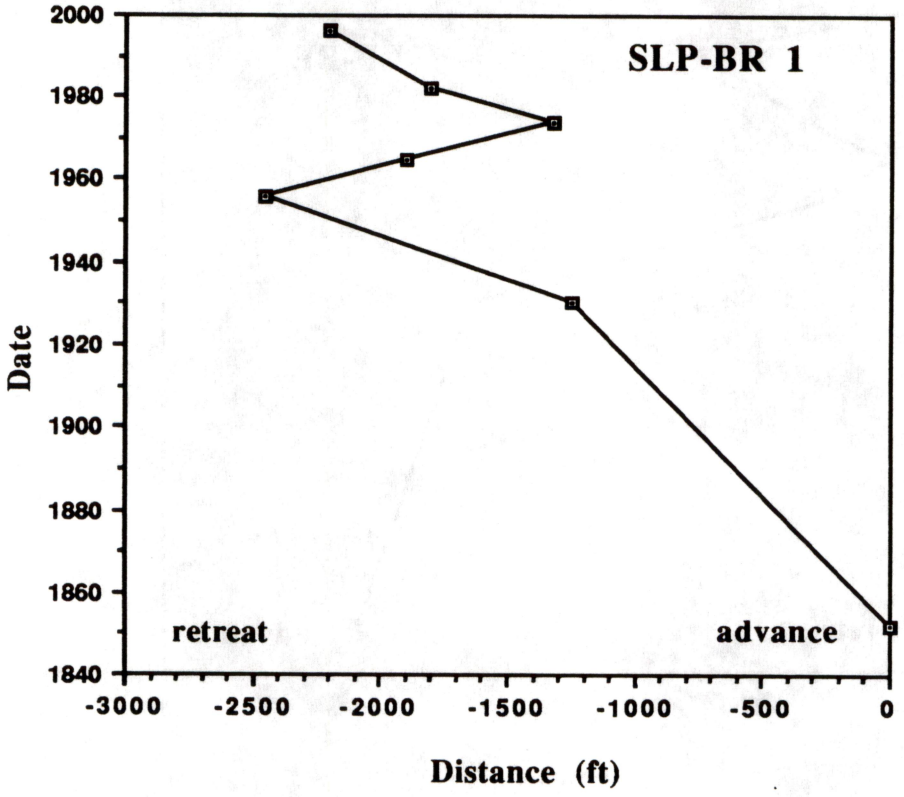
SLP-BR 1
2000
1980
1960
1940
1920
1900
1880
1860
1840
Date
retreat
advance
-3000
-2500
-2000
-1500
-1000
-500
0
Distance (ft)

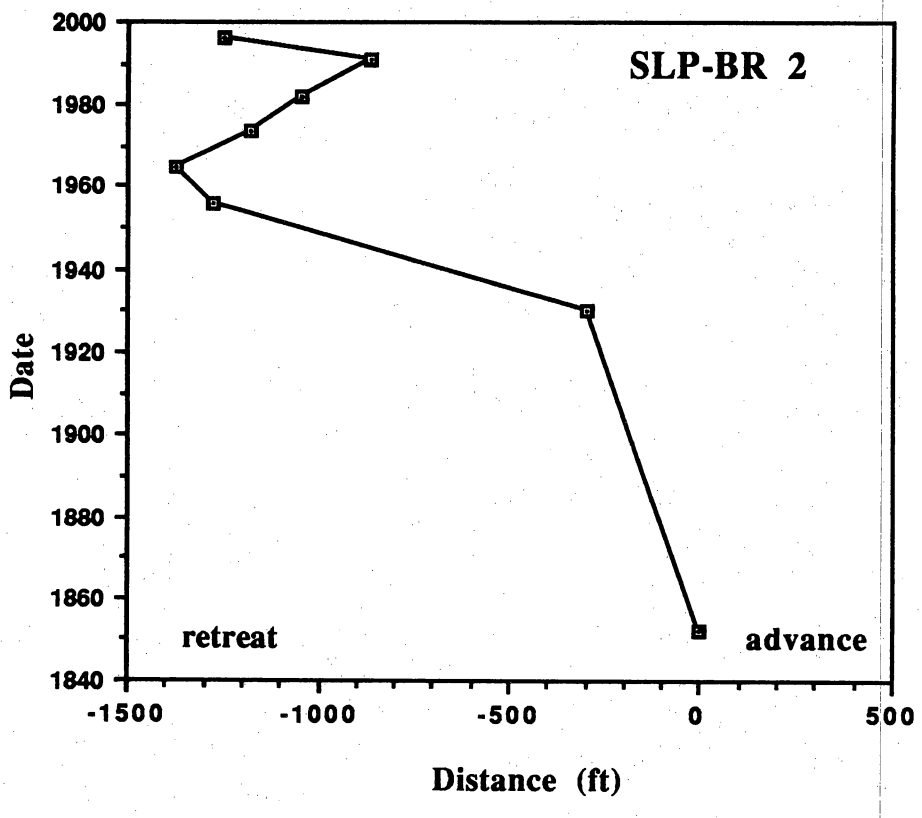
SLP-BR 2
2000
1980
1960
1940
1920
1900
1880
1860
1840
Date
retreat
advance
-1500
-1000
-500
0
500
Distance (ft)

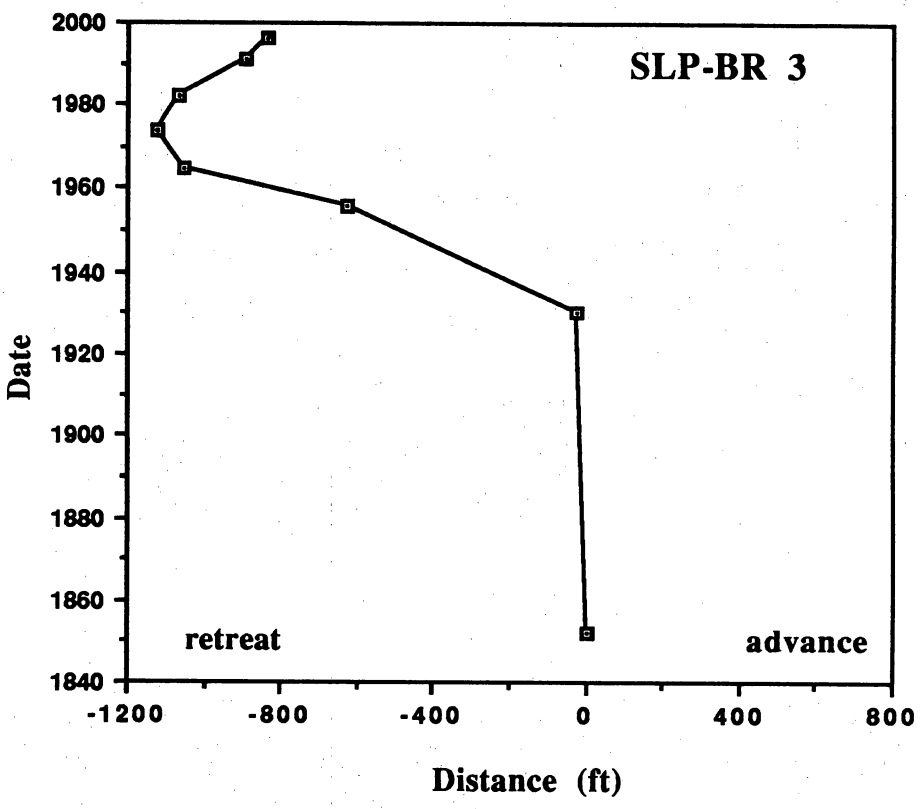
SLP-BR 3
2000
1980
1960
1940
1920
1900
1880
1860
1840
Date
retreat
advance
-1200
-800
-400
0
400
800
Distance (ft)

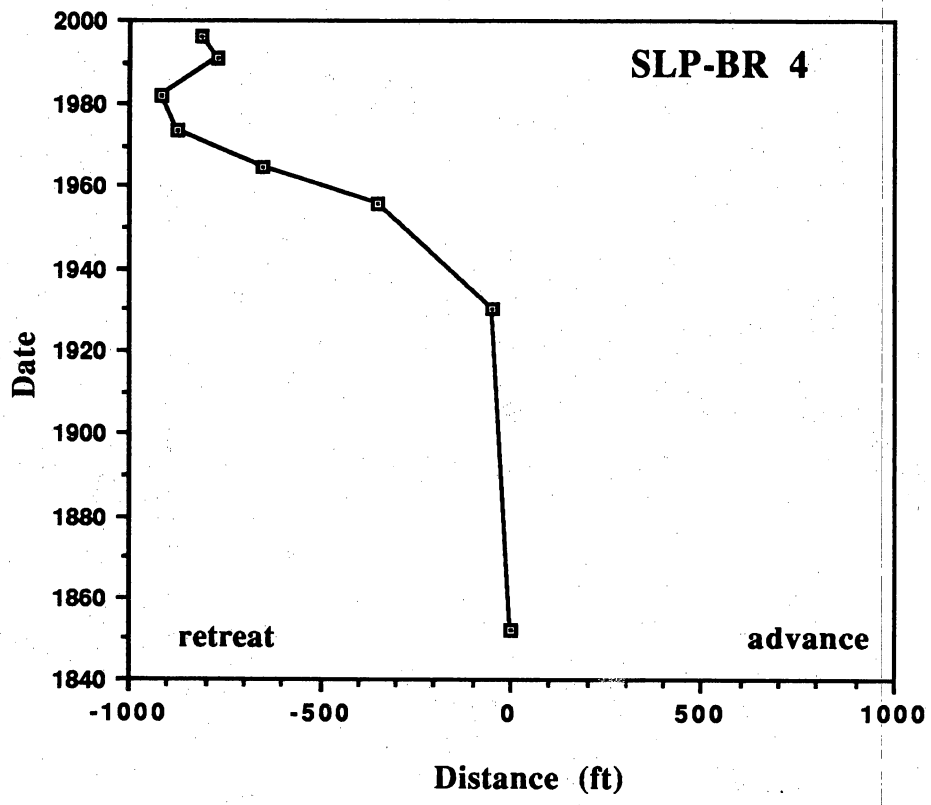
SLP-BR 4
Date
2000
1980
1960
1940
1920
1900
1880
1860
1840
retreat
advance
-1000
-500
0
500
1000
Distance (ft)

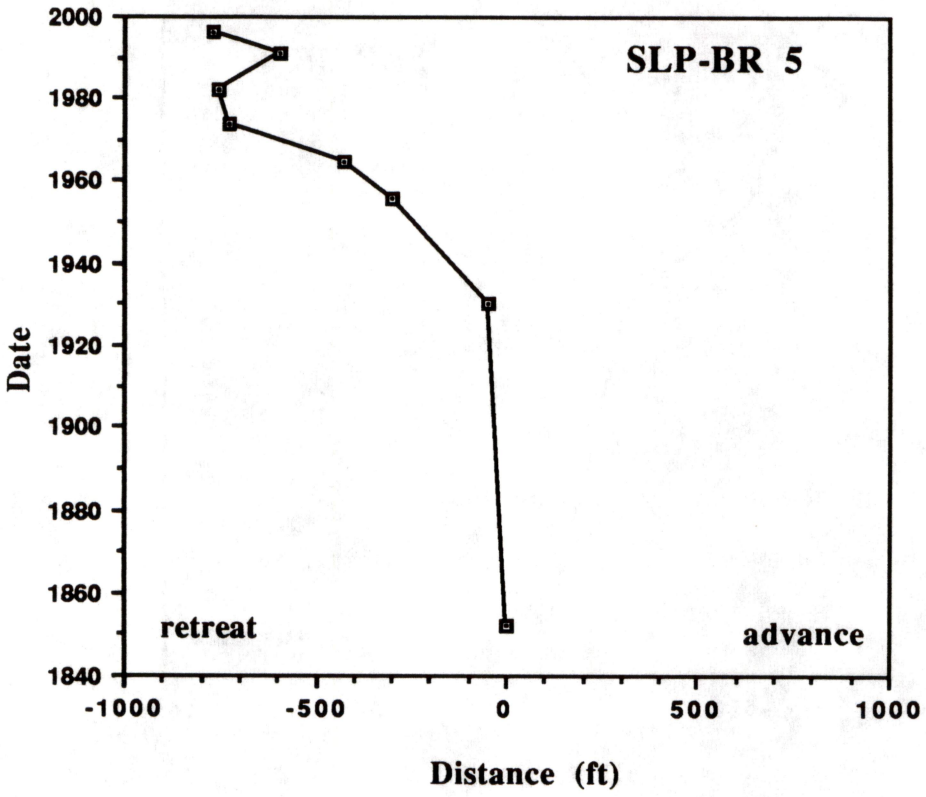
SLP-BR 5
Date
2000
1980
1960
1940
1920
1900
1880
1860
1840
retreat
advance
-1000
-500
0
500
1000
Distance (ft)

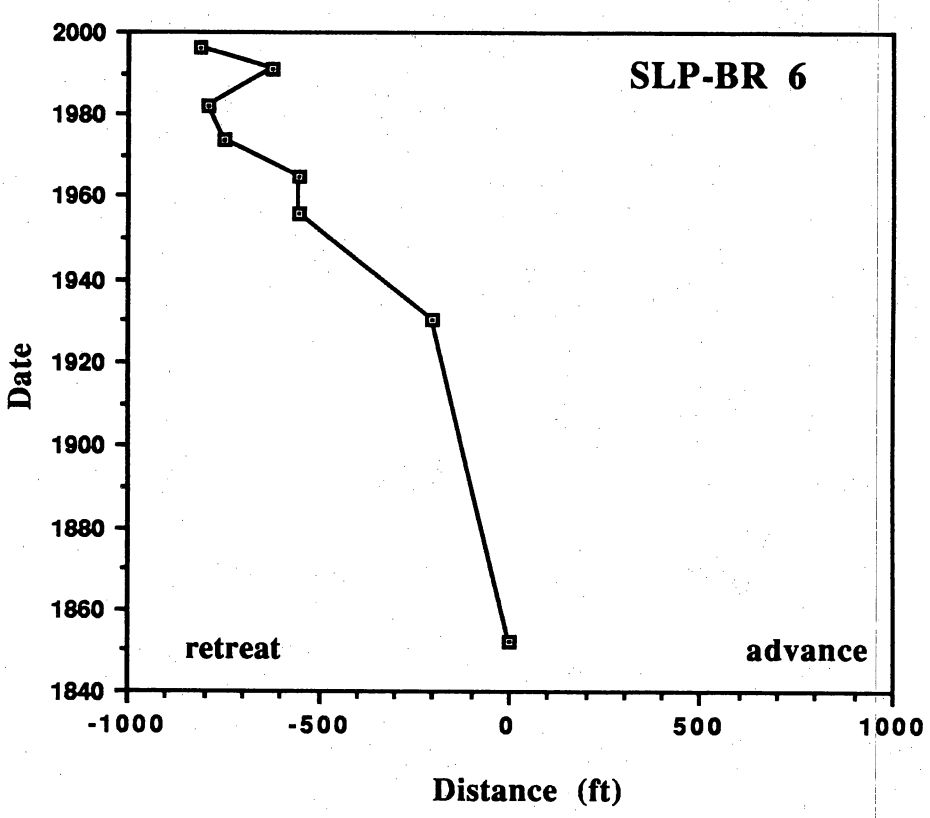
SLP-BR 6
Date
2000
1980
1960
1940
1920
1900
1880
1860
1840
retreat
advance
-1000
-500
0
500
1000
Distance (ft)

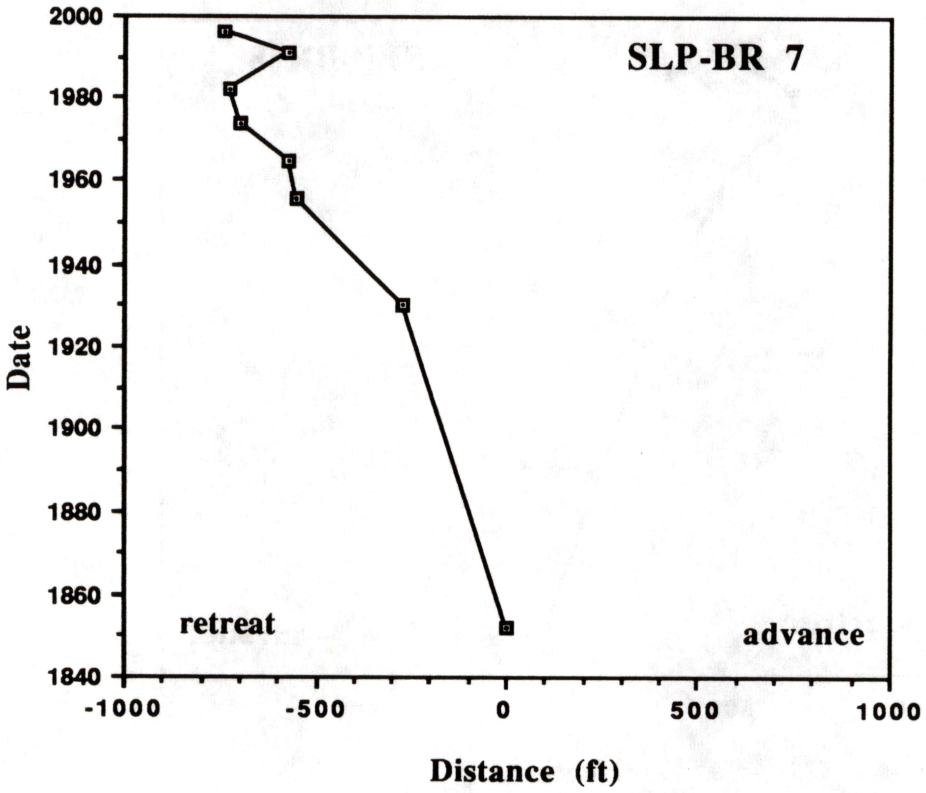
SLP-BR 7
Date
2000
1980
1960
1940
1920
1900
1880
1860
1840
retreat
advance
-1000
-500
0
500
1000
Distance (ft)

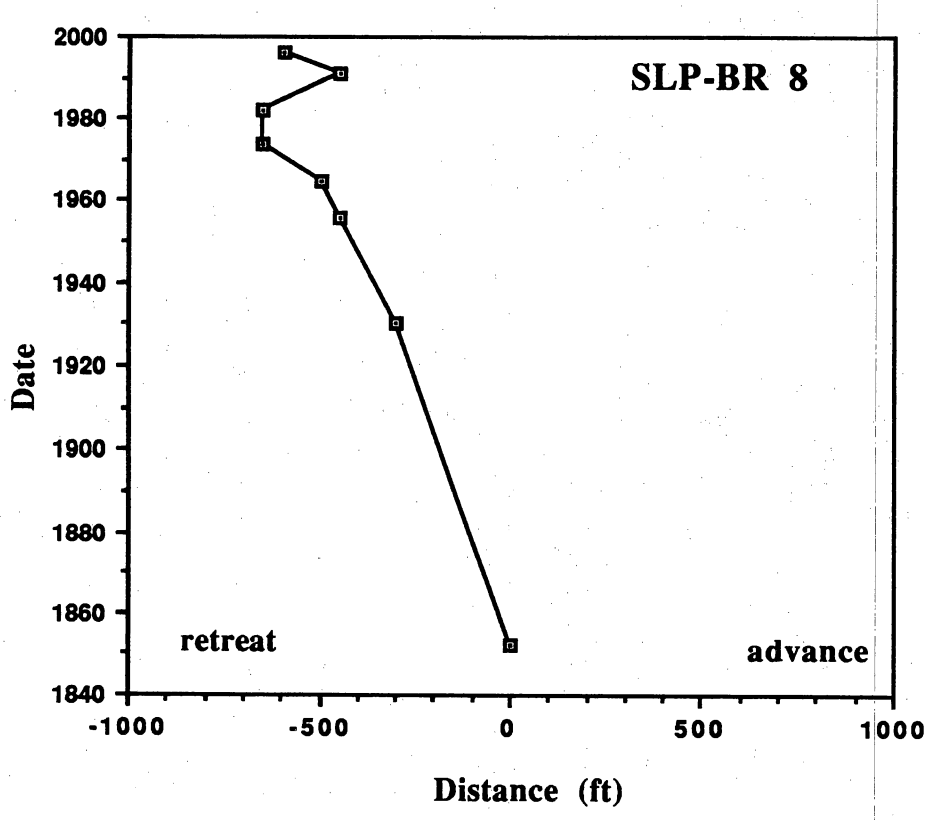
SLP-BR 8
2000
1980
1960
1940
1920
1900
1880
1860
1840
Date
retreat
advance
-1000
-500
0
500
1000
Distance (ft)

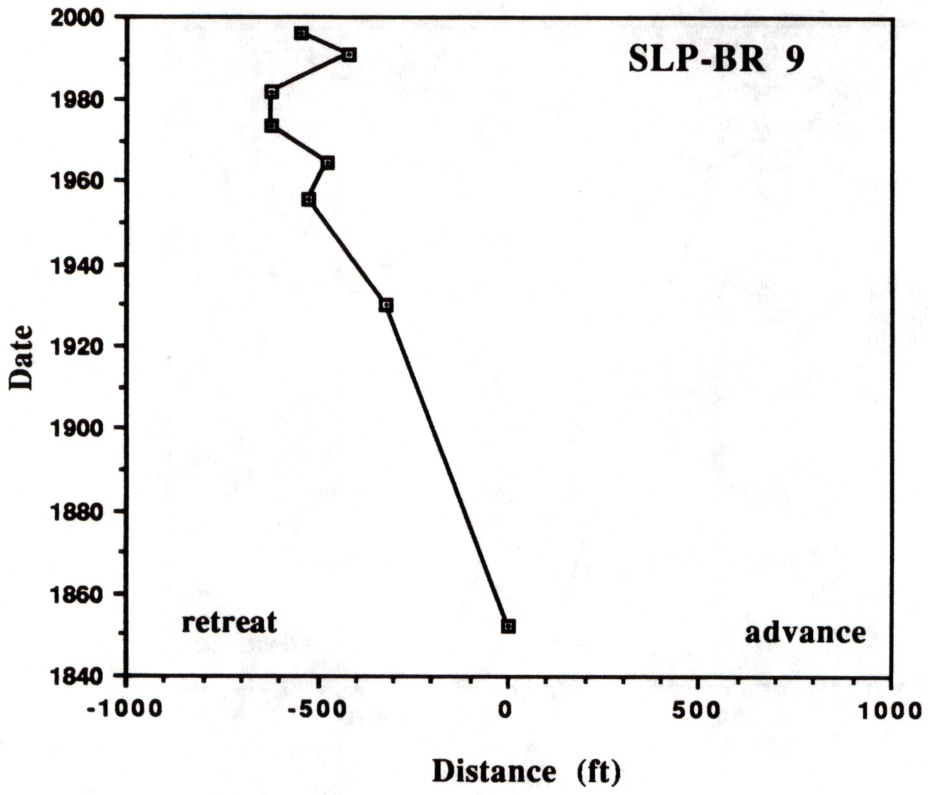
SLP-BR 9
Date
2000
1980
1960
1940
1920
1900
1880
1860
1840
retreat
advance
-1000
-500
0
500
1000
Distance (ft)

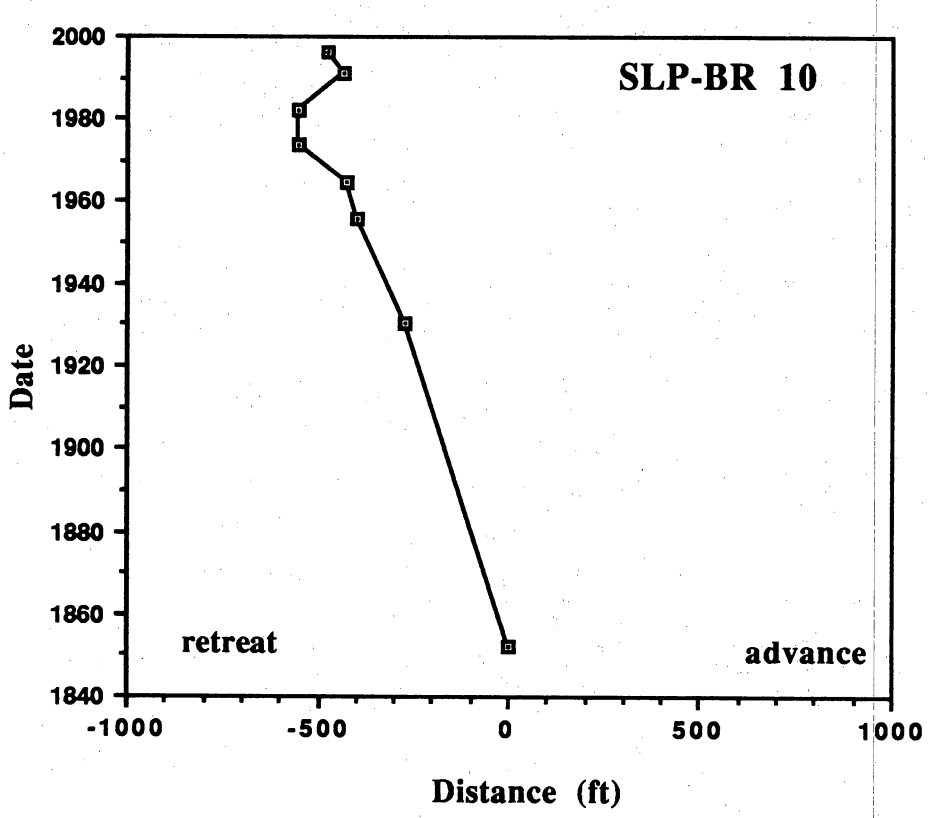
SLP-BR 10
2000
1980
1960
1940
1920
1900
1880
1860
1840
Date
retreat
advance
-1000
-500
0
500
1000
Distance (ft)

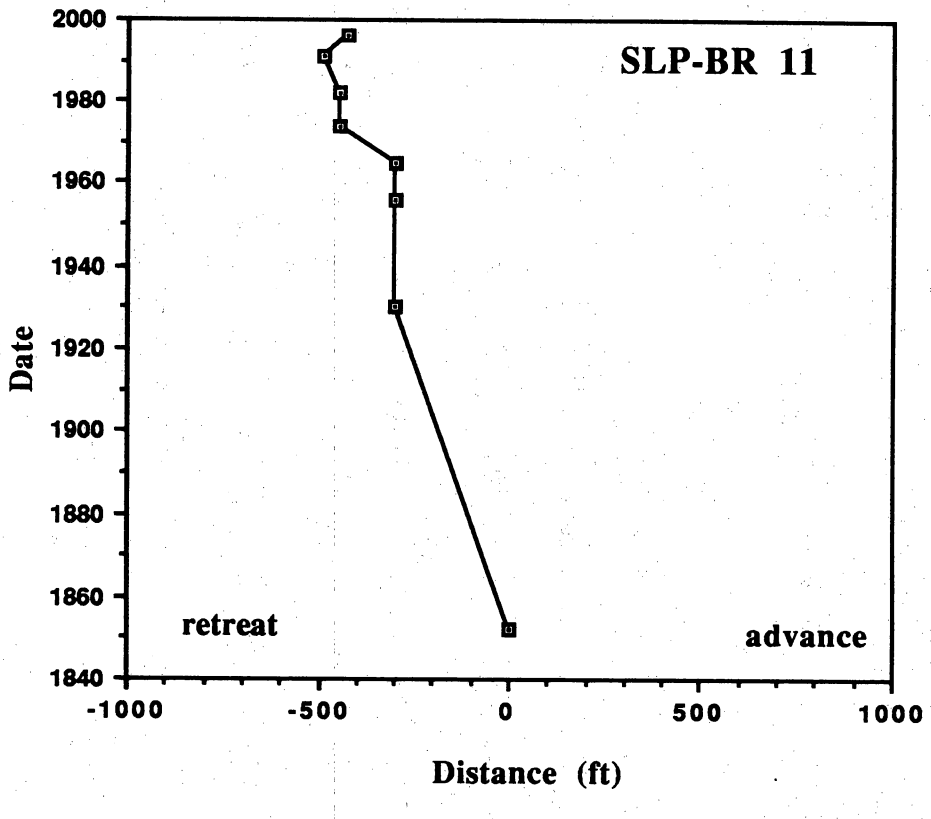
SLP-BR 11
Date
2000
1980
1960
1940
1920
1900
1880
1860
1840
retreat
advance
-1000
-500
0
500
1000
Distance (ft)

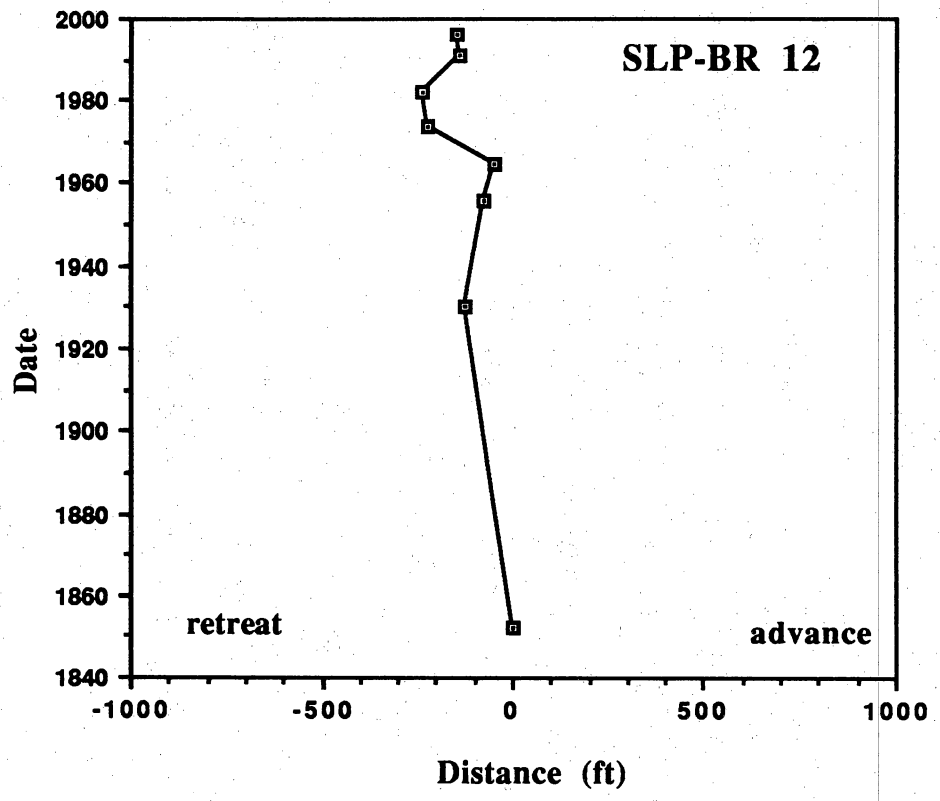
SLP-BR 12
Date
2000
1980
1960
1940
1920
1900
1880
1860
1840
retreat
advance
-1000
-500
0
500
1000
Distance (ft)

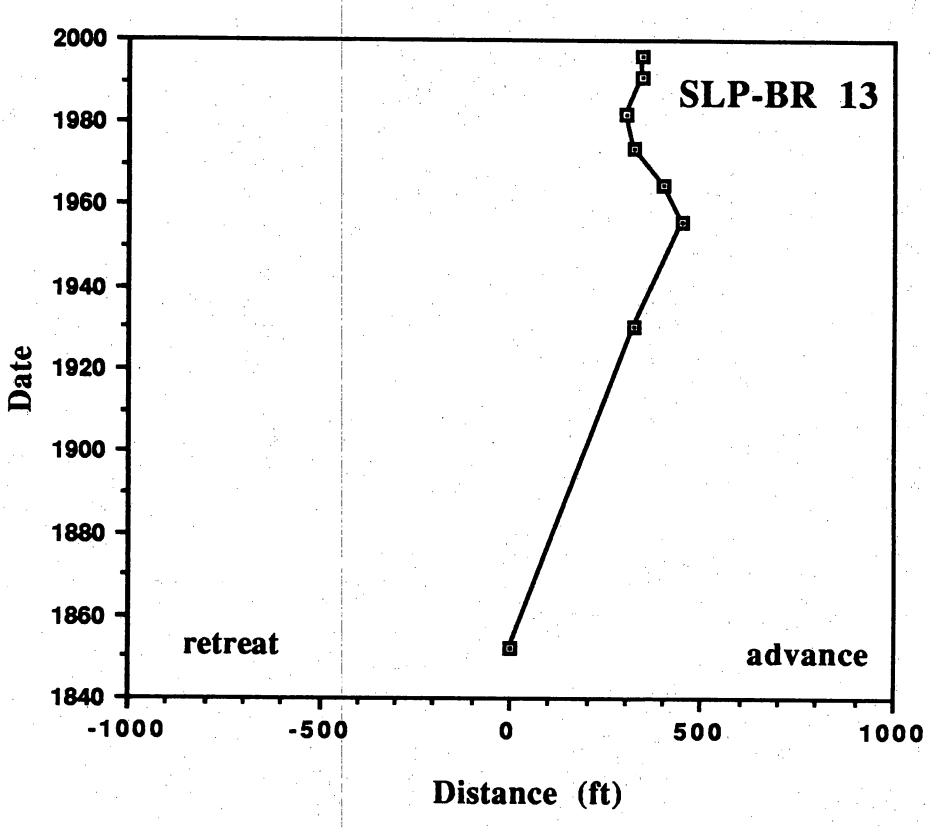
SLP-BR 13
Date
2000
1980
1960
1940
1920
1900
1880
1860
1840
retreat
advance
-1000
-500
0
500
1000
Distance (ft)

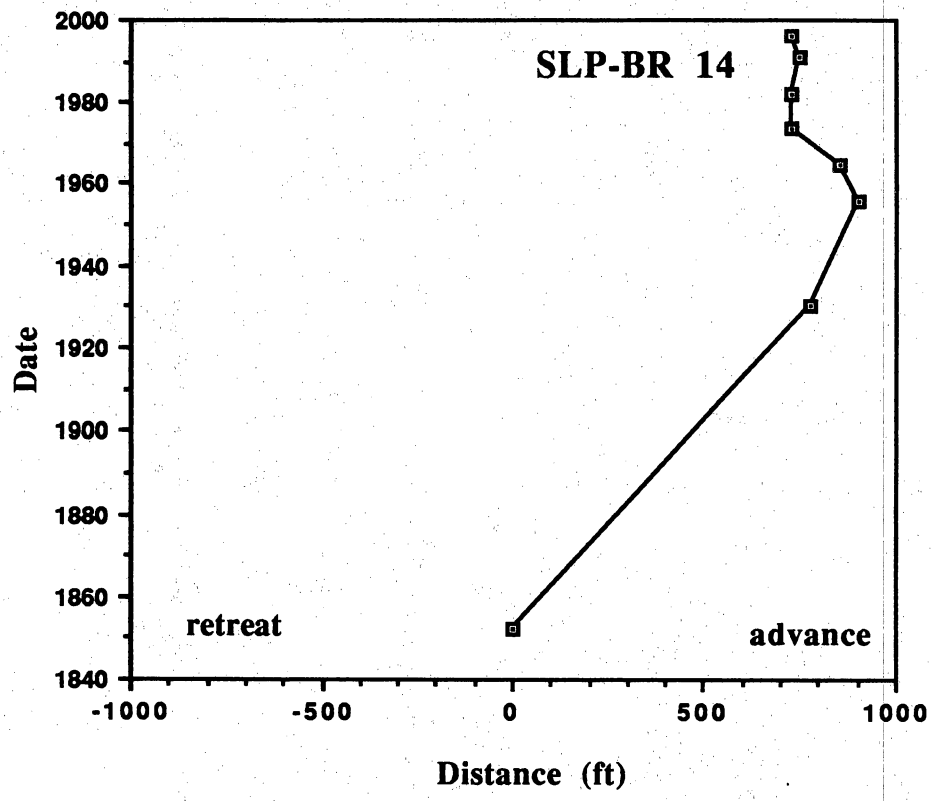
SLP-BR 14
2000
1980
1960
1940
1920
1900
1880
1860
1840
Date
retreat
advance
-1000
-500
0
500
1000
Distance (ft)

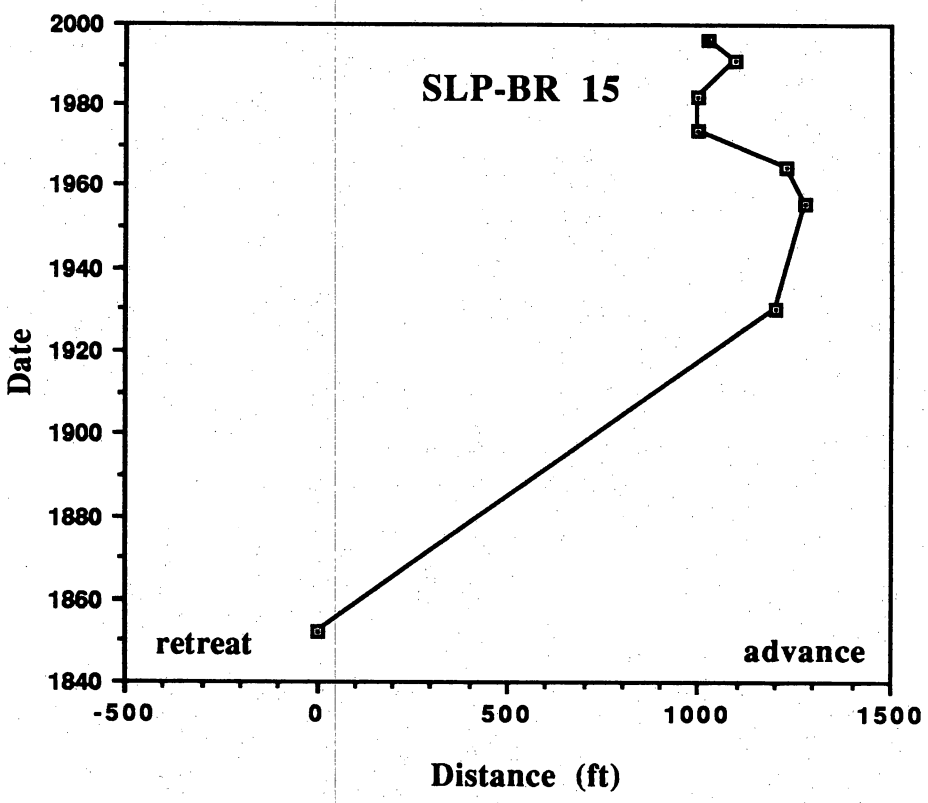
SLP-BR 15
2000
1980
1960
1940
1920
1900
1880
1860
1840
Date
retreat
advance
-500
0
500
1000
1500
Distance (ft)

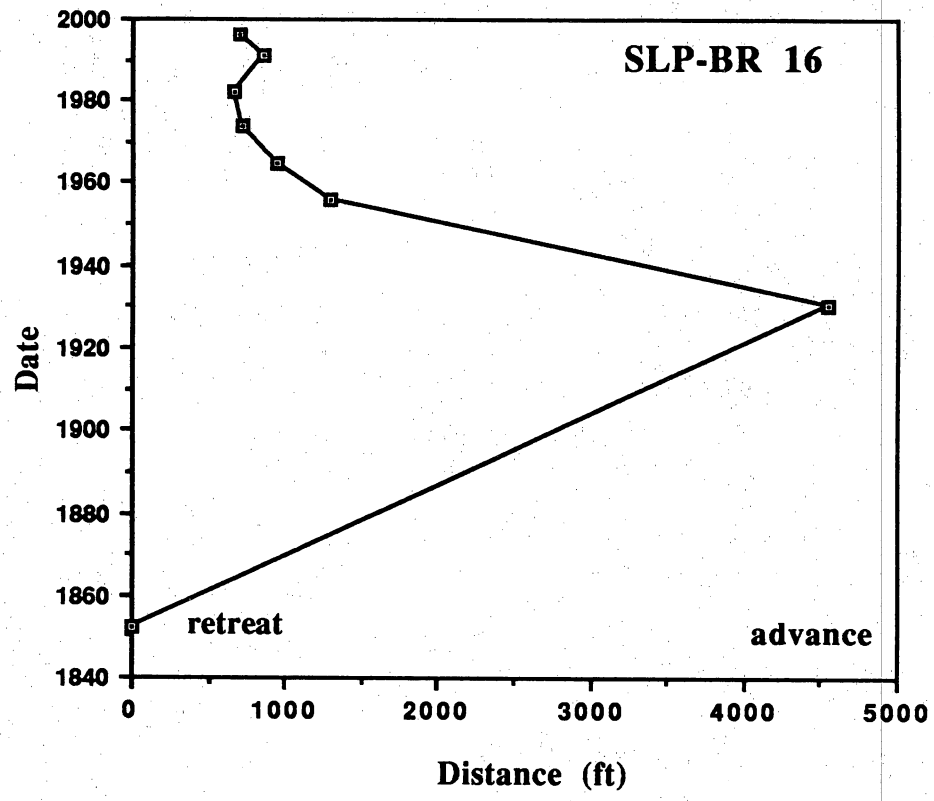
SLP-BR 16
2000
1980
1960
1940
1920
1900
1880
1860
1840
Date
retreat
advance
0
1000
2000
3000
4000
5000
Distance (ft)

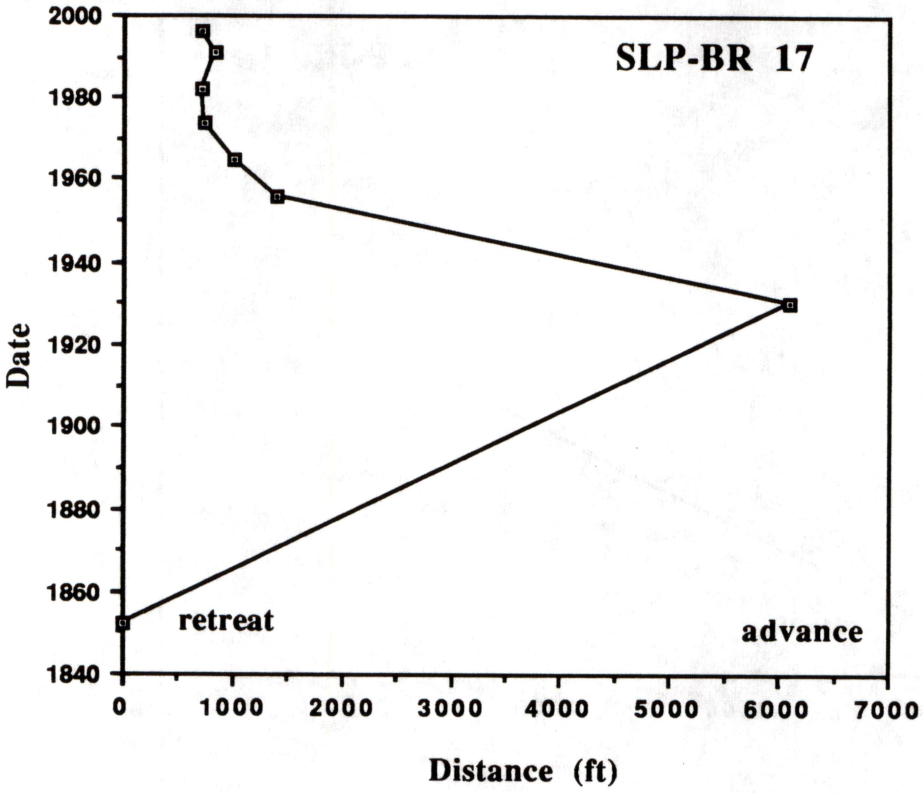
SLP-BR 17
Date
2000
1980
1960
1940
1920
1900
1880
1860
1840
retreat
advance
0
1000
2000
3000
4000
5000
6000
7000
Distance (ft)

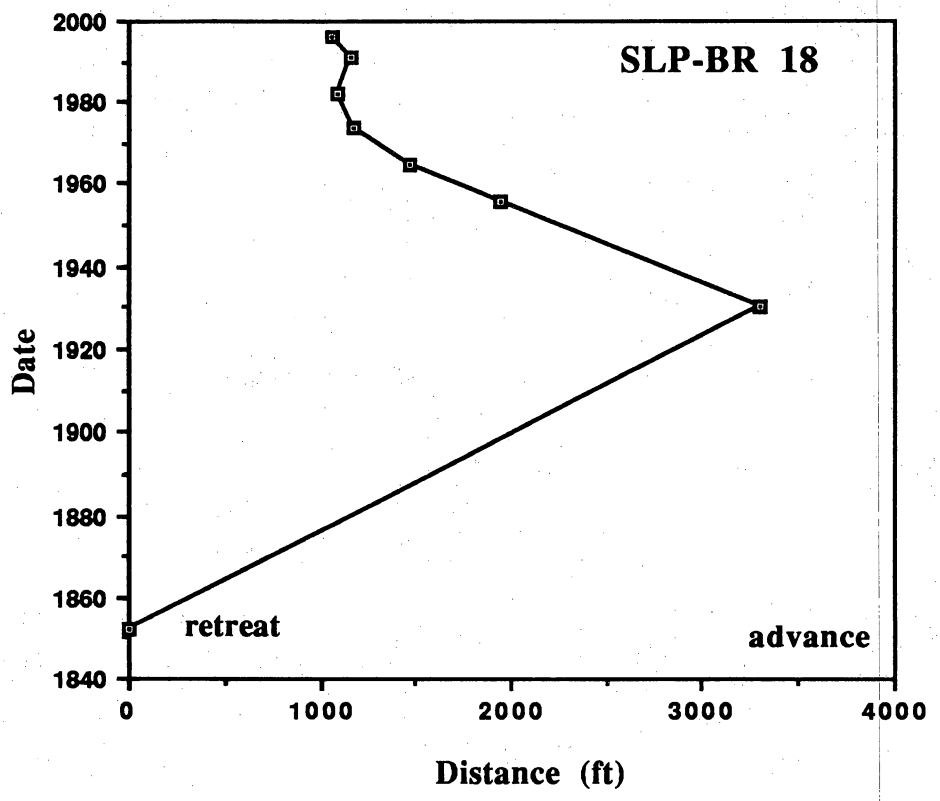
SLP-BR 18
2000
1980
1960
1940
1920
1900
1880
1860
1840
Date
retreat
advance
0
1000
2000
3000
4000
Distance (ft)

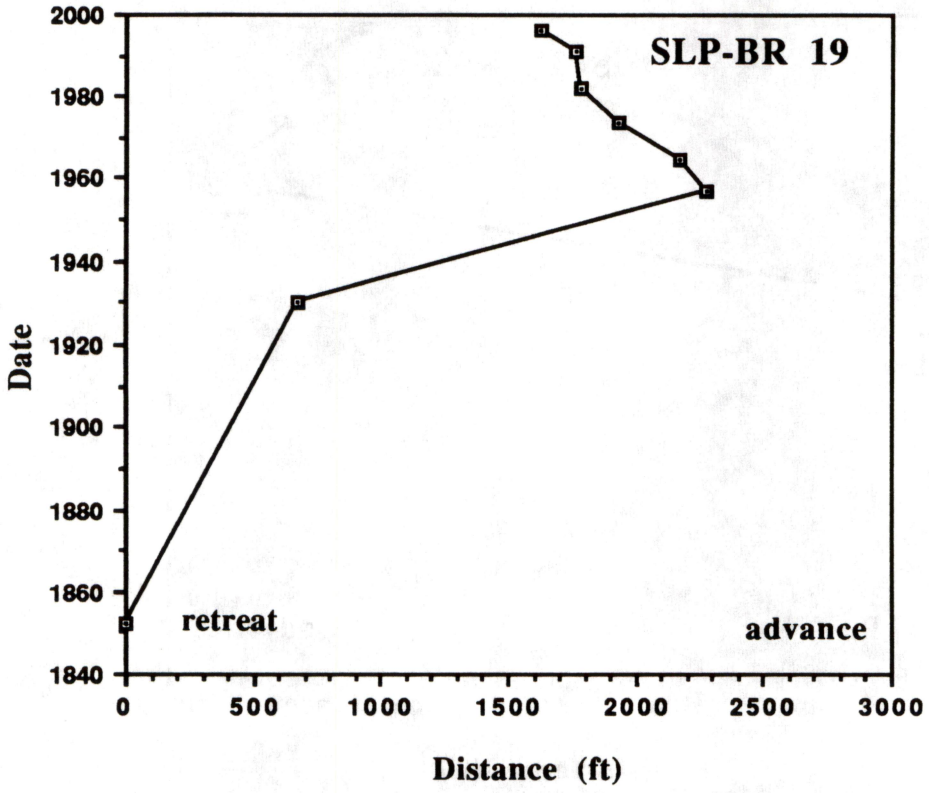
SLP-BR 19
Date
2000
1980
1960
1940
1920
1900
1880
1860
1840
retreat
advance
0
500
1000
1500
2000
2500
3000
Distance (ft)

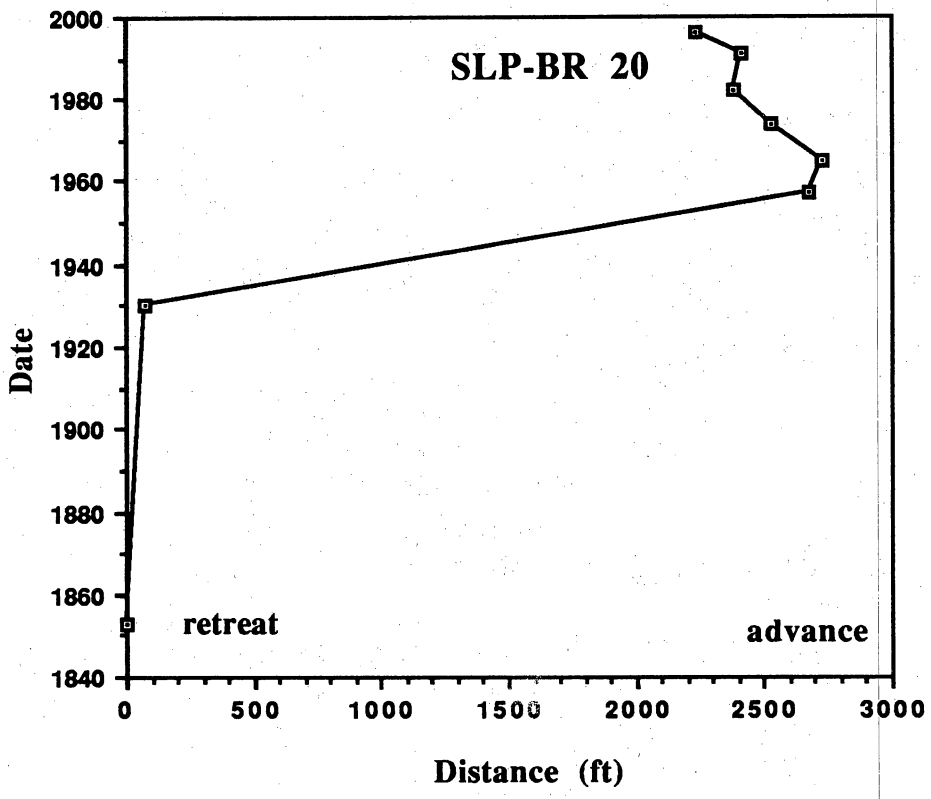
SLP-BR 20
2000
1980
1960
1940
1920
1900
1880
1860
1840
Date
retreat
advance
0
500
1000
1500
2000
2500
3000
Distance (ft)

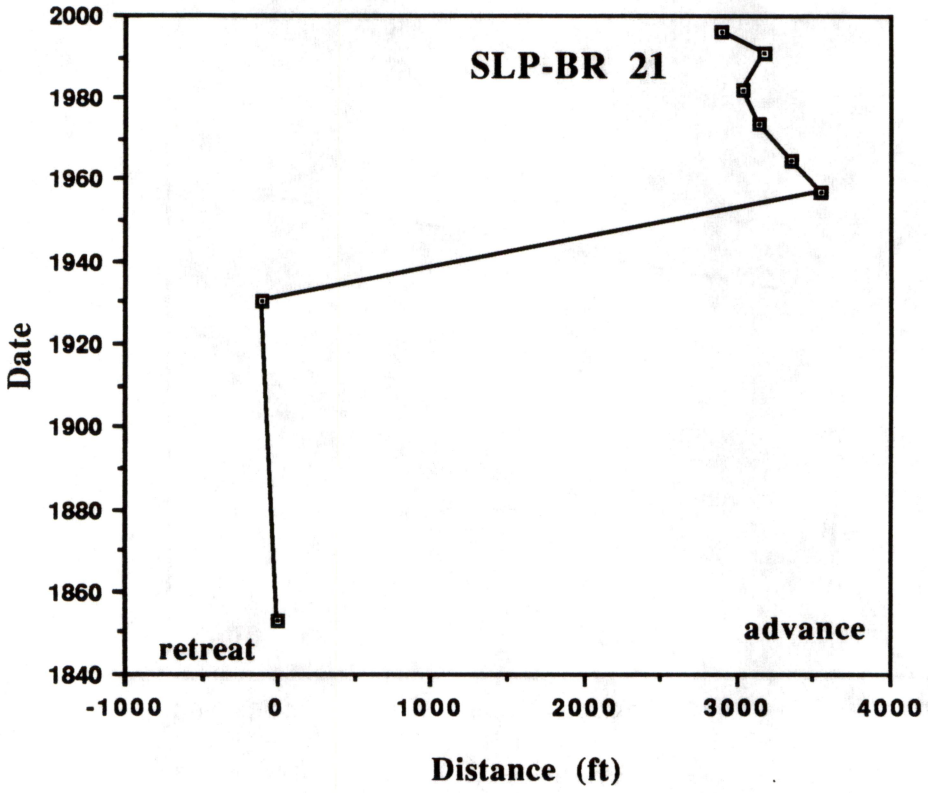
SLP-BR 21
2000
1980
1960
1940
1920
1900
1880
1860
1840
Date
-1000
0
1000
2000
3000
4000
Distance (ft)
retreat
advance

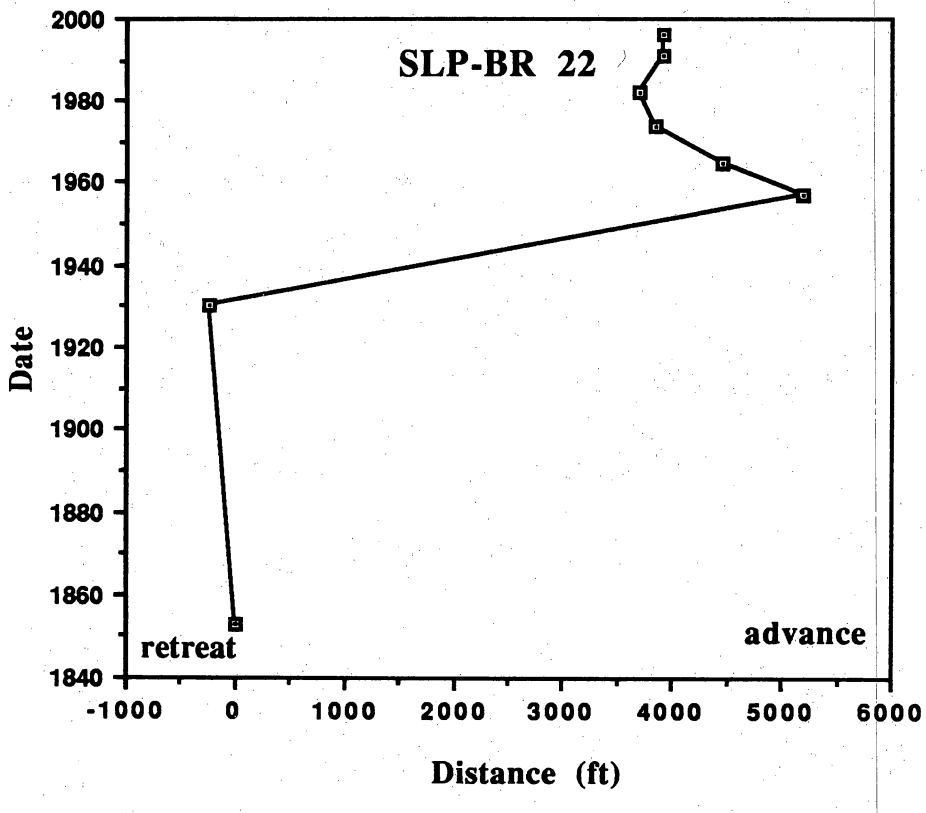
SLP-BR 22
Date
2000
1980
1960
1940
1920
1900
1880
1860
1840
retreat
advance
-1000
0
1000
2000
3000
4000
5000
6000
Distance (ft)

Addendum 2

Comparison of ^{210}Pb-Derived Sedimentation Rates in Differing Fluvial-Deltaic Settings, Texas Gulf Coast

COMPARISON OF ^{210}PB-DERIVED SEDIMENTATION RATES IN DIFFERING FLUVIAL-DELTAIC SETTINGS, TEXAS GULF COAST

William A. White and Robert A. Morton

Bureau of Economic Geology
The University of Texas at Austin
University Station Box X
Austin, TX 78713

ABSTRACT

Continuing submergence of fluvial-deltaic marshes near the mouths of Texas coastal rivers emphasizes the need to examine in detail the processes that establish and maintain, as well as degrade, these biologically productive environments. Among major processes affecting wetland losses are rates of sediment accumulation. Using a simple ^{210}Pb-dating model that assumes a constant flux of unsupported ^{210}Pb and a constant rate of sedimentation, we determined sedimentation rates in cores from three Texas fluvial-deltaic systems (Trinity, Lavaca-Navidad, and Nueces Rivers), each separated by approximately one degree of latitude. Average rates of river valley sedimentation decreased southwestward from 0.37 cm/yr in the Trinity, 0.24 cm/yr for the Lavaca-Navidad, to 0.18 cm/yr in the Nueces. Sedimentation rates correlate positively with a number of parameters that define the differing fluvial-deltaic settings, including size of coastal drainage basin, average rainfall, suspended sediment load, thickness of Holocene mud, rates of relative sea-level rise, and rates of wetland loss. There is some evidence that upstream reservoirs have reduced sedimentation rates, which are being outpaced by rates of relative sea-level rise, suggesting that marshes will continue to be lost as a result of submergence and erosion.

INTRODUCTION

Replacement of wetlands by water and barren flats in the lower alluvial valleys and deltas of major rivers in Texas suggests that relative sea-level rise and reductions in sediment supply have rendered the fluvial-deltaic systems incapable of maintaining sufficient elevation to prevent submergence (White and Calnan, 1991). From the 1950s to 1980s more than 2,000 ha of wetlands were lost along the Trinity, Lavaca-Navidad, and Nueces rivers. Losses were most extensive along the Trinity River, followed by the Lavaca-Navidad, and Nueces Rivers. Each river system has in the past transported a significant load of suspended sediment with the Trinity maintaining the largest load (Longley, 1992). The construction of upstream dams and reservoirs has greatly reduced the volume of sediment reaching deltaic marshes and other wetland habitats. Reductions in sediment supply and

high rates of subsidence are important factors contributing to wetland loss. Still, there remains a potential for the various rivers to deliver enough sediment to offset subsidence and submergence of wetlands.

This paper synthesizes the results of three different studies (White and Morton, 1993, 1995, and 1996) designed to determine past rates of sedimentation for fluvially dominated areas near river deltas along the Texas coast. Analysis of sedimentation rates in conjunction with rates of relative sea-level rise and river sediment load helps to quantify major processes that affect wetland resources in fluvial-deltaic settings. The paper focuses on the relationship between average sedimentation rates and various parameters, such as precipitation, basin size, stream sediment load, tidal levels, thickness of Holocene mud fill, wetland losses, relative sea-level rise, and elevation, i.e., parameters that help characterize fluvial-deltaic systems.

SETTING OF STUDY AREAS

Although the three fluvial-deltaic systems investigated are situated on the Gulf coastal plain, they are each separated by approximately 1 degree of latitude and occupy different climatological settings (Fig. 1). Average rainfall decreases southwestward along the coast, from the Trinity valley to the Nueces valley. Natural environments of the deltas and alluvial valleys consist of salt, brackish, and fresh marshes; transitional areas; flats; open water (including lakes and abandoned river channels); fluvial woodlands, and uplands (White et al., 1983, 1985, and 1989). These habitats have developed on alluvial valley fill within the entrenched valleys. Inland parts of the alluvial valley are dominated by fluvial processes in contrast to deltaic areas where estuarine processes are more influential. Brackish water marshes are dominant in the Trinity River delta whereas salt and brackish marshes characterize the Lavaca-Navidad and Nueces River deltas. In inland reaches of the study areas, fresh water marshes are present. Bay water salinities increase down the coast, reflecting decreasing precipitation and increasing evapotranspiration.

The floodplain hydrologies of all three alluvial valleys have been modified by human structures. Embankments associated with highways and railroads partition each of the valleys, and reservoirs have been constructed in each of the drainage basins. Fresh water impoundments nearest the coast (Fig. 1) include Lake Livingston along the Trinity constructed in 1969, Lake Texana on the Navidad constructed in 1980, and Lake Corpus Christi on the Nueces, initially constructed in 1929 and enlarged in 1958. Dramatic reductions in suspended sediment along the Trinity and Nueces Rivers have been documented below Lake Livingston (Fig. 2) and Lake Corpus Christi (Liebbrand, 1987).

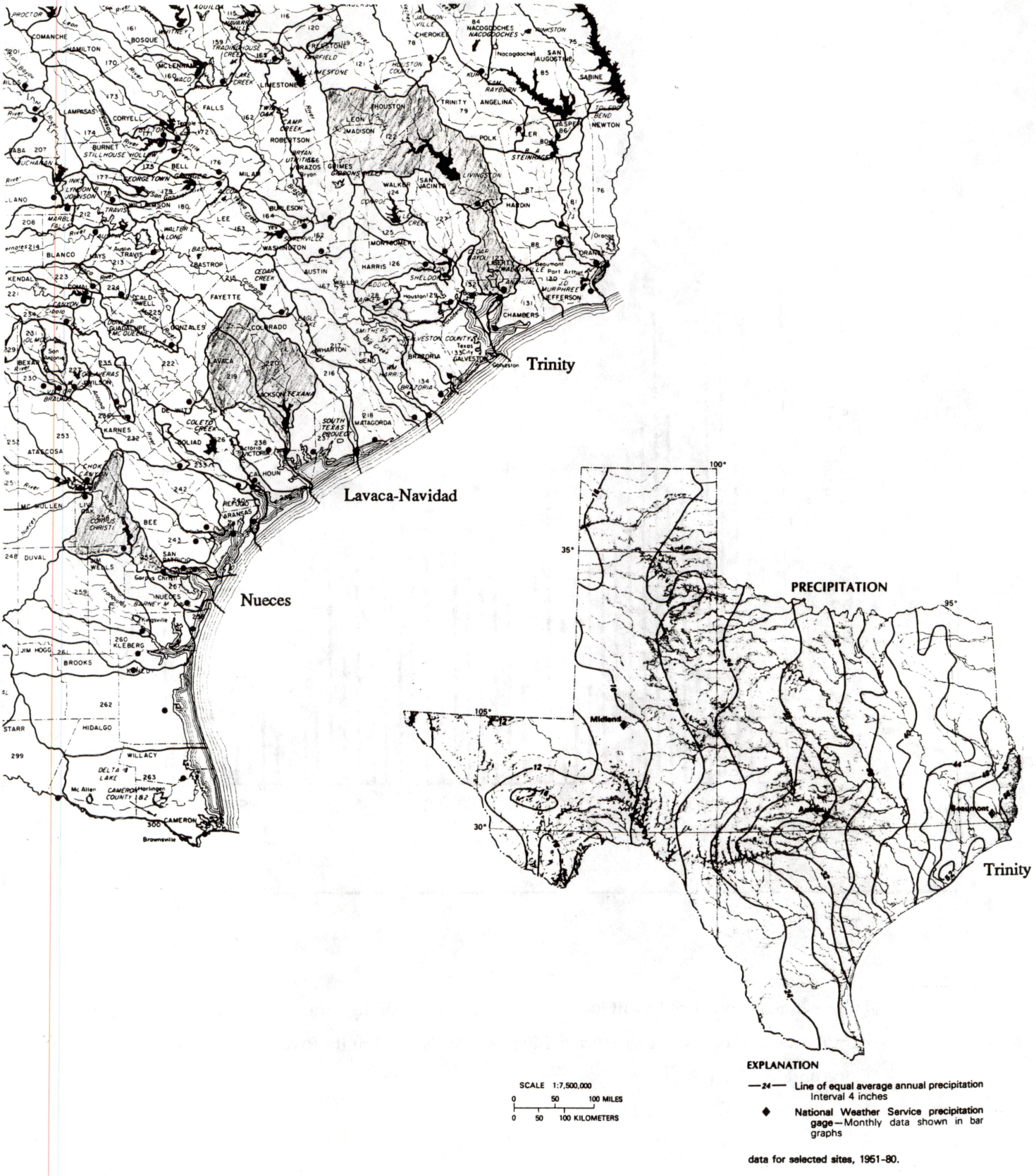

Figure 1. Annual precipitation and sizes of coastal drainage basins for the Trinity, Lavaca-Navidad, and Nueces River systems. Annual precipitation map from USGS (1986), and coastal drainage basins from Greiner (1982).

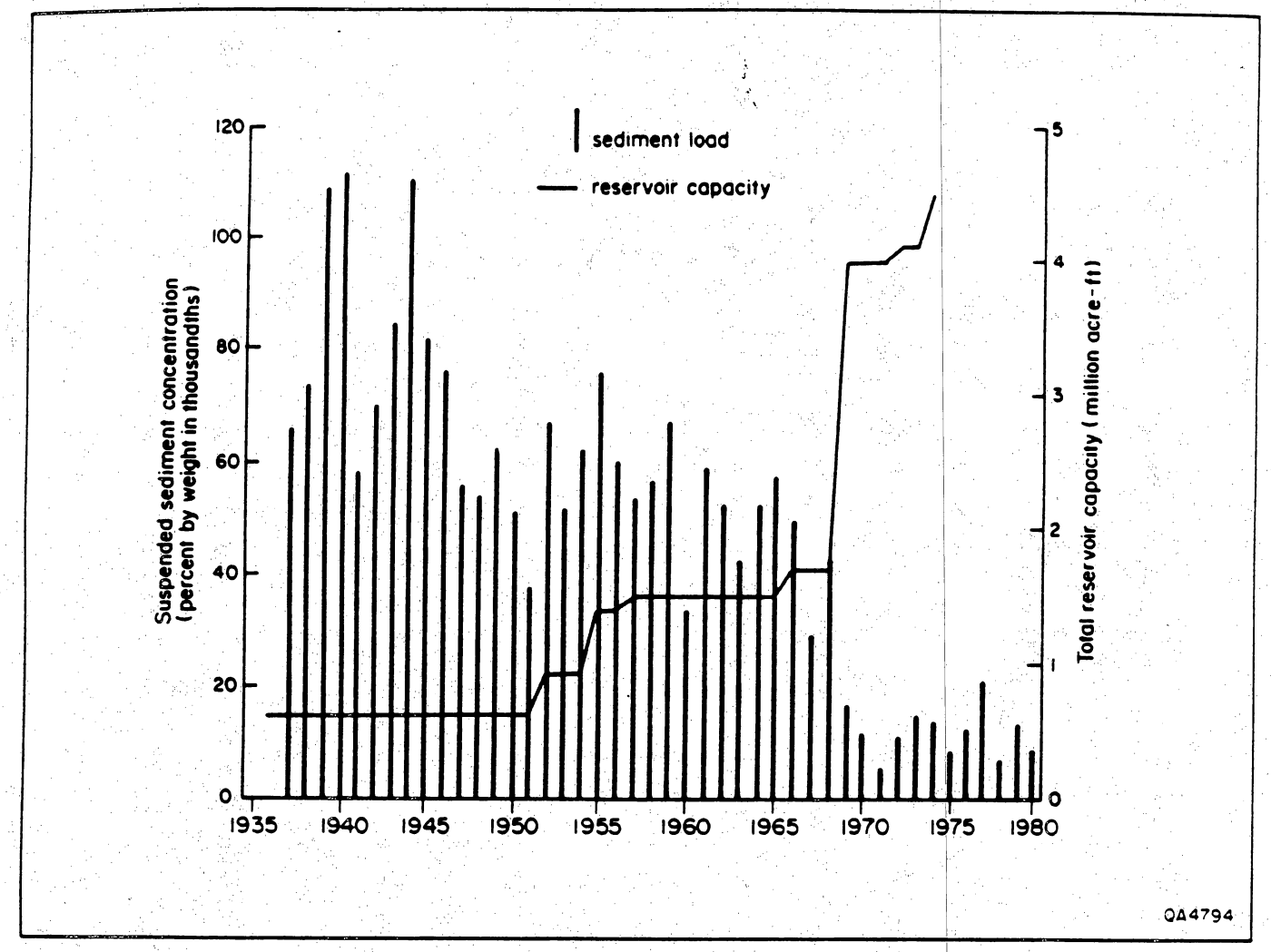

Figure 2. Suspended-sediment load (percent by weight) of the Trinity River at Romayor, and cumulative authorized water storage in reservoirs of the Trinity River basin (entire). From Paine and Morton (1986).

METHODS

^{210}Pb Dating Theory

Sedimentation rates were determined through analysis of ^{210}Pb activities in shallow cores. ^{210}Pb is a naturally occurring radioactive isotope in the uranium 238 (^{238}U) series (Robbins, 1978). It has been used by numerous researchers to determine dates and sedimentation rates in various settings including lakes, continental shelf, and wetlands (Koide et al., 1973; Robbins, 1978; Armentano and Woodwell, 1975; Nittrouer et al., 1979; Smith and Walton, 1980; McCaffrey and Thomson, 1980; Church et al., 1981; Oldfield and Appleby, 1984; Sharma et al., 1987; DeLaune et al., 1987; Bricker-Urso et al., 1989; Allen et al., 1993; and Kearney et al., 1994). A half life of 22.2 years makes ^{210}Pb a useful "tool" in dating sediments deposited during the past 100 to 150 years. Robbins (1978) and Oldfield and Appleby (1984) provide comprehensive discussions of ^{210}Pb and its applications.

Use of ^{210}Pb for dating purposes is based on its assumed constant atmospheric concentration and subsequent accumulation in sediments at the earth's surface. Radium-226 (^{226}Ra) in the earth's crust decays into radon gas (^{222}Rn), some of which escapes into the atmosphere and decays through a series of short lived isotopes to ^{210}Pb. ^{210}Pb is removed from the atmosphere by precipitation and dry sedimentation and is sorbed by sediment particles at the earth's surface. This atmospheric addition of ^{210}Pb is designated as "excess" or "unsupported", in contrast to "supported" ^{210}Pb, which is a decay product of, and assumed to be in equilibrium with, ^{226}Ra in the sediments. Supported ^{210}Pb remains relatively constant with depth and is sometimes referred to as "background" activity. Excess ^{210}Pb activity in undisturbed sediments decreases exponentially with depth. Excess, or unsupported, ^{210}Pb is determined by subtraction of supported ^{210}Pb from total ^{210}Pb activities.

Inventories of excess ^{210}Pb in the sediment provide the basis for determining dates and accumulation rates using various models or equations. In this investigation, we used the simplest model, which is known as the constant flux:constant sedimentation (CFS) model (Robbins, 1978; Oldfield and Appleby, 1984).

The CFS model assumes a constant rate of flux of ^{210}Pb to the sediment, and a constant rate of sediment accumulation. Sedimentation rates are determined through logarithmic plots of excess ^{210}Pb activity against depth or against cumulative dry mass using the following equation (notations from Oldfield and Appleby, 1984):

$$C=C_{(0)}e^{-km/r}$$

where C is the unsupported ^{210}Pb concentration at any given depth in the sediment, $C_{(0)}$ is the unsupported ^{210}Pb concentration at the sediment water interface, m is the depth or cumulative dry-

mass of the sediment, r is the sedimentation rate, and k is the ^{210}Pb decay constant (0.03114 yr^{-1}). The logarithmic plot of unsupported ^{210}Pb (C) against depth (or cumulative dry mass) will ideally be linear with slope of -k/r and thus, r=-k/slope.

Analytical Methods

Isotopic analyses of core samples were completed under the supervision of Dr. Charles Holmes of the U.S. Geological Survey using procedures developed by the USGS (Holmes and Martin, 1976; Martin and Rice, 1981), which is a modified version of that described by Flynn (1968). The specific activity of ^{210}Pb was measured indirectly by determining the activity of the granddaughter isotope ^{210}Po. In general, samples were analyzed at 1-cm intervals down to a depth of 20 to 21 cm, below which analyses were at 2-cm intervals.

In the Lavaca-Navidad and Nueces fluvial-deltaic systems, supported ^{210}Pb activities were determined by the USGS from analysis of ^{226}Ra, which is the source of supported ^{210}Pb (Robbins, 1978). In the Trinity fluvial-deltaic system, supported ^{210}Pb activities were estimated on a core by core basis by examining a plot of total ^{210}Pb activity against depth. Supported ^{210}Pb was assumed to be equivalent to the lowest activities in a core where the profile of total ^{210}Pb versus depth flattened out as "background," or constant activity, levels were approached, i.e., where unsupported or excess ^{210}Pb is zero.

Selection of Coring Sites

Ten to twelve short cores were taken in each river system. Criteria used in selecting sites included location with respect to the modern river channels and abandoned channels; location with respect to the estuarine system, relative elevations, susceptibility to flooding, and types of wetland vegetation; and location with respect to existing human modifications. The approach was to sample several different wetland environments but avoid local human alterations that may have affected sedimentation rates. Coring sites were located throughout the alluvial valleys with preference given to more inland areas where fluvial processes were dominant (Figs. 3-5). Only core 11 on the Nueces delta (Fig. 5) was taken on the margin of one of the bays.

Coring Methods

Cores of the marsh substrate were taken by twisting and, where necessary, driving a thin-walled, sharpened metal tube, approximately 1 m long and 11.5 cm in diameter. Lengths of sediment recovered varied depending on the difficulty of penetrating the substrate and the amount of shortening.

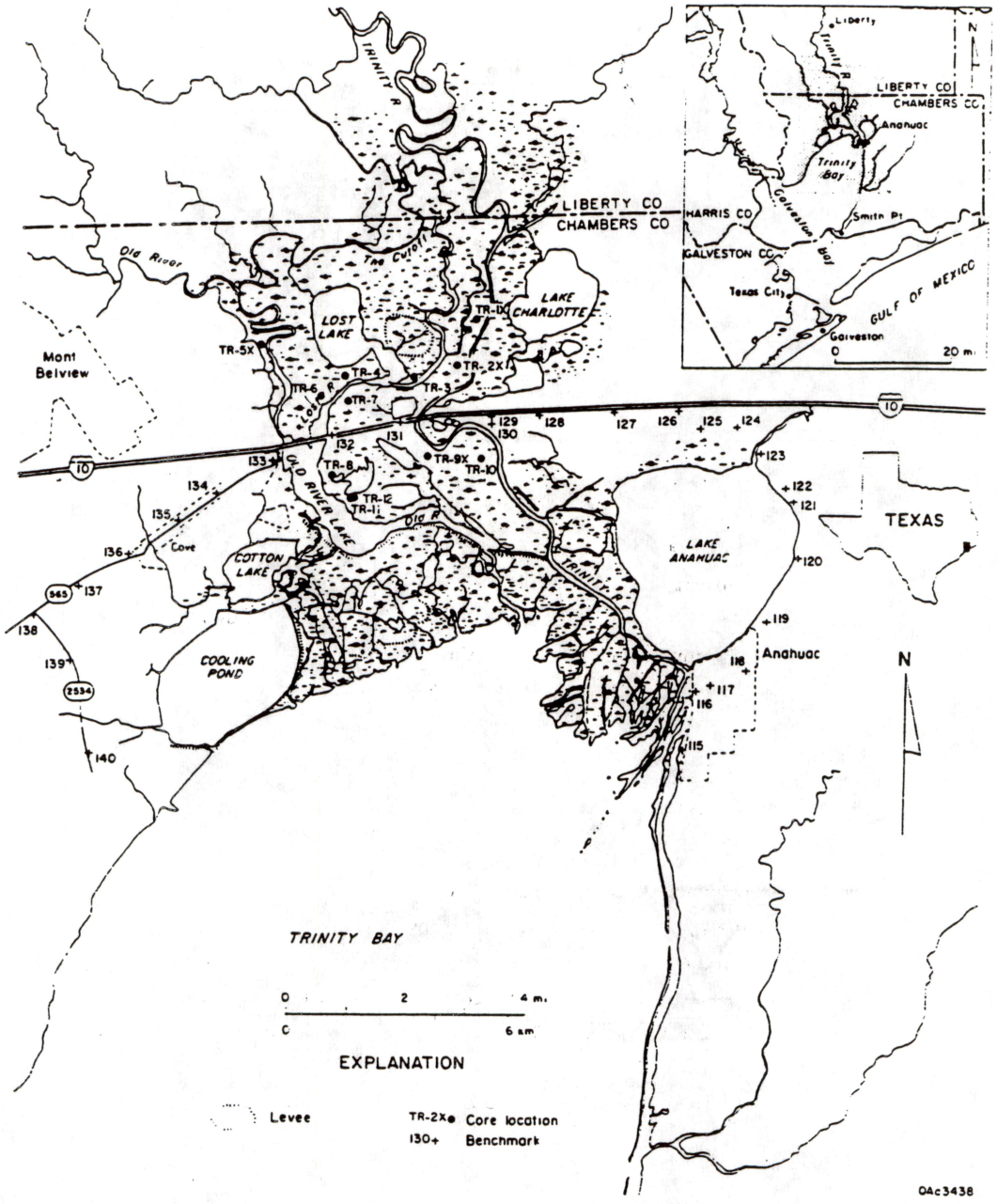

Figure 3. Trinity River fluvial-deltaic system study area showing locations of coring sites and benchmarks.

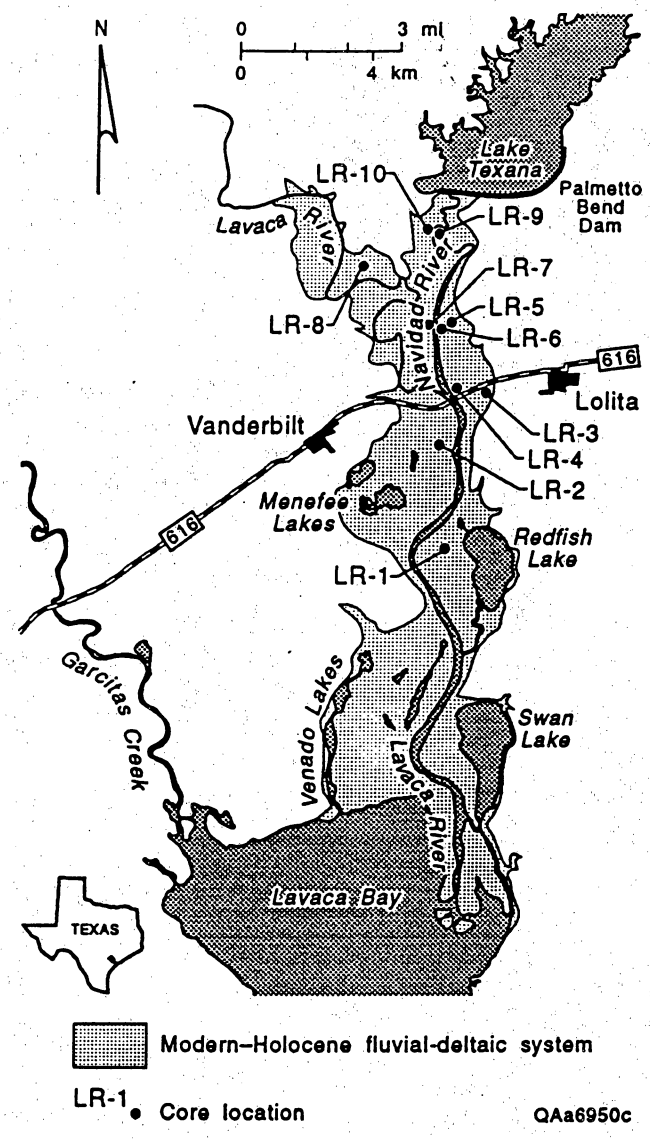

Figure 4. Lavaca-Navidad River fluvial-deltaic system study area showing locations of coring sites.

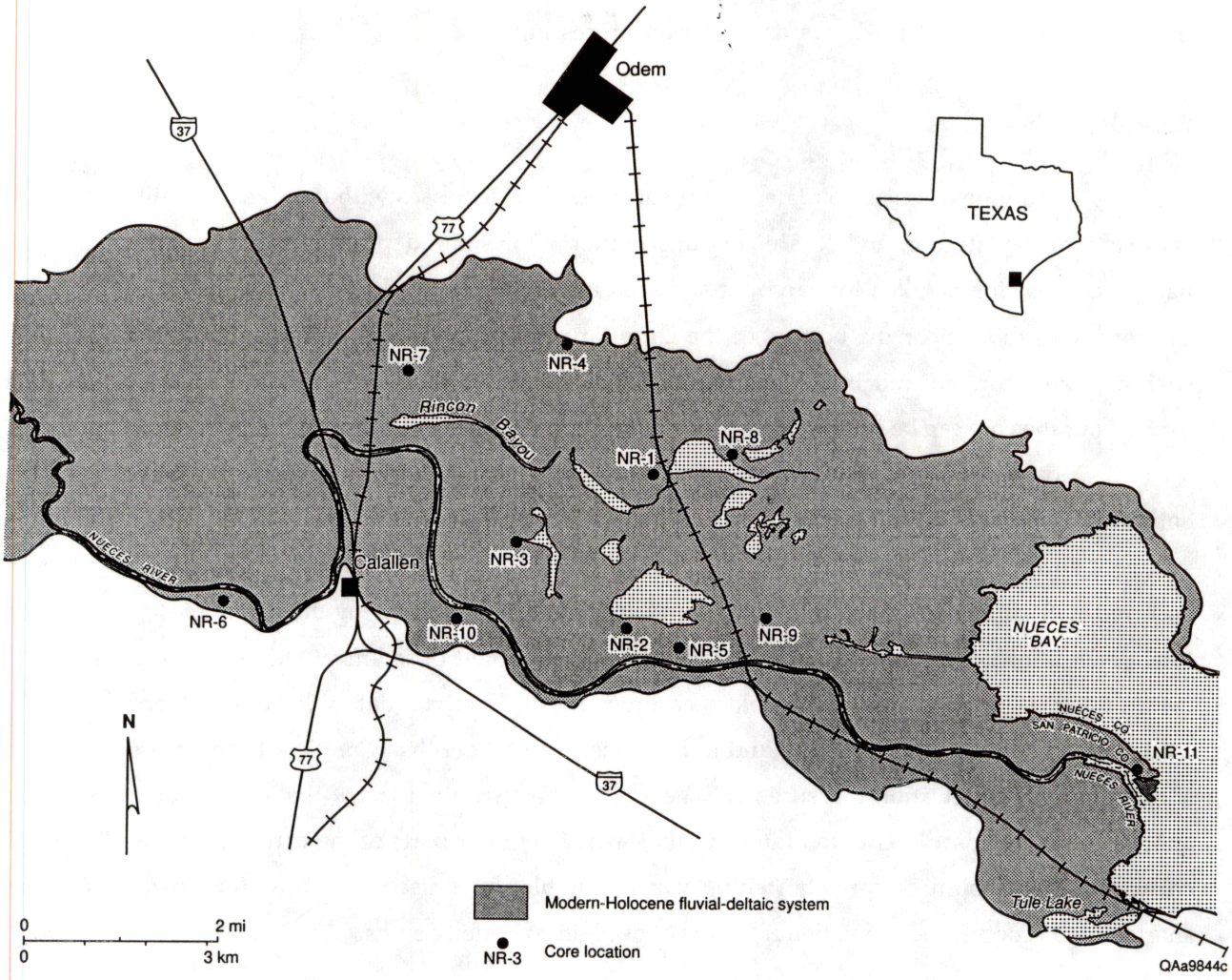

Figure 5. Nueces River fluvial-deltaic system study area showing locations of coring sites.

Some sediment bypassing and thinning occurred in deeper sections of cores where stiff clayey sediments were encountered, especially in transitional area levee-flank environments. Cores were dug out of the marsh soils to minimize loss of material during extraction from the substrate. The end of each core was covered with rubber caps that were tightened down with ring clamps and taped. The cores were transported to the BEG Core Research Center for processing.

Core Shortening

The volume of unconsolidated sediments normally decreases with depth as a result of physical compaction, dewatering, and loss of organic matter. For some depth-dependent relationships, the natural compaction is taken into account and the data are normalized to equate values near the top of the core with those near the bottom of the core. Physical properties affected by natural compaction, such as water content and bulk density, are used to remove the effect of compaction so that data throughout the core can be compared on a postcompaction basis (Morton and White, in press).

Most cores from the three river systems underwent some shortening, most from 1 to 6 cm for the entire core lengths of up to 80 cm. During coring, distance measurements were periodically made to the sediment surface inside and outside of the core barrel to determine the amount of core shortening that occurred with depth. By making these two measurements and by knowing the length of the core barrel, total penetration of the core barrel, and core length, the amount of sediment shortening was calculated (Morton and White, in press). The field measurements and derived data were used to reconstruct the interval thickness before shortening and to calculate restored depths. Core lengths estimated from the shortening and penetration measurements generally agree within 1 cm of the actual core length. For analysis of average sedimentation rates in this paper, the upper parts of the cores, generally the top 20 cm where the amount of core shortening was negligible, were used. In those few instances where shortening did occur, sedimentation rates were based on corrected depths.

Core Preparation and Handling

Cores were split in half by first cutting horizontally down each side of the metal tubes and then by cutting the core in half with a thin wire or band saw. The top section of each core, and in several cases the entire core, was cut with a fine-toothed band saw to limit disturbance of the root-matted zone. The two half cores were then separated, each half retained in the half tube. One half of the core was wrapped in plastic, sealed in an airtight clear plastic liner, and transported to the USGS laboratory in Denver for x-radiography and analysis of ^{210}Pb and ^{226}Ra activity, moisture content, loss on ignition, bulk density, and texture.

The other halves of the cores were archived and retained in the BEG Core Research Center where they were subsampled for other physical and chemical analyses. Each half core was trimmed with an osmotic knife and physically described. Information recorded on core description sheets included core depth, sediment color, sediment type (visual description), nature of contacts, textural trends, sedimentary structures, state of oxidation, and presence of accessories (organic material and caliche nodules). The cores were then photographed to produce large-format color prints and 35-mm slides.

Textural Analysis

Textural analysis were completed for representative samples in a number of cores in the Trinity and Lavaca-Navidad fluvial-deltaic systems, and for all samples in the Nueces system. Samples were analyzed for percent sand, silt, and clay following procedures detailed by Starkey et al. (1984) and Gee and Bauder (1986). In general, disaggregated samples were wet sieved through a 230-mesh sieve to separate particles larger than sand size, >62 μm from silt and clay. The silt and clay fractions were separated using a hydrometer or pipette.

Salinity Analysis

Excess ^{210}Pb activities can be affected by a high salt content (Church et at., 1981). Salinities in the fluvial-deltaic areas increase down the coast from a low in the Trinity River system to a high in the Nueces River system. Total chloride was measured in samples in a selected number of cores in the Lavaca-Navidad and Nueces fluvial-deltaic systems by ion chromatography following Bureau of Economic Geology procedures (Specific Work Instruction 1.15: Determination of anions by ion chromatography). Three samples from each core (top, middle, and bottom) were analyzed. Chlorinity was converted to salinity using a factor of 1.80655 (Duxbury, 1971).

Vegetation Assemblages and Elevations

Prevalent plant species were surveyed at the coring sites in each fluvial-deltaic system. In addition, elevations were estimated from USGS 7.5 minute topographic maps, field observations, and aerial photographs. Because the contour interval on the topographic maps is 5 feet, estimates of elevation must be considered as gross approximations (Fig. 6).

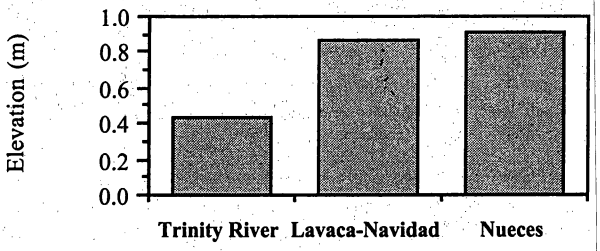

Figure 6. Estimated average elevations of coring sites in the Trinity, Lavaca-Navidad, and Nueces fluvial-deltaic systems.

Trinity River Fluvial-Deltaic System

In the Trinity River fluvial-deltaic system, coring sites varied from brackish-water marshes characterized in some areas by Spartina patens, to fresh-water marshes characterized at one site by Zizaniopsis miliacea. The most abundant plant at coring sites was Alternanthera philoxeroides. It was the dominant species at about half of the coring sites and was part of the vegetation community at 9 of the 12 sites. Sites were located in low and high marshes. Estimated elevations range from greater than 0.6 m to less than 0.3 m. Coring site TR-1X had the highest estimated elevation, and TR-5X the lowest. Levee flank sites (TR-1X, TR-2X, TR-9X, and TR-10) were generally in high-marsh environments and were the most difficult to core because clay stiffness greatly increased with depth. Low marshes, which were composed predominantly of Alternanthera philoxeroides or Zizaniopsis miliacea, were less consolidated and easier to core.

Lavaca-Navidad River Fluvial-Deltaic System

In the Lavaca-Navidad fluvial-deltaic system, coring sites included brackish-water marshes characterized by an assemblage of Distichlis spicata, Paspalum vaginatum, and Juncus romerianus, fresh-water marshes dominated by Zizaniopsis miliacea, transitional areas with virtually homogeneous stands of Spartina spartinae, transitional areas with mixtures of short grasses including Cynodon dactylon and unidentified composites, and fluvial woodlands with abundant Sabal minor. Estimated elevations ranged from greater than 1.5 m to less than 0.45 m. Coring site LR-8 had the highest estimated elevation, and sites LR-2, LR-3, and LR-6 the lowest. Sites in transitional areas (LR-4, LR-5, LR-7, LR-8 and LR-10) were generally at higher elevations, and were the most difficult to

core because of increasing stiffness of clay with depth. Low marshes were composed predominantly of Scirpus californicus, Zizaniopsis miliacea, and Distichlis-Paspalum.

Nueces River Fluvial-Deltaic System

In the Nueces River fluvial-deltaic system, coring sites included salt-water marshes characterized by assemblages of Spartina alterniflora and Salicornia-monanthochloe-Suaeda; brackish-water marshes characterized by Spartina spartinae, Borrichia frutescens, and Distichlis spicata; and fresh to brackish assemblages of Scirpus californicus, Typha, Scirpus maritimus, and Eleocharis sp. Estimated elevations range from approximately 1.2 m to less than 0.3 m. Coring sites NR-1 and NR-7 had the highest estimated elevations, and site NR-11 had the lowest. Sites in high marshes and transitional areas, were characterized by Spartina spartinae and Borrichia frutescens. Low marshes were composed predominantly of Spartina alterniflora, Scirpus californicus, Typha, and Distichlis spicata.

RESULTS AND DISCUSSION

Sediment in cores consisted primarily of homogeneous mud (silt and clay), but sand was abundant in some sediment samples, especially in the Lavaca-Navidad fluvial-deltaic system. Textural variations can influence excess ^{210}Pb activity. Activity levels are higher in finer sediments, apparently because Pb, like many other metals, is sequestered by fine-grained particles such as clay minerals, organic matter, and Fe-Mn oxides (Nittrouer et al., 1979). Because analytical methods differed somewhat in the three study areas, we had to normalize sediment samples using textural composition in order to compare ^{210}Pb activities among river systems. In the Nueces system, core samples were separated by texture before isotopic analysis, and only the mud fractions (silt and clay, or particles <62 μm in size) were analyzed for ^{210}Pb activity. Sediments in cores of the Trinity River were predominantly mud with minimal sand content. Of 59 samples analyzed in three cores from the Trinity River system, the average sand content was less than 5 percent, the remainder of the sediment consisting of mud (silt and clay). Thus, we concluded that analysis of ^{210}Pb was effectively of the mud fraction in Trinity River core samples. However, in some Lavaca-Navidad cores, sand was relatively abundant, ranging from 15 to 56 percent in one core. In order to be consistent with analyses of the fines in the other two fluvial-deltaic systems, ^{210}Pb activities in the Lavaca-Navidad system were calculated on a sand-free basis before sedimentation rates were determined.

Mean bay water salinities adjacent to the fluvial-deltaic systems was another variable among the three study areas. Salinities increase from a low of 8.95 ppt in Trinity Bay, to 13.17 ppt in Lavaca

Bay, to 21.49 ppt in Nueces Bay (Fig. 7) (Diener, 1975). Marsh assemblages in the fluvial-deltaic systems mirror this trend, with the most saline marshes occurring in the Nueces system and least saline marshes occurring in the Trinity system. On the basis of several chlorinity analyses, however, we concluded that the salt content did not significantly affect unsupported ^{210}Pb activities and sedimentation rates (Church et al., 1981). ^{210}Pb activities were calculated on a salt-free basis in several cores from the Nueces fluvial-deltaic system, which had the highest measured salinities (ranging from 0.3 to 4 percent salt in upper 12 cm of sediment). Sedimentation rates determined on a salt-free basis, were generally not significantly different from rates calculated without considering the effect of salt.

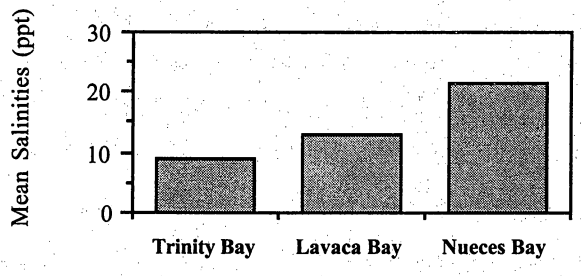

Figure 7. Mean salinities of the bay water in which the fluvial-deltaic systems have prograded. From Diener (1975).

Because sediment bulk densities were not adequately measured in the Trinity fluvial-deltaic system, we decided to compare sedimentation rates among the three systems on a relative basis, without accounting for possible compaction of sediments. Furthermore, linear trends of ^{210}Pb activity plotted against depth for only the upper part of the cores were used in a piece-wise fashion (Brugam, 1978, for example). Log normal plots of excess ^{210}Pb against depth show linear trends with depths for at least some measurable section in most cores (Figs. 8-10). However, in the Trinity River system most excess ^{210}Pb profiles leveled off in the top few centimeters. We attributed this relatively uniform ^{210}Pb activity in near surface layers (Fig. 8) to a zone of bioturbation and mixing of sediments (Nittrouer et al., 1979). Bioturbation was most extensive in Trinity River cores, affecting the upper 2 to 5 cm of sediments. In the Lavaca-Navidad and Nueces River cores, distinct evidence of bioturbation was not apparent in either X-rays or cores examined in reflected light. Below the root zones, cores appear to be homogeneous and profiles of excess ^{210}Pb against depth show that activities generally decline in a relatively linear fashion to depths of about 10 to <30 cm, below which there is a flattening of the profile for most cores. When possible, cores were taken at sites with no evidence of surface

disturbance such as burrows and cattle trails. However, effects of cattle and deer tracks were difficult to avoid in some areas because grazing is widespread in marsh areas.

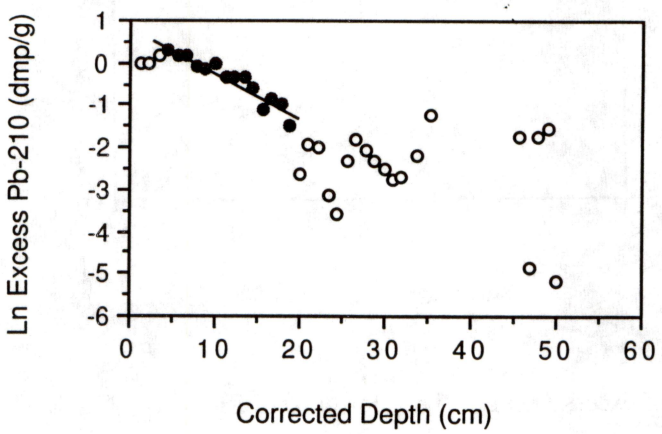

Figure 8 Log normal plot of excess ^{210}Pb activity for Trinity River core TRX-1. Linear segment used to determine sediment rate shown by straight line. Depressed activities in top 4 cm is attributed to bioturbation, and were excluded from the regression analysis.

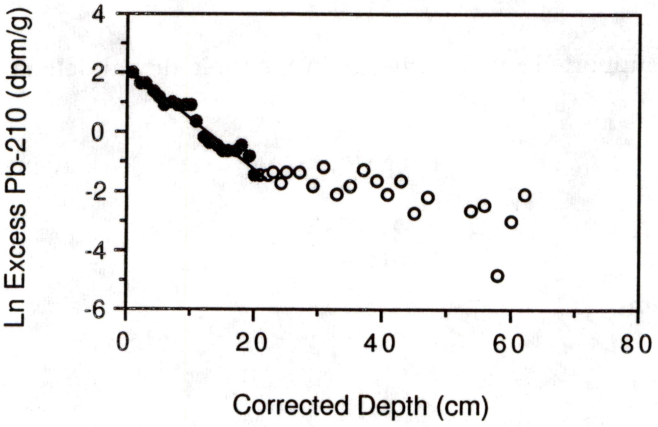

Figure 9. Log normal plot of excess ^{210}Pb activity for Lavaca-Navidad River core LR-3. Linear segment used to determine sedimentation rate shown by dark circles and line of regression.

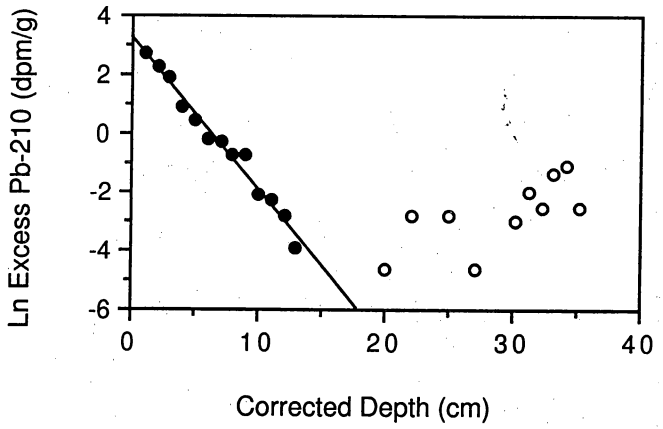

Figure 10. Log normal plot of excess ^{210}Pb activity for Nueces River core NR-1. Linear segment used to determine sedimentation rate shown by dark circles and line of regression.

The range in supported ^{210}Pb activities in the Trinity, Lavaca-Navidad, and Nueces River fluvial-deltaic systems were 0.5 to 1.0 dpm/g, 0.5 to 0.8 dpm/g, and 0.9 to 1.6 dpm/g, respectively (Table 1). The higher supported activities in the Nueces River fluvial-deltaic system may be partly related to the location of South Texas uranium deposits in the Nueces River drainage basin, and to analysis of only the fine fraction in Nueces River sediments. Sand may have slightly diluted the concentrations of supported ^{210}Pb in Lavaca-Navidad sediments for example.

Table 1. Range and average supported ^{210}Pb activities in the three fluvial-deltaic systems

Fluvial-Deltaic System	Range (dpm/g)	Average (dpm/g)
Trinity River System	0.5 - 1.0	0.7
Lavaca-Navidad River System	0.5 - 0.8	0.6
Nueces River System	0.9 - 1.6	1.1

Sedimentation Rates

Vertical accretion rates derived from the CFS model show that the highest average rates occurred in the Trinity River fluvial-deltaic system, followed by the Lavaca-Navidad and Nueces. Average rates were 0.37 cm/yr in the Trinity, 0.24 cm/yr in the Lavaca-Navidad, and 0.18 cm/yr in the

Nueces (Fig. 11). Rates in the Trinity River ranged from a high of 0.62 cm/yr at core site TR-7 to a low of 0.22 cm/yr at core site TR-9X (Table 2; Fig. 12). Because bioturbation was common in the upper few cm of each core from the Trinity River system, the linear plot below this zone was used to determine sedimentation rates (Fig. 8). In the Lavaca-Navidad fluvial-deltaic system, rates ranged from 0.49 cm/yr to 0.13 cm/yr (Table 3; Fig. 13), and in the Nueces system, from 0.45 cm/yr to 0.06 cm/yr (Table 4; Fig 14). It should be noted that core NR-11 in the Nueces River delta was not included in the average for the Nueces River system (Fig. 11) because it was collected on the edge of Nueces Bay in a tidally influenced estuarine marsh. This location is substantially different from all other core locations in the three study sites, which were taken more than 3 km inland from the bay shorelines (Figs. 3-5).

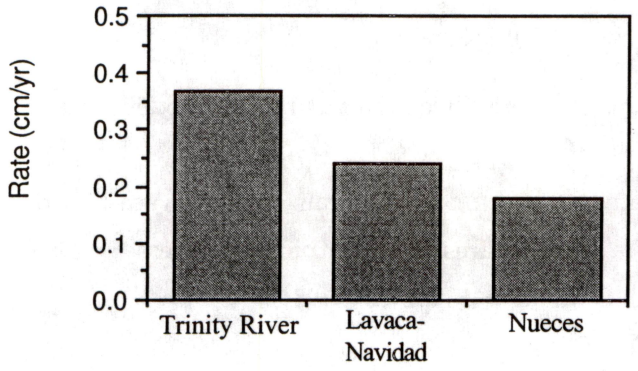

Figure 11. Average sedimentation rates determined in cores using the CFS model.

Table 2. Average sedimentation rates for given core intervals in the Trinity River fluvial-deltaic system. Rates are based on a least-squares fit of Ln plots of excess ^{210}Pb against corrected depths (CFS model, Oldfield and Appleby, 1984).

Core Number	CFS rate (cm/yr)	Corrected Depth (cm)	R^2	Supported ^{210}Pb (dpm/g)	Anomalies excluded
TR-1X	0.28	4-19	0.921	0.80	
TR-2X	0.26	5-30	0.877	0.90	
TR-3	0.26	4-15	0.849	1.00	
TR-5X	0.42	2-21	0.804	0.50	
TR-6	0.32	6-20	0.929	0.60	
TR-7	0.62	6-21	0.809	0.60	
TR-8	0.32	2-17	0.880	0.60	
TR-9X	0.22	2-18	0.945	1.00	2
TR-10	0.50	1-21	0.930	0.60	1
TR-11	0.47	11-27	0.735	0.60	

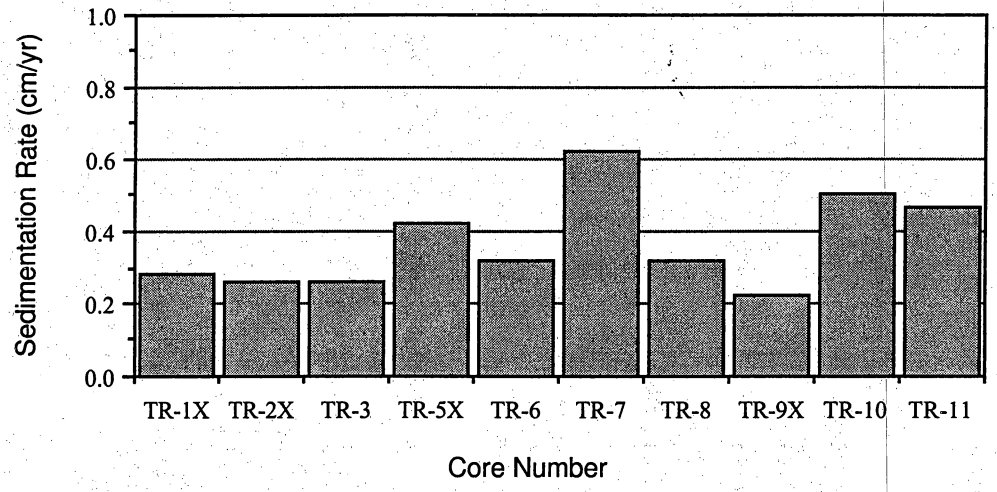

Figure 12. Average sedimentation rates of Trinity River cores using CFS model (table 2).

Table 3. Average sedimentation rates for given core intervals in the Lavaca-Navidad River fluvial-deltaic system. Rates are based on a least-squares fit of Ln plots of excess ^{210}Pb (sand-free basis) against corrected depths (CFS model, Oldfield and Appleby, 1984).

Core Number.	CFS Rate (cm/yr)	Corrected depth (cm)	R^2	Supported ^{210}Pb (dpm/g)
LR-1	0.18	1-14	0.988	0.67
LR-2	0.33	1-32	0.931	0.79
LR-3	0.19	1-20	0.948	0.77
LR-4	0.10	1-14	0.965	0.45
LR-5	0.13	1-20	0.836	0.50
LR-6	0.32	1-24	0.773	0.56
LR-7	0.24	1-25	0.968	0.56
LR-8	0.26	1-24	0.881	0.55
LR-9	0.49	1-30	0.776	0.65
LR-10	0.19	1-19	0.844	0.65

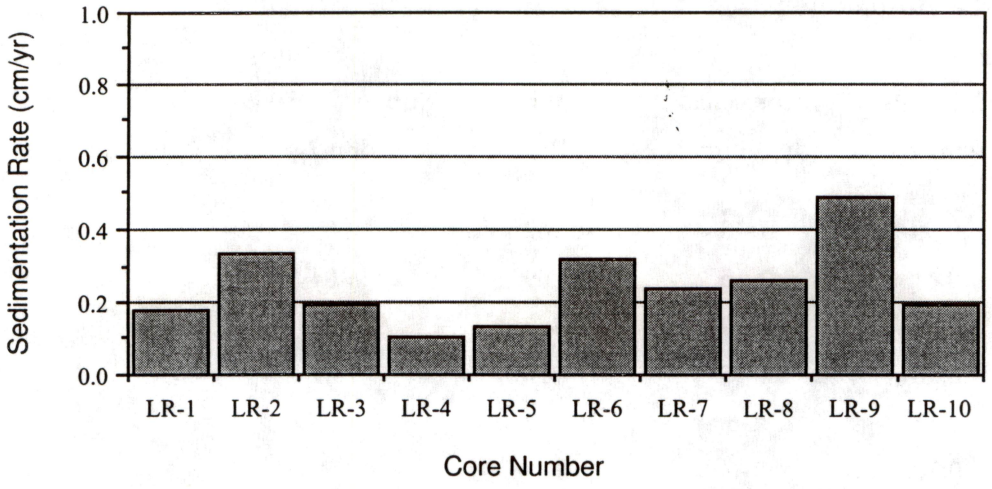

Figure 13. Average sedimentation rates of Lavaca River cores using CFS model (table 3).

Evidence Supporting ^{210}Pb Rates in the Nueces River Fluvial-Deltaic System

In the Nueces River fluvial-deltaic system, sedimentation rates at coring sites range from less than 1 mm/yr to more than 4 mm/yr (Table 4 and Fig. 14). The lowest sedimentation rate of 0.6 mm/yr at core NR-1 is supported independently by a rate based on archeological evidence found at the edge of a bayou near the coring site. The archeological evidence, which consists of a thin stratum of shells and faunal bones, was discovered at a depth of 25 cm by Mike Blum (University of Nebraska) and was dated by Bob Ricklis (Archeologist, Corpus Christi) at 500 to 1,000 years B.P. Using the more recent date of 500 years yields an average sedimentation rate of 0.05 cm/yr for the 25 cm of sediment above the archeological horizon. This rate is within 0.01 cm/yr of the rates determined from ^{210}Pb data. The low sedimentation rate is consistent with the geomorphic setting of coring site NR-1 . The site is approximately 3 km north of the Nueces River (Fig. 5) and is partially "protected" from flooding by an upland terrace that curves around the western (upstream) side of the site.

One of the highest rates of sedimentation in the Nueces River fluvial-deltaic system was at core site NR-11, an intertidal Spartina alterniflora marsh on the edge of Nueces Bay and the Nueces River. The average rate of sedimentation at this site is 0.45 cm/yr, which is equivalent to the rate of relative sea-level rise for a period from the 1940s to mid 1980s at the Rockport tide gauge (Fig. 15).

Table 4. Average sedimentation rates for given core intervals in the Nueces River fluvial-deltaic system. Rates are based on a least-squares fit of Ln plots of excess ^{210}Pb against corrected depths (CFS model, Oldfield and Appleby, 1984).

Core Number.	CFS Rate (cm/yr)	Corrected depth (cm)	R^2	Supported ^{210}Pb (dpm/g)	Anomalies Excluded
NR-1	0.06	1-13	0.962	1.09	
NR-2	0.41	1-15	0.769	1.04	
NR-3	0.20	1-10	0.872	1.29	
NR-4	0.20	1-15	0.917	1.09	1
NR-5	0.13	1-6	0.912	1.15	
NR-6	0.10	1-6	0.916	0.87	
NR-7	0.16	1-12	0.926	0.98	
NR-8	0.13	1-13	0.832	0.91	1
NR-9	0.10	1-9	0.918	0.99	
NR-10	0.32	1-20	0.852	1.57	3
NR-11	0.45	1-25	0.899	0.94	3

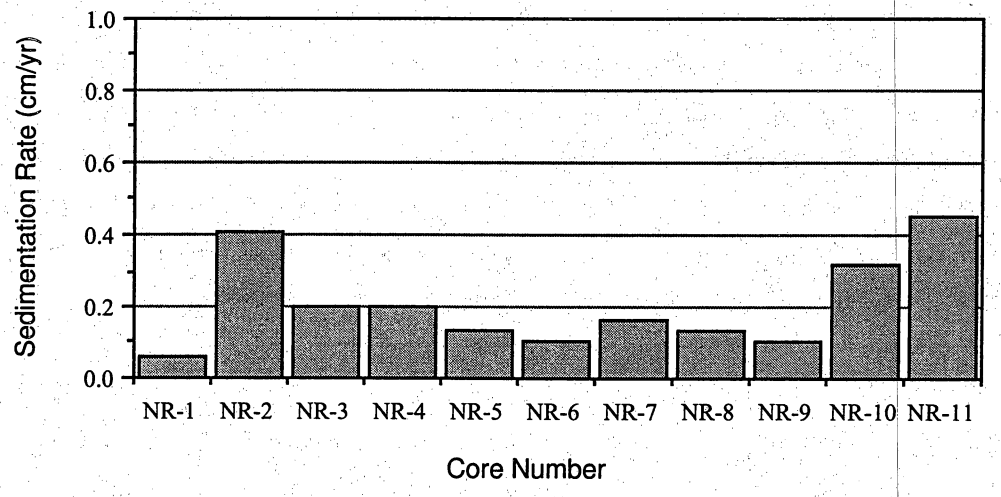

Figure 14. Average sedimentation rates of Nueces River cores using CFS model (table 4). Depths are generally less than 15 cm. Supported ^{210}Pb for each core is based on average ^{226}Ra.

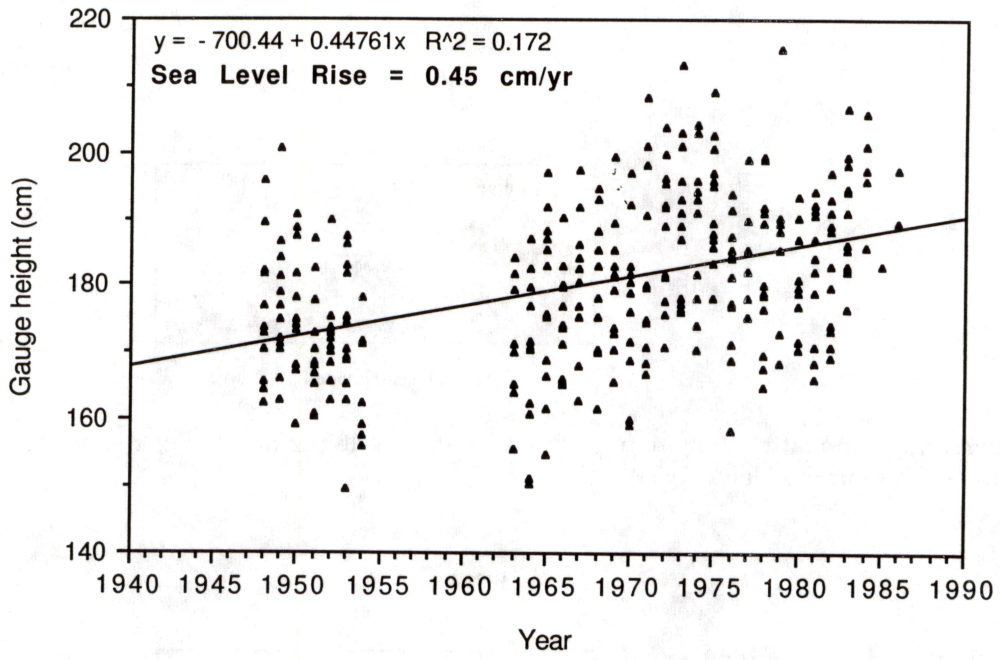

Figure 15. Average rate of sea-level rise at the Rockport, TX, tide gauge for the period from the 1940s to mid-1980s. Average monthly tide levels from National Oceanic and Atmospheric Administration (NOAA). See Figure 20 for location of Rockport gauge.

Comparison of Active Processes in the Three Fluvial-Deltaic Systems

Analysis of active processes in the three study areas reveals some interesting trends, some of which may influence sedimentation rates. As previously mentioned, the three fluvial-deltaic systems are in different climatic settings, each separated by about 1 degree of latitude. Salinities increase southwestward as a result of decreasing rainfall and increasing evapotranspiration. These changes are mirrored by other processes that have a down the coast variance such as sediment load, Holocene valley fill thickness, sea-level rise, bay tide levels, and rates of wetland loss.

Rainfall, Basin Size, and Sediment Load

Average rainfall decreases from a high of approximately 137 cm/yr in the Trinity River basin, to 99 cm/yr in the Lavaca-Navidad, to 76 cm/yr in the Nueces (Fig. 16). The sizes of the drainage basins that lie within the coastal plain also decrease southwestward from 10,287 km^2 for the Trinity, to 5,978 km^2 for the Lavaca-Navidad, to 3,398 km^2 for the Nueces (Figs. 1 and 17). Average annual streamflow and suspended sediment load decrease down the coast, as well, from a high along the Trinity to a low along the Nueces (Fig. 18). The annual streamflow and suspended load of the combined

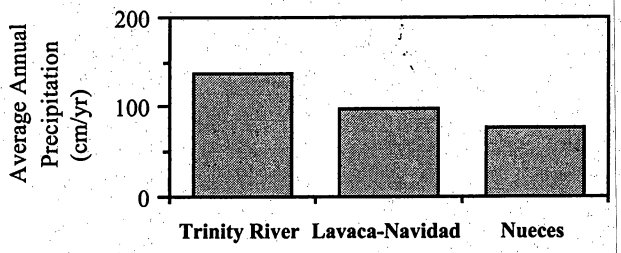

Figure 16. Average annual precipitation for the three fluvial-deltaic areas. For the period 1961 to 1990. From Dallas Morning News (1993).

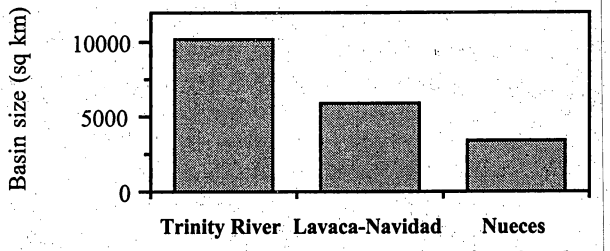

Figure 17. Relative sizes of drainage basins within the coastal plain for the three river systems. From Greiner (1982).

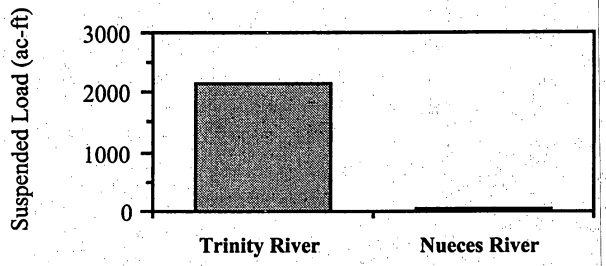

Figure 18. Average annual suspended load for the Trinity River at Romayor, TX and Nueces River at Mathis, TX. Similar records for the Lavaca-Navidad are not available because of lack of stream gauging station on the Navidad near the coast. Measurements for the Trinity are from 1937-1984 and for the Nueces 1943-1988. Data from Texas Water Development Board.

Lavaca and Navidad Rivers fall between the Trinity and Nueces, but a true measure of streamflow and suspended load near the mouth of the Navidad could not be determined because the gauging station from which suspended load is measured is located in the upper part of the drainage basin, and measurements at this upstream site underestimate the volume of streamflow and load reaching the Lavaca-Navidad River fluvial-deltaic system.

Modern–Holocene Valley-Fill Deposits

The entrenched valleys of each river system, which formed during lower stands of sea level during the Pleistocene (Price 1933), have been partly filled with Holocene sediments. Cross sections based on geotechnical studies along highways crossing the valleys reveal thick sands with some gravel overlain by mud deposits. Holocene mud deposits are thickest in the Trinity River valley, averaging 8.7 m, are thinner in the Lavaca River valley, averaging 4.4 m, and are thinnest in the Nueces River valley, averaging 2.1 m (Fig. 19).

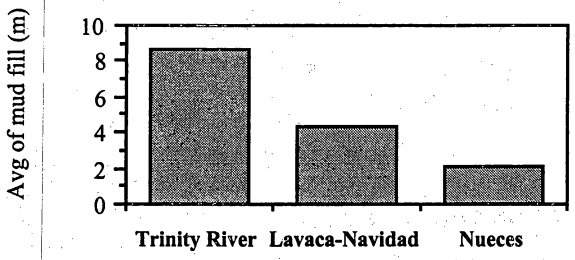

Figure 19. Average thickness of Holocene mud fill in fluvial-deltaic systems.

Relative Sea-Level Rise

Sea-level rise can affect intertidal marsh accretion rates (for example, McCaffrey and Thomson, 1980). Relative sea-level rise as used here is the relative vertical rise in water level with respect to a datum at the land surface, whether it is caused by a rise in mean-water level or subsidence of the land surface. Along the Texas coast, both eustatic sea-level rise and subsidence are part of the relative sea-level rise equation. Subsidence, especially associated with pumpage of ground water and oil and gas, is the predominant component. As defined in this report, relative sea-level rise does not include the offsetting effects of vertical accretion.

Over the past century, sea level has been rising on a worldwide (eustatic) basis at an average rate of about 1.2 mm/yr, with a rate in the Gulf of Mexico and Caribbean region of 2.4 mm/yr (Gornitz et al., 1982; Gornitz and Lebedeff, 1987). Adding subsidence to these rates yields a relative sea-level rise that at some locations along the Texas coast exceeds 10 mm/yr (Swanson and Thurlow, 1973; Penland et al., 1988). But these rates are locally dwarfed by human-induced subsidence, for example in the Houston area, where subsidence rates greater than 75 mm/yr near the center of the subsidence bowl have been recorded (Gabrysch and Coplin, 1990). The major cause of human-induced subsidence is the withdrawal of underground fluids, principally ground water, oil, and gas (Pratt and Johnson, 1926; Gabrysch 1969; and Kreitler, 1977).

Each of the three fluvial-deltaic systems is affected to some degree by subsidence. Subsidence resulting from ground water production in the Houston area is well known, and the margins of the subsidence bowl encompass the Trinity River fluvial deltaic system (Gabrysch and Coplin, 1990). In contrast, subsidence in the Lavaca-Navidad and Nueces fluvial-deltaic systems appears to have been affected more by oil and gas production (Ratzlaff, 1980).

Benchmark releveling surveys along highways or railroads that cross each valley provide another measure of subsidence. In the Trinity River fluvial-deltaic system, the average subsidence rate of four benchmarks along Interstate Highway 10 is 8.1 mm/yr for the period 1973-1978. Rates of subsidence in this area apparently decreased during and after the 1970s. For example, the westernmost benchmark had a subsidence rate of 10.9 mm/yr from 1963-1978 and 9.7 mm/yr from 1973-1978, a reduction of about 12 percent. Other benchmarks to the west also had lower rates of subsidence for the more recent period, apparently as a result of reductions in groundwater pumpage (Gabrysch and Coplin, 1990). A conservative estimate would be to assume that the average rate of subsidence for the Trinity Valley is about 10 percent higher, or about 9 mm/yr, for the longer period of 1963 to 1978. Adding the average sea-level rise for the Gulf of Mexico (Gornitz et al., 1982) to this rate of subsidence yields a relative sea-level rise of about 11.3 mm/yr for the Trinity River fluvial-deltaic system.

Tide gauge records and benchmark releveling surveys also provide data for determining rates of relative sea-level rise in the Lavaca River and Nueces River valleys. Paine (1993) compiled data on vertical movement using regional first-order levelings conducted by the National Geodetic Survey (NGS) in the 1950s, late 1970s and early 1980s. Vertical movement at each benchmark in the network was determined with reference to an arbitrarily chosen benchmark at the town of Sinton (Fig. 20). The geodetic network was referenced to sea level through leveling lines to tide gauge stations at Galveston, Rockport, and Port Isabel (Fig. 20). These data provide relative sea-level rise rates at benchmarks along the main leveling line that crosses the Lavaca River valley and Nueces River valley.

Rates of subsidence in millimeters per year for the period 1951–1982 were determined for 3 or 4 benchmarks that cross the Lavaca and Nueces River valleys. Rates of relative sea-level rise were

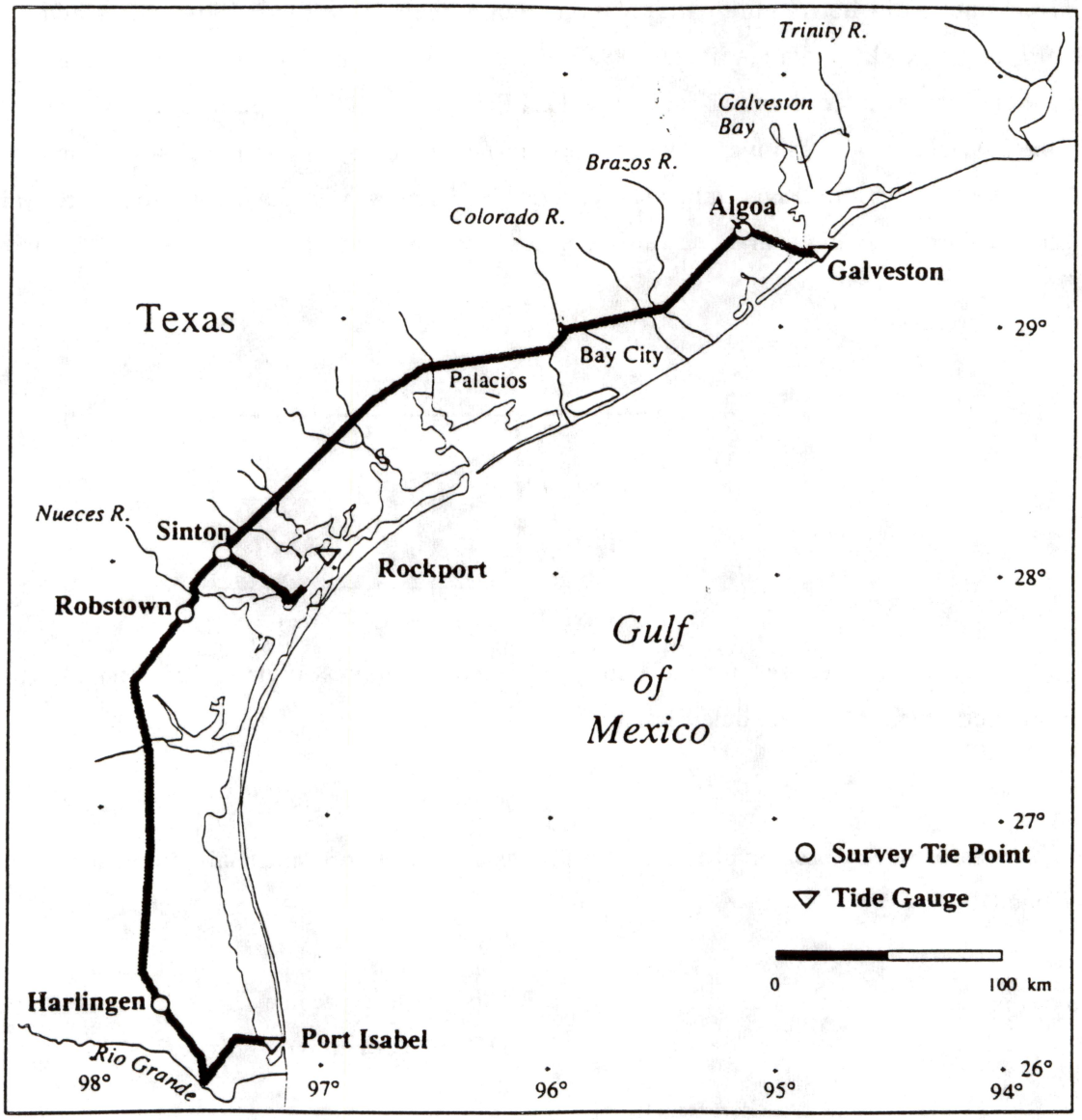

Figure 20. Location of National Geodetic Survey leveling lines and National Ocean Survey tide gauges. From Paine (1993).

estimated relative to a tide gauge at Port Isabel, Texas (Fig. 20) because dates of leveling surveys between Algoa and Harlingen and Harlingen and Port Isabel were in close agreement, and use of the Port Isabel gauge did not require extrapolation from a benchmark several kilometers away as was necessary for the Rockport gauge (Paine, 1993). Rates of relative sea-level rise are also relative to the reference benchmark near Sinton, Texas. Based on these data, the average rates of relative sea-level rise in the Lavaca and Nueces River valleys are 8.1 mm/yr and 6.3 mm/yr, respectively. Comparison of these rates with the Trinity River valley shows a decline in rates from the Trinity to Nueces (Fig. 21). Tide gauge records also, in general, indicate a decline in sea-level rise down the coast (Table 5).

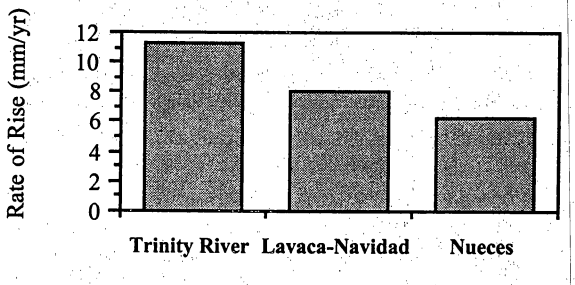

Figure 21. Relative sea-level rise for the Trinity, Lavaca, and Nueces fluvial-deltaic systems. See text for period over which rates were determined.

Table 5. Rates of relative sea-level rise at the Port Isabel, Rockport, and Galveston Pier 21 gauges. From Paine (1993).

Tide gauge	Relative sea-level rise rate 1951 to 1982 (mm/yr)
Port Isabel	4.6
Rockport	5.4
Galveston Pier 21	8.2

Historical Wetland Losses

Approximately 2,000 ha of wetlands have been lost in the three fluvial-deltaic systems since the 1950s (White and Calnan, 1990; White and Tremblay, 1995). Losses, which are primarily the

result of submergence and the replacement of emergent vegetation by open water, have been most extensive in the Trinity fluvial-deltaic system and least extensive in the Nueces (Fig. 22).

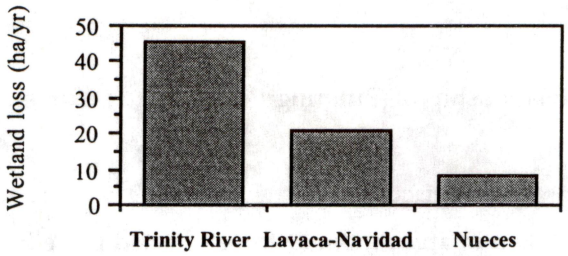

Figure 22. Rate of marshland loss from the 1950s to 1979/80s in the Trinity, Lavaca, and Nueces fluvial-deltaic systems.

The Trinity River delta, at the head of Trinity Bay, is the only natural bayhead delta in Texas that has undergone significant progradation in recent historic times. Historical analysis of the Trinity River delta using aerial photographs (White and Calnan, 1991) shows that delta progradation continued from 1930 to 1956, adding approximately 600 ha of marshland. This trend in marsh gain was reversed between 1956 and 1974, when more than 1,400 ha of marshland was converted to open water and unvegetated flat. Vegetated wetlands continued to shrink by an additional 90 ha between 1974 and 1988. Although some wetland losses around the Trinity River delta have resulted from bay shore erosion (Paine and Morton, 1986), the most extensive losses have occurred in interior marshes. From 1953 to 1989, wetland losses exceeded 1,742 ha in the delta and lower reaches of the Trinity River alluvial valley (White et al., 1993; White and Tremblay, 1995). Approximately 40 percent of the submergence of wetlands in the Trinity River delta and alluvial valley resulted from construction of a power plant cooling reservoir (more than 1,010 ha in size) in the southwestern part of the delta. Most of the remaining 60 percent of marsh loss (1045 ha), however, was due to submergence apparently associated with subsidence and declining river sediment loads (Fig. 2).

Losses of marsh habitat in the Lavaca River valley amounted to more than 430 ha between the 1950's and 1979 (White and Calnan, 1990). Losses were due primarily to the replacement of emergent vegetation by water and barren flats, and were most pronounced in the Menefee Flats area and downstream near Venado Lakes on the western side of the valley (Fig. 4). Among the probable causes for the losses are subsidence and relative sea-level rise, compartmentalization of marshes by roads, levees, and canals, and possibly disposal of brine (Mackin, 1971).

In the Nueces River valley, more than 130 ha of marsh habitat was lost between the 1950s and 1979 (White and Calnan, 1990). The losses were a result of the transformation of emergent vegetation to open water and barren flats, primarily in the delta near Nueces Bay. Delta progradation and marsh expansion ended sometime between 1930 and 1959 (Morton and Paine, 1984). Among the probable causes for the losses in wetlands are reductions in the volume of fluvial sediments reaching the delta and relative sea-level rise.

Relationship of Differing Processes to Sedimentation Rates

Several of the processes discussed in the preceding section may influence sedimentation rates. Most of the cores were taken in areas thought to be affected more by fluvial processes, i.e., cores were collected at least 3 km up the valley from bay margins. The low relief and funnel shape of the entrenched valleys, however, make them susceptible to hurricane storm surge flooding from the estuaries. All the sites were inundated by storm surge during Hurricane Carla in 1961, and by storm surge and aftermath rains during Hurricane Beulah in 1967. In addition, water levels at some of the sites are undoubtedly affected by abnormally high tides. Still, the location of most of the coring sites in the fluvial portion of the fluvial-deltaic systems suggest that they are also influenced largely by fluvial processes and those factors that may influence them, such as basin size, rainfall, basin denudation rate, sediment load, elevation, and relative sea-level-rise. A plot of sedimentation against these factors shows consistent relationships among the three basins (Figs. 23-24). This trend, of decreasing sedimentation rates from the Trinity to the Nueces, also has a positive correlation with the thickness of Holocene mud fill that caps the valley fill sequences (Fig. 25). Only average elevation, as expected, has an inverse or negative correlation with rates of sedimentation (Fig. 24)

In the Nueces fluvial-deltaic system, preliminary relationships between sedimentation rates, river suspended sediment loads, dam construction, and relative sea-level rise were investigated for several cores (White and Morton, 1996). Among the findings was a decrease in sedimentation rates since approximately the 1930s (Fig. 26). The Mathis Dam at Lake Corpus Christi was constructed in 1929 and is estimated to have trapped 75 percent of the suspended sediment load delivered along the Nueces River (Brune, 1953). The Seale Dam, which flooded the Mathis Dam at Lake Corpus Christi, was completed in 1958 and traps more than 95 percent of the suspended sediment (Liebbrand, 1987).

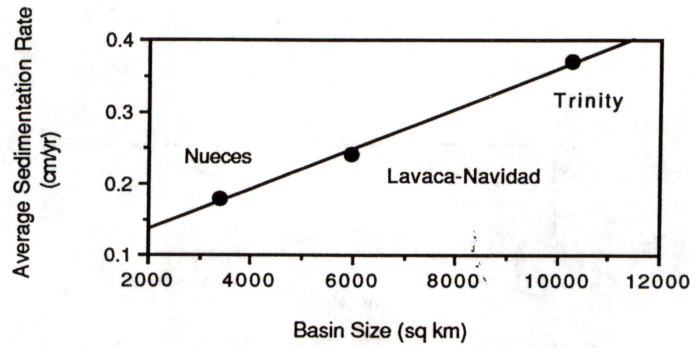

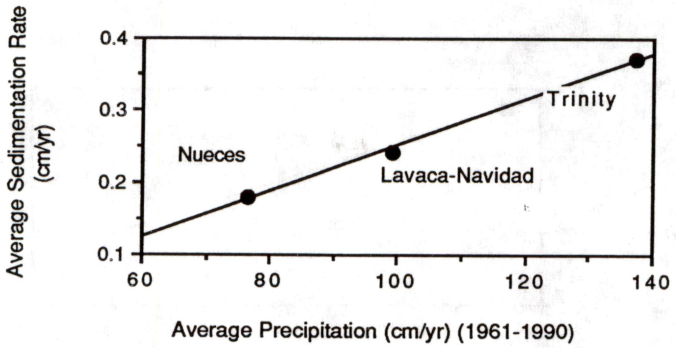

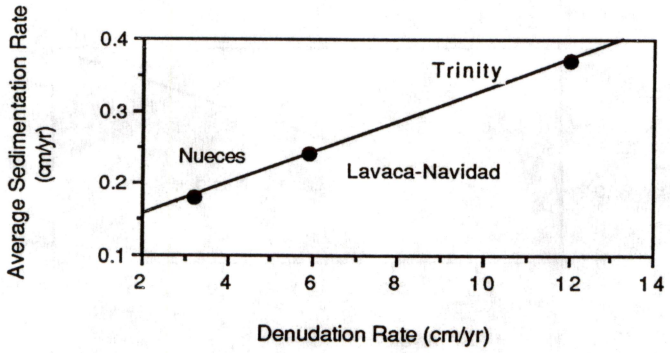

Figure 23. Relationships between average sedimentation rates and coastal basin size, annual rainfall, and denudation rates in the three river systems. See Figure 1 for basin locations. Average annual rainfall for period 1961-1990 at Liberty, Hallettsville, and Corpus Christi from the Dallas Morning News (1993). Denudation rates from Winker (1979).

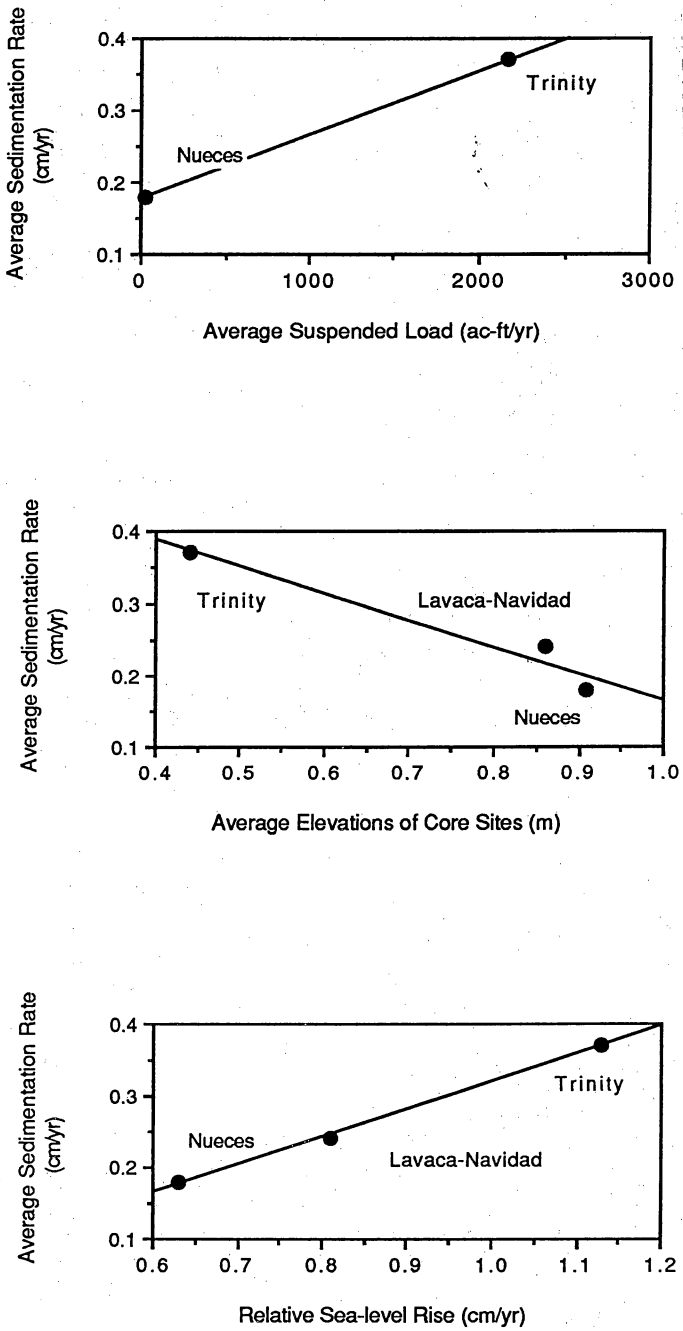

Figure 24. Relationships between average sedimentation rates and river suspended load, estimated average elevations of coring sites, and rates relative sea-level rise. See text for sources.

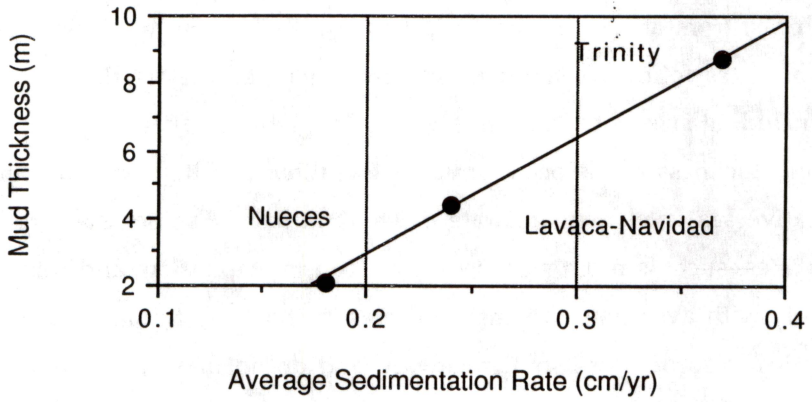

Figure 25. Relationship between average sedimentation rate and average thickness of Holocene mud as measured in cross-sections across the three fluvial-deltaic systems.

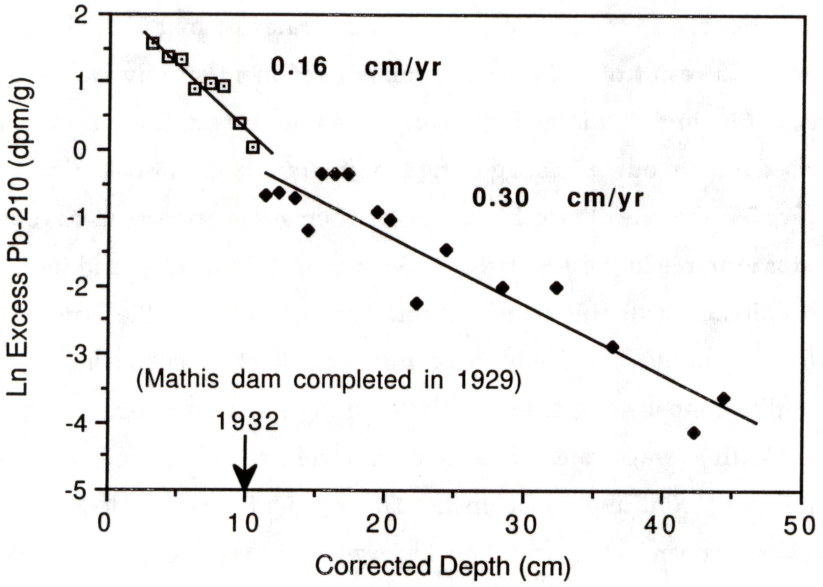

Figure 26. ^{210}Pb profile of core NR-3 showing decreasing rates of sedimentation after the Mathis Dam was constructed on the Nueces River in 1929. Based on CFS model and corrected depth. Also, note that top 2 cm excluded because of bioturbation.

CONCLUSIONS

Using a simple ^{210}Pb model (CFS), average sedimentation rates were measured in cores from fluvial-deltaic systems located on the north, central, and south Texas coastal plain. Sedimentation rates decrease down the coast from of 0.37 cm/yr, to 0.24 cm/yr, to 0.18 cm/yr. This southwestward decrease in sedimentation rates follows a trend of several other parameters that characterize the fluvial-deltaic systems, including size of the coastal plain drainage basin, average precipitation, river suspended sediment load, thickness of Holocene mud in the alluvial valleys, average elevations of coring sites, average relative sea level rise, and rate of wetland loss. Factors that are expected to influence sedimentation rates, such as basin size, sediment load, precipitation, and relative sea-level rise, all correlate positively with average sedimentation rates in the three fluvial-deltaic systems.

Rates of wetland loss also decrease southwestward and do not have an inverse relationship with sedimentation rates like one might expect. For example, where rates of sedimentation are lowest in the Nueces valley, rates of wetland loss are also lowest. The reason is possibly related to rates of subsidence, which are also lowest in the Nueces River system. In the Trinity River delta and alluvial valley as a whole, subsidence appears to be a significant contributing factor to marsh loss at least up to the 1970's (White and Tremblay, 1995). The higher rates of subsidence compared to sedimentation suggest that subsidence is a contributing factor to the replacement of marshes by open water and has apparently outpaced rates of sedimentation. In addition, rates of marsh sedimentation may have declined through time as a result of reductions in marsh sediment supply from upstream reservoir development. For example, in the Nueces River fluvial-deltaic system, there is evidence that rates of sedimentation decreased after about 1930 suggesting that impoundment of Lake Corpus Christi in 1929 was responsible. However, the rate at which marshes are being lost appears to have decreased during more recent periods, for example in the Trinity River delta from 1974 to 1988, and in the Nueces delta in the 1970s (White and Calnan, 1990). This change in rate of wetland loss in the Trinity delta may be due partly to the sharp declines in rates of subsidence on the east side of the subsidence bowl after 1978 as a result of reductions in the pumpage of groundwater. Nevertheless, decreasing sediment loads along the river systems, coupled with average rates of relative sea-level rise that exceed rates of sedimentation, suggest that wetlands will continue to be lost. The rates of wetland loss as well as rates of sedimentation, however, appear to be controlled in large part by the characteristics that define the differing fluvial-deltaic settings along the Texas Coast.

ACKNOWLEDGMENTS

Funding for this report was provided by the Texas Water Development Board under Research and Planning Fund Grant, and USGS as part of a cooperative study on coastal erosion and wetland loss along the upper Texas Coast. Cores were analyzed for isotopic elements, weight loss-on-ignition, water content, mineral matter, bulk density, and texture (texture in the Nueces River study area only) by Dr. Charles Holmes of the U.S. Geological Survey, Denver. Textures (in the Trinity River study area) and sediment salinities were analyzed by Steve Tweedy, Chemist in Charge of the BEG Mineral Studies Laboratory. Textural analyses in the Lavaca-Navidad study area were completed by the Department of Geography, University of Wisconsin at Milwaukee. Word processing and pasteup of figures were by Susan Lloyd. Others providing assistance in the Bureau's Core Research Center included George Bush, Alex Colunga, James Donnelly, and Robert Sanchez. The authors are especially grateful to numerous landowners in the study areas who gave permission to enter their property and take cores.

REFERENCES

Allen, J. R. L., Ray, J. E., Longworth, G., Hasler, S. E., and Ivanovich, M., 1993, A comparison of the ^{210}Pb dating technique with three other independent dating methods in an oxic estuarine salt-marsh sequence: Estuaries, v. 16, no. 3B, p. 670-677.

Armentano, T. V., and Woodwell, G. M.,1975, Sedimentation rates in a Long Island marsh determined by ^{210}Pb dating: Limnology and Oceanography, v. 20, no. 3, p. 452-456.

Bricker-Urso, S., Nixon, S. W., Cochran, J. K., Hirschberg, D. J., and Hunt, C., 1989, Accretion rates and sediment accumulation in Rhode Island salt marshes: Estuaries, v. 12, no. 4, p. 300-317.

Brugam, R. B.,1978, Pollen indicators of land-use change in Southern Connecticut: Quaternary Research, v. 9. p. 349-362.

Brune, G. M., 1953, Trap efficiency of reservoirs: Transactions of the American Geophysical Union, v. 34, p. 407-418.

Church, T. M., Lord, C. J., III, and Somayajulu, B. L. K., 1981, Uranium, thorium, lead nuclides in a Delaware salt marsh sediment: Estuarine, Coastal and Shelf Science, v. 13, p. 267–275.

Dallas Morning News, 1993, Texas Almanac, 672 p.

DeLaune, R. D., Smith, C., J., Patrick, W. H., Jr., and Roberts, H. H., 1987, Rejuvenated marsh and bay-bottom accretion on the rapidly subsiding coastal plain of U. S. Gulf coast: A second order effect of the emerging Atchafalaya delta: Estuarine Coastal and Shelf Science, v. 25, p. 1-9.

Diener, R. A., 1975, Cooperative Gulf of Mexico estuarine inventory and study—Texas: area description: U. S. Department of Commerce, National Oceanic and Atmospheric Administration, Technical Report NMFS CIRC-393, 129 p.

Duxbury, A. C., 1971, The earth and its oceans: Reading, Massachusetts, Addison-Wesley Publishing Company, 381 p.

Flynn, W. W., 1968, The determination of low levels of polonium-210 in environmental materials: Analytica Chimica Acta, v. 43, p. 221–227.

Gabrysch, R. K., 1969, Land-surface subsidence in the Houston–Galveston region, Texas: United Nations Educational, Scientific and Cultural Organization (UNESCO), Studies and Reports in Hydrology, Land Subsidence Symposium, v. 1, p. 43–54.

Gabrysch, R. K., and Coplin, L. S., 1990, Land-surface subsidence resulting from ground-water withdrawals in the Houston–Galveston region, Texas, through 1987: U.S. Geological Survey Report of Investigations No. 90-01, 53 p.

Gee, G. W., and Bauder, J. W., 1986, Particle-size analysis, in, Methods of soil analysis, Part 1. Physical and mineralogical methods, Agronomy Monograph no. 9, 2nd ed: Madison, Wisconsin, American Society of Agronomy--Soil Science of America, p. 383-410.

Gornitz, V., and Lebedeff, S., 1987, Global sea-level changes during the past century: Society of Economic Paleontologists and Mineralogists, Special Publication No. 41, p. 3–16.

Gornitz, V., Lebedeff, S., and Hansen, J., 1982, Global sea level trend in the past century: Science, v. 215, p. 1611–1614.

Greiner, J. H., Jr., 1982, Erosion and sedimentation by water in Texas, average annual rates estimated in 1979: Texas Department of Water Resources, Report 268, 145 p.

Holmes, C. W., and Martin, E. A., 1976, Rates of sedimentation, in Holmes, C. W., et al., Environmental studies, South Texas Outer Continental Shelf, 1976, Geology report for the Bureau of Land Management prepared by the U.S. Geological Survey, 626 p.

Kearney, M. S., Stevenson, J. C., and Ward, L. G., 1994, Spatial and temporal changes in marsh vertical accretion rates in Monie Bay: Implications for sea-level rise: Journal of Coastal Research, v. 10, no. 4, p. 1010-1020.

Koide, M., Bruland, K. W., and Goldberg, E. D., 1973, $^{228}Th/^{232}Th$ and ^{210}Pb geochronologies in marine and lake sediments: Geochimica et Cosmochimica Acta, v. 37, p. 1171-1187.

Kreitler, C. W., 1977, Faulting and land subsidence from ground-water and hydrocarbon production, Houston–Galveston, Texas: The University of Texas at Austin, Bureau of Economic Geology Research Note 8, 22 p.

Liebbrand, N. F., 1987, Estimated sediment deposition in Lake Corpus Christi, Texas, 1972–1985: U.S. Geological Survey Open-File Report 87-239, 26 p.

Longley, W. L., 1992, Freshwater inflow to Texas bays and estuaries: ecological relationships and methods for determining needs: Texas Water Development Board and Texas Parks and Wildlife Department, 366 p.

Mackin, J. G., 1971, A study of the effect of oil field brine effluents on biotic communities in Texas estuaries: Texas A&M University Research Foundation Report, Project 735, 72 p.

Martin, E. A., and Rice, C. A., 1981, ^{210}Pb geochronology and trace metal concentrations of sediments from Upper Klamath Lake and Lake Euwana, Oregon: Northwest Science, v. 55, no. 4, p. 269–280.

McCaffrey, R. J., and Thomson, John, 1980, A record of the accumulation of sediment and trace metals in a Connecticut salt marsh, in, Saltzman, Barry, ed, Estuarine Physics and Chemistry: Studies in Long Island Sound, Advances in Geophysics, Volume 22: New York, Academic Press, p. 165-236.

Morton, R. A., and Paine, J. G., 1984, Historical shoreline changes in Corpus Christi, Oso, and Nueces Bays, Texas Gulf Coast: The University of Texas at Austin, Bureau of Economic Geology Geological Circular 84-6, 66 p.

Morton, R. A., and White, W. A., in press, Characteristics and corrections for core shortening: Journal of Coastal Research.

Nittrouer, C. A., Sternberg, R. W., Carpenter, R., and Bennett, J. T., 1979, The use of Pb-210 geochronology as a sedimentological tool: application to the Washington continental shelf: Marine Geology, v. 31, p. 297–316.

Oldfield, F., and Appleby, P. G., 1984, Empirical testing of ^{210}Pb-dating models for lake sediments, in Haworth, E. Y., and Lund, J. W. G., eds., Lake sediments and environmental history: Minneapolis, Minnesota, University of Minnesota Press, p. 93–124.

Paine, J. G., 1993, Subsidence in the Texas coast: inferences from historical and late Pleistocene sea levels: Tectonophysics, v. 222, p. 445–458.

Paine, J. G., and Morton, R. A., 1986, Historical shoreline changes in Trinity, Galveston, West, and East Bays, Texas Gulf Coast: The University of Texas at Austin, Bureau of Economic Geology Geological Circular 86-3, 58 p.

Penland, Shea, Ramsey, K. E., McBride, R. A., Mestayer, J. T., and Westphal, K. A., 1988, Relative sea level rise and delta-plain development in the Terrebone Parish region: Baton Rouge, Louisiana Geological Survey, Coastal Geology Technical Report No. 4, 121 p.

Pratt, W. E., and Johnson, D. W., 1926, Local subsidence of the Goose Creek oil field: Journal of Geology, v. 34, p. 577–590.

Price, W. A., 1933, Role of diastrophism in topography of Corpus Christi area, South Texas: American Association of Petroleum Geologists Bulletin, v. 17, no. 8, p. 907-962.

Ratzlaff, K. W., 1980, Land-surface subsidence in the Texas coastal region: U.S. Geological Survey Open-File Report 80-969, 19 p.

Robbins, J. A., 1978, Geochemical and geophysical applications of radioactive lead, in Nriagu, J. O., ed., The biogeochemistry of lead in the environment, Part A. Ecological cycles: New York, Elsevier/North-Holland Biomedical Press, chap. 9, p. 285–393.

Sharma, P., Gardner, L. R., Moore, W. S., and Bollinger, M. S., 1987, Sedimentation and bioturbation in a salt marsh as revealed by ^{210}Pb, ^{137}Cs, and ^{7}Be studies: Limnology and Oceanography, no. 32, no. 2, p. 313-326.

Smith, J. N., and Walton, A., 1980, Sediment accumulation rates and geochronologies measured in Saguenay Fjord using the Pb-210 dating method: Geochimica et Cosmochimica Acta, v. 44, p. 225-240.

Starkey, H. C., Blackmon, P. D., and Hauff, P. L., 1984, The routine mineralogical analysis of clay-bearing samples: U.S. Geological Survey Bulletin 1563, 32 p.

Swanson, R. L., and Thurlow, C. I., 1973, Recent subsidence rates along the Texas and Louisiana coasts as determined from tide measurements: Journal of Geophysical Research, v. 78, no. 5, p. 2665–2671.

U.S. Geological Survey, 1986, National water summary 1985—hydrologic events and surface-water resources: Water-Supply Paper 2300, 506 p.

White, W. A., and Calnan, T. C., 1990, Sedimentation and historical changes in fluvial-deltaic wetlands along the Texas Gulf Coast with emphasis on the Colorado and Trinity River deltas: The University of Texas at Austin, Bureau of Economic Geology, report prepared for the Texas Parks and Wildlife Department and Texas Water Development Board under interagency contract (88-89) 1423, 124 p., 6 appendices.

White, W. A., and Calnan, T. C., 1991, Submergence of vegetated wetlands in fluvial-deltaic areas, Texas Gulf Coast, in Coastal depositional systems in the Gulf of Mexico: Quaternary framework and environmental issues: 12th Annual Research Conference, Society of Economic Paleontologists and Mineralogists, Gulf Coast Section, Houston, Texas, p. 278–279.

White, W. A., Calnan, T. C., Morton, R. A., Kimble, R. S., Littleton, T. G., McGowen, J. H., Nance, H. S., and Schmedes, K. S., 1983, Submerged lands of Texas, Corpus Christi area: sediments, geochemistry, benthic macroinvertebrates, and associated wetlands: The University of Texas at Austin, Bureau of Economic Geology Special Publication, 154 p.

White, W. A., Calnan, T. R., Morton, R. A., Kimble, R. S., Littleton, T. G., McGowen, J. H., Nance, H. S., and Schmedes, K. E., 1985, Submerged lands of Texas, Galveston-Houston area: sediments, geochemistry, benthic macroinvertebrates, and associated wetlands: The University of Texas at Austin, Bureau of Economic Geology, Special Publication, 145 p.

White, W. A., Calnan, T. R., Morton, R. A., Kimble, R. S., Littleton, T. G., McGowen, J. H., and Nance, H. S., 1989, Submerged lands of Texas, Port Lavaca area: sediments, geochemistry, benthic macroinvertebrates, and associated wetlands: The University of Texas at Austin, Bureau of Economic Geology, Special Publication, 165 p.

White, W. A., and Morton, R. A., 1993, Determining recent sedimentation rates of the Trinity River, Texas: The University of Texas at Austin, Bureau of Economic Geology, report prepared for the Texas Water Development Board under interagency contract no. 93-483-356, 50 p., 3 appendices.

White, W. A., and Morton, R. A., 1995, Determining recent sedimentation rates of the Lavaca-Navidad River System, Texas: The University of Texas at Austin, Bureau of Economic Geology, report prepared for the Texas Water Development Board under interagency contract no. 93-483-013, 76 p., 5 appendices.

White, W. A., and Morton, R. A., 1996, Determining recent sedimentation rates of the Nueces River System, Texas: The University of Texas at Austin, Bureau of Economic Geology, report prepared for the Texas Water Development Board under interagency contract no. 93-483-075, 123 p..

White, W. A., and Tremblay, T. A., 1995, Submergence of wetlands as a result of human-induced subsidence and faulting along the upper Texas Gulf Coast: Journal of Coastal Research, v. 11, no. 3, p. 788-807.

White, W. A., Tremblay, T. A., Wermund, E. G., Jr., and Handley, L. R., 1993, Trends and status of wetland and aquatic habitats in the Galveston Bay System, Texas: Galveston Bay National Estuary Program, GBNEP-31, Webster, Texas, 225 p.

Winker, C. D., 1979, Late Pleistocene Fluvial-deltaic deposition Texas Coastal Plain and Shelf: M.A. Thesis, The University of Texas at Austin, 187 p.

Addendum 3

Descriptions of Vibracores, Galveston Island and Bolivar Peninsula

CORE LOG

sand flat PAGE 1 OF 2
8. mile Rd

CORE #GIV-96la TYPE Vibra LOCATION Galveston Island
LATITUDE _____ LONGITUDE _____ SURFACE ELEVATION _____
DEPTH PENETRATED _____ LENGTH RECOVERED _____ % SHORTENING _____

OBTAINED BY Morton, Garner, Angle DATE 6/96
DESCRIBED BY Ed Garner DATE 7/96

PROFILE (ft, m) DESCRIPTION

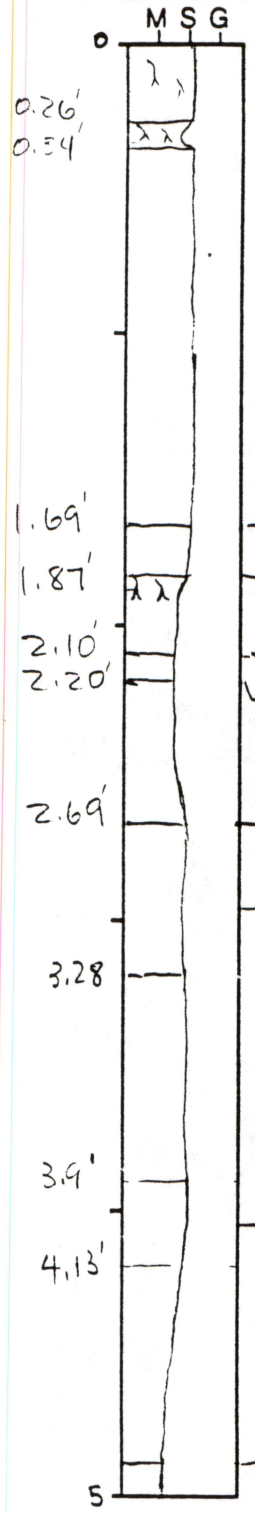

tan and gray fine sand with organic lumps and organic material (roots & grass); disturbed.

tan to light gray sandy mud with organic material (roots)

tan fine sand and muddy sand

tan muddy sand with brown-gray mottles (Organic)

sharp contact, roots at top

gray silty mud with brown-gray mottles (organic)

dark gray muddy fine sand.

dark gray sandy mud

intermixed mud zone

light gray muddy fine sand with tan streaks;

dk gray mottles

CORE LOG

CORE # GIV-961a TYPE _____ LOCATION _____
LATITUDE _____ LONGITUDE _____ SURFACE ELEVATION _____
DEPTH PENETRATED _____ LENGTH RECOVERED _____ % SHORTENING ___

OBTAINED BY _____ DATE _____
DESCRIBED BY _____ DATE _____

PROFILE (ft. m) DESCRIPTION

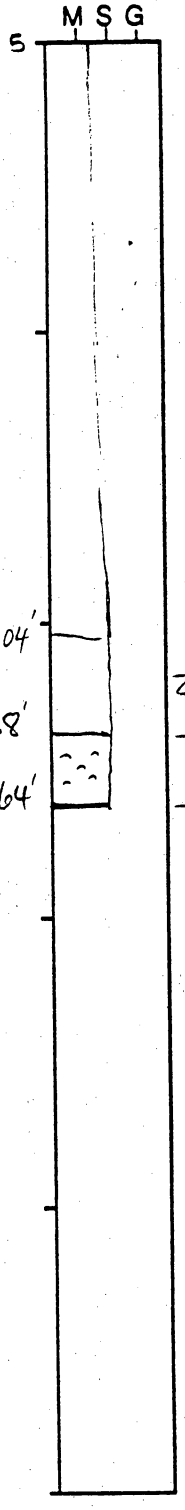

Dark gray muddy fine sand with tan streaks
increase in mud content toward top of unit, burrowed

2 dark gray mottles

light gray fine sand with shell fragments and dark gray mottles, roots

Augered 3ft clean tan sand

CORE LOG

CORE # GIV962a TYPE Vibra LOCATION ridge crest B-mile Rd Galveston Island
LATITUDE ____ LONGITUDE ____ SURFACE ELEVATION ____
DEPTH PENETRATED ____ LENGTH RECOVERED ____ % SHORTENING ____

OBTAINED BY Morton, Garner, Angle DATE 6/96
DESCRIBED BY Ed Garner DATE 7/96

PROFILE (ft, m) DESCRIPTION

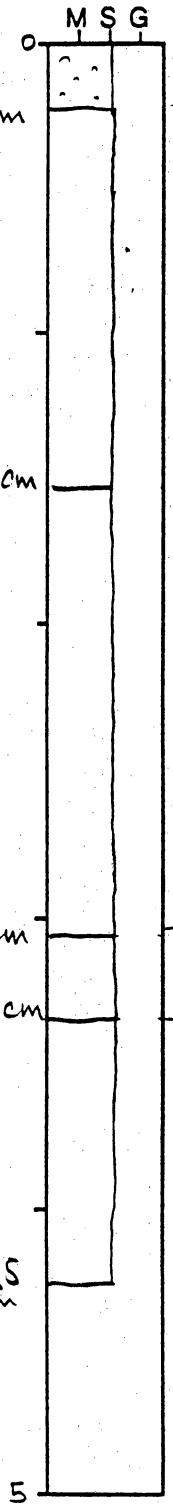

light brown to tan fine sand with shells and shell fragments.

Gray fine sand with tan streaks and dark gray (organic) mottles and nodules. burrowed and root traces

Gray fine sand with tan streaks and red-brown mottles; iron stone nodules in red brown mottles, iron staining around roots

Gray fine sand with tan streaks and dark gray (organic) mottles

Disturbed / gray and tan fine sand

TD

Augered 9ft

PAGE 1 OF 1

CORE LOG

ridge crest, ranch house

CORE # BPV-96a TYPE vibra LOCATION Bolivar Pen.
LATITUDE _____ LONGITUDE _____ SURFACE ELEVATION _____
DEPTH PENETRATED 14.25 LENGTH RECOVERED 3.64 % SHORTENING _____

5.25 pen
3.64 rec
1.61 shr

OBTAINED BY Morton Garner, Angle DATE 6/96
DESCRIBED BY Ed Garner DATE 7/96

PROFILE (ft, m) DESCRIPTION

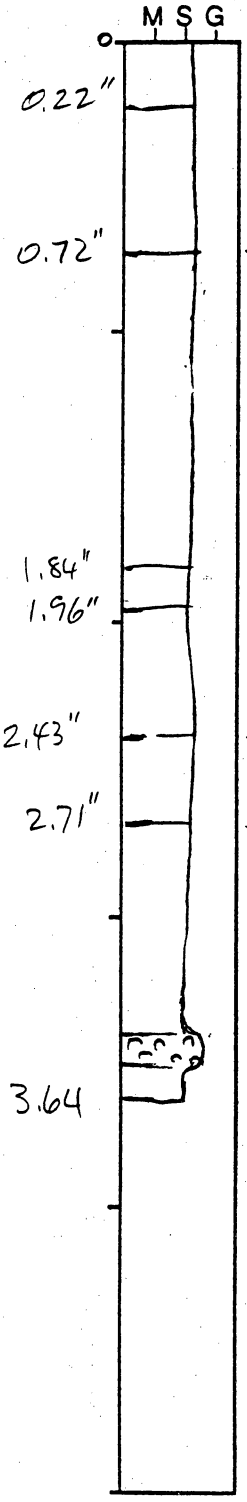

Brown fine sand

Tan fine sand with red-brown mottles

Tan fine sand with scattered shell fragments

2 Black heavy mineral streak

Reddish tan fine sand

Tan fine sand

2 scattered shell fragments

TD

base of p.t
1.5' lt tan sand / roots
1.1' darker tan sand / orange root traces
2.4' dark brown fine sd / orange root traces and organics

CORE LOG

Sand p.t, ridge crest ranch house

CORE # BV-96-1 TYPE Vibra LOCATION Bolivar Peninsula
LATITUDE _____ LONGITUDE _____ SURFACE ELEVATION _____
DEPTH PENETRATED 14.25 LENGTH RECOVERED 9.4 % SHORTENING _____

14.25
9.40
5.8 = shorten

OBTAINED BY Morton, Garner, Angle DATE 6/96
DESCRIBED BY Ed Garner DATE 7/96

PROFILE (ft. m) DESCRIPTION

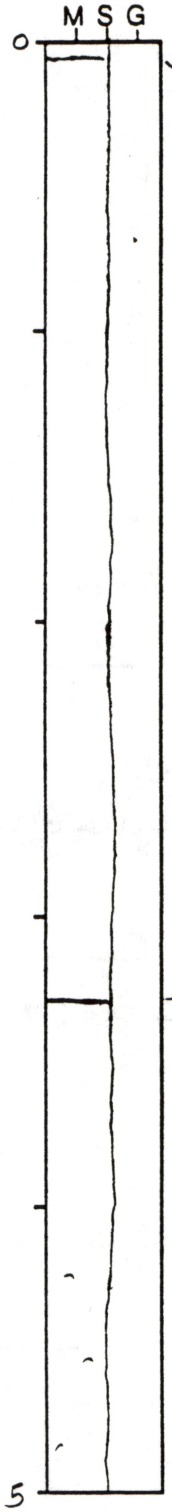

Dark gray fine sand with organic matter

Green gray fine sand

Green gray fine sand with scattered shell fragments

CORE LOG

CORE # BPJ-962a TYPE _____ LOCATION _____
LATITUDE _____ LONGITUDE _____ SURFACE ELEVATION _____
DEPTH PENETRATED _____ LENGTH RECOVERED _____ % SHORTENING ___

OBTAINED BY _____ DATE _____
DESCRIBED BY _____ DATE _____

PROFILE (ft. m) DESCRIPTION

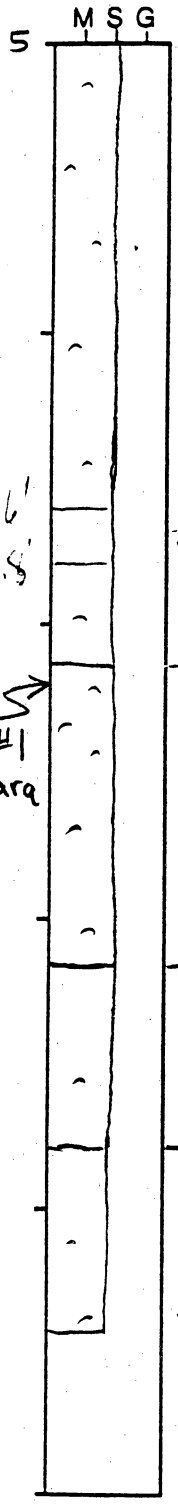

scattered shell fragments

← black organic streak

Gray fine to med. sand with coarse shells and shell fragments

Gray fine to med. sand with fine shell fragments

shell fragments

Dark gray fine sand with scattered fine shell fragments.

CORE LOG

CORE # BPV-963a TYPE vibra LOCATION barren flat, Crystal Beach Bolivar Peninsula
LATITUDE _____ LONGITUDE _____ SURFACE ELEVATION _____
DEPTH PENETRATED 13.5 LENGTH RECOVERED 10.4 % SHORTENING 3.1'

OBTAINED BY Morton, Garner, Angle DATE 6/96
DESCRIBED BY Ed Garner DATE 7/96

PROFILE (ft. m) DESCRIPTION

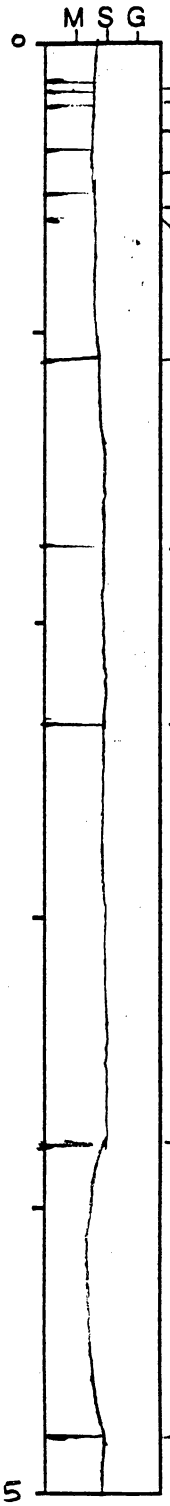

.13'
.16'
.21'
.38'
.52'
0.61' Dark Brown muddy fine sand with shell fragments, blackmottles
Black mud with shell fragments
Brown fine sand with shell fragments, organics
Dark brown muddy fine sand with shell fragments
Dark brown to black sandy mud
Dark gray to black mud with organics

1.12' Black mud

1.77' Dark gray to gray mud with black streaks and mottles, root traces

2.36 Tan to gray fine to medium sand with shells and shell fragments; dark brown mottles and streaks, root traces

Gray fine to medium sand with shells and shell fragments

3.81 Gray mud with fine to medium sand-filled burrows; sand contains shell fragments

4.82 Gray fine to medium sand with shells and shell fragments.

CORE LOG

CORE # BPV-963a TYPE _____ LOCATION _____
LATITUDE _____ LONGITUDE _____ SURFACE ELEVATION _____
DEPTH PENETRATED _____ LENGTH RECOVERED _____ % SHORTENING ___

OBTAINED BY _____ DATE _____
DESCRIBED BY _____ DATE _____

PROFILE
(ft, m) DESCRIPTION

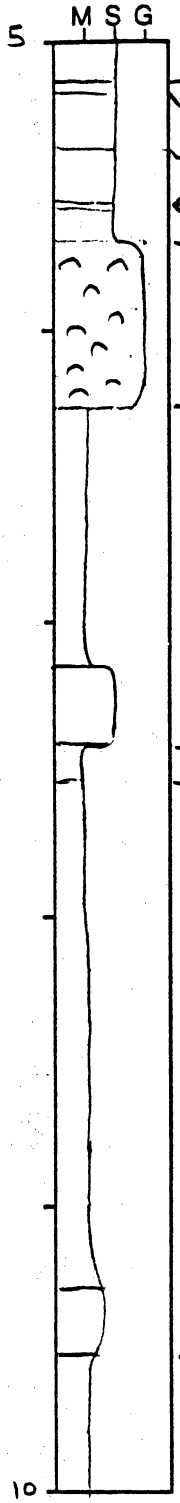

2
5
8
6
8
9

Dark brown "Coffee Ground" organic zone
Gray muddy sand with shell fragments & dark brown organics
Gray muddy fine sand
← coffee ground zone (dk brown)

Shell bed, shells and shell fragments including oysters

6.28 sharp contact

Dark gray mud

7.17 Dark gray fine sand w/ shell fragments

7.27 Dark gray mud
7.55

Dark gray mud with shells and shell fragments

9.32 Dark gray sandy mud
9.51

Dark gray mud with black mottles

CORE LOG

CORE # BPV-963a TYPE _____ LOCATION _____
LATITUDE _____ LONGITUDE _____ SURFACE ELEVATION _____
DEPTH PENETRATED _____ LENGTH RECOVERED _____ % SHORTENING ___

OBTAINED BY _____ DATE _____
DESCRIBED BY _____ DATE _____

PROFILE
(ft. m) DESCRIPTION

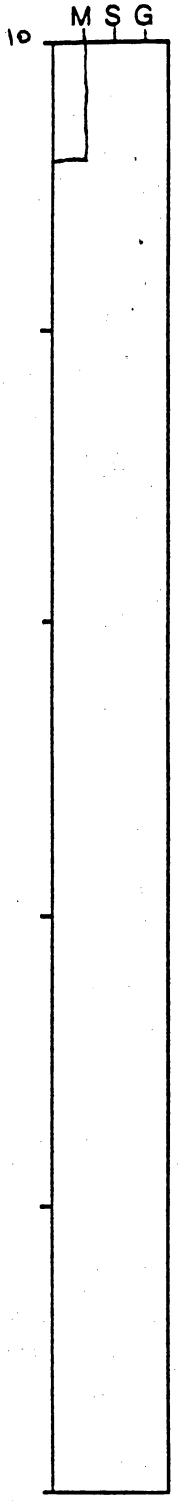

Dark gray mud with black mottles

10.42 TD

Augered 6 ft lt tan fine sand

CORE LOG

sand pit ridge crest, Crystal Beach

CORE # BPV-96-10 TYPE Vibra LOCATION Bolivar Peninsula
LATITUDE _____ LONGITUDE _____ SURFACE ELEVATION _____
DEPTH PENETRATED 14.25 LENGTH RECOVERED 7.5 % SHORTENING 0.75

8.25
7.50
0.75

OBTAINED BY Morton, Garner, Angle DATE 6/96
DESCRIBED BY Ed Garner DATE 7/96

PROFILE (ft, m) DESCRIPTION

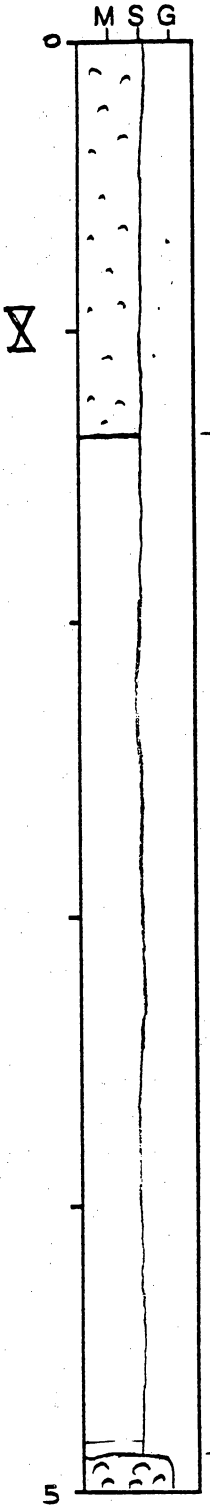

Tan medium to coarse sand with shell fragments

disseminated shell, some oyster, C^{14} sample, 0.8-1.1

1.38

Gray medium to coarse sand with shell fragments, less shell matl. compared to upper unit

4.92

dark zone
shell bed slight upward fining

CORE LOG

CORE # _____ TYPE _____ LOCATION _____
LATITUDE _____ LONGITUDE _____ SURFACE ELEVATION _____
DEPTH PENETRATED _____ LENGTH RECOVERED _____ % SHORTENING ___

OBTAINED BY _____ DATE _____
DESCRIBED BY _____ DATE _____

PROFILE
(ft. m) DESCRIPTION

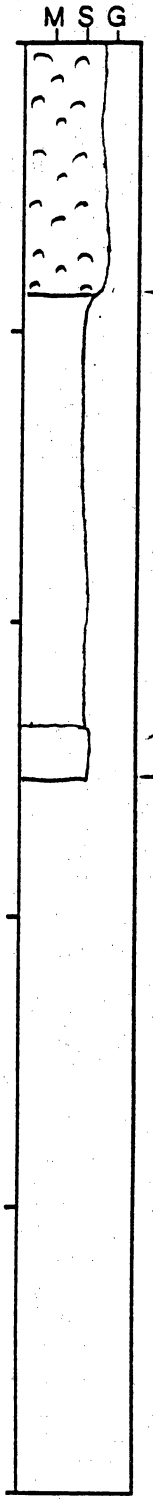

Shell bed

5.69 Sharp contact

Dark gray medium to coarse muddy sand with shells and shell fragments scattered

contains ~ 30% shells

7.53 TD

2 ft dark organic rich mud

Augered core top — 3.2 ft gray muddy sand

PAGE 1 OF 2

CORE LOG

CORE # BPV-965a TYPE Vibra LOCATION marsh, Gab Lake Bolivar Peninsula

LATITUDE _____ LONGITUDE _____ SURFACE ELEVATION _____

DEPTH PENETRATED 14.25 LENGTH RECOVERED 8.43 % SHORTENING 0.62

9.05
8.43
0.62

OBTAINED BY Morton, Garner, Ansle DATE 6/96

DESCRIBED BY Ed Garner DATE 7/96

PROFILE (ft, m)

DESCRIPTION

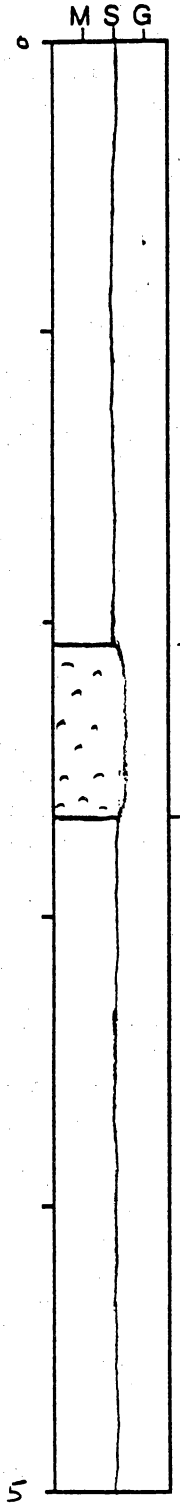

Gray fine sand with 10-15% fine to coarse shell fragments

Gray fine sand with ~25% fine to coarse shell fragments and shells.

Gray fine sand with 5% fine to coarse shell fragments.

CORE LOG

CORE # BPV-965a TYPE _____ LOCATION _____
LATITUDE _____ LONGITUDE _____ SURFACE ELEVATION _____
DEPTH PENETRATED _____ LENGTH RECOVERED _____ % SHORTENING ___

OBTAINED BY _____ DATE _____
DESCRIBED BY _____ DATE _____

PROFILE (ft, m) DESCRIPTION

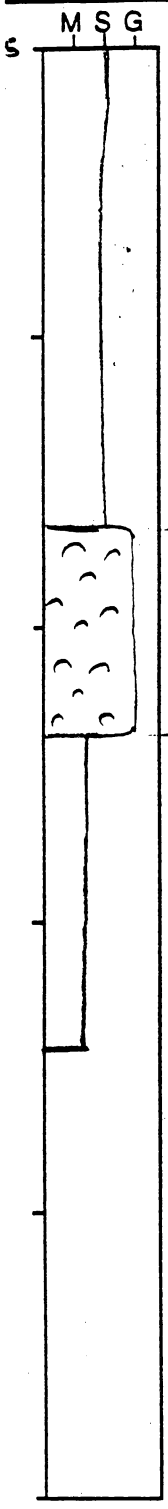

gray fine sd with shell frags

6.68

slight upward fining
Shell bed with fine sand shells and shell fragments, Ranges

7.38

sharp contact

Dark gray sandy mud; shelly near top, sand filled burrows near base

8.43

-TD

Augered 4.75' tan fine sand

CORE LOG

ridge crest, Crab Lake

CORE # BPV-966a TYPE _____ LOCATION Bolivar Peninsula
LATITUDE _____ LONGITUDE _____ SURFACE ELEVATION _____
DEPTH PENETRATED 5.6 LENGTH RECOVERED 4.75 % SHORTENING 0.85'

5.60
4.75
.85

OBTAINED BY Morton, Garner, Angle DATE 6/96
DESCRIBED BY Ed Garner DATE 7/96

PROFILE (ft, m) DESCRIPTION

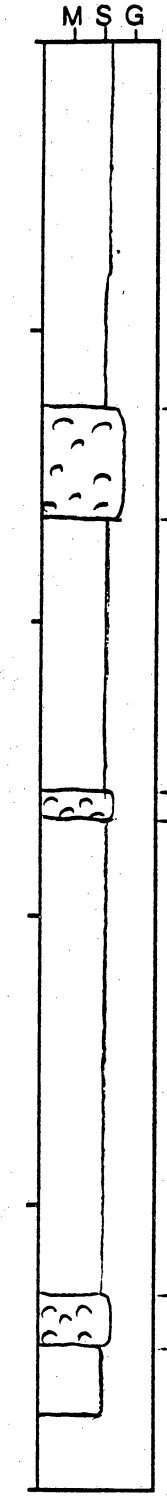

Tan fine sand with ~10% fine to coarse shell fragments

1.28 — Shell bed with ~ 40% fine sand oysters

1.67 — Tan fine sand with fine to coarse shell fragments (10% shell)

2.59
2.69 — Shell bed with 15% fine sand drag — Donax, oyster

Gray fine sand with < 5% fine to med. shell fragments.

4.30
4.49 — Shell bed; shells and shell fragments w/10% fine sand — Busycon, oys mulinea incisura

4.75 TD — Gray fine sand with < 5% fine to coarse shell frags.

Augered 3.5 ft (: ft organic muddy sand

PAGE 1 OF 2

CORE LOG

ridge flank, Elm Grove

CORE #BPV-967a TYPE vibra LOCATION Bolivar Peninsula
LATITUDE _____ LONGITUDE _____ SURFACE ELEVATION _____
DEPTH PENETRATED 14.25 LENGTH RECOVERED 7.45 % SHORTENING 33

10.75
7.45
3 30

OBTAINED BY Morton, Garner, Angle DATE 6/96
DESCRIBED BY Ed Garner DATE 7/96

PROFILE (ft. m) DESCRIPTION

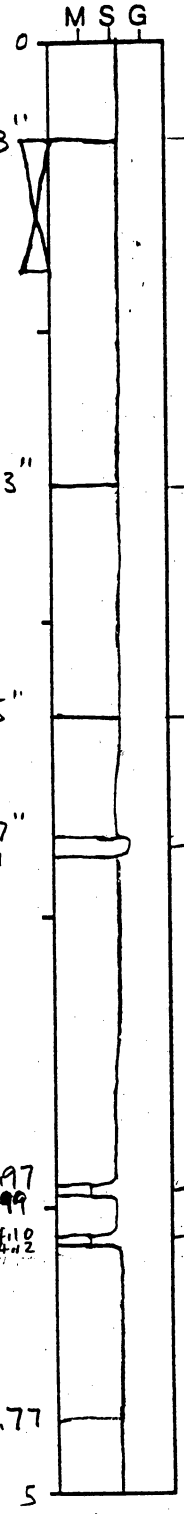

Tan fine to medium sand with dark gray to black mottles (organic) and medium to coarse shell fragments.

Tan medium to fine sand with coarse shell fragments and shells.

disseminated shell C^{14} sample 0.33 - 0.7

Tan fine to medium sand with fine to medium shell fragments

thin shell bed

Gray fine to medium sand with shell fragments

gray mud

dark gray mud

Gray fine sand to med?

CORE LOG

CORE # BPV-967a TYPE _____ LOCATION _____
LATITUDE _____ LONGITUDE _____ SURFACE ELEVATION _____
DEPTH PENETRATED _____ LENGTH RECOVERED _____ % SHORTENING ___

OBTAINED BY _____ DATE _____
DESCRIBED BY _____ DATE _____

PROFILE (ft, m) DESCRIPTION

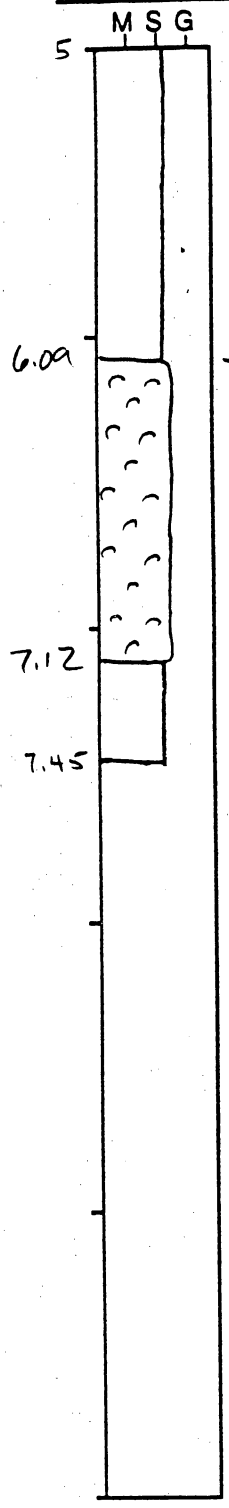

Gray fine to med? sand

shell bed; shells and shell fragments <50% sand includes reworked oyster

Gray fine to coarse sand with shells and shell fragments

TD

CORE LOG

marsh, Elm Grove

CORE # EPI-968a TYPE vibra LOCATION Bolivar Peninsula
LATITUDE _____ LONGITUDE _____ SURFACE ELEVATION _____
DEPTH PENETRATED 11 LENGTH RECOVERED 6.1 % SHORTENING 4.9'

11.0
6.1

OBTAINED BY Morton, Garner, Angle DATE 6/96
DESCRIBED BY Ed Garner DATE 7/96

PROFILE
(ft. m) DESCRIPTION

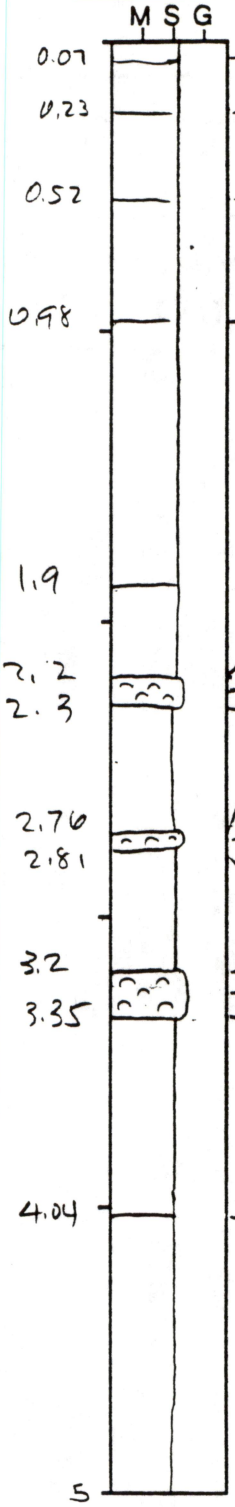

Brown fine sand with roots and grass

Brown fine sand with coarse shell fragmen ~2%

Dark gray fine sand with organics and roots

Gray fine sand with black streaks (organics)

Green gray fine sand with tan mottles

Gray fine sand with fine to coarse shell fragments (50%)

~ shell bed with 40% fine sand

Tan fine sand with fine to coarse shell fragments (5

~ shell bed; medium to coarse shell frags; 40% fine sand

Gray fine sand with fine to coarse shell fragments

~ shell bed; shells and shell fragments; 40% fine sand

Gray fine sand with < 5% fine shell fragments

Gray fine sand with 10% fine to coarse shell fra

CORE LOG

CORE # BFN-968a TYPE _____ LOCATION _____
LATITUDE _____ LONGITUDE _____ SURFACE ELEVATION _____
DEPTH PENETRATED _____ LENGTH RECOVERED _____ % SHORTENING _____

OBTAINED BY _____ DATE _____
DESCRIBED BY _____ DATE _____

PROFILE (ft. m) DESCRIPTION

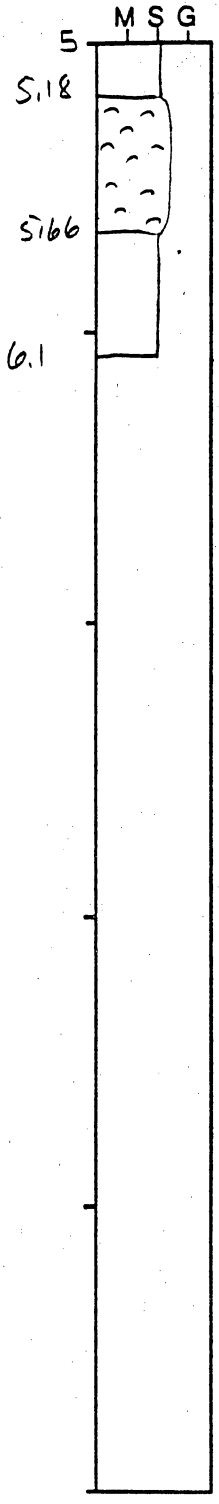

Shell bed; 40% fine - coarse sand
oyster & disseminated

Gray fine sand with fine to coarse shell (10-15%)

TD

0.5' lt tan gray silty sand
organic conc. — 1.6' tan silt
2.5' brown silty clay
core top
Augered 5.7'

PAGE 1 OF 1

CORE LOG rd along channel near East Bay

CORE # RLV-96la TYPE vibra LOCATION Robinson Lake
LATITUDE ____ LONGITUDE ____ SURFACE ELEVATION ____
DEPTH PENETRATED ____ LENGTH RECOVERED 4.8 % SHORTENING ____

OBTAINED BY Morton, Garner, Angle DATE 6/96
DESCRIBED BY Ed Garner DATE 7/96

PROFILE (ft. m) DESCRIPTION

M S G

0 — Gray brown sandy mud

0.26 — Gray sandy mud; mottled with red brown and dark gray., iron staining along root traces

0.97 — Gray stiff mud mottled with red brown and dark gray to black, iron staining along root traces

4.77" — TD

Addendum 4

GPS Locations of Vibracores, Galveston Island and Bolivar Peninsula

GPS Locations of Vibracores

Galveston Island/Bolivar Peninsula, Galveston County Texas

Core	Latitude	Longitude	Date Collected
GIV961	29°15'53.339029"N	94°53'47.776896"W	06/10/96
GIV962	29°15'50.176732"N	94°53'45.860604"W	06/10/96
BPV961	29°24'19.424903"N	94°43'29.634322"W	06/11/96
BPV962	29°24'22.832145"N	94°43'33.789977"W	06/11/96
BPV963	29°27'58.810988"N	94°38'03.206531"W	06/11/96
BPV964	29°27'52.563145"N	94°37'51.408095"W	06/11/96
BPV965	29°29'59.645460"N	94°32'27.032999"W	06/11/96
BPV966	----------	No Data, Bad PDOP	06/11/96
BPV967	29°27'58.415813"N	94°40'20.995134"W	06/12/96
BPV968	29°28'00.279376"N	94°40'22.237147"W	06/12/96
RLV961	29°33'53.164769"N	94°35'50.697125"W	06/13/96

Addendum 5

Effects of Structures, Nearshore Bathymetry, and Offshore Shoals on Wave Refraction, Shoreline Erosion, and Grain Size Patterns, Southeast Texas Coast

Effects of Structures, Nearshore Bathymetry, and Offshore Shoals on Wave Refraction, Shoreline Erosion, and Grain Size Patterns: Southeast Texas Coast

James C. Gibeaut
Bureau of Economic Geology
The University of Texas at Austin
University Station Box 'X'
Austin, Texas 78713
U.S.A.
fax: 512-471-0140
e-mail: gibeautj@begv.beg.utexas.edu

ABSTRACT

Wave refraction and shoaling can cause alongshore variation in the amount of wave energy reaching a shoreline. A wave refraction model was developed for 300 km of the generally erosional southeastern Texas and western Louisiana coast to qualitatively assess the effects of wave refraction on shoreline rates-of-change and nearshore sediment grain size. Wave hindcast data computed by the U.S. Army Corps of Engineers provided 20 years of deep-water wave height and direction data for the period from 1956 through 1975 for input to the model. Shoreline rates-of-change for nearly the same period and inner-shelf sediment samples obtained in 1976/77 were compared to nearshore wave heights computed by the model using average deep-water wave conditions.

Sabine and Heald Banks are shoals that are more than 25 km offshore of the eastern half of the study area and have crests shallower than 10 m. These shoals focus wave energy on the shoreline and cause a variance in wave heights of at least 30% of the deep-water heights as computed by the wave refraction model. The western half of the study area, west of Galveston Bay, has steeper offshore gradients and no prominent offshore shoals. Shoreline wave heights here are generally higher than east of Galveston Bay but show less and more local variability. Local wave-height variance is caused by refraction and shoaling on ebb-tidal deltas and the Brazos River Delta. Variation in shoreline rates-of-change match shoreline wave-height variation (relatively high wave heights correspond with relatively high retreat rates) except where jetties, dredged channels, and the Galveston Island seawall have interrupted littoral drift, which is the

most important source of beach sand along this coast. Landward of Sabine and Heald Banks, between Bolivar Roads (the main entrance to Galveston Bay) and Sabine Pass, the curve showing the alongshore rate of shoreline change and the curve showing wave heights occurring at the 4-m isobath for the average, onshore wave condition are remarkably similar. Peaks in nearshore grain size for this 90-km stretch of coast also correspond with peaks in wave heights.

Wave refraction across nearshore features such as headlands and embayments tends to focus energy on shoreline protuberances causing higher rates of erosion and hence acting to smooth the shoreline. Refraction caused by offshore shoals that are not part of the littoral drift system, however, may cause shoreline irregularities. Sabine and Heald Banks are such offshore shoals, and their effects on wave propagation may impart a large-scale rhythmic topography by causing alongshore variance in the shoreline rate-of-change. The actual development and permanency of this topography depends on the temporal variation in wave direction, height, and period, and the reaction time required for the shoreline to adjust to new average wave conditions.

KEYWORDS

ocean waves, propagation, shoaling, Texas, jetties, shoals, shorelines , changes

(1.0) INTRODUCTION

It is well established that offshore ridges and troughs cause wave refraction and the convergence and divergence of wave energy along shorelines (Shepard and Inman, 1950,1951; U.S. Army Corps of Engineers, 1984, pp. 2–60 to 2–74). It has also been shown that alongshore variation in wave energy is an important cause of alongshore variation in shoreline change (e.g. Goldsmith et al., 1975; Inman and Dolan, 1989). Goldsmith (1976) used a wave refraction model to relate alongshore variation in wave energy arriving at the shoreline to shoreline change from Cape Henlopen to Cape Hatteras on the United States east coast. He also generally related beach grain size distribution to variation in wave energy as derived from wave refraction modeling. More recently, Barua and Kana (1995) related convergence and divergence of wave energy, as computed by a wave refraction program, to general shoreline grain size and morphology along the Ganges-Brahmaputra Delta coast. The focus of this study is to determine the effect that offshore bathymetry, particularly offshore shoals, has on wave refraction patterns and the alongshore distribution of wave energy along the southeast Texas coast (Fig. 1). Furthermore, shoreline change and nearshore sediment grain size is compared to computed alongshore wave heights for a representative wave condition.

(2.0) PHYSICAL SETTING OF STUDY AREA

(2.1) Processes

The southeastern shore of Texas is a microtidal, wave-dominated coast in the classification of Hayes (1979). Tides are chiefly diurnal with a diurnal range of 0.85 m on Sabine Bank (Fig. 1) (National Ocean Service, 1979). Mean significant wave height (Hs), as determined from 20 years of hindcast data, is 1.2 m with a mean peak wave period (Tp) of 5.8 s (Hubertz and Brooks, 1989, station number 12) (Fig. 1). The hindcast data show that mean Hs varies from 0.9 m in July and August to 1.4 m in December, January, February, March, and April when cold fronts traverse the area. Waves from the southeast are the most common, occurring 49% of the time and have the

highest mean Hs of 1.4 m and a mean Tp of 6.1 s (Fig. 2). Two years of nondirectional wave data were collected from May 1993 through April 1995 by a buoy of the National Data Buoy Center at mooring number 42035 (Fig. 1). The buoy mooring is located in 15 m water depth and 45 km northwest and landward of WIS station number 12. These data are hourly and nearly continuous over the 2 years. The mean Hs was 0.91 m, and the mean Tp was 5.6 s. The lower wave heights measured by the buoy data compared to the hindcast data are partly explained by the buoy being closer to shore than the hindcast station. Other explanations include the different time periods and biases in the data.

The above hindcast study and buoy data did not include waves generated by tropical cyclones. The study area, however, is greatly affected by both tropical storms and hurricanes. Tide records from the bay side of Galveston Island show that storm surges exceeded 1.2 m about every 5 years from 1908 to 1983 (Morton and Paine, 1985). In a hurricane hindcast study that included storms occurring from 1956 to 1975, the return interval for a Hs of 6.2 m was determined to be 5 years (Abel et al., 1989, station number 12). Hurricane Alicia, in 1983, was the most recent hurricane to strike the southeast Texas coast. Alicia was a minimal category 3 storm (Garcia and Flor, 1984) and crossed the coast at San Luis Pass (Fig. 1) causing extensive property damage and beach and dune erosion along Galveston and Follets Islands (Morton and Paine, 1985; Morton et al. 1994).

The U.S. Army Corps of Engineers (1985) used Summary of Synoptic Meteorological Observations (SSMO) data to estimate littoral drift rates in the study area. Ten years of SSMO data provided deep-water wave statistics that were then transformed to alongshore wave energy flux at 17 locations between Sargent Beach and Sabine Pass. The wave energy flux determinations were verified with observational data and a wave gauge. The energy data were converted to littoral drift rates and combined with drift caused by wind-generated currents to determine gross and littoral drift rates and directions. The net overall littoral drift was determined to be to the southwest at about 38,000 m^3/yr for unobstructed stretches of shoreline. Gross transport rates due to waves

only were calculated as being much lower to the east of Bolivar Roads than to the west (Fig. 1). Between Bolivar Roads and Sabine Pass, gross transport rates averaged about 90,000 m^3/yr. Between Bolivar Roads and Sargent Beach, they averaged 230,000 m^3/yr.

(2.2) Shoreline Features

The southeast Texas coast consists of sandy, transgressive and regressive barrier islands, spits, and beaches (Morton, 1979). Transgressive shoreline deposits occur at headlands formed of delta-plain sediments of the Holocene Brazos-Colorado delta and the Pleistocene Trinity delta. Brazos River delta deposits formed a headland between East Matagorda Bay and West Bay, and the Trinity River delta deposits formed a headland between High Island and Sabine Pass (Fig. 1). These headlands probably protruded seaward much more 3,500 years ago, when sea level approached its present level (Frazier, 1974), than they do today (Morton, 1977). Since sea-level stillstand, the headlands eroded and sediment dispersed to the inter-deltaic areas forming prograding spits and regressive barrier islands. This process created the relatively linear shoreline configuration present today (Morton, 1979).

A wide range in naturalness, size, and type of coastal openings occurs along the southeast Texas coast. These openings affect shoreline change and nearshore sediment textures through their effect on wave refraction patterns and alongshore sediment transport. On the southwest end of the study area, the new Brazos River entrance has built an arcuate, wave-dominated delta that protrudes 2 km into the Gulf of Mexico. This delta formed in 1929 when the Brazos River was diverted from the Freeport channel to its present location (U.S. Army Corps of Engineers, 1992a). No jetties are at this new Brazos River entrance. Freeport channel (old Brazos River entrance) is 10 km northeast of the new Brazos River (Fig. 1). Jetty construction and dredging activities began at Freeport channel in the 1880's (U.S. Army Corps of Engineers, 1992a). Currently, two jetties extend about 1 km seaward of the natural shoreline trend to depths of 4 m. The dredged channel at Freeport extends 5 km offshore to surrounding depths of 12 m. The 14-m isobath protrudes 10 km

seaward in an arcuate configuration along 30 km of shoreline centered on the Brazos River and Freeport entrances (Fig. 1). Apparently, this bathymetry reflects the relict Holocene Brazos-Colorado deltaic headland at the time of sea-level stillstand (Morton, 1977; Morton, 1979; Morton and Winker, 1979).

The Galveston Bay system exchanges water with the Gulf of Mexico through three tidal inlets. San Luis Pass, is a natural, unjettied and undredged tidal inlet separating Follets and Galveston Islands (Fig. 1). San Luis Pass maintains a mixed-energy, ebb-tidal delta configuration (Gibeaut and Davis, 1993) that is offset to the southwest and extends 2 km offshore as outlined by the 6-m isobath. The ebb-tidal delta extends 5 km alongshore and is currently bypassing most littoral drift. San Luis Pass locally affects shoreline change within a few kilometers distance (Morton et al., 1994; Morton et al. 1995). Bolivar Roads separates Galveston Island and Bolivar Peninsula (Fig. 1). Dredging and jetty construction at this large tidal inlet began in the 1870's, and, by 1910, the jetties were completed to their present length extending more than 7 km offshore (U.S. Army Corps of Engineers, 1992a). The jetties terminate in surrounding depths of 8 m. Much of the sediment of the ebb-tidal delta moved shoreward in response to jetty construction and dredging (White et al., 1985), but in the 1960's, the 10-m isobath indicated a large down-drift offset ebb-tidal delta/shoreface deposit (Fig. 1). This deposit extends about 8 km offshore and 20 km alongshore. Rollover Pass is a flood-dominated tidal inlet that cuts across Bolivar Peninsula and is only about 60 m wide (Bales and Holley, 1989). Dredging created this pass during the winter of 1954/55 (U.S. Army Corps of Engineers, 1992a). Construction of seawalls and bulkheads in the channel stabilized it by 1959, and it remains open today.

Sabine and Calcasieu Lakes (Fig. 1) open to the Gulf of Mexico through jettied and dredged tidal channels. Sabine Pass on the Texas-Louisiana border has a large ebb-tidal delta that is offset to the west and extends 13 km offshore and about 35 km alongshore as delineated by the 10-m isobath. Jetties at Sabine Pass extend 5 km into the Gulf of Mexico to surrounding depths of 4 m. A dredged shipping channel extends to seaward of Sabine Bank. The ebb-tidal delta associated

with Calcasieu Pass is also offset to the west and protrudes about 5 km offshore and extends about 15 km alongshore as delineated by the 6-m isobath. Jetties at Calcasieu Pass extend about 1.5 km into the Gulf to surrounding depths of 3 m. A dredged channel extends seaward and to the east of Sabine Bank.

The Galveston seawall and groin field on the east end of Galveston Island (Fig. 1) have affected shoreline change by preventing erosion at the seawall and interrupting littoral drift that supplied beaches to the southwest of the seawall. Construction of the seawall began in 1902 and was completed to its current length of 16 km in 1963 (U.S. Army Corps of Engineers, 1992b). In the 1930's, 13 150-m-long groins were constructed in front of the seawall.

(2.3) Offshore Features

The complexity of offshore bathymetry between the landward, 10-m isobath and the seaward edge of the study area (about 30 m depth) is quite variable (Fig. 1). Generally, the bathymetry is less complicated and deeper for the southwestern 100 km of the study area. The regional offshore slope from the shoreline to 30 m depth decreases to the northeast. Seaward of Sargent Beach the slope is 0.8 m/km, seaward of Galveston Island it is 0.4 m/km, Bolivar Peninsula 0.3 m/km, and Ocean View Beach 0.2 m/km. The slopes from the shoreline to 10 m depth also decrease to the northeast with offshore of Sargent Beach being 3.4 m/km, Galveston Island 2.9 m/km, Bolivar Peninsula 1.4 m/km, and Ocean View Beach 0.8 m/km.

Bathymetry of the eastern 200 km of the study area is complicated by Sabine and Heald Banks. These Banks are inner shelf, sandy shoals interpreted as remnants of barrier islands formed during the Holocene sea-level rise (Nelson and Bray, 1970). They are aligned northeast-southwest and are parallel to the present shoreline trend. Sabine Bank is delineated by the 10-m isobath about 25 km offshore of Sabine Pass (Fig. 1). The main body of Sabine Bank extends 50 km and is about 7.3 km wide at its widest section. A few small shoals detached from Sabine Bank exist to the

east. The shallowest portions of the Bank are on the eastern end where depths are as shallow as 4.5 m but deepen to more than 9 m at the southwest end. Surrounding depths are 12 m, hence Sabine Bank has a maximum relief of about 8 m. Heald Bank is 55 km offshore of the entrance to Galveston Harbor (Bolivar Roads) (Fig. 1). Heald Bank is not as well defined as Sabine Bank and has a relatively small area that is shallower than 10 m (Fig. 1). The 14-m isobath encloses a much larger area extending 30 km to the southwest from the eastern shallow areas. The trend of Heald Bank may be extended another 30 km to the southwest as delineated by the 20-m isobath.

(3.0) METHODS

(3.1) Wave Refraction Modeling

This study uses the Regional Coastal Processes Wave (RCPWAVE) Propagation Model (Ebersole et al., 1986). The Waterways Experiment Station of the U.S. Army Corps of Engineers developed RCPWAVE with the goal of predicting natural and human-induced coastal change across an extensive length of shoreline. RCPWAVE can predict linear, plane-wave propagation over a coastal region with varying bathymetry. The model includes refractive and bottom-induced diffractive effects but does not include nonlinear effects. Wave input is monochromatic and unidirectional. RCPWAVE was modified to run on the Bureau of Economic Geology's (Bureau) SUN 1000 workstation. It was also modified to provide output suitable for input into the CPS-3 mapping and contouring program (Schlumberger GeoQuest, 1994) for graphical display of the results.

RCPWAVE provides output of several wave parameters for each grid cell. For this study, wave height, which is proportional to wave energy, is contoured and plotted in gray scale over bathymetric contours (Fig. 3). For more direct comparisons with shoreline change and nearshore sediment texture, a wave-height profile was generated depicting heights occurring along the 4-m isobath (Figs. 4,5). A shallower isobath was not chosen for the wave-height profile because bathymetry shallower than 4 m is relatively unreliable due to dynamic conditions and boundary

effects during the gridding process. The 4-m depth approximates the limit of normal sediment exchange with the beach or the "depth of closure." At depths greater than the depth of closure, bathymetric change is relatively small compared to shallower depths. Williams et al. (1979), using the method of Hallermeier (1977), estimated the depth of closure to be approximately 4.4 m for the Galveston Island coast. Brown and Kraus (1994), using the method of Hallermeier (1983) and 20 years of wave hindcast data (discussed below) (Hubertz and Brooks, 1989), estimated the depth of closure to be between 4.6 and 7 m along Galveston Island. Hallermeier's 1983 method involves multiplying the estimated average of the highest waves occurring for 12 hours in a year by 2.3. A better way to determine the depth of closure is to compare time series of beach and nearshore profiles over at least several years, but these data are not available.

Isobaths deeper than the 4-m isobath were not chosen for the wave-height profile because of the desire to compare wave heights occurring close to the shoreline with shoreline rates-of-change. Another reason is to ensure that currently active wave processes have a significant impact on surficial sediment texture so that a comparison between patterns of wave height and texture could be made. Inner shelf mean grain sizes of the mud and sand fractions in the study area are fine sand or finer (White et al., 1985; White et al., 1987; White et al., 1988). The bottom orbital velocity required to initiate sediment motion for fine sand is approximately 18 cm/s for wave periods of 6 s (Komar and Miller, 1973, 1975). Using the linear Airy wave equation and shallow-water wave parameters of height = 1.2 m, period = 6 s, and water depth = 4 m, it is determined that bottom orbital velocities reach 80 cm/s. Thus waves commonly cause sediment motion and suspension at 4-m depth, and sediment texture at this depth will reflect varying wave conditions.

(3.2) Bathymetry

Because complicated bathymetry in the form of Sabine and Heald banks occurs 50 km offshore, a large area must be considered in the wave refraction model. This analysis includes 300 km of the southeast Texas and western Louisiana coast between the Calcasieu River on the northeast and East Matagorda Bay on the southwest (Fig. 1). The area extends about 100 km

offshore to depths of 30 m. Digital bathymetric data used to construct the grid for wave refraction analyses were obtained from the U. S. National Geophysical Data Center (NGDC) through the U.S. Geological Survey in St. Petersburg, Florida. The bathymetric data consist of digitized smooth sheets of National Oceanographic and Atmospheric Administration surveys. Horizontal coordinates are in the Universal Transverse Mercator zone 15R coordinate system and related to the 1927 North American Datum. Depths are relative to mean low water (Gulf Coast low water datum), but, for the wave refraction analyses, the depths were deepened by 0.21 m to estimate depths at mean tide level.

To obtain full coverage of the area, bathymetric surveys from the 1930's and 1960's had to be combined. Care was taken to use the latest available data for a particular area, and the data were filtered to eliminate obvious errors. Approximately 70% of the study area is covered by 1960's surveys including the entire area east of Galveston Island from the shoreline to seaward of Sabine and Heald Banks (Fig. 1). Over 419,000 soundings were used to construct the grid with the widest spacing between survey lines being about 2 km on the seaward edge of the area. Data density increases greatly toward shore with survey line spacing less than 100 meters and soundings along the lines even more closely spaced. A rectilinear bathymetric grid was constructed using CPS-3 (Schlumberger GeoQuest, 1994) mapping software. The grid has 600 cells, which are 500 m long, in the alongshore direction, and 800 cells, which are 125 m wide, in the normal to shore direction. Soundings in a 2-km boundary surrounding the grid area were considered by the gridding routine to eliminate edge effects. The grid is not smoothed for the wave refraction analyses.

The depth at which waves begin to significantly transform is typically _ the wavelength. For a wave with a 6 s period, the deep-water wavelength is approximately 56 m. The depth at which this wave will begin to change as it propagates onshore, therefore, is 14 m (56 m/4). For an 8.5-s period wave, the beginning transformation depth is 28 m. It is determined, therefore, that the bathymetric grid used in this study begins seaward of where typical waves begin to transform as

they propagate onshore and that the shallow portions of Sabine and Heald Banks are expected to affect wave propagation.

(3.3) Wave Data

Wave parameters used in this study are from the U.S. Army Corps of Engineers Coastal Engineering Research Center's Wave Information Study (WIS) for the Gulf of Mexico (Hubertz and Brooks, 1989). This data set is a hindcast of wave conditions for coastal and offshore locations for the period 1956 to 1975. Tropical storm and hurricane conditions are excluded. For the hindcast, a wind field is computed from an atmospheric pressure field and merged with observed wind data (Resio et al., 1982). A discrete spectral model then uses the merged wind field to determine the generation of waves (Resio, 1982). The results of the hindcast are 20-year time series from 1956 to 1975 of directional wind and wave data at 3-hour intervals. Data for discrete locations are compiled in percent occurrence tables for 22.5-degree direction intervals.

Hubertz and Brooks (1992) evaluated the accuracy of the hindcast estimates by comparing them with measured wind and wave data from six oceanographic buoys and a coastal wave gauge. Measured data were not widely available during the original hindcast period, therefore, a new 1-year time series of hindcast data was generated for 1988. The hindcast accuracy for Hs was determined to be low in the mean by 0.1 m compared to measured data and to have a root mean square difference (RMSD) of 0.25 m. Tp was low in the mean by 1 s with a RMSD of 2 s. The largest discrepancies between hindcast and measured values occurred during times of rapid shifts in wind direction and speed. These shifts occur with passing cold fronts in the fall and winter when southerly winds rapidly shift northerly after fronts pass to the south and east. Northerly winds are directed offshore along the southeast Texas coast, therefore, an under prediction of the Hs and Tp for waves generated during these times has a minimal effect on the wave hindcast statistics used in this study. The measured wave data were nondirectional; hence a wave direction comparison could not be made. However, a climatic summary of measured wind direction is available for buoys over a 13-year period from 1976 to 1988. A comparison using these climatic

data to determine accuracy of the hindcast wind data assumes that the wind climate was statistically the same during the hindcast and measured periods. Hubertz and Brooks (1992) found that the frequency distribution of wind direction for 20-degree intervals generally agreed within 5% between the hindcast and measured data sets.

Data from WIS station number 12 (Fig. 1) located 70 km offshore of Bolivar Peninsula and in 20-m water depth were used in this study to determine beginning offshore wave conditions for wave refraction analyses. For wave cases one through seven, the mean Hs and Tp for each 22.5-degree onshore wave direction interval were used (Table 1). For case eight, the mean Hs, Tp, and direction of waves for onshore wave conditions only (wave directions between 55 and 235 degrees) were computed from the 3-hourly data.

Case nine estimates Hurricane Alicia conditions in 1983 based on data presented in Garcia and Flor (1984) (Table 1). Hurricane Alicia made landfall near San Luis Pass with winds up to 115 mph on the morning of August 18, 1983. The Coastal Engineering Research Center operated wave and tide gauges on three Shell Oil Company Platforms during Alicia's westerly passage through the Gulf of Mexico. The closest gauge to the study area was at the Vermillion 22 platform, which is 80 km to the southeast of Calcasieu Pass (Fig. 1). This gauge was in 10 m water depth and located about 16 km off the Louisiana coast. The highest Hs recorded at this gauge was about 2 m for a 12-hour period during the afternoon and evening on August 17. The corresponding Tp was about 8.5 s. No directional information is available other than the observance of dominantly southeast waves (Garcia and Flor, 1984). Storm surge at the Vermillion 22 platform was estimated to be about 0.38 m above the expected tide range. The highest water levels on the Gulf coast occurred on the west end of Galveston Island and reached 3.36 m above mean tide level. For the current study, water depths were not adjusted for surge caused by Alicia. Wave refraction results for estimated Hurricane Alicia conditions (case nine) are presented to provide contrast to the nonstorm, average conditions presented in cases one through eight.

(3.4) Shoreline Change Data

The distribution of wave heights along the coast is compared with shoreline change rates. Shoreline change data for the shoreline from Sargent Beach northeast to Sabine Pass (Fig. 1) are taken from Bureau published reports (Morton, 1974; Morton and Pieper, 1975; Morton, 1975; Morton et al., 1976). These reports provide the amounts and rates of shoreline movement at points spaced 1,524 m alongshore. Shoreline change data are given for several time intervals spanning the period from the 1800's to the 1970's. The Coastal Studies Institute, Louisiana State University provided shoreline change data for the Louisiana coast from Sabine Pass east to Calcasieu Pass (Fig. 1). These data include rates of shoreline change at locations spaced 50 m apart for several time intervals from 1883 to 1994 for all but 4.96 km to the east of Sabine Pass where 1994 data are not available (Byrnes et al., 1995).

For comparison with alongshore wave height patterns, shoreline rate-of-change data were selected for the time interval that most closely matched the period of the WIS hindcast data (1956 to 1975). For the Texas coast from Sargent Beach to 6 km west of Sabine Pass (Fig. 1), shoreline change for the period from the mid-1950's (1955, 1956, or 1957) to the mid 1970's (1973 or 1974) are used. For the shoreline 6 km west of Sabine Pass, the time period from 1955 to 1970 is used, and for the Louisiana shoreline 4.96 km east of Sabine Pass to Calcasieu Pass, the period from 1947/54 to 1994 is used (Fig. 1). Shoreline rate-of-change is computed by dividing the distance between shorelines by the number of years separating shorelines.

(3.5) Sediment Texture

Nearshore sediment texture data are from published Bureau reports (White et al., 1985; White et al., 1987; White et al., 1988). Surface sediment samples comprising the upper 4 to 10 cm of sediment were collected during 1976 and 1977 using a grab sampler. Sample sites are 1.6 km apart and extend from the Gulf shoreline to about 18 km offshore for the entire Texas coast. The reports provide contour maps of various textural properties of the sediments including mean grain

size for the sand and mud fraction. The textural parameters were contoured by hand and published on 1:250,000 scale maps along with the actual data value for each sample location. For this study, the published maps were used to produce, by hand, an alongshore profile of mean grain size occurring between the 3.6-m and 5.5-m isobaths. This profile is compared with the wave-height profile along the 4-m isobath (Figs. 4,5).

(4.0) RESULTS

(4.1) Wave Transformation

When viewing contour maps of wave height (Fig. 3), the effect of the offshore shoals, such as Sabine and Heald Banks, on wave transformation is readily apparent. Wave energy is focused landward of the shoals causing zones of relatively high- and low-wave heights along the shoreline (Fig. 3). These zones shift along the coast with the change in wave direction. For the more common directions of cases three (Fig. 3c), four (Fig. 3d), eight (Fig. 3h) (average onshore condition), and nine (Fig. 3i) (storm condition), the variance in alongshore wave heights caused by the shoals only occurs east of Bolivar Roads. For these directions, four zones of high- and five zones of low-wave heights occur between Bolivar Roads and Sabine Pass. The eastern high-wave height zone is enhanced by the additional focusing and shoaling of waves on the large ebb-tidal delta at Sabine Pass, and the western low-wave height zone is enhanced by the sheltering effect of the ebb-tidal delta at Bolivar Roads (Fig. 3h). Between Sabine Pass and Calcasieu Pass, two high-wave height zones and three low-wave height zones occur. The relatively high waves are caused by offshore wave interaction with the eastern portion of Sabine Bank, and the eastern high-wave height zone is further enhanced by focusing and shoaling on the delta at Calcasieu Pass.

West of Bolivar Roads, along Galveston Island, Follets Island, and Sargent Beach, wave heights are relatively constant except for local variation caused by waves refracting and shoaling on the ebb-tidal deltas at Bolivar Roads and San Luis Pass and the Brazos River delta. During average onshore wave conditions, the amount of variation in alongshore wave heights east of Bolivar

Roads is as much as 0.5 m (Fig. 4b), whereas west of Bolivar Roads the variation is generally less than 0.1 m except for local variance around deltas. The average wave height is slightly higher west of Bolivar Roads than east of Bolivar Roads by about 0.1 m (Fig. 4b).

Cases three and nine (Figs. 3c and 3i) both have a wave direction of 135 degrees, but case nine represents a long-period, large-wave height storm condition estimated to have occurred during Hurricane Alicia in 1983. The variance in alongshore wave height between Bolivar Roads and Sabine Pass is about 1 m for hurricane conditions or 50% of the initial wave height of 2 m (case nine, Fig. 3i). Wave heights for nonstorm conditions (case three, Fig. 3c), on the other hand, vary by about 0.3 m or only 25% of the initial wave height of 1.2 m. Wave height zones are also shifted about 4 km to the east for long-period hurricane conditions compared to nonstorm conditions.

(4.2) Shoreline Change, Sediment Texture, and Wave Height

The alongshore wave height measured at the 4-m isobath for the average onshore wave condition of case eight is plotted with shoreline rate-of-change and sediment texture in Fig. 4. West of Bolivar Roads, shoreline change rates and wave heights correspond and vary sharply in the vicinity of the Brazos River, Freeport jetties, and San Luis Pass. Shoreline rate-of-change is also relatively high and variable along Sargent Beach, but wave heights are nearly constant. High shoreline advance rates on the west side of the Brazos River occur in an area of low-wave heights. At the mouth and immediately east of the Brazos River, a prominent peak in the retreat rate of -24.5 m/yr corresponds with a sharp peak in wave height of 1.33 m. Farther to the east between the Brazos River and Freeport jetties, retreat rates significantly decrease, and a distinct low in wave heights occurs. Another prominent peak in shoreline retreat of -13 m/yr is present on the west side of the Freeport jetties and corresponds with a peak in wave height of 1.28 m. East of the Freeport jetties, shoreline retreat rates are slightly elevated and correspond with a small peak in wave height of 1.22 m.

The central region of Follets Island has fairly low shoreline retreat rates (less than -3.5 m/yr) and constant wave heights. Near the east end of Follets Island there is a peak in retreat rates of minus 8.9 m/yr, and farther to the east, immediately west of San Luis Pass, there is a zone of advance of 19 m/yr. Wave heights do not correspond well with shoreline retreat and advance in this area on the west side of San Luis Pass. Wave heights, however, are high on the south and northeast sides of the ebb-tidal delta and correspond with high-retreat rates immediately east of the Pass. There are two zones of locally high-retreat rates along West Beach (the eastern zone includes a double peak) that may correspond to two subtle peaks of wave height. Rates of shoreline retreat increase from -1.5 to -5.5 m/yr eastward toward the Galveston Island seawall, but no corresponding change in wave height occurs. Wave heights east of the seawall and immediately west of Bolivar Roads are very high. Shoreline change data are not shown in Fig. 4 for this area, but this has been a zone of shoreline advance since the jetties were constructed.

On the northeastern end of the study area, between Sabine Pass and Calcasieu Pass, the shoreline both advanced and retreated during the period from 1947/54 and 1994 (Fig. 4a). Alongshore wave heights vary by as much as 0.5 m along this stretch of shoreline (Fig. 4b). For a distance of 5 km west of Calcasieu Pass, erosion rates sharply increase from -5 m/yr to more than -10 m/yr (Byrnes et al., 1995) (Fig. 4a), and correspond with a peak in wave heights. Farther to the west, erosion rates and wave heights decrease. Erosion rates increase again to the west and reach a peak midway between Calcasieu Pass and Sabine Pass just east of Ocean View Beach. A distinct low in wave heights occurs in this area. Farther toward Sabine Pass the shoreline advanced, but within about 10 km of the Sabine Pass jetty the rate of advance decreased. A zone of high-wave heights occurs at this same location.

Between Bolivar Roads and Sabine Pass, alongshore wave heights vary by as much as 0.3 m for the average condition, and the shoreline change and wave height curves have similar shapes (Figs. 4a and 4b). For this section of shoreline, the shoreline change data and wave data used to determine the average onshore wave conditions closely correspond in time. Fig. 5 illustrates the

same data as Fig. 4 but is expanded to show more detail between Bolivar Roads and Sabine Pass. Shaded lines drawn on Fig. 5 show the hypothesized correlation between peaks in wave height and peaks in shoreline erosion. Zones of high-wave heights are shifted about 8 km to the east of zones of high-erosion rates except for the area 5 to 15 km west of Sabine Pass. Morton (1975) determined this area to have the highest, long-term (1880's to 1970's) erosion rates (more than 5 m/yr) for the shoreline between Sabine Pass and Bolivar Roads. Zones of high-wave heights also occur in this area for cases three through seven corresponding to wave directions from 135 to 225 degrees (Figs. 3c,d,e,f,g).

Fig. 4c is an alongshore plot of mean grain size of the sand and mud fraction of surficial sediments occurring between the 3.6- and 5.5-m isobaths. Mean grain size is markedly coarser west of Bolivar Roads than to the east. Sediments to the west are mostly very fine sand (3 to 4 phi) with coarse silt (4 to 5 phi) being the finest texture. From Bolivar Roads east to Sabine Pass, sediments become finer and change from coarse silt to very fine silt (7 to 8 phi). There are three zones of relatively large grain size between Bolivar Roads and Sabine Pass which are hypothesized to correspond with zones of high-wave energy as indicated in Fig. 5.

(5.0) DISCUSSION

The wave refraction model used in this study can only accept monochromatic and unidirectional waves. Vincent and Briggs (1989), in a controlled laboratory experiment, compared the transformation of monochromatic, unidirectional waves and directionally-spread, irregular waves over an elliptical mound. They determined that focusing of waves behind the mound caused wave heights to increase by 50 to over 100% more than they did for directionally-spread, irregular waves. They also determined that the amount of directional spread is the main cause of differences in height transformation rather than the amount of spread in energy frequency. As the directional spread increased, the increase in wave height caused by the mound lessened. These results indicate that wave height variance caused by the offshore shoals as determined for this study, which modeled only monochromatic and unidirectional waves, may be too large. The wave-height

patterns, however, would not be affected, and the qualitative comparisons with shoreline change and grain size made in this study are valid. More quantitative analyses will require a spectral wave refraction model such as Resio (1988).

The overall erosional state of the southeast Texas coast is largely due to a lack of sediment. With the exception of the new Brazos River entrance, sandy sediment delivered to the coastal zone by rivers is largely trapped in Galveston Bay, Sabine Lake, and Calcasieu Lake (Fig. 1) or farther upriver in reservoirs. The offshore supply of sandy sediment has largely been depleted over the past 3,500 years since sea-level stillstand (Cole and Anderson, 1982). The remaining major supply of sediment is from updrift beach and shoreface erosion. These sources, however, have been significantly interrupted by the construction of jetties, groins, and dredged channels that trap sediment and by the Galveston Island seawall that prevents erosion. Morton (1979) estimated that jetties along the Texas coast have trapped more than 50% of sand supplied by shoreline erosion since their construction beginning in the late 1800's.

Shoreline change patterns from the mid-1950's to the mid-1970's reflect the influence of these coastal structures, but variance in alongshore wave height also has a discernible effect. Because of steeper offshore gradients, waves arriving at the 4-m isobath are overall slightly higher west of Bolivar Roads than they are east of Bolivar Roads (Fig. 4). The relatively high erosion rates along Sargent Beach are caused by the high-wave heights and a lack of sand. Apparently the new Brazos River delta acted as a sediment sink from the 1950's to the 1970's preventing alongshore transport to Sargent Beach. The shoreline of the southwestern side of this delta advanced at a rate of more than 30 m/yr during this time (Morton and Pieper, 1975) and continued to advance from 1974 to 1982 (Paine and Morton, 1989). Waves diverge on the southwest side of the delta causing a low in wave heights for dominant southeast wave conditions (Figs. 3,4) and a likely local reversal to the northeast in the direction of littoral drift.

The shoreline between the Brazos River and Freeport jetties retreated at relatively high rates from the mid-1950's to the mid-1970's. This retreat was enhanced by the interruption of

southwestward littoral drift by the Freeport jetties. On the northeast, updrift side of the jetties, retreat rates decreased dramatically indicating the effect that the jetties have on downdrift rates. Peaks in retreat rates between the Brazos River and Freeport jetties coincide with wave height peaks, which indicates that wave refraction and shoaling are also factors in determining local rates of shoreline change.

Overall, shoreline retreat rates are relatively low along the central parts of Follets and Galveston Islands (Fig. 4a), but they have relatively high wave heights (Fig. 4b). A large supply of nearshore sandy sediment (Fig. 4c) helps prevent high shoreline retreat rates here. On the east end of Follets Island, there are zones of high-retreat and high-advance rates that indicate a local reversal in littoral drift direction. Wave height variation is small in this area, and correspondence with shoreline change is not clear, but changes in wave direction caused by refraction around the ebb-tidal delta at San Luis Pass can explain the pattern. Along West Beach, shoreline retreat rates decrease from east to west away from the influence of the Galveston Island seawall and groin field (Fig. 4a). Here the interruption of littoral drift and sediment supply by updrift erosion has been the dominant factor in creating the shoreline change pattern. Farther to the west, however, local variation in retreat rates along Galveston Island is probably caused by variation in wave heights.

The jetties at Bolivar Roads have trapped sediment causing the shoreline to advance on both sides of the inlet. Even though wave heights are very high on the west side of the jetties, the shoreline advanced about 2 m/yr from 1956 to 1970 (Morton, 1974). Clearly, the jetties have caused this shoreline change pattern in spite of the high waves occurring at the 4-m isobath (Fig. 4c). Shoreline advancement on the east side of the jetties was over 5 m/yr, and this corresponds with a low-wave height zone (Fig. 5). The littoral drift blocking effect of the jetties, however, is the overriding factor causing the shoreline advancement, not the low-wave heights.

As waves propagate across the shallowest portions of Sabine and Heald Banks they converge, and heights increase landward of these shoals (Fig. 3). This wave-focusing effect of the offshore shoals causes significant variation in the distribution of wave heights arriving at the

shoreline east of Bolivar Roads. The variation in total wave energy is even greater because energy is proportional to the square of the height. These offshore shoals, therefore, are expected to have a significant effect on shoreline change. The similarity in the shapes of the alongshore curves of wave height and shoreline change between Sabine Pass and Bolivar Roads is striking (Fig. 5). The alongshore alignment of high- and low-retreat rates with high- and low-wave heights, however, is not exact. There are several possible reasons for this misalignment: (1) A single average wave condition cannot precisely represent the wave climate, particularly across 300 km of coast; (2) Hindcast wave conditions may have a biased error, particularly in direction; (3) Shoreline change rates are computed over a period that does not exactly correspond to the hindcast period; and (4) The effect of wave direction and variance in the rates of littoral drift are not modeled here.

Between Sabine Pass and Calcasieu Pass, high- and low-retreat rates do not align with high- and low-wave heights (Fig. 4). This misalignment is caused by the period of available shoreline change data being so different from the period of the wave hindcast data. The shoreline change data cover the period from 1947/54 to 1994. Nineteen ninety-four is 18 years beyond the ending year of 1976 for the hindcast data. The east end of the study area may also have a significantly different wave climate as indicated by the hindcast study. More easterly and landward hindcast stations have more southerly wave directions than station 12 used for this analysis (Hubertz and Brooks, 1989, stations 13 and 14). The relatively large variation in wave height and the prominent zones of shoreline advance and retreat, however, suggests that eastern Sabine Bank has a significant impact on shoreline change patterns between Sabine and Calcasieu Passes.

The highest wave heights between Sabine Pass and Bolivar Roads occur 5 to 15 km west of Sabine Pass and correspond with the highest rates of historical erosion along this stretch of shoreline (Morton, 1975). Waves begin to focus on this high-erosion location as they propagate across the shallowest part of Sabine Bank. A nearshore bathymetric protuberance associated with the ebb-tidal delta and shoreline progradation further focuses waves on the shoreline resulting in the high-wave heights. Waves focus on this part of the shoreline for a wide range of wave

directions (135 to 225 degrees) (Figs. 3c,d,e,f,g), and, hence, the high, long-term erosion rates are expected. An area of relatively coarse sediment also occurs in this area (Fig. 5c), further indicating high-wave energy conditions.

Wave refraction across nearshore features such as headlands and embayments tends to focus energy on shoreline protuberances causing higher rates of erosion and hence acting to smooth the shoreline. Refraction caused by offshore shoals that are not part of the littoral drift system, however, may cause shoreline irregularities. Sabine and Heald Banks are such offshore shoals, and their effects on wave propagation may impart a large-scale rhythmic topography by causing alongshore variance in the shoreline rate-of-change between Bolivar Roads and Sabine Pass. The actual development and permanency of this topography depends on the temporal variation in wave direction, height, and period, and the reaction time required for the shoreline to adjust to new average wave conditions. Wave heights and periods used in this study did not cause waves to break on the Banks. Based on Galvin's (1969) empirical relationship of the ratio of wave height to depth when wave breaking occurs (0.83), it is expected that significant wave breaking will occur on the Banks when wave heights exceed about 5 m. During hurricanes, therefore, these shoals may act to lower wave heights along the stretch of shoreline in their shadow rather than to focus wave energy.

(6.0) CONCLUSIONS

1. The construction of jetties, dredged channels, and the Galveston seawall have significantly affected shoreline change patterns since the late 1800's along the southeast Texas coast, but variance in alongshore wave heights caused by wave refraction also has a discernible effect. East of Bolivar Roads, modeled relative wave heights also generally correlate with known changes in nearshore sediment grain size.

2. Shoreline wave heights west of Bolivar Roads are, on average, higher than they are east of Bolivar Roads because of steeper offshore gradients.

3. Variation in wave heights west of Bolivar Roads is generally less and more local than east of Bolivar Roads and is mostly caused by local refraction and shoaling on the ebb-tidal deltas of Bolivar Roads and San Luis Pass and the Brazos River Delta. High and low wave heights occur at locations of relatively high and low shoreline rates-of-change except where shoreline change is dominated, in an opposite sense, by the interruption of littoral drift caused by jetties, dredged channels, and the Galveston seawall.

4. Variation in wave heights between Bolivar Roads and Sabine Pass is largely caused by wave focusing by offshore shoals. This variation correlates with the pattern of shoreline rate-of-change and nearshore sediment grain size.

5. Wave refraction over offshore shoals, which are not in the littoral drift system, is a process that acts to impart shoreline irregularities by causing spatial variance in the shoreline rate-of-change. The temporal variability of the wave climate and the reaction time of the shoreline to adjust to new average wave conditions determine if spatial variance in wave heights results in large-scale rhythmic topography.

(7.0) ACKNOWLEDGMENTS

Grants from the U.S. Geological Survey Coastal Geology Program and the U.S. Minerals Management Service supported this work. Jay Raney provided a helpful review of an earlier draft. Publication authorized by the Director, Bureau of Economic Geology, The University of Texas at Austin.

(8.0) LITERATURE CITED

Abel, C. E., Tracy, B. A., Vincent, C. L. and Jensen, R. E., 1989. Hurricane hindcast methodology and wave statistics for Atlantic and Gulf hurricanes from 1956–1975. Wave Information Study Report 19, Waterways Experiment Station, U.S. Army Corps of Engineers, Vicksburg, Mississippi.

Bales, J.D. and Holley, E.R., 1989. Sand transport in Texas tidal inlet. Journal of Waterway, Port, Coastal, and Ocean Engineering, 115: 427–443.

Barua, D.K. and Kana, T.W., 1995. Deep water wave hindcasting, wave refraction modeling, and wind and wave induced motions in the east Ganges-Brahmaputra Delta coast. Journal of Coastal Research, 11: 834–848.

Brown, C. A. and Kraus, N. C., 1994. Reconnaissance study of wave refraction and shoreline change for the Galveston, Texas, beach nourishment borrow sites. Final report prepared for the Texas General Land Office and the City of Galveston, Conrad Blucher Institute for Surveying and Science, Texas A&M University-Corpus Christi.

Byrnes, M. R., McBride, R. A., Tao, Q. and Duvic, L., 1995. Historical shoreline dynamics along the chenier plain of southwestern Louisiana. Gulf Coast Association of Geological Societies Transactions, 45: 113–122.

Cole, M.L. and Anderson, J.B., 1982. Detailed grain size and heavy mineralogy of sands of the northeastern Texas Gulf Coast: implications with regard to coastal barrier development. Transactions-Gulf Coast Association of Geological Societies, 32: 555–563.

Ebersole, B. A., Cialone, M. A. and Prater, M. D., 1986. Regional coastal processes numerical modeling system report 1 RCPWAVE-A linear wave propagation model for engineering use.

Technical Report CERC-86-4, U.S. Army Engineer Waterways Experiment Station, Vicksburg, MS.

Frazier, D. E., 1974. Depositional-episodes: their relationship to the Quaternary stratigraphic framework in the northwestern portion of the Gulf basin. Geological Circular 74-1, The University of Texas at Austin, Bureau of Economic Geology.

Galvin, C. J., 1969. Breaker travel and choice of design wave height. Journal of the Waterways and Harbors Division, 6569: 175–200.

Garcia, A. W. and Flor, T. H., 1984. Hurricane Alicia storm surge and wave data. Technical Report CERC-84-6, Department of the Army, Waterways Experiment Station, Corps of Engineers, Vicksburg, Mississippi.

Gibeaut, J. C. and Davis, R. A., Jr., 1993. Statistical geomorphic classification of ebb-tidal deltas along the west-central Florida coast. Journal of Coastal Research, SI 18: 165-184.

Goldsmith, V., 1976. Wave climate models for the continental shelf: critical links between shelf hydraulics and shoreline processes. In: R. A. Davis, Jr. and R. L. Ethington (Editors), Beach and Nearshore Sedimentation. Society of Economic Paleontologists and Mineralogists, Special Publication No. 24, pp. 24–47.

Goldsmith, V., Byrne, R.J., Sallenger, A.H. and Drucker, D.M., 1975. The influence of waves on the origin and development of the offset coastal inlets of the southern Delmarva Peninsula, Virginia. In: L.E. Cronin, (Editor), Estuarine Research. Academic Press, New York, pp. 183–200.

Hallermeier, R. J., 1977. Calculating a yearly limit depth to the active beach profile. TP 77-9, U.S. Army Corps of Engineers, Coastal Engineering Research Center, Fort Belvoir, Virginia.

Hallermeier, R. J., 1983. Sand transport limits in coastal structure design. Proceedings of Coastal Structures '83, American Society of Civil Engineers, pp. 703–716.

Hayes, M.O., 1979. Barrier island morphology as a function of tidal and wave regime. In: S. P. Leatherman (Editor), Barrier Islands from the Gulf of St. Lawrence to the Gulf of Mexico. Academic Press, New York, pp. 1–28.

Hubertz, J. M. and Brooks, R. M., 1989. Gulf of Mexico hindcast wave information. Wave Information Studies of U.S. Coastlines, WIS Report 18, Department of the Army, Corps of Engineers, Waterways Experiment Station, Vicksburg, Mississippi.

Hubertz, J. M. and Brooks, R. M., 1992. Verification of the Gulf of Mexico hindcast wave information. Wave Information Studies of U.S. Coastlines, WIS Report 28, Department of the Army, Corps of Engineers, Waterways Experiment Station, Vicksburg, Mississippi.

Inman, D.L. and Dolan, R., 1989. The Outer Banks of North Carolina: budget of sediment and inlet dynamics along a migrating barrier system. Journal of Coastal Research, 5, 193–237.

Komar, P. D. and Miller, M. C., 1973. The threshold of sediment movement under oscillatory water waves. Journal of Sedimentary Petrology, 43: 1101–1110.

Komar, P. D. and Miller, M. C., 1975. On the comparison between the threshold of sediment motion under waves and unidirectional currents with a discussion of the practical evaluation of the threshold. Journal of Sedimentary Petrology, 362–367.

Morton, R. A., 1974. Shoreline changes on Galveston Island (Bolivar Roads to San Luis Pass): an analysis of historical changes of the Texas Gulf shoreline. Geological Circular 74-2, Bureau of Economic Geology, The University of Texas at Austin, Austin, Texas.

Morton, R. A., 1975. Shoreline changes between Sabine Pass and Bolivar Roads: an analysis of historical changes of the Texas Gulf shoreline. Geological Circular 75-6, Bureau of Economic Geology, The University of Texas at Austin, Austin, Texas.

Morton, R. A., 1977. Historical shoreline changes and their causes, Texas Gulf Coast. Gulf Coast Association of Geological Societies Transactions, 27: 352–364.

Morton, R. A., 1979. Temporal and spatial variations in shoreline changes and their implications, examples from the Texas Gulf Coast. Journal of Sedimentary Petrology, 49: 1101–1112.

Morton, R. A. and Pieper, M. J. 1975. Shoreline changes in the vicinity of the Brazos River Delta (San Luis Pass to Brown Cedar Cut): an analysis of historical changes of the Texas Gulf shoreline. Geological Circular 75-4, Bureau of Economic Geology, The University of Texas at Austin, Austin, Texas.

Morton, R. A., Pieper, M. J., and McGowen, J. H., 1976. Shoreline changes on Matagorda Peninsula (Brown Cedar Cut to Pass Cavallo): an analysis of historical changes of the Texas Gulf shoreline. Geological Circular 76-6, Bureau of Economic Geology, The University of Texas at Austin, Austin, Texas.

Morton, R. A. and Winker, C. D., 1979. Distribution and significance of coarse biogenic and clastic deposits on the Texas inner shelf. Gulf Coast Association of Geological Societies Transactions, 29: 306–320.

Morton, R.A. and Paine, J.G., 1985. Beach and vegetation-line changes at Galveston Island, Texas: Erosion, deposition, and recovery from Hurricane Alicia. Geological Circular 85-5, Bureau of Economic Geology, University of Texas at Austin, Austin, Texas.

Morton, R. A., Paine, J. G. and Gibeaut, J. C., 1994. Stages and durations of post-storm beach recovery, southeastern Texas coast, U.S.A. Journal of Coastal Research, 10: 884–908.

Morton, R. A., Gibeaut, J. C. and Paine, J. G., 1995. Meso-scale transfer of sand during and after storms: implications for prediction of shoreline movement. Marine Geology, 126: 161–179.

National Ocean Service, 1979. Tide tables 1979, high and low water predictions east coast of North and South America including Greenland: National Ocean Survey, National Oceanic and Atmospheric Administration, U.S. Department of Commerce.

Nelson, H. F. and Bray, E. E., 1970. Stratigraphy and history of the Holocene sediments in the Sabine-High Island area, Gulf of Mexico. In: J. P. Morgan and R. H. Shaver (Editors), Deltaic Sedimentation, Modern and Ancient. Society of Economic Paleontologists and Mineralogists Special Publication 15, pp. 48–77.

Paine, J.G. and Morton, R.A., 1989. Shoreline and vegetation-line movement, Texas Gulf Coast, 1974 to 1982. Geological Circular 89-1, Bureau of Economic Geology, The University of Texas at Austin, Austin, Texas.

Resio, D. T., 1982. The estimation of wind-wave generation in a discrete spectral model. Wave Information Studies of U.S. Coastlines, WIS Report 5, Department of the Army, Waterways Experiment Station, Corps of Engineers, Vicksburg, Mississippi.

Resio, D.T., 1988. A steady-state wave model for coastal applications. In: B.L. Edge (editor), Coastal Engineering 1988 Proceedings. American Society of Civil Engineers, New York, New York, pp. 929–940.

Resio, D. T., Vincent, C. L. and Corson, W. D., 1982. Objective specification of Atlantic Ocean wind fields from historical data. Wave Information Studies of U.S. Coastlines, WIS Report 5, Department of the Army, Waterways Experiment Station, Corps of Engineers, Vicksburg, Mississippi.

Schlumberger GeoQuest, 1994. CPS-3 Version 4.0, Schlumberger GeoQuest, Houston, Texas.

Shepard, F.P. and Inman, D.L., 1950. Nearshore circulation related to bottom topography and wave refraction. Transactions American Geophysical Union, 31: 555–565.

Shepard, F.P. and Inman, D.L., 1951. Nearshore circulation. Proceedings 1st Conference Coastal Engineering, pp. 50–59.

U.S. Army Corps of Engineers, 1984. Shore Protection Manual Volume 1. Coastal Engineering Research Center, Department of the Army, Waterways Experiment Station, Vicksburg, Mississippi.

U.S. Army Corps of Engineers, 1985. Galveston County shore erosion study feasibility report and environmental impact statement, volume 2. Report, Galveston District.

U.S. Army Corps of Engineers, 1992a. Inlets along the Texas Gulf coast. Planning Assistance to States Program Section 22 Report, U.S. Army Engineer District, Galveston Southwestern Division.

U.S. Army Corps of Engineers, 1992b. Galveston Beach groinfield and maintenance material placement. Planning Assistance to States Program Section 22 Report, U.S. Army Engineer District, Galveston Southwestern Division.

Vincent, C.L. and Briggs, M.J., 1989. Refraction—diffraction of irregular waves over a mound. Journal of Waterway, Port, Coastal, and Ocean Engineering, 115: 269–284.

White, W. A., Calnan, T. R., Morton, R. A., Kimble, R. S., Littleton, T. G., McGowen, J. H., Nance, H. S. and Schmedes, K. E., 1985. Submerged lands of Texas, Galveston–Houston

area: sediments, geochemistry, benthic macroinvertebrates, and associated wetlands. The University of Texas at Austin, Bureau of Economic Geology Special Publication.

White, W. A., Calnan, T. R., Morton, R. A., Kimble, R. S., Littleton, T. G., McGowen, J. H. and Nance, H. S., 1987. Submerged lands of Texas, Beaumont–Port Arthur area: sediments, geochemistry, benthic macroinvertebrates, and associated wetlands: The University of Texas at Austin, Bureau of Economic Geology Special Publication.

White, W. A., Calnan, T. R., Morton, R. A., Kimble, R. S., Littleton, T. G., McGowen, J. H. and Nance, H. S., 1988. Submerged lands of Texas, Bay City–Freeport area: sediments, geochemistry, benthic macroinvertebrates, and associated wetlands: The University of Texas at Austin, Bureau of Economic Geology Special Publication.

Williams, S. J., Prins, D. A. and Meisburger, E. P., 1979. Sediment distribution, sand resources, and geologic character of the inner continental shelf off Galveston County, Texas. Miscellaneous Report No. 79-4, U.S. Army Corps of Engineers, Coastal Engineering Research Center, Fort Belvoir, Virginia.

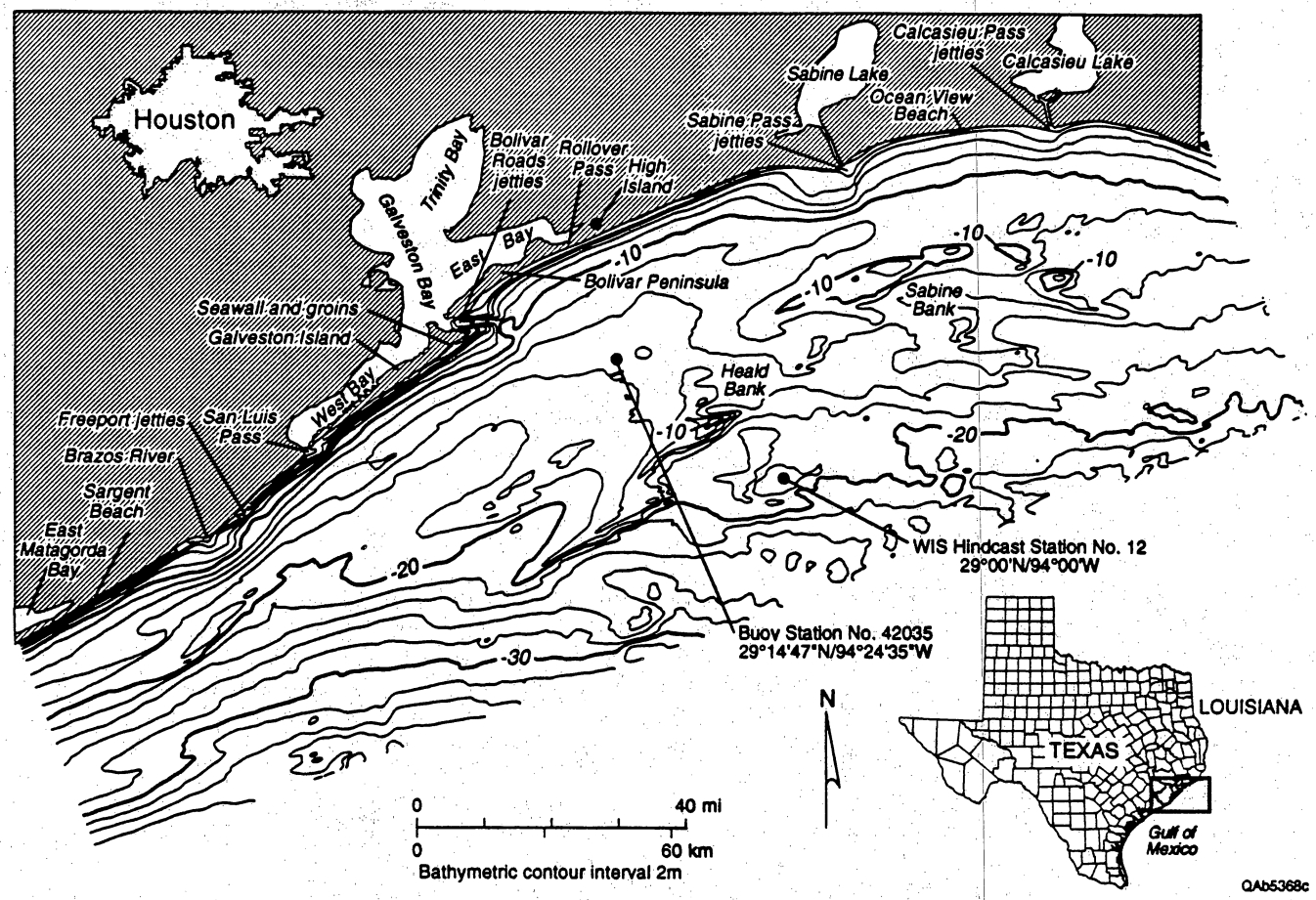

Figure 1. Bathymetric map of the study area. Isobaths are smoothed and have a 2-m interval. Depths are related to mean tide level.

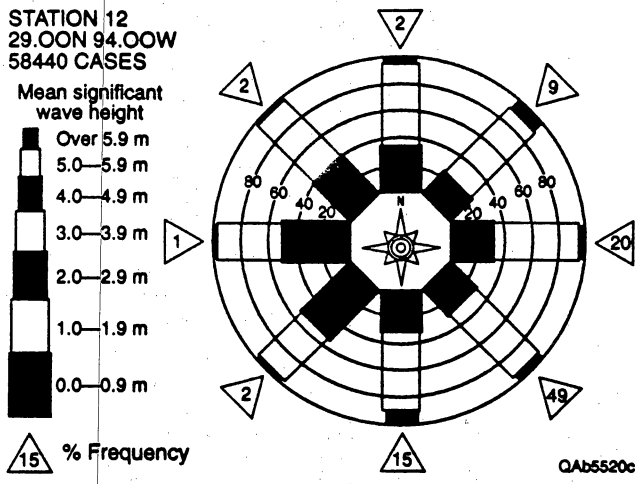

Figure 2. Wave rose diagram for WIS hindcast station 12, from Hubertz and Brooks (1989).

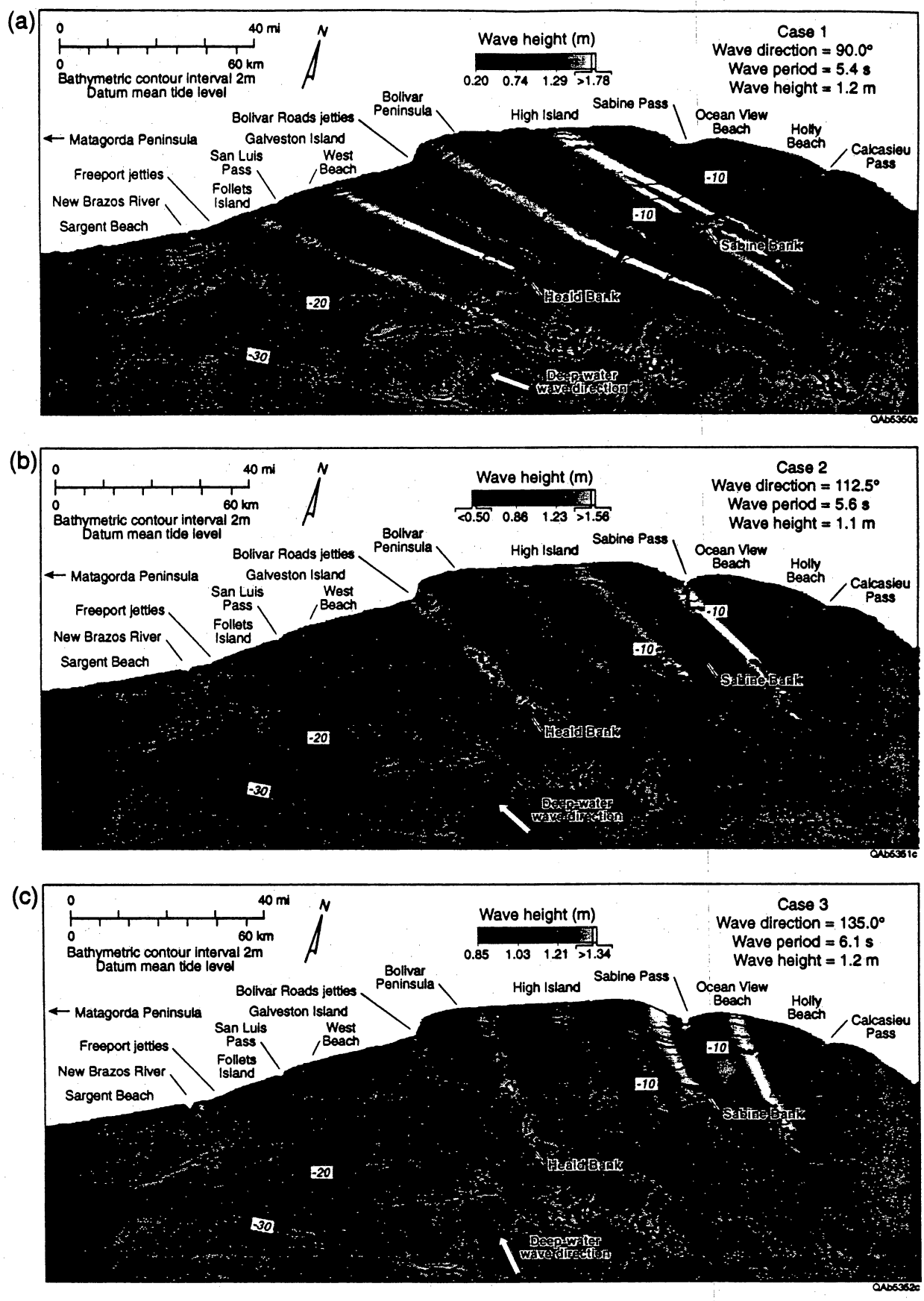

Figure 3. Bathymetry and wave heights for wave conditions one through nine. Isobaths are not smoothed. Note that the gray scale used to depict wave height varies from case to case.

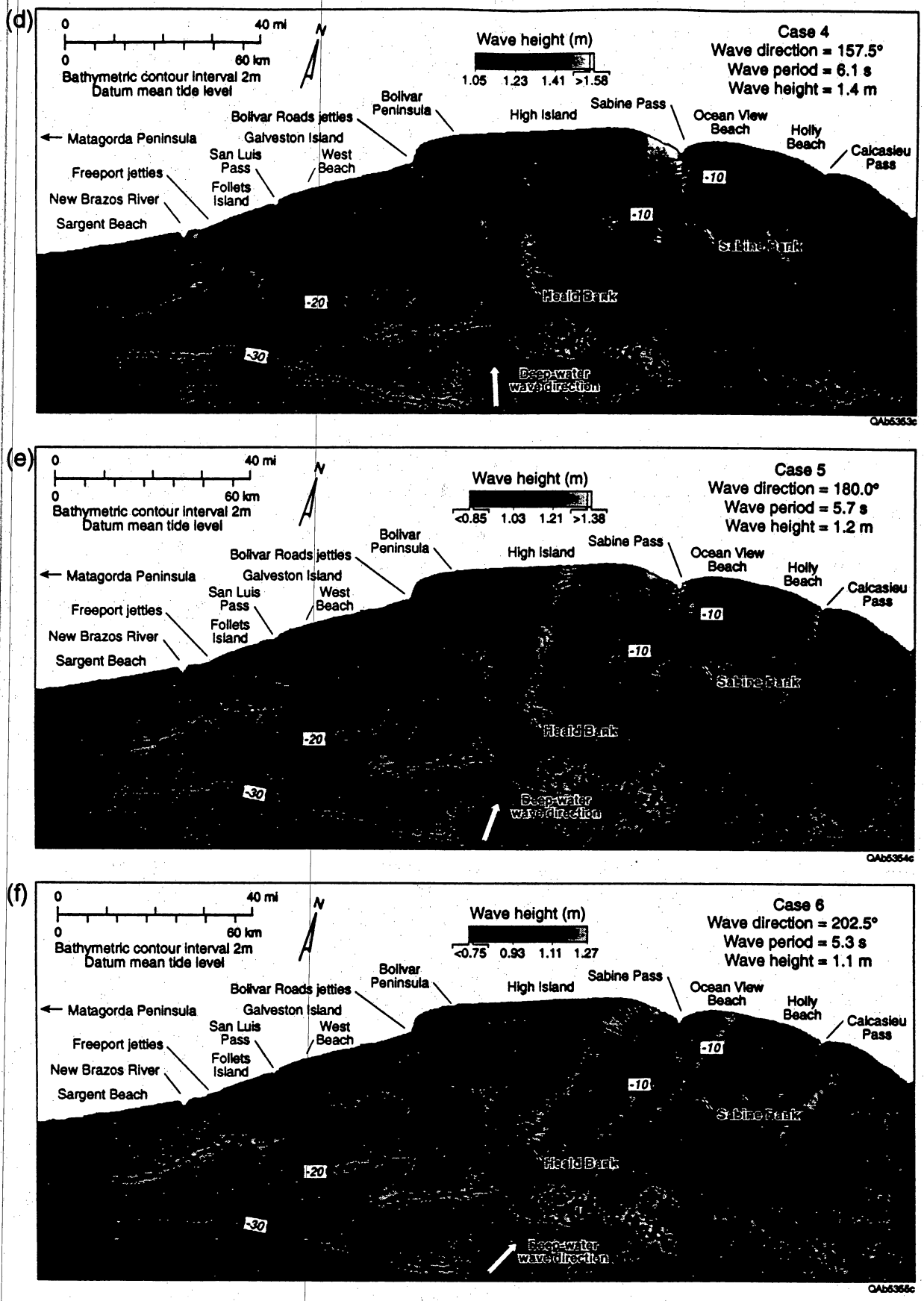

Figure 3. (cont.)

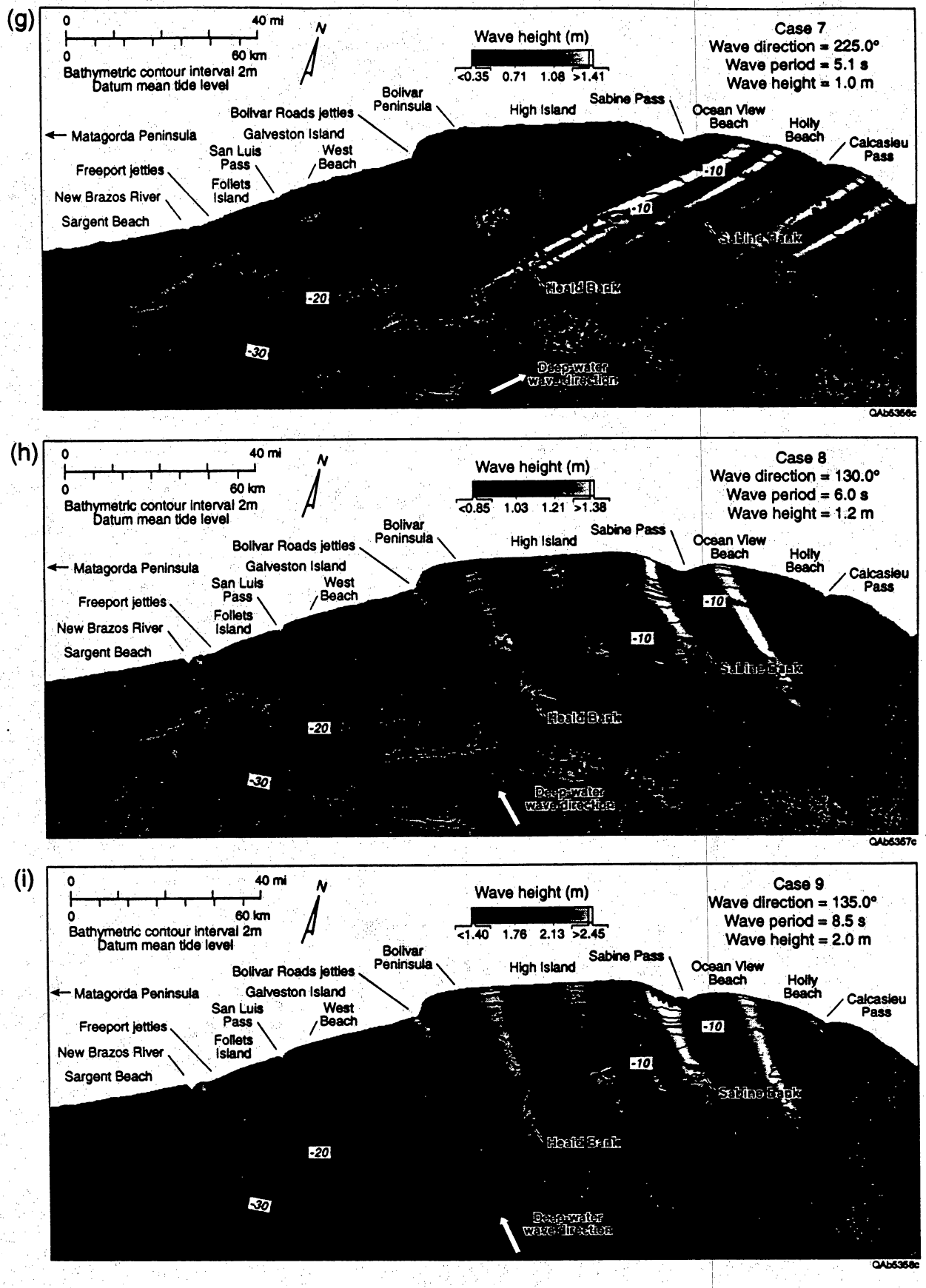

Figure 3. (cont.)

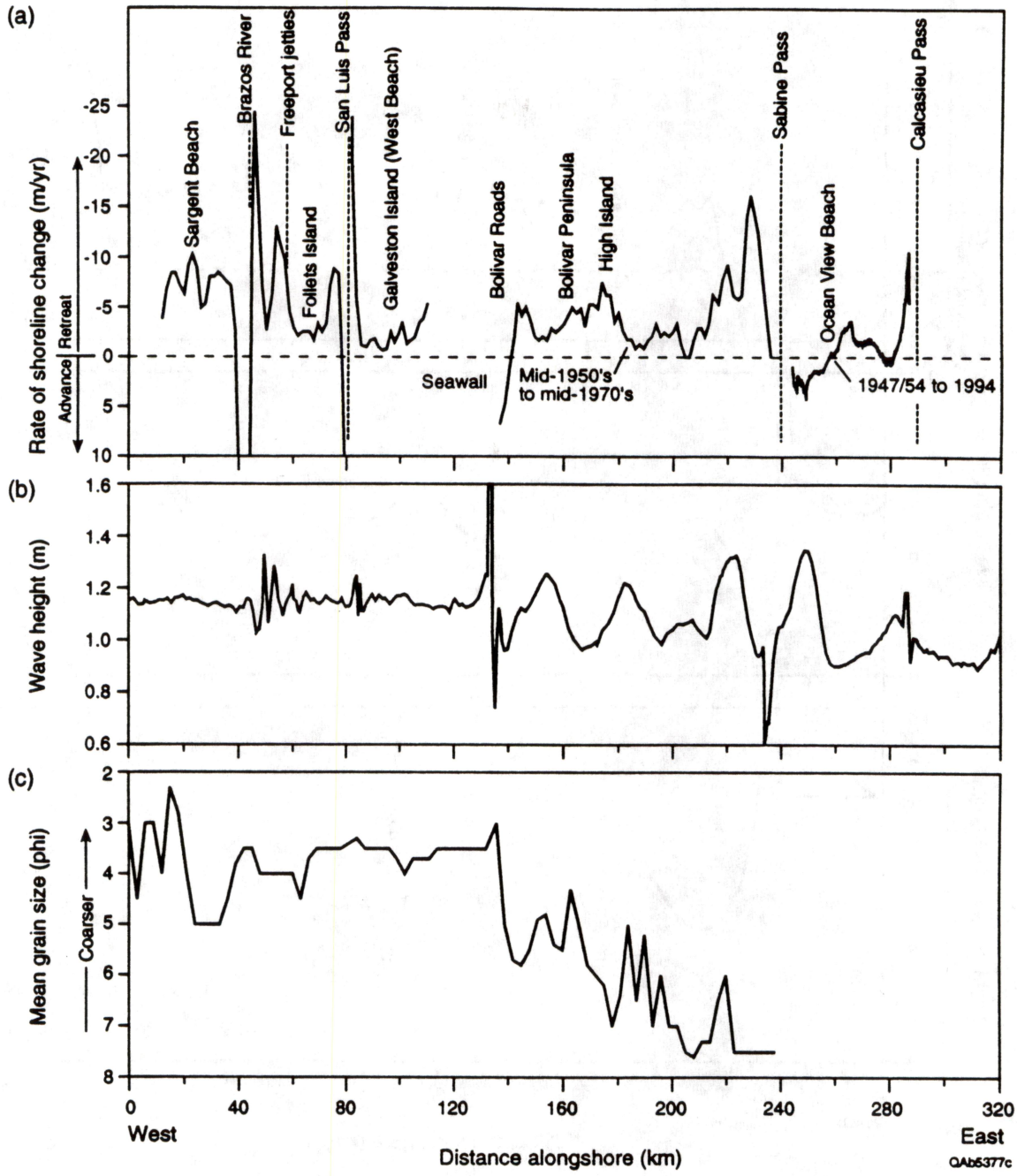

Figure 4. Alongshore plots of shoreline change, wave height, and grain size from Sargent Beach to Calcasieu Pass. (a) Shoreline change. (b) Wave height along the 4-m isobath. (c) Mean grain size of surface sediment between 3.6 and 5.5 m water depth for the mud and sand fraction.

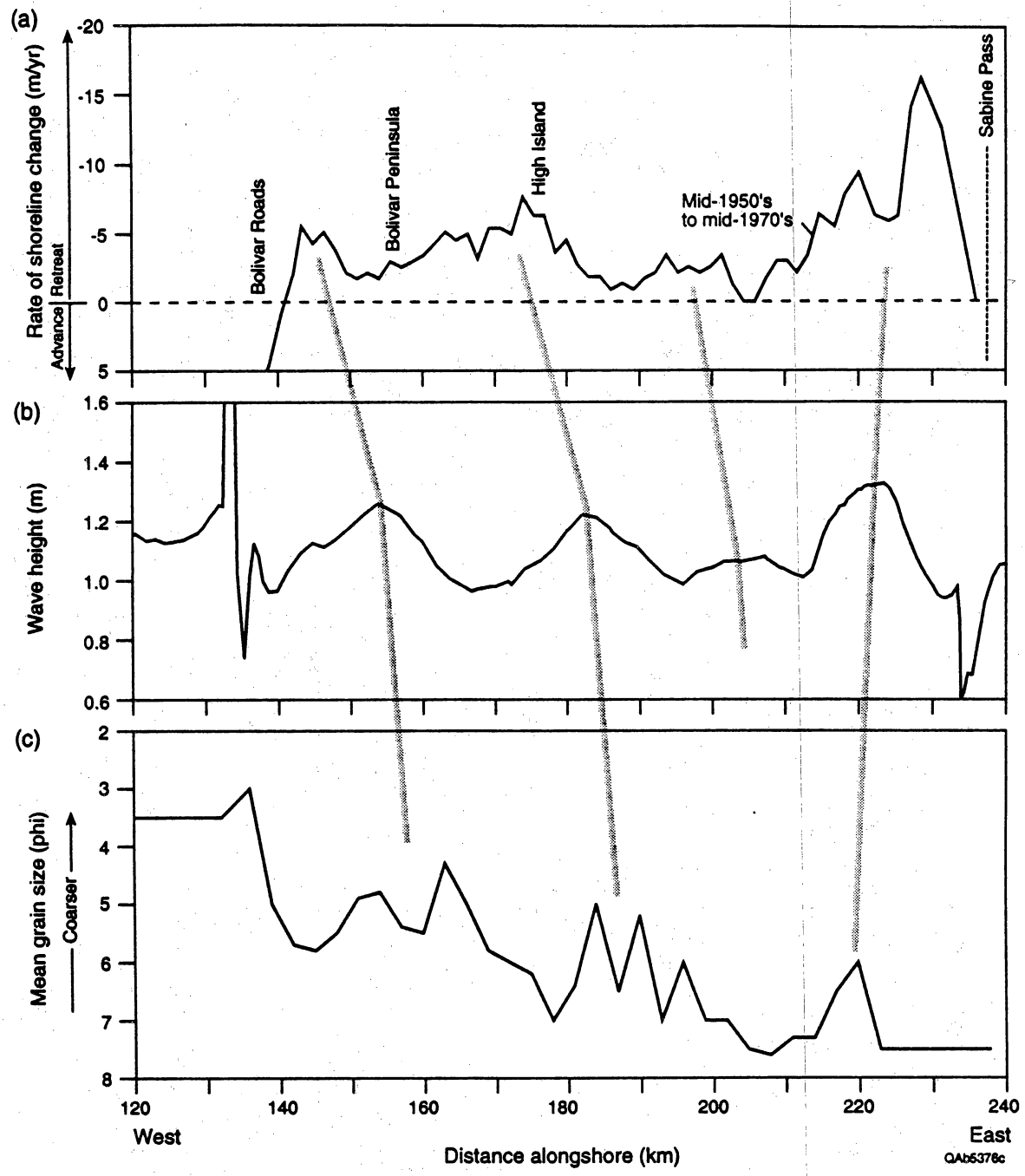

Figure 5. Alongshore plots of shoreline change, wave height, and grain size from Bolivar Roads to Sabine Pass. Shaded lines indicate interpreted correlations between peaks. (a) Shoreline change. (b) Wave height along the 4-m isobath. (c) Mean grain size of surface sediment between 3.6 and 5.5 m water depth for the mud and sand fraction.

TABLES

Table 1. - Wave parameters used in model runs displayed in Fig. 3. Hs= significant wave height, WIS= Wave Information Study. Frequency is percent occurrence of all waves approaching from 78.75 to 236.25 degrees (onshore direction).

Case	height (m)	period (s)	true direction	frequency (%)	comments
1	1.2	5.4	90.0	12.1	Mean Hs and mean period for wave directions in a 22.5-degree arc centered around 90 degrees; WIS station #12
2	1.1	5.6	112.5	17.4	Mean Hs and mean period for wave directions in a 22.5-degree arc centered around 112.5 degrees; WIS station #12
3	1.2	6.1	135.0	35.5	Mean Hs and mean period for wave directions in a 22.5-degree arc centered around 135 degrees; WIS station #12
4	1.4	6.1	157.5	23.5	Mean Hs and mean period for wave directions in a 22.5-degree arc centered around 157.5 degrees; WIS station #12
5	1.2	5.7	180.0	8.1	Mean Hs and mean period for wave directions in a 22.5-degree arc centered around 180.0 degrees; WIS station #12
6	1.1	5.3	202.5	2.4	Mean Hs and mean period for wave directions in a 22.5-degree arc centered around 202.5 degrees; WIS station #12
7	1.0	5.1	225.0	1.1	Mean Hs and mean period for wave directions in a 22.5-degree arc centered around 225 degrees; WIS station #12
8	1.2	6.0	130.0	N/A	Mean Hs and mean period for wave directions between 55 and 235 degrees true; WIS station #12
9	2.0	8.5	135.0	N/A	Estimated Hurricane Alicia conditions from Garcia and Flor (1984). Data from Shell Oil platform (Vermillion 22, 25 ft deep). Hs and period are measured but directions are absent other than statement of predominantly southeast waves, therefore used southeast compass direction for model.

Addendum 6

Predicting Shorelines Based on Past Shoreline Change: Effect of Rate-of-Change Calculation Method and Baseline Selection

Predicting Shorelines Based on Past Shoreline Change: Effect of Rate-of-Change Calculation Method and Baseline Selection

James C. Gibeaut
Bureau of Economic Geology
The University of Texas at Austin
University Station, Box X
Austin, Texas 78713, U.S.A.

ABSTRACT

There are several methods used to calculate shoreline rate-of-change given the spatial and temporal distribution of past shorelines along a transect. Five of these methods studied here include: (1) end point (EP), (2) linear regression (LR), (3) jackknife (JK), (4) average of rates (AOR), and (5) minimum description length (MDL). These methods may give very different values; but the trend of the baseline, from which the transects are drawn, relative to the trend of the shoreline also affects the rate-of-change calculation. Furthermore, the position and shape of the predicted shoreline are determined not only by the calculated rate-of-change but by the position and shape of the latest shoreline in the time series, from which the predicted shoreline is projected, and the shoreline projection vector. The projection vector has a magnitude equal to the rate-of-change multiplied by the desired number of years and direction determined by the orientation of the transect and the sign of the rate-of-change. This study uses a computer program that automatically determines baselines that conform to shoreline orientation. Using time series of simulated shorelines and actual shorelines from Galveston Island, Texas, the effect of baseline orientation and rate-of-change calculation method on rate-of-change statistics and shoreline prediction is explored.

Absolute shoreline change rates calculated using multiple conformal baselines may produce higher or lower rates-of-change than those calculated using nonconformal baselines. The difference depends on the rate-of-change method used and increases with

increasing shoreline change, increasing shoreline curvature, and increasing discrepancy between shoreline and baseline orientation. Simulated and actual shoreline data indicate that differences in the rates-of-change may commonly exceed 0.5 m/yr. The LR method of rate-of-change calculation appears to be the most stable with respect to baseline selection. Comparisons of 60-year predicted shorelines determined using conformal and nonconformal baselines show the potential for differences of more than 30 m along shorelines with moderate amounts of change and curvature. Discrepancies between predicted shorelines are enhanced in areas with alongshore gradients in the rate of shoreline change. There is also the potential for the prediction of different shoreline shapes when using different baselines.

The calculation method has a large effect on computed shoreline change rates along Galveston Island, Texas, which vary from 1 to 9 m/yr among the EP, LR, JK, AOR, and MDL methods. The MDL method appears to account for changes in littoral drift caused by a seawall and groin system. The MDL and AOR methods, however, show locally abrupt alongshore differences in rates-of-change that may cause predicted shorelines to have unnatural shapes. One should consider predicted shoreline shape when evaluating the reliability of rates-of-change and baselines.

ADDITIONAL INDEX WORDS: shoreline erosion, shoreline shape, shoreline change analysis, future shoreline prediction, shoreline mapping computer program

INTRODUCTION

The prediction of the future position of shorelines is of great importance to coastal managers who need this information to generate maps of flood zones and to determine setback distances for construction. It is currently not practical to use deterministic models of shoreline change to predict shoreline positions more than a few years into the future. This is one reason why much work has been completed on determining past and inferring

future shoreline change using time series analysis of past shoreline positions. This work falls into four categories: (1) the acquisition and merging of shoreline data obtained from maps, photographs, and Global Positioning System surveys, and the errors in determining the relative positions of past shorelines (DOLAN et al., 1980; CROWELL et al., 1991), (2) the effect on shoreline change determination of sparse temporal data and the timing of shoreline data relative to storms and water level variations (DOLAN et al., 1991; MORTON, 1991), (3) mathematical methods for determining shoreline rate-of-change using time series of shoreline positions (FOSTER and SAVAGE, 1989; DOLAN et al., 1991; FENSTER et al., 1993), and (4) the effects of various spatial sampling schemes on shoreline change determination (DOLAN et al., 1992).

A required product from a management perspective is not just the rate-of-change along a shoreline but the estimated future position of the shoreline – i.e., a map or aerial photograph with the expected future shoreline drawn on it. To do this, one must determine the magnitude and direction (vector) in which to project the future shoreline from the current shoreline. Typically, distances between past shorelines are measured along transects, and these distances are used to determine the rate of shoreline change using various formulas. Multiplying the rate-of-change by the desired number of years into the future provides the magnitude of the vector, and the transect orientation and sign of the rate-of-change provide the direction of the vector for projecting future shorelines. Previous work has not considered the effect of transect orientation relative to the shoreline trend on rate-of-change statistics, predicted shoreline position, and predicted shoreline shape. This paper explores that effect and also considers the implications of using various methods for computing the rate of shoreline change along Galveston Island, Texas (Figure 1).

Predicting Future Shoreline Positions

The shoreline change rate and the horizontal direction of shoreline movement are required to project future shoreline positions. Both of these elements, however, are affected by the orientation of the transects relative to the shoreline trend. In practice, transects are oriented perpendicular to a baseline which is drawn approximately parallel to the shoreline. Variation in the orientation between baselines and shorelines causes variation in the computed rate-of-change. This is illustrated in Figure 2a where the distance between shorelines measured from a baseline that does not conform to the shoreline trend is greater than the distance measured from a baseline that is more conformal to the trend where the shorelines are parallel. This effect translates into higher computed rates-of-change for the nonconformal baseline situation compared to the conformal baseline situation. The relationship is complicated, however, by shorelines that converge and diverge alongshore (i.e., shorelines with alongshore gradients in their rate-of-change). Figure 2b shows that distances between shorelines computed using conformal baselines are even less than those computed with nonconformal baselines than would be expected if the shorelines were parallel. Figure 2c shows that nonparallel shorelines cause distances computed with conformal baselines to be greater than those computed with nonconformal baselines potentially resulting in lower rates-of-change when using nonconformal baselines. The differences for the cases shown in Figure 2 increase with greater separation of the shorelines (i.e., higher shoreline rate-of-change). The use of a single straight baseline along a coast that has shoreline curvature, will, therefore, introduce alongshore variation in rate-of-change values solely related to shoreline shape and baseline selection.

The effect of baseline orientation on the direction of future shoreline projection is obviously affected by baseline selection because transects oriented perpendicular to the baseline provide the direction when combined with the sign of the rate-of-change (retreat

or advance). What is less obvious, however, is the combined effect of differences in the rate-of-change computed for differently oriented baselines and the different directions of projection on the position of a future shoreline. If the desired end result of shoreline change analysis is to draw an expected future shoreline on a map, then one must consider not just the separate effects on the rate-of-change and direction of projection due to baseline selection but also their combined effect.

METHODS

Computer Program

To study the effects of using various methods for computing shoreline change rates, and the selection of baseline orientation on rate-of-change statistics and future shoreline positions, we developed the Shoreline Shape and Prediction Program (SSAPP). SSAPP is a computer program that automates shoreline change analysis beginning with the geographic positions of past shorelines in an electronic form and ending with the coordinates of projected shorelines. The program has the following features: (1) rapid calculation of five shoreline rate-of-change methods for any desired transect spacing, (2) the ability to automatically construct baseline segments of user-selected length that conform to past shoreline orientations or to accept a predetermined baseline, (3) the ability to map predicted shoreline positions using selected future dates and rate-of-change methods, (4) the ability to use data from and provide results to a Geographic Information System (GIS) such as ARC/INFO or a Computer-Aided Drafting (CAD) system such as AUTOCAD, and (5) the ability to accept shoreline data that are in no particular order, which is a significant advantage because shoreline segments are often digitized out of order and reside in geographical data bases in no particular order. With SSAPP, we can quickly calculate shoreline rates-of-change and project future shoreline positions in a GIS or CAD

program for long stretches of shoreline using various baselines, transect spacing, and rate-of-change calculation methods.

Rate of Shoreline Change Calculation Methods

Five methods of calculating the rate of shoreline change from time series of past shoreline positions are considered in this study. DOLAN et al. (1991) reviewed four of these methods including the end point method (EP), the average of rates method (AOR), (FOSTER and SAVAGE, 1989), the linear regression method (LR), and the jackknife method (JK) (EFRON, 1982). FENSTER et al. (1993) presented a new method here termed the minimum description length (MDL) method. Subroutines in SSAPP calculate the rate-of-change based on each of these methods, which are briefly described below.

End Point Rate-of-Change (EP)

This is a simple method that takes the distance between the earliest and latest shoreline positions and divides by the number of years.

Linear Regression Rate-of-Change (LR)

For this method, all the available data are used in a linear regression. The slope of the regression line is the shoreline rate-of-change.

Jackknife Rate-of-Change (JK)

This routine uses the Jackknife method as described by EFRON (1982). A family of linear regression lines are computed by successively eliminating a single and different shoreline position in the time series. The slopes of these regression lines are then averaged to yield a rate-of-change.

Average of Rates Rate-of-Change (AOR)

FOSTER and SAVAGE (1989) developed this technique using data from Florida. It involves averaging the end point rates computed for all possible combinations of two shorelines in a time series. Each combination of shoreline positions must pass a minimum time criterion (T_{min}), however, to be included in the average. T_{min} is defined as follows:

$$T_{min} = [\sqrt{(E_1)^2 + (E_2)^2}\ ] / R_1$$

where E_1 and E_2 are the assumed error ranges for shoreline position measurements 1 and 2, respectively, and R_1 is the end point rate for the longest time span in the time series. The end point combinations with time spans greater than T_{min} are considered "long-term" rates, and their rates are averaged to yield the rate-of-change value. The error range for shoreline position used in this study is 8.5 m. This value is based on analyses performed by CROWELL et al. (1991) regarding the various errors involved in locating shorelines on T-sheets made prior to 1930 and on aerial photography, which are both used here.

Minimum Description Length Rate-of-Change (MDL)

This method was presented by FENSTER et al. (1993). First an optimum polynomial is fitted to a time series of shoreline positions based on the minimum description length criterion (MDL) as follows:

$$MDL_K = MSE_K + [\ln(N) \times K \times s^2] / N$$

where MDL_K is the minimum description length for a model with K terms, MSE_K is the mean squared error of the model, N is the number of data points, and s^2 is the noise variance that, for this study, is taken as the assumed error range for shoreline position measurements. The error range used for this study is 8.5 m, which is the same used for the AOR method. The model with the smallest MDL_K is called the optimum polynomial and is selected for further analysis.

Once the optimum polynomial is determined, points where the slope changes sign are found. These "critical points" indicate a change in the direction of shoreline movement at particular times. If there are no changes in the sign of the slope (i.e., no critical points), then the slope of a linear regression is used as the rate-of-change. If changes of sign in the slope do occur, the most recent time when the slope changes is selected, and all data prior to that time, are weighted to zero. A new linear regression is calculated called the "zero-weight line." The user has the option to select the slope of this line as the best rate-of-change value. This would be the case if specific knowledge of a change in coastal processes suggests that the earlier data should be completely disregarded (weighted to zero).

Often specific knowledge of coastal processes is not available, or it is not clear to what extent the earlier data should be considered. The MDL method allows an objective means to value data that are available before a change in trend. This is accomplished by incrementally increasing the weights of the earlier data (shoreline positions earlier than the critical point) and recalculating the linear regression and MDL_K. The weights are increased until the MDL_K is equal to or just less than that of the MDL_K for the optimum polynomial. Thus a nonlinear model is forced to be linear through a weighted linear regression technique. For the analyses in this study, SSAPP calculated the MDL method with no intervention based on specific knowledge of coastal processes. SSAPP did limit, however, the maximum order of the polynomial to be considered to 3 (K=4).

Automatic Baseline and Transect Determination

SSAPP invokes a baseline and transect determination routine that acts on a time series of digitized shorelines. SSAPP does this by first calculating the linear trend of all combined shoreline data. All data are then rotated around the average northing and easting position so that the shoreline trend is zero (horizontal in an x,y plot). Using the value for

baseline length provided by the user, the program then makes increments to the left of the average point (rotation point) and searches for all shoreline points lying within that increment (baseline segment) along the rotated trend line (x-axis). For each shoreline year within this segment, a linear regression is performed. The slopes and y-intercepts of each shoreline within the segment are then averaged. The end points of the initial baseline are determined by using this average line formula and the x-values bounding the increment. This baseline is subsequently adjusted and the rest of the baseline calculations proceed differently as described below.

To adjust the initial baseline and calculate the remaining baselines, SSAPP searches for points lying within an x-axis interval the length of the selected baseline length. This interval is centered on the x-value determined by adding the baseline length to the last end point of the previous baseline segment. When adjusting the initial baseline, the search is centered around the last end point of the current baseline segment. All y-values for shoreline positions within this interval are then averaged. The new baseline is now defined by the coordinates of the previous baseline end point and the x-value obtained by adding the baseline length to the x-value of the previous end point and the average y-value. If the difference between the new y-value (average y-value) and the y-value of the previous baseline end point is greater than 0.01, then all shoreline data are rotated around the previous baseline end point by the amount of the angle formed by the juncture of the previous baseline and the newly determined baseline. Thus all shoreline data are realigned to the trend of the new baseline, and a new search and end point calculation are made. This continues until the 0.01 tolerance is met or 30 iterations are made. If the number of iterations reaches 30, the last 2 y-values are averaged. (The 0.01 tolerance value and 30 maximum iterations were found to adequately determine the baselines for this study while limiting unnecessary computer time.) When the end of the shoreline data is reached to the left, the routine begins again at the center of the data and proceeds to the right.

Transects are automatically placed along the baselines at user-selected intervals. The first transect is placed at the end point of a baseline and is oriented so that it bisects the angle formed between the adjacent baselines. Subsequent transects within a baseline are oriented perpendicular to the baseline. If the selected baseline length and transect interval are equal, then transects are placed in the middle of baselines and are oriented perpendicular to the baselines. Figure 3 is an example of baselines and transects automatically constructed by SSAPP.

Once each baseline is determined, SSAPP then proceeds to determine the distance from the baseline of each shoreline that crosses the transect. The program searches for points spanning the transect for each shoreline. Once the closest points on each side of the transect are found, a linear interpolation is made to determine the point where the transect crosses the shoreline. The distance from the baseline for each shoreline is then calculated, and these numbers are used in the various rate-of-change calculation routines. To predict a future shoreline, SSAPP determines a projection vector the length of which is determined by multiplying the desired rate-of-change value for a particular transect by the desired number of years into the future for a prediction. The direction of the vector is determined by the sign of the rate-of-change (retreat or advance), and the orientation of the transect. To determine the predicted shoreline position, this vector is added to the point at which the latest shoreline crosses the transect.

Shoreline Data

Simulated Shorelines

To explore the effects of baseline selection on rates-of-change and predicted shoreline positions, both simulated and actual shoreline data are used. Simulated shorelines are used to estimate effects for specific amounts of shoreline and baseline nonconformity and shoreline rates-of-change. Maps of the different shoreline shapes are

shown in Figure 4. Shape "a" is simply a series of parallel and straight shorelines oriented so that a baseline drawn east to west forms a 30-degree angle with the shoreline trend. The spacing between these shorelines is the same as spacing along an actual transect taken from the center of Galveston Island, Texas (Figure 1). Figure 5 is a plot of shoreline distance versus time (shoreline history plot) illustrating the distribution in space and time of the shorelines along a transect. Shapes "b," "c," and "d" are sine waves with successive years offset a constant distance landward to simulate retreat (Figure 4). Thus, a shoreline history plot for a transect across these shorelines would be a straight line. For specific simulations, the distances between shorelines are increased or decreased to change retreat rates. Table 1 provides the shape parameters and rates-of-change for each simulation. The shapes and rates were chosen to reflect what are commonly encountered along barrier island/headland coasts. SSAPP was used to calculate erosion rates and predicted shorelines using single, nonconformal baselines (Figure 4) and multiple, 200-m long conformal baselines as automatically constructed by SSAPP.

Galveston Island

Historical shorelines along Galveston Island, Texas (Fig. 1), were used to evaluate the effects of the various methods for determining the shoreline rate-of-change and for the effects of baseline selection on projected future shoreline positions. For most of the Island, there are six digitized shorelines: 1838/50, 1930/34, 1955, 1965, 1970/74, and 1990. These shorelines originally were transferred from maps (1850 and 1934) or vertical aerial photographs (post-1934 dates) to 1:24,000-scale U.S. Geological Survey 7.5-minute quadrangle topographical maps, then later digitized into a geographical information system.

For this study, SSAPP automatically constructed multiple, conformal baselines 200 m in length and transects with a spacing of 50 m. A baseline length of 200 m appeared to

adequately follow the shapes of the shorelines, particularly toward the southwest end of the island (Figure 3). The transect spacing of 50 m provided a relatively smooth projected shoreline for the scale of this analysis. For comparison, an analysis was also performed using a single, nonconformal baseline, which was determined by a linear regression of all shoreline points for the entire island.

RESULTS

Simulated Shoreline Data: Effect of Baseline Selection on Rate-of-Change Calculations and Predicted Shoreline Position and Shape

Considering results from simulated shorelines with simple geometry allows the partial isolation of the causes of differences in rate-of-change values and predicted shorelines caused by baseline selection. Table 2 presents data for simulation 1. These shorelines are straight, and have an alongshore spacing the same as an actual transect from near the middle of Galveston Island (Figure 5). Rate-of-change calculations and future shoreline projections were performed using a baseline oriented at a 30-degree angle to the shoreline trend (nonconformal) and a baseline oriented parallel (conformal) to the shoreline trend. The calculated rates-of-change using the nonconformal baseline are always higher than the conformal baseline. Rates differ by 0.1 to 0.3 m/yr, or by 13% to 20%. The rates calculated by the EP, LR, JK, and MDL methods for their respective conformal and nonconformal baselines all differ by 13% to 14%, but the AOR method differs by 20%. The AOR method shows a greater difference because T_{min} for the nonconformal case is 13.98 years whereas for the conformal case it is 16.24 years. This difference in T_{min} causes the 1974–1990 shoreline pair to fail the minimum time criterion for the conformal case and thus to be dropped from the average.

Even though the rate-of-change values for the two baseline orientations differ for all the calculation methods, there are no differences in the 60-year projected shoreline

positions for the EP, LR, and JK methods. This is because the different directions of the transects (projection vector) along which the shoreline is projected compensate for the differences in rates-of-change. The MDL 60-year projected shoreline differs by only 0.7 m, but the AOR shoreline projected from the nonconformal baseline is 6.52 m landward of the shoreline projected from the conformal baseline.

Shoreline simulations 2 through 10 (Table 1) have shoreline trends that vary alongshore as a sine wave. Analyses of time series of evenly spaced shorelines with sine wave shapes are used to determine the effect of conformal and nonconformal baselines for different shoreline curvatures and rates-of-change. Table 3 presents the results from these analyses for rates-of-change of 2, 3, and 4 m/yr paired with 3 shoreline shapes with different curvatures (Figure 4, Table 1). Because shorelines for each time series are spaced equally, all the rate-of-change calculation methods yield the same values as presented in Table 3.

When shorelines are curved, discrepancies of shoreline rate-of-change values and projected shoreline positions for conformal and nonconformal baselines increase as rates-of-change or shoreline curvatures increase (Table 3). Because the shorelines are parallel, the rate-of-change values computed using conformal baselines are always less than those computed using nonconformal baselines (Table 3). The percent average rate-of-change difference for each shoreline shape is fairly constant for different rates-of-change and increases from about 2.3% to 12.5% for increasing shoreline curvature. Average absolute differences in the rates-of-change range from 0.05 m/yr for low curvature, low rate-of-change shorelines to 0.48 m/yr for high curvature, high rate-of-change shorelines. Absolute maximum differences in the rates-of-change are nearly twice the average differences.

Table 3 also presents the absolute differences in projected 60-year shoreline positions using conformal and nonconformal baselines. The differences in projected

shoreline positions are not as great as might be expected from the differences in rate-of-change values. The largest average absolute difference in this analysis is 12.3 m for the case with a rate-of-change of 4 m/yr and a high curvature (simulation #10) (Tables 1 and 3). Maximum differences, however, are more than twice the average differences and reach 29.0 m. Figure 6 shows how the differences in projected shoreline position and rate-of-change values are distributed alongshore for the intermediate curvature and rate-of-change case (simulation #6, Table 1). Figure 6 shows that the 60-year shoreline projected using the conformal baseline is seaward of the shoreline projected using the nonconformal baseline in the area of the seaward protuberance, but the opposite is true for the embayment. The two shorelines converge, however, at the apexes of the protuberance and embayment where the conformal and nonconformal baselines have similar orientations (Figure 5, 8). Also shown in Figure 6 is the rate-of-change computed for the conformal baseline case. The nonconformal rate-of-change was 3 m/yr and did not vary alongshore because of the way the simulated shorelines were constructed. The conformal rates-of-change vary smoothly along the shoreline, and, at the apexes, are nearly the same as the nonconformal rates. Rates are most different between the apexes where the shoreline trend is at its highest angle to the nonconformal baseline orientation.

Galveston Island: Differences Between Various Shoreline Rate-of-Change Calculation Methods

Figure 7a is a plot of the values of five methods for calculating the rates-of-change along the Galveston Island shoreline. The rates are determined using 200-m conformal baselines automatically selected by SSAPP, and with a transect spacing of 50 m. The alongshore shapes of the rate-of-change curves computed using the EP, LR, JK, and AOR methods are similar. On the extreme northeast end of the island, all methods reflect the accretion that has occurred from impoundment of sand by the jetty at Bolivar Roads. There is local erosion, however, southwest of the impoundment area and east of the

seawall and groins at around 41 km distance from the southwest end of the island (Figure 7a). Littoral drift along this northeast portion of the island is to the east, and the seawall and groins have interrupted littoral drift supply to the beach adjacent to the east end of the seawall causing local erosion. This section of shoreline is apparently west of the direct influence of the sediment impoundment caused by the jetty.

In front of a relatively old part of the seawall between 35 and 40 km from the southwest end of the island, the shoreline is nearly stable with rates-of-change of less than -1.0 m/yr (Figure 7a). Farther to the west, all methods of rate-of-change calculation show that rates of erosion gradually increase and reach a maximum of almost -3.0 m/yr just west of the seawall at a distance of 28 km. Littoral drift here is to the southwest, and, as is the case on the east end of the seawall, the seawall and groin field have interrupted littoral drift supply causing erosion. From about 28 km (about 2.5 km west of the seawall) to 22 km, erosion rates gradually decrease for all methods except the MDL method. From 22 km to 15 km, the shoreline is stable to slightly erosional (less than -0.5 m/yr) for all the methods except the MDL method, which shows erosion rates of more than -2.0 m/yr. Although the AOR method generally conforms with the EP, LR, and JK methods between 22 and 15 km, it is relatively erratic with several transects showing slight accretion.

From 15 km to about 7 km, erosion rates for all methods gradually increase. This increase, however, is more pronounced in the AOR and MDL methods. From about the 7 km point southwest to San Luis Pass, erosion rates slightly decrease then increase. The southwest end of the island has prograded to the southwest, but this analysis does not include that portion. Variance in rates-of-change from 0 to 7 km shows the effects of San Luis Pass. Along this stretch, the LR method shows the least variance and the lowest rates-of-change. The JK and EP methods show only slightly more variance, but the AOR and MDL methods show large swings in rates-of-change.

As mentioned above, all methods except the MDL method have a similar alongshore shape in their rate-of-change curves. Figure 7b shows the alongshore difference between EP and MDL rates. The MDL method departs dramatically from the EP method and the other methods for about 16 km west of the seawall between the 13 and 23 km marks. Along this 10 km of shoreline, the MDL method computed erosion rates of -2 to -4 m/yr while the other methods determined the shoreline to be nearly stable (Figure 7a). Differences in computed rates between the MDL and EP methods increase to 8 m/yr on the southwest end of the island with the MDL method providing much higher erosion rates than the EP method. The AOR method also determines relatively high erosion rates in this area.

Figures 7c and 7d are plots of the differences in the rate-of-change between adjacent transects for the EP and MDL methods, respectively. These plots illustrate the distribution of high-frequency variance alongshore and the amount of spatial dependence among adjacent measurement sites. The vertical scales of the plots are the same as the rate-of-change plot in Figure 7a so that a direct visual comparison may be made. Figure 7c shows well that the EP method has high spatial autocorrelation with adjacent measurements never varying by more than 0.08 m/yr southwest of the seawall and 0.28 m/yr in front of and to the northeast of the seawall. The MDL method, however, shows areas of large shifts in adjacent values centered around 3, 15, and 24 km and for the stretch of shoreline northeast of 33 km. These adjacent differences for the MDL calculated rates exceed 1 m/yr. Although a difference plot is not shown for the AOR method, it is apparent in the rate-of-change plot (Figure 7a) that the AOR method also shows relatively large shifts in adjacent rate-of-change values. The MDL and AOR methods also show relatively large-scale alongshore variance in their rates compared to the other methods.

Table 4 shows the mean and variance of the rate-of-change for all of Galveston Island and for each method of calculation. The mean values for the EP, LR, JK, and AOR methods are similar and range from an erosion rate of -0.91 to -1.11 m/yr. The mean rate-of-change for the MDL method, however, is -2.06 m/yr. Table 4 also presents the variance in rates for all of Galveston Island. The EP, LR, and JK methods have relatively low variances of 0.49 to 0.62 m^2/yr^2, and the AOR method has a higher variance of 0.92 m^2/yr^2. The MDL method, however, has a variance of more than twice the other methods at 2.06 m^2/yr^2.

Galveston Island: Differences in Predicted Shoreline Positions Caused by Baseline Selection

Figure 8a illustrates the effects of using conformal 200-m long baselines versus using one nonconformal straight baseline on predicting the Galveston Island shoreline 60 years into the future. Figure 8a is an alongshore plot of the distances between shorelines predicted using conformal and nonconformal baselines for the EP and MDL methods. It shows that, for the EP method, differences are almost always less than 5 m, but that there are some isolated locations with differences of more than 5 m. There is a slight increase in the differences on each end of the island and adjacent to and in front of the seawall. These are areas where greater shoreline curvature, greater rates-of-change, and relatively high alongshore gradients in the rate-of-change occur (Figure 7). The MDL method shows greater differences in predicted shoreline positions with some areas and scattered locations being more than 10 m different. The southwest end, where erosion rates and shoreline curvature increase, shows a discrepancy of up to 40 m with the shoreline computed using the conformal baseline seaward of the nonconformal case. Large, but more localized discrepancies occur about 4 km west of the seawall, in front of the seawall, and on the northeast end of the island.

Figure 8b shows the alongshore difference in rate-of-change for the conformal and nonconformal baseline cases for the MDL method. Rates are commonly different by more than 0.1 m/yr and roughly correspond with the differences in predicted shoreline positions (Figure 8a). The southwest end generally shows a lower erosion rate for the conformal baseline by as much as 0.2 m/yr. This much difference in erosion rate alone, however, cannot account for the 40 m discrepancy in predicted shoreline positions for this area. The rapid decrease in the rate-of-change from the southwest end to the northeast (Figure 7a) and the different directions of the projection vectors are responsible for most of the differences between the predicted shorelines. Because of the different orientations of the baselines, the transect (projection vector) that projects the predicted shoreline point for the conformal case is northeast of the transect that projects the corresponding point for the nonconformal case. The point predicted using the conformal baseline, therefore, was determined with a lower rate-of-change due to the alongshore gradient in rate-of-change. The mean rate-of-change and variance in the rate-of-change along the entire island is the same for both the conformal and nonconformal cases (Table 4).

DISCUSSION

The method for calculating the rate of shoreline change has a large effect on determining the rate-of-change along Galveston Island (Figure 7a, Table 4) and, consequently, on the predicted shoreline position. It is beyond the scope of this paper to determine which shoreline change calculation method is best for Galveston Island, but it is important to point out some differences among them. The EP, LR, and JK methods yield similar results and usually the lowest erosion rates (Figure 7a, Table 4). These methods also show low alongshore variance compared to the AOR and MDL methods. The MDL method departs radically from the other methods west of the seawall (Figure 7a). Inspection of the weights and critical points reveals that the MDL method completely

Table 1. Shape Characteristics of Simulated Shorelines. Letter designations for shapes correspond to Figure 4.

Simulation	shape	form	amplitude (m)	period (m)	maximum angle between shorelines and nonconformal baseline (degrees)	maximum shoreline curvature (2nd derivative)	spatial shoreline distribution	rate-of-change along non-conformal baseline (m/yr)
1	a	linear	N/A	N/A	30.0	0	variable	-0.86 (EP)
2	b	sine wave	100	2000	18.0	0.00099	constant	-2.00
3	b	sine wave	100	2000	18.0	0.00099	constant	-3.00
4	b	sine wave	100	2000	18.0	0.00099	constant	-4.00
5	c	sine wave	175	2000	31.5	0.00173	constant	-2.00
6	c	sine wave	175	2000	31.5	0.00173	constant	-3.00
7	c	sine wave	175	2000	31.5	0.00173	constant	-4.00
8	d	sine wave	250	2000	45.0	0.00247	constant	-2.00
9	d	sine wave	250	2000	45.0	0.00247	constant	-3.00
10	d	sine wave	250	2000	45.0	0.00247	constant	-4.00

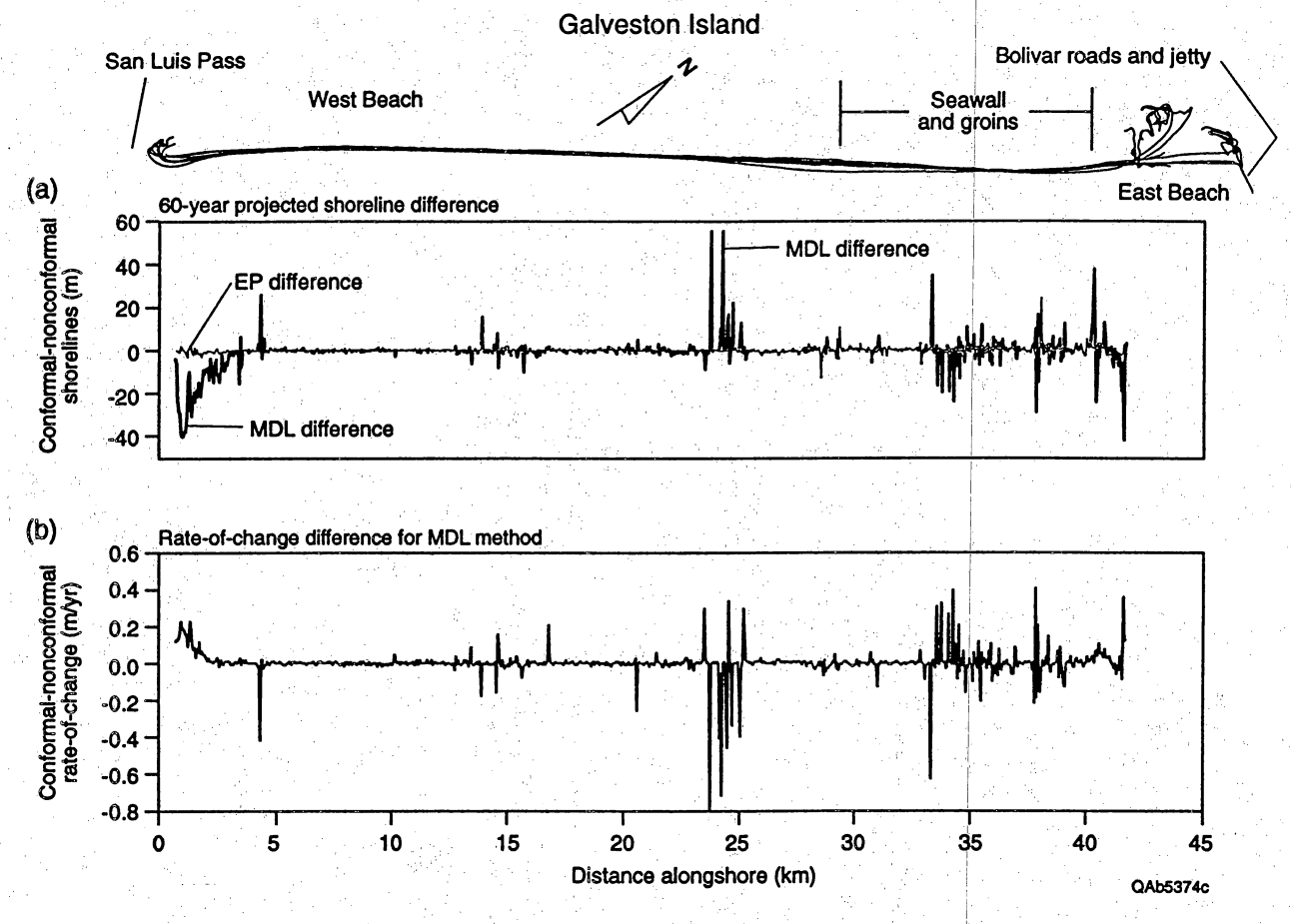

Figure 8. Plots of the alongshore differences in shorelines predicted 60 years into the future and rates-of-change determined using conformal and nonconformal baselines along Galveston Island. The computer program SSAPP automatically selected 200-m long baselines to conform to the historical shoreline trend and projected the future shorelines along transects spaced 50 m apart. The nonconformal baseline is the linear regression line computed using all the historical shoreline points and also had transects spaced 50 m apart. All data were linearly interpolated along the nonconformal baseline (linear regression line) for consistent comparison. (a) Alongshore plot of the distance between shorelines predicted with conformal and nonconformal baselines for the EP and MDL methods. Values less than zero indicate that the shoreline predicted using conformal baselines is seaward of the shoreline predicted using the nonconformal baseline. (b) Alongshore plot of difference in the rate-of-change calculated by the MDL method and using conformal and nonconformal baselines. Values greater than zero indicate that the rate using the conformal baselines is less erosional or more accretional than the rate calculated using the nonconformal baseline. Values less than zero indicate that the conformal rate is more erosional or less accretional than the nonconformal rate.

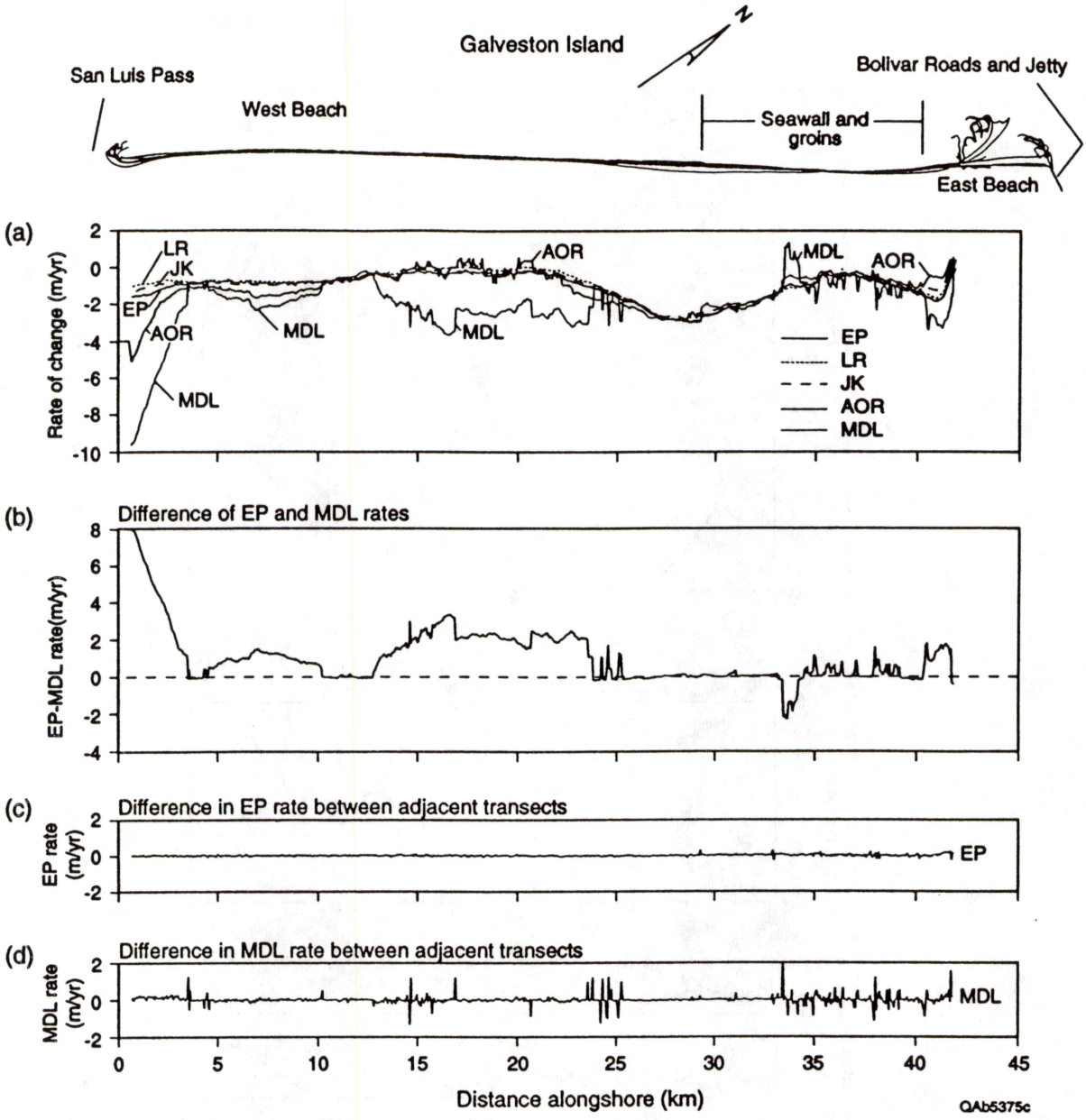

Figure 7. Results of rate-of-change analysis for Galveston Island, Texas, computed using 200-m long baselines that were automatically selected by the computer program SSAPP to conform to the historical shoreline trend. Transect spacing is 50 m. (a) Alongshore plot of rate-of-change calculated by five methods: EP= end point rate; LR= linear regression; JK= jackknife; AOR= average of rates; and MDL= minimum description length. Values less than zero indicate erosion. (b) Difference between the EP and MDL rates-of-change. There are large differences on the southwest end (left) and west (left) of the Galveston seawall and groin system. The EP method calculates lower erosion rates than the MDL method. (c and d) Difference in the rate-of-change for adjacent transects using the EP and MDL methods, respectively. Scale is the same as in (a) for direct visual comparison. The EP method shows little differences between adjacent transects indicating high spatial autocorrelation at a scale of 50 m (the transect spacing). The MDL method shows significant differences between adjacent transects. Both plots, however, show considerably less variation than the rate-of-change plots shown in (a).

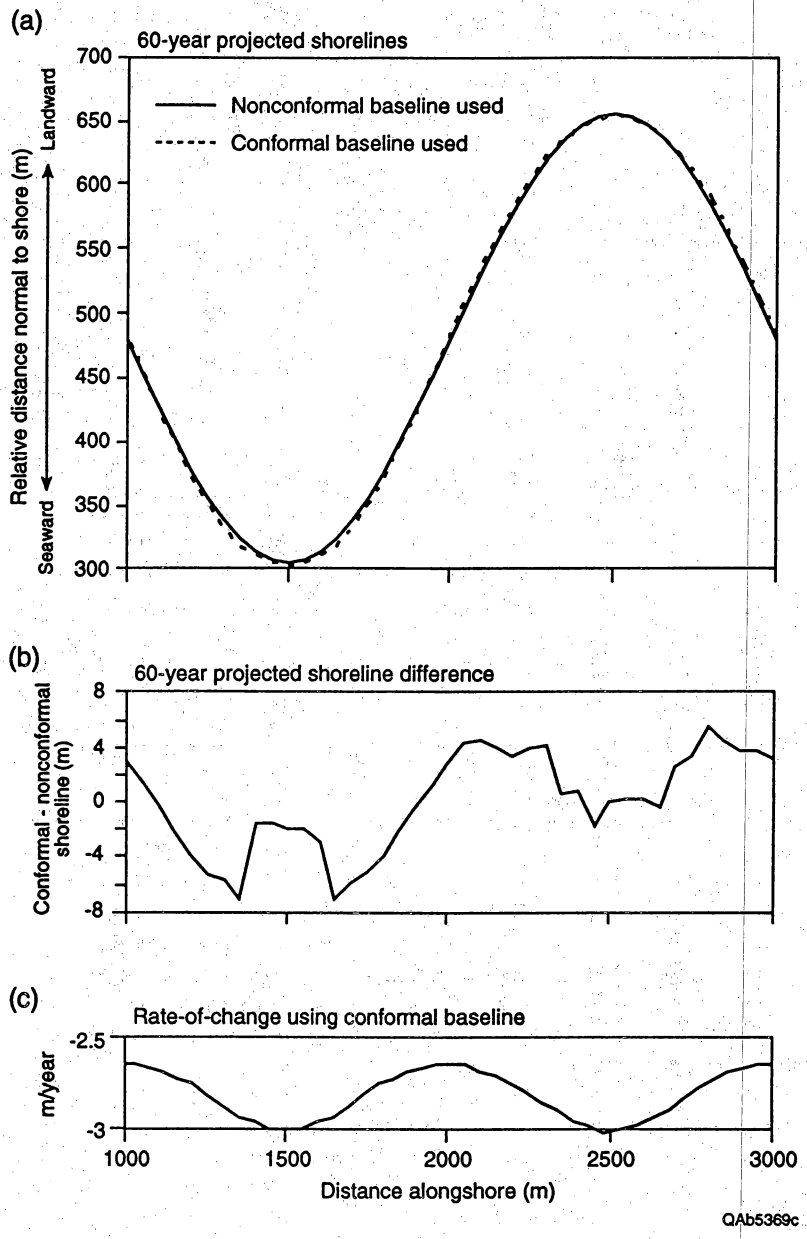

Figure 6. Results of rate-of-change and shoreline prediction analysis for simulation #6, a moderate erosion and shoreline curvature case. (a) Plot of predicted shorelines for 60 years into the future. The shoreline predicted using 200-m long baselines, which were automatically selected by the computer program SSAPP to conform to the shoreline trend, and one predicted with a nonconformal, single and straight baseline parallel to the x-axis are shown. Transect spacing is 50 m. The plot is stretched in the direction of the y-axis to better illustrate differences. (b) Distances between the predicted shorelines as interpolated along the x-axis and measured parallel to the y-axis. (c) Alongshore rates-of-change computed using conformal baselines. The simulated shorelines were constructed such that the rates-of-change for the nonconformal baseline are constant alongshore at -3.0 m/yr. The conformal rates-of-change are equal to or less than the nonconformal rates.

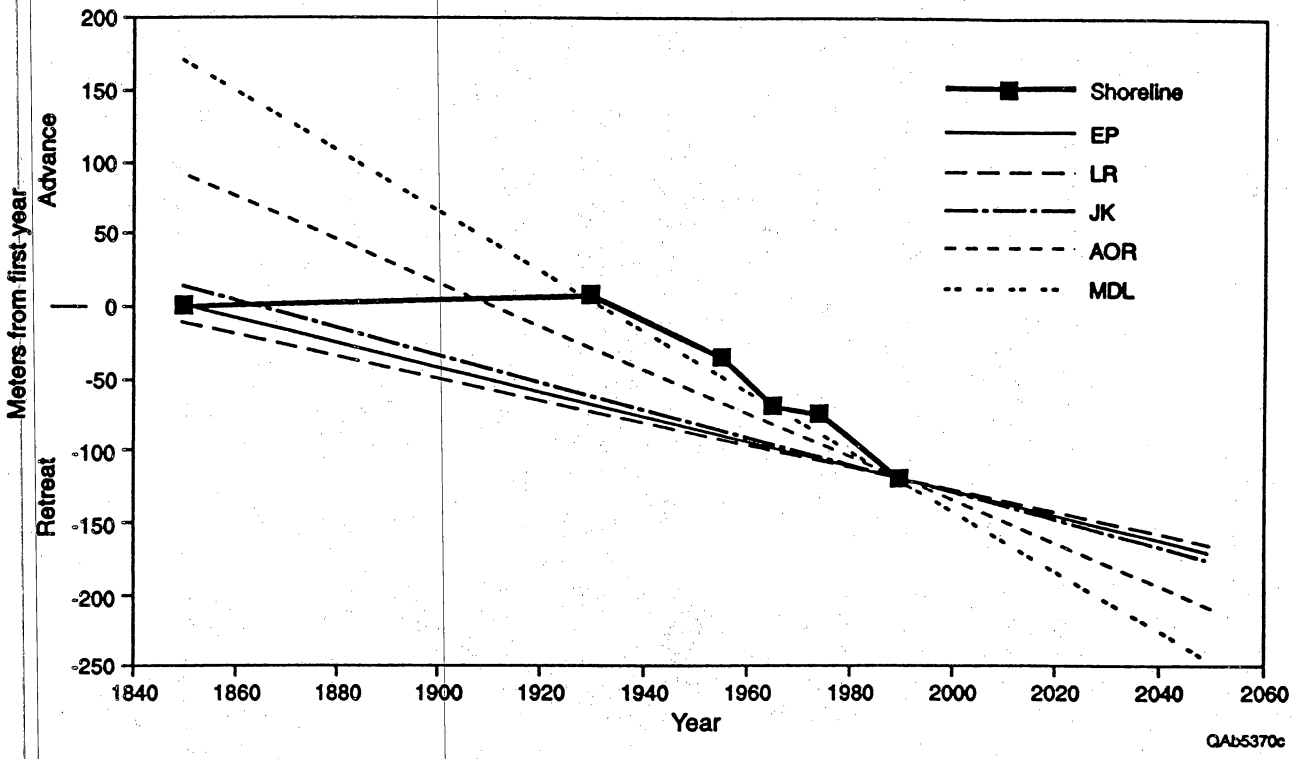

Figure 5. Shoreline history plot from central Galveston Island, Texas, used to locate shorelines in space and time for simulation #1. Also shown are lines with slopes equal to the shoreline rate-of-change as calculated by the EP, LR, JK, AOR, and MDL methods. Each line is forced to go through the latest shoreline position of 1990 and extends 60 years into the future to the year 2050. The spatial difference of the lines in the year 2050 indicates the significance of selecting the method of rate-of-change calculation when predicting future shorelines.

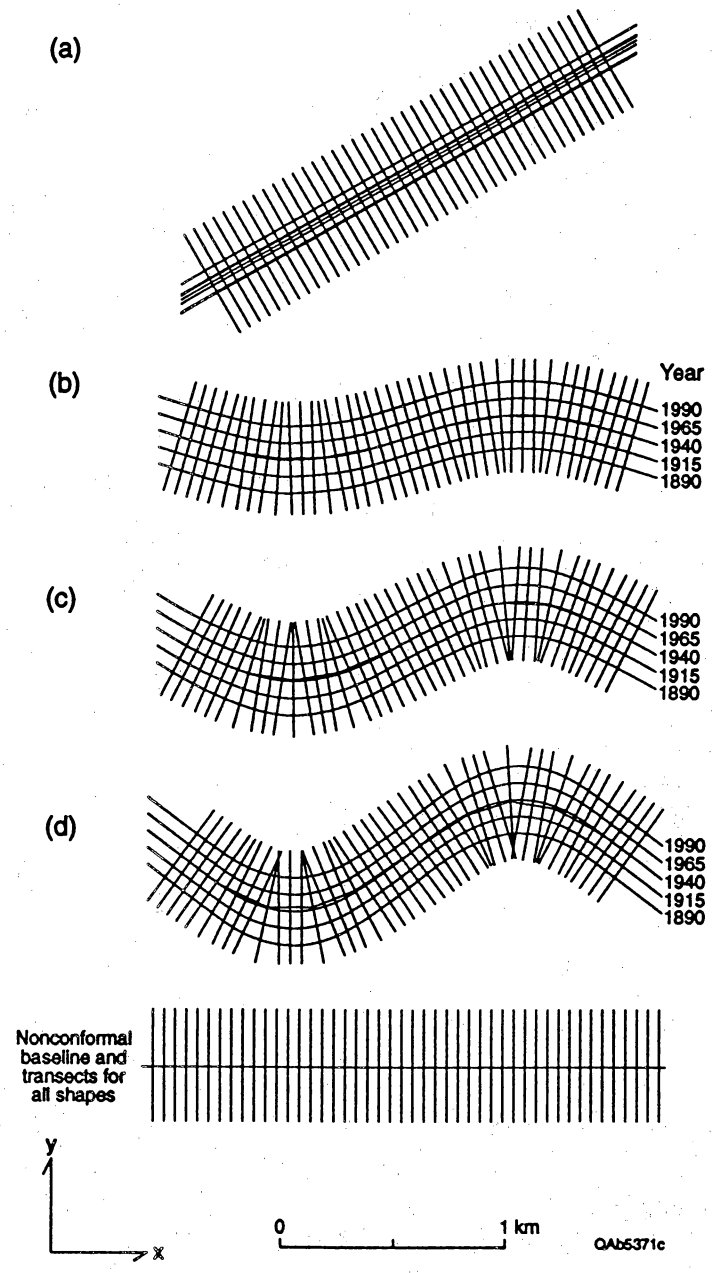

Figure 4. Map views of simulated shoreline shapes and the conformal baselines and transects constructed by the computer program SSAPP. Baseline segments are 200 m long, and transect spacing is 50 m. Table 1 presents the parameters used to generate each shape (a) Straight shorelines with spacing equal to spacing along a transect near the center of Galveston Island (see shoreline history plot in Figure 5). (b, c, d) Shapes constructed using a sine function. For individual simulations listed in Table 1, the shoreline dates were held constant and shoreline spacing was evenly adjusted along the y-axis. This changed the rate-of-change of the time series for the simulations.

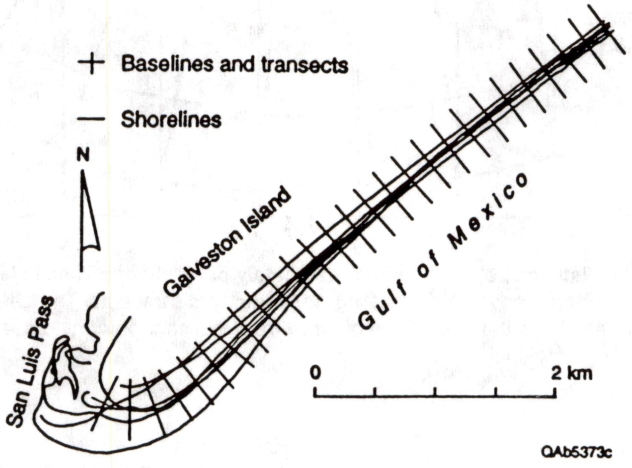

Figure 3. Historical shorelines, baselines, and transects from the southwest end of Galveston Island showing how well the baseline construction algorithm in SSAPP follows the trend of the shoreline. The baselines are 200 m long, and the transects are 200 m apart.

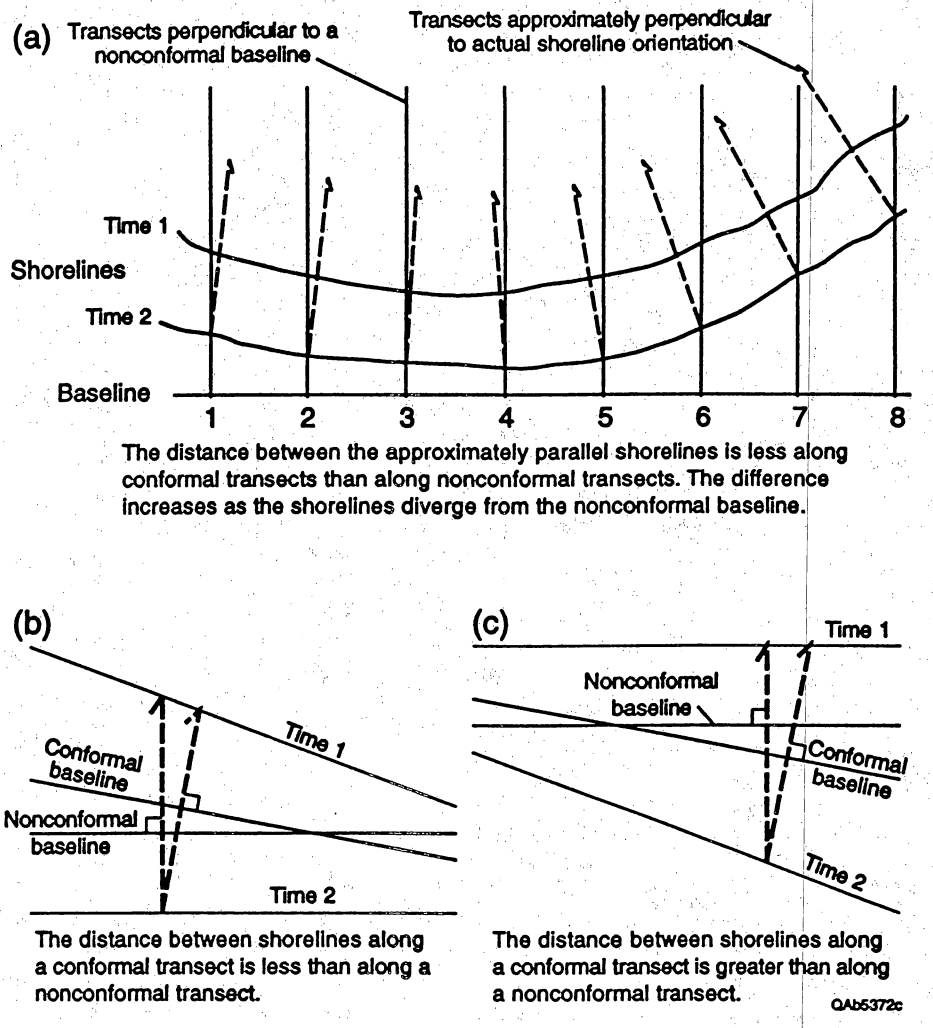

Figure 2. Illustration of how measured distances between shorelines, and, thus, calculated rates-of-change may vary when using transects drawn perpendicular to conformal and nonconformal baselines. (a) Parallel shorelines. (b) Nonparallel shorelines converging to the right. (c) Nonparallel shorelines converging to the left.

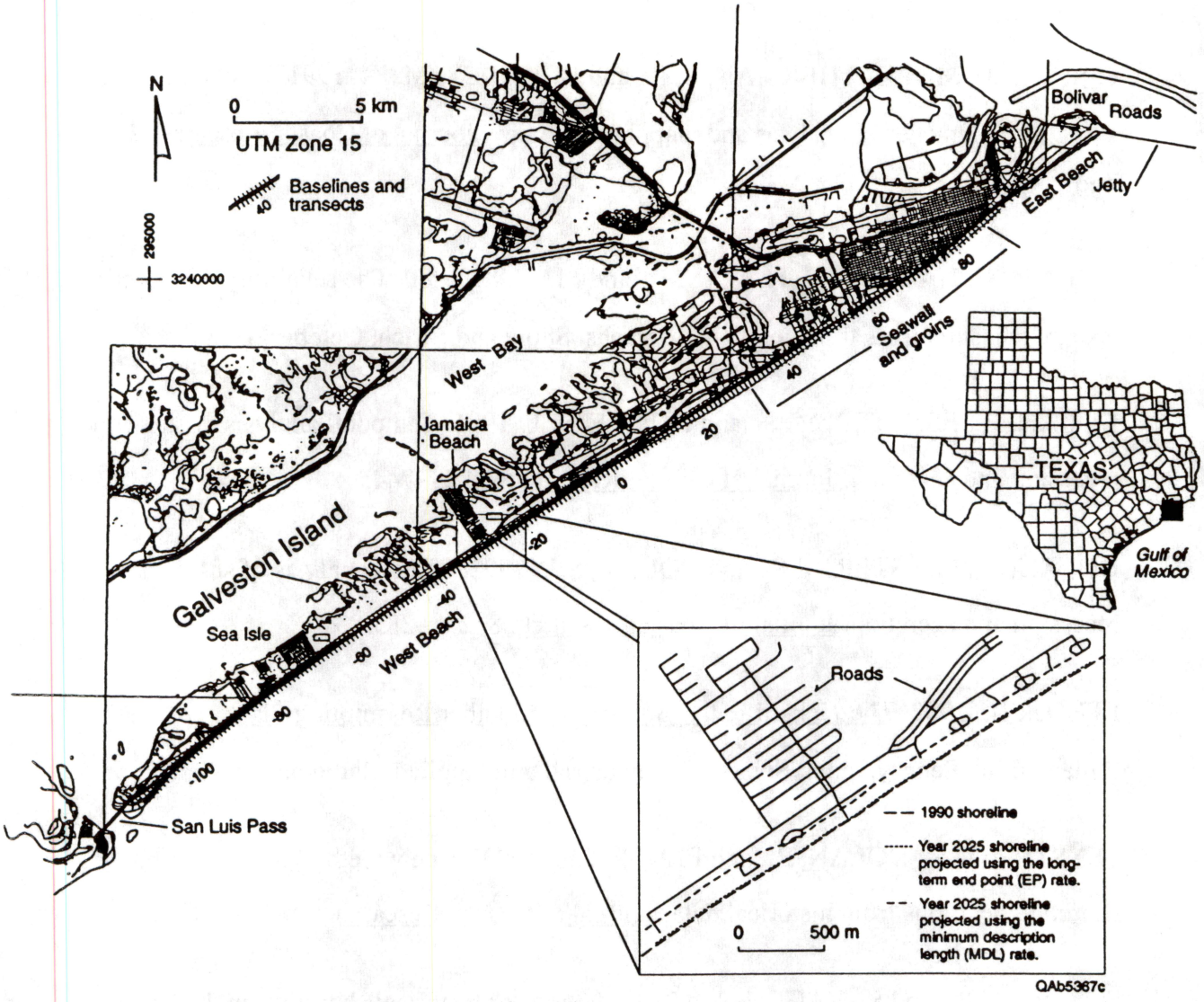

Figure 1. Galveston Island, Texas, showing the seawall and groin system, the south jetty at Bolivar Roads, East and West Beaches, and the natural tidal inlet of San Luis Pass. Transects along the Gulf of Mexico coast are spaced 200 m apart, and their orientations are perpendicular to 200-m long baselines. The SSAPP computer program automatically determined the baselines to follow the trend of historical shorelines. Map inset shows enlarged area of Jamaica Beach with 1990 shoreline and 2025 shorelines predicted with the EP and MDL methods. The MDL method calculated a higher erosion rate than the EP method, thus the MDL 2025 shoreline is about 100 m landward of the EP 2025 shoreline. The MDL 2025 shoreline has an unnatural bend in it caused by an abrupt alongshore change in the calculated rate-of-change.

LITERATURE CITED

CROWELL, M.; LEATHERMAN, S. P., and BUCKLEY, M. K., 1991. Historical shoreline change: error analysis and mapping accuracy. Journal of Coastal Research, 7, 839–852.

DOLAN, R.; HAYDEN, B. P., MAY, P., and MAY, S., 1980. The reliability of shoreline change measurements from aerial photographs. Shore and Beach, October, 1980.

DOLAN, R.; FENSTER, M. S., and HOLME, S. J., 1991. Temporal analysis of shoreline recession and accretion. Journal of Coastal Research, 7, 723–744.

DOLAN, R.; FENSTER, M.S., and HOLME, S.J., 1992. Spatial analysis of shoreline recession and accretion. Journal of Coastal Research, 8, 263–285.

EFRON, B., 1982. The Jackknife, the Bootstrap and Other Resampling Plans. Philadelphia, Pennsylvania: Society for Industrial and Applied Mathematics, 92p.

FENSTER, M.S.; DOLAN, R., and ELDER, J.F., 1993. A new method for predicting shoreline positions from historical data. Journal of Coastal Research, 9, 147–171.

FOSTER, E.R., and SAVAGE, R.J., 1989. Methods of historical shoreline analysis. Coastal Zone '89, 5, 4434–4448.

MORTON, R. A., 1991. Accurate shoreline mapping: past, present, and future. Coastal Sediments '91, American Society of Civil Engineers, 997–1010.

curvature of the shoreline, and the amount of discrepancy between the shoreline trend and baseline. The long-term linear regression method of rate-of-change calculation is probably the most stable with respect to baseline selection.

3. The difference between a shoreline position projected 60 years into the future using a single linear baseline orientation and one using multiple conformal baseline orientations may be significant from a coastal management perspective along barrier island/headland coasts where shoreline curvature caused by structures, shoreline interaction with tidal inlets, and headlands and bays occurs. The difference increases with increasing curvature of the shoreline, increasing rates of shoreline change, and higher alongshore gradients in the rate-of-change.

4. The selection of calculation method has a large effect on shoreline change rates along Galveston Island, Texas. The rates of shoreline change commonly vary by more than 1 m/yr and up to 9 m/yr among the EP, LR, JK, AOR, and MDL methods. The MDL method appears to account for changes in littoral drift caused by a seawall and groin system.

5. Large and abrupt alongshore differences in rates-of-change may cause predicted shorelines to have unnatural shapes. One should consider predicted shoreline shape when evaluating the reliability of rates-of-change and baseline orientations.

ACKNOWLEDGMENTS

This work was supported by a grant from the U.S. Geological Survey Coastal Geology Program. Robert Morton and Jay Raney provided helpful reviews of an earlier draft. Publication authorized by the Director, Bureau of Economic Geology, The University of Texas at Austin.

constructed, then the shoreline predicted with the nonconformal baseline would also have been erroneous.

It is clear that selection of baselines can have a significant effect on shoreline change analysis and the prediction of future shorelines. The time series of simulated shorelines used here do not cover all possible configurations of shoreline time series, but their analysis serves to point out that the selection of baselines will affect rate-of-change statistics, predicted shoreline position, and the shape of predicted shorelines. The effect will be most pronounced along shorelines with high rates-of-change, large variations in shoreline orientation, and alongshore gradients in the rate-of-change. Barrier islands with tidal passes on their ends often have recurved spits or areas of sediment impoundment with rates of shoreline change and shoreline curvature great enough to cause differences of more than 0.5 m/yr in rate-of-change values and more than 30 m in 60-year projected shoreline positions. For these areas and other areas with shoreline curvature, one should consider the effect of baseline selection. Using conformal baselines should produce more realistic predicted shorelines and more consistent rates-of-change than nonconformal baselines.

CONCLUSIONS

1. The algorithm in the Shoreline Shape and Prediction Program (SSAPP) uses time series of shoreline data to determine baseline orientations, and it is an effective and objective method to automatically select baseline and transect orientation for shoreline prediction and change analysis.

2. Absolute shoreline change rates calculated using multiple conformal baselines can be significantly less than those calculated using a single linear baseline along coasts with time series of parallel or nearly parallel shorelines. The amount of difference depends on the rate-of-change calculation method used, the magnitude of shoreline change, the

shown by its relatively low percent difference in rate-of-change in Table 2. The AOR and MDL methods are potentially more sensitive to different baseline orientations than the LR method. This is because of the way these methods evaluate the usefulness of the shorelines in the time series. A slight shift in the spacing of the shorelines may cause the elimination of a shoreline pair in the average of the AOR method or cause a shift in the critical time or the number of terms (K) in the optimum polynomial in the MDL method. The EP method also may be relatively sensitive to baseline selection because of its reliance on just two shorelines.

Conformal baselines will provide lower rates of change indicating more stable conditions than nonconformal baselines for time series of shorelines that are parallel. The greater the angle formed between baselines and shoreline trends, the greater the difference will be. The difference in the positions of predicted shorelines, however, is a function of differences in the calculated rate-of-change plus the direction of projection, shoreline shape (amount of curvature), alongshore gradient in rate-of-change, and amount of shoreline change. The simulation shown in Figure 6 shows how baseline selection also can affect predicted shoreline shape. Conformal baselines acted to broaden the protuberances and embayments and caused the shoreline between the protuberances and embayments to change orientation relative to the shoreline projected with the nonconformal baseline. The simulated shorelines were constructed as if all the shorelines in the time series had the same and constant beach slopes alongshore and that all shoreline movement was caused by relative sea level rise. This being the case, the predicted shoreline should have the same shape as the shorelines in the time series, as is the case with the shoreline predicted with the nonconformal baseline. The shape of the shoreline predicted with conformal baselines, therefore, is erroneous. If the nonconformal baseline, however, had not been chosen to be parallel to the x-axis of the coordinate system in which the simulated shorelines were

discounted (applied zero weights to) data prior to 1915 or 1950 along this stretch. Therefore, the MDL method automatically considered the change in littoral processes caused by the seawall located in the updrift direction. The MDL method holds promise for a relatively objective, unsupervised way of computing rates-of-change.

On the other hand, the alongshore, high-frequency variance in the rate-of-change for the MDL and AOR methods as shown in Figures 7a and 7d is of concern when projecting predicted shorelines. This variability is caused by varying availability of shorelines through the years for adjacent transects and by actual variance in the shapes of the shorelines. Even if the rate-of-change variance does reflect actual shoreline shape and change variability over the time period of analysis, projecting a new shoreline using those rates will likely produce an unnatural shoreline shape. An example of this is shown in the inset in figure 1 where projected shorelines using the EP and MDL rates are mapped. The MDL method predicts shoreline retreat of about 75 m over a 30-year period, but there is a prominent bend in the predicted shoreline that probably would not form given the lack of structures in the area and the lack of natural processes to form such a feature. The rates-of-change for the EP, LR, and JK methods are much smoother alongshore (Figure 7a,c) because they are not as affected by the alongshore shapes and availability of shorelines in the time series used to compute them. When determining the reliability of predicted shorelines, one must consider the naturalness of the alongshore shape of the predicted shoreline. Predicted shorelines that have unnatural shapes would suggest that unreasonable rate-of-change values were used or that projection vectors need to be changed.

Our analyses show that baseline conformity to shorelines can significantly affect rate-of-change statistics and predicted shoreline positions. This effect, however, is not the same for all rate-of-change methods considered here. The LR method, which considers all shorelines equally, is probably the least sensitive to different baseline orientations as

Table 2. Effect of baseline orientation on rate-of-change determination and 60-year predicted shoreline position for simulation #1. Values less than zero indicate retreat and conformal shoreline seaward of nonconformal shoreline.

	rate-of-change				
method	baseline and shorelines form 30-degree angle (nonconformal) (m/yr)	baseline and shorelines are parallel (conformal) (m/yr)	difference (m/yr)	difference (%)	difference between 60-year projected shoreline positions (m)
EP	-0.86	-0.74	0.12	-13.95	0.00
LR	-0.77	-0.67	0.10	-12.99	0.00
JK	-0.95	-0.82	0.13	-13.68	0.00
AOR	-1.51	-1.21	0.30	-19.87	-6.52
MDL	-2.08	-1.79	0.29	-13.94	-0.70

EP= end point, LR= linear regression, JK= jackknife, AOR= average of rates, MDL= minimum description length

Table 3. Effect of baseline selection on position of 60-year projected shoreline and calculated rate-of-change for various rates of shoreline change and curvature. Shoreline shape designations correspond to Figure 4. Results from simulations 2 through 10 are presented. Values are absolute differences between those computed using conformal and nonconformal baselines.

	Rate of simulated shoreline change calculated using nonconformal baseline orientation											
	-2 m/yr				-3 m/yr				-4 m/yr			
shoreline shape	average 60-year shoreline difference (m)/(%)	maximum 60-year shoreline difference (m)/(%)	average rate-of-change difference (m/yr)/(%)	maximum rate-of-change difference (m/yr)/(%)	average 60-year shoreline difference (m)/(%)	maximum 60-year shoreline difference (m)/(%)	average rate-of-change difference (m/yr)/(%)	maximum rate-of-change difference (m/yr)/(%)	average 60-year shoreline difference (m)/(%)	maximum 60-year shoreline difference (m)/(%)	average rate-of-change difference (m/yr)/(%)	maximum rate-of-change difference (m/yr)/(%)
b	0.30/0.25	0.70/0.58	0.05/2.50	0.09/4.50	0.6/0.33	1.30/0.72	0.07/2.33	0.14/4.67	1.30/0.54	3.30/1.38	0.09/2.25	0.18/4.50
c	1.20/1.00	2.60/2.17	0.13/6.50	0.25/12.50	3.00/1.67	7.10/3.94	0.20/6.67	0.37/12.33	5.20/2.17	13.70/5.71	0.26/6.50	0.48/12.00
d	2.90/2.42	6.00/5.00	0.25/12.50	0.42/21.00	6.70/3.72	14.00/7.78	0.37/12.33	0.63/21.00	12.30/5.12	29.00/12.08	0.48/12.00	0.84/21.00

Table 4. Mean and variance of rate-of-change values computed by five methods and for conformal and nonconformal baselines. Shoreline data from Galveston Island.

Method	Mean (m/yr)		Variance (m^2/yr^2)	
	conformal baseline	nonconformal baseline	conformal baseline	nonconformal baseline
EP	-1.04	-1.04	0.54	0.54
LR	-0.91	-0.91	0.62	0.62
JK	-0.96	-0.96	0.49	0.49
AOR	-1.11	-1.10	0.92	0.92
MDL	-2.06	-2.06	2.06	2.06

Addendum 7

Reports Published by Bureau of Economic Geology Research Staff Related to the Five-Year Program

Publication Reference	Work Elements
Morton, R. A., 1991, Response of Holocene depositional systems tracts to sediment influx, northern Gulf of Mexico: Proceedings Gulf Coast Section SEPM 12th Annual Research Conference, p. 149-158.	WE-2
White, W. A., and Calnan, T. R., 1991, Submergence of vegetated wetlands in fluvial-deltaic areas, Texas Gulf Coast: Proceedings Gulf Coast Section SEPM 12th Annual Research Conference, p. 278-279.	WE-1
Westphal, K. A., Penland, S., Seal, R. W., and Morton, R. A., 1992, Aerial videotape survey of coastal Texas and Louisiana: Center for Coastal, Energy, and Environmental Resources, Louisiana State University, Coastal Geology Map Series No. 13, 210p.	WE-1
Morton, R. A., Leach, M. P., Paine, J. G., and Cardoza, M. A., 1993, Monitoring beach changes using GPS surveying techniques: Journal of Coastal Research, v. 9, p. 702-720.	WE-1
Morton, R. A., Paine, J. G., and Gibeaut, J. C., 1993, Large-scale transfer of sand during storms: implications for modeling and prediction of shoreline movement:, in List, J. H., ed., Large Scale Coastal Behavior '93, U.S. Geological Survey Open-file Report 93-381, p.129-132.	WE-3,4
Morton, R. A., Paine, J. G., and Gibeaut, J. C., 1994, Stages and durations of post-storm beach recovery, southeastern Texas Coast: Journal of Coastal Research, v. 10, p. 884-908.	WE-1,3
Morton, R. A., 1994, Texas Barriers, *in* Davis, R. A., ed., Geology of Holocene Barrier Islands: Springer-Verlag, Berlin, p. 75-114.	WE-2
White, W. A., and Tremblay, T. A., 1995, Submergence of wetlands as a result of human-induced subsidence and faulting along the upper Texas Gulf coast: Journal of Coastal Research, v. 11 p. 788-807.	WE-1
Morton, R. A., Gibeaut, J. C., and Paine, J. G., 1995, Meso-scale transfer of sand during and after storms: implications for prediction of shoreline movement: Marine Geology, v. 126, p. 161-179.	WE-1,3,4
Blum, M. D., Morton, R. A., and Durbin, J. E., 1995, "Deweyville" terraces and deposits of the Texas Gulf Coastal Plain: Transactions Gulf Coast Association of Geological Societies, v. 45, p. 53-60.	WE-2
Morton, R. A., 1996, Geoindicators of coastal wetlands and shorelines, *in* Berger, A. R., and Iams, W. J., eds., Geoindicators: Assessing rapid environmental changes in earth systems: A. A. Balkema, Rotterdam, p.207-230.	WE-1,4
White, W. A., and Morton, R. A., in press, Wetland losses related to fault movement and hydrocarbon production, southeastern Texas coast: Journal of Coastal Research.	WE-1,3
Morton, R. A., and White, W. A., in press, Characteristics of and corrections for core shortening in unconsolidated sediments: Journal of Coastal Research.	WE-1
Paine, J. G., Morton, R. A., and Garner, L. E., in press, Site dependency of shallow seismic data quality in saturated, unconsolidated coastal sediments: Journal of Coastal Research.	WE-2
Stewart, L. B., Morton, R. A., and Lagoe, M. B., 1996, Holocene development of the southeastern Texas coast, Sabine Lake area, from foraminiferal biofacies: Transactions Gulf Coast Association of Geological Societies, in press.	WE-2

Morton, R. A., Blum, M. D., and White, W. A., 1996, Valley fills of incised coastal plain rivers, southeastern Texas: Transactions Gulf Coast Association of Geological Societies, in press.	WE-2
Morton, R. A., Kindinger, R. A., and Stewart, L. B., in preparation, Depositional environments and geologic history of the southeastern Texas coast during the last sea-level cycle: Transactions Gulf Coast Association of Geological Societies, in press.	WE-2
Morton, R. A., in preparation, Gulf shoreline movement between Sabine Pass and the Brazos River, Texas - 1974-1996: Bureau of Economic Geology, Geological Circular	WE-1
White, W. A, 1996, Wetland changes associated with faulting and subsidence: Proceedings Sabine Lake Conference, Sept. 13-14, 1996, Beaumont, Texas.	WE-2
Morton, R. A., 1996, Geological and historical development of Sabine Lake - an overview: Proceedings Sabine Lake Conference, Sept. 13-14, 1996, Beaumont, Texas.	WE-2

Addendum 8

Oral Presentations Made by Bureau of Economic Geology Research Staff
Related to the Five-Year Program

Speaker	Title	Meeting
R. A. Morton	Response of Holocene depositional systems tracts to sediment influx, northern Gulf of Mexico	Gulf Coast Section SEPM 12th Annual Research Conference, Houston Tx
W. A. White	Submergence of vegetated wetlands in fluvial-deltaic areas, Texas Gulf Coast	Gulf Coast Section SEPM 12th Annual Research Conference, Houston Tx
R. A. Morton	Geo-Indicators of Coastline and Wetland Changes	International Union of Geological Sciences Workshop on Geological Indicators of Rapid Environmental Change, Corner Brook, Newfoundland, Canada.
R. A. Morton	Global impact of mining and urbanization on earth surface processes and geomorphology in the coastal zone	International Union of Geological Sciences Workshop, Madrid, Spain.
W. A. White	Marsh Loss in the Galveston Bay System, Texas	Society of Wetland Scientists, Portland, Oregon
R. A. Morton	Evolution of incised coastal plain rivers, southeast Texas coast	SEPM meeting, St. Petersburg, Fla
J. C. Gibeaut	High-accuracy bathymetric surveys for coastal research	SEPM meeting, St. Petersburg, Fla
J. C. Gibeaut	Shallow water high-accuracy, high resolution bathymetric surveying system	Water for Texas Conference, Austin Tx
R. A. Morton	Shoreline changes in Texas	Coastal Erosion Technical Transfer Meeting, Texas General Land Office, Galveston Tx
R. A. Morton	Coastal Land Loss Short Course	1995 Annual GSA, New Orleans
W. A. White	Active faults and their effect on wetlands, upper Texas Gulf Coast	Society of Wetland Scientists, Boston, Mass
R. A. Morton	Mapping Shoreline Boundaries - Geological and Legal Implication	University of Maryland Department of Geography and Coastal Research Laboratory, College Park, Maryland
R. A. Morton	Recent erosion rates at Sargent Beach and their causes	Town Meeting, Sargent Tx
R. A. Morton	Differential kinematic GPS beach surveys: Key to improving models of nearshore sediment flux	South-central GSA, Austin Tx
J. C. Gibeaut	Accurate and rapid bathymetric surveys for coastal research	South-central GSA, Austin Tx
W. A. White	Geomorphic change in wetlands as a result of subsidence along active surface faults, Texas Gulf Coast	South-central GSA, Austin Tx
R. Gutierrez	Geoid variations and beach morphology: A regional approach to shoreline surveying using the Global Positioning System	South-central GSA, Austin Tx

J. G. Paine	Site dependency of shallow seismic data quality in beach, floodplain, and marsh environments of the Texas coastal plain	South-central GSA, Austin Tx
R. A. Morton	Valley fills of incised coastal plain rivers, southeastern Texas	Gulf Coast Association of Geological Societies
L. B. Stewart	Holocene development of the southeastern Texas coast, Sabine Lake area, from foraminiferal biofacies	Gulf Coast Association of Geological Societies
R. A. Morton	Geological and historical development of Sabine Lake - an overview	Sabine Lake Conference, Beaumont Tx
W. A. White	Wetlands changes associated with faulting and subsidence	Sabine Lake Conference, Beaumont Tx

Addendum 9

List of Electronic Files Submitted for CD-ROM

Documents

All Macintosh applications
CG=Cricketgraph

Folder	Folder	Folder	Document	Application
			c14	Word
			coreloc	Word
			dunes	Word
			seismic	Word
			shoretypes	Word
JCR/GPS				
			GPSBEACH	Word
			pkBall	CG
			319/320	CG
			319B	CG
			320B	CG
	GPS profiles		P2B 11/91(m)	Excel
			P2C 11/91(m)	Excel
			P2D 11/91(m)	Excel
			P2C 5x100	Excel graph
			P2A 5x100	Excel graph
			P2A 5x150 comparison	Excel graph
			P2B 5x100	Excel graph
ivfGCAGS				
			table ages	Word
			tablesizes	Word
			text	Word
coreshorten				
			shortjcr	Word
			tables	Word
			coreabst	Word
	figs		cum	CG
			fig3	Word
			figscale	Word
			int	CG
			LR4%	CG

Folder	Folder	Folder	Document	Application
			scale	Freehand
		TR-10	LOI	CG
			min	CG
			Pb/unc&cordepth	CG
			TR-10	CG
			TR-10 %WATER	CG
			TR-10 density adj	Excel
			TR-10 Pb vs Depth	CG
			TR-10 Pb vs depth (n)	CG
			TR-10 slope	CG
			TR-10 USGS	Excel
			TR-10.tx	Excel
			water	CG
	figs cont'd		TR10	CG
			TR10cumshort	CG
			TR10intshort	CG
forams				
			GCAGS96	Word
Galgrains				
			Galveston Sed Samples	Excel
			psa	Excel
			sieve	Excel
	cumulative curves		1-70	CG
			graph data 2	CG
GCAGS Deweyville				
	freehandfigs		Freehand 4.0 #0001-#0006.data	Freehand 4.0
			text	Word
geoindi				
			afig11	CG
			afig8	CG
			afig9	CG
			data	CG
			fig 6	Freehand
			shorehistory	Freehand

Folder	Folder	Folder	Document	Application
			text	Word
JCR beachrecovery				
			table 1	Word
			text 1	Word
	figs		%cumrecov	CG
			%profile recov	CG
			profile1-5	Word
			profile7-8	Word
	profiles-CG		profile1-5	CG
			profile7-8	CG
			profile1'-5'	CG
			profile7'	CG
	recov data		% recov	CG
			% recov.tx	CG
			alongshore rec.	CG
			alongshore %	CG
			alongshorevol	CG
			format plot	CG
			profile recov	CG
			rec 1-5	CG
			rec 7	CG
			vol recov	CG
LSCB				
			list	Word
			isoabst	Word
			revtext	Word
	figs		1 & 3	Word
			4 & 8	Word
			beach height	CG
			data	CG
			fig 7	Word
			follets	CG
			g1	CG
			g2	CG
			p1tower	CG
			p3cisle	CG
			p4slp	CG

Folder	Folder	Folder	Document	Application
			Profile 1 (m)	CG
			Profile 3 (m)	CG
			Profile 8 (m)	CG
			Profile4 (m)	CG
		plot	3x	CG
			Profile 1 (m) copy	CG
			Profile 3 (m) copy	CG
			Profile 8 (m) copy	CG
			Profile4 (m) copy	CG
			x1	CG
			x4	CG
			x8	CG
		tables	1VOL REC	Word
			2Vol change	Word
			3effects	Word
		volume	10yr	CG
			1984	CG
			1985	CG
			87-93	CG
			Aug 88-Sept 89	CG
			Aug 90-Nov 91	CG
			Aug-Dec 84	CG
			Dec 83-Feb 84	CG
			Dec 84-Feb 85	CG
			Feb-May 84	CG
			Feb-May 85	CG
			May-Aug 84	CG
			May-Sept 85	CG
			Nov 91-Apr 93	CG
			Oct 87-Aug 88	CG
			profile recov	CG
			Sept 85-Oct 87	CG
			Sept 89-Aug 90	CG
			vol change	CG
			vol recovy	CG
			volchangeword	Word

Folder	Folder	Folder	Document	Application
SB/HBgrains				
	cumulative curves		1-4	CG
			8-12	CG
			13-18	CG
			19-23	CG
			26-36	CG
			40-47	CG
			49-53	CG
			54-61	CG
			62-66	CG
			67-72	CG
			73-77	CG
			graph data pt 1	CG
			graph data pt 2	CG
	textures		hydrom	Excel
			sieve	Excel
			table	Excel
shorehist				
	galveston 96 data	1996 shoreline plts Galvs	96 transects 1-31 Galvs	CG
			GI 01-04 1996	CG
			GI 13-31 1996	CG
Bill's folders				
			USGS coast erosion files	Word
WhiteandMorton(inpress)				
			CaplenFieldFigure13	Excel
			ClamLakeFigure10	Excel
			FaultFigurecapsrevised	Word
			FinalFaulttext	Word
			PortNechesFigure9	Excel
			Readme	Word
			Table1faultlengths	Word
			Table2soilsacrossfault	Word
			Table3Marshloss	Word
WhiteTremblay(1995)				
			White&Tremblay(1995)	Word

Scans

Scanned core descriptions

geographic area	well names and cores taken
Coastal Erosion	CE 2-15
McFaddin Vibracores	McFV 1-7
Sabine Lake Vibracores	SLV 1-30
Sabine Shelf Vibracores	SSV 1-6
Sabine Bank Vibracores	SBV 1-25
Heald Bank Vibracores	HBV 1-7
Galveston Island-Bolivar Peninsula	GI-BP 1-12

Addendum 10

Extended Abstracts Presented at the Sabine Lake Conference

GEOLOGICAL AND HISTORICAL DEVELOPMENT OF SABINE LAKE - AN OVERVIEW

Robert A. Morton
Bureau of Economic Geology
The University of Texas at Austin

Reconstruction of the late Pleistocene geologic history of the southeastern Texas coast illustrates how climate and sea-level fluctuations influenced the location and morphology of Sabine Lake and the composition of sediments filling the Lake. Sabine Lake is an estuary and unfilled former river valley that was constructed during the last glacial period (Kane, 1959). As continental glaciers in North America expanded and sea level began falling about 100,000 years ago, the Sabine and Neches Rivers began excavating a valley in response to lowered base level. Maximum incision of the valley to a depth of about 120 ft below Sabine Lake (Kane, 1959) occurred about 20,000 years ago when sea level was at its lowest position, or about 300 ft below present sea level. As the ice masses melted about 18,000 years ago, sea level began rising rapidly and the incised valley beneath Sabine Lake was flooded about 9,000 years ago when sea level was at about -70 ft (Nelson and Bray, 1970; Anderson et al., 1991; Morton et al., 1995). Initially fresh water marsh formed on the abandoned floodplain of the Deweyville river deposits. Small bayhead deltas also formed where the Sabine and Neches Rivers entered the drowned valley. Later, as sea level rose irregularly and with minor reversals toward its present position, the valley was inundated by more saline water and began filling with estuarine and marine sediments characterized by oysters and brackish water clams. About 3,500 years ago, when sea level reached its present position, Sabine Lake was separated from the Gulf of Mexico by advancement of the Gulf shoreline and deposition of the beach ridge/mudflat complex that is known as the chenier plain (Gould and McFarlan, 1959). High volume fresh-water inflow into Sabine Lake helped maintain Sabine Pass as a narrow link between the water bodies.

Depositional remnants of the late Pleistocene Sabine and Neches Rivers are collectively referred to as "Deweyville" on the basis of elevated terraces and associated fills that are preserved along the valley walls. These terrace features were first recognized in the Sabine valley at the town of Deweyville by Bernard (1950). The late Pleistocene rivers were characterized by moderately large bed-load streams with relatively uniform discharge that migrated laterally and filled the incised valley with sandy point-bar deposits. Because muddy overbank sediments are noticeably absent in these late Pleistocene river deposits, they are mined extensively for sand and gravel aggregate. Along the valley margins and at the base of the valley, three Deweyville terraces are preserved like stair steps that are progressively lower and located toward the valley axis. The youngest (lowest) terrace controls gradients, channel

patterns, positions, and surficial drainage of the modern Sabine and Neches Rivers. The modern rivers are narrow, sinuous, flashy-discharge streams that transport a muddy organic-rich suspended load. The muddy overbank deposits of these rivers help maintain fixed channels that change position by meander-bend cutoff and avulsion during deep floods. The lack of abundant abandoned courses and oxbows within the modern floodplain indicate that the modern rivers have not substantially reworked the Deweyville deposits.

The differences in channel pattern, sediment composition, and depositional style between the late Pleistocene and Holocene rivers suggest fundamentally different physical processes. River discharge during the late Pleistocene must have been largely contained within the channel banks, whereas overbank flooding and vertical aggradation of the floodplain during the Holocene and modern was frequent. Greater and more uniform annual river discharge during the late Pleistocene can be attributed to a cooler and wetter climate that produced precipitation throughout the year and thick soils in the drainage basins. Cooler temperatures and restricted size of the Gulf of Mexico when sea level was lower also would have hindered or prevented the formation of tropical cyclones. Thus annual distribution of precipitation would have been relatively uniform, and the thick upland soils would have minimized surface runoff and contributed to more uniform river discharge. Post-glacial changes in upland vegetation, stripping of upland soils, and generation of tropical cyclones produced flashy peak river discharge, frequent overbank flooding, and loads of suspended sediment (mud) that characterize the Holocene rivers.

Extant discharges of the Sabine and Neches Rivers are largely moderated by flood control structures and freshwater impoundments upstream of Sabine Lake. The volume of sediment presently reaching the Sabine/Neches floodplains and associated coastal marshes in Sabine Lake and the volume of sediment needed to sustain wetlands in these areas is unknown and represents one of the major gaps in scientific data for the river/estuarine system. Artificial reductions in peak discharge of the rivers may have reduced the volume of sediment deposited on the floodplains, in the delta regions, and in Sabine Lake, which would contribute to the historical loss of wetlands observed.

Morphological changes in the rivers during historical time have been related primarily to human activities. The lower reaches of the rivers initially were cleared of log rafts and snags, realigned, and deepened to improve navigation by steamboats (U.S. Army Corps of Engineers, 1880). Subsequent dredging of the river channels and deposition of dredged material on the river banks was conducted to permit navigation by deep draft vessels. Alterations to the river floodplains included removal of dense stands of large cypress trees that were logged for lumber and construction of high mounds of dredged material along the natural levees. These high

mounds alter the floodplain hydrology and may prevent some overbank sediment from being deposited on the floodplain.

Marshes composing the Louisiana side of Sabine Lake have remained essentially natural whereas the Texas side of the Lake has been greatly altered by the dredging of the Sabine-Neches channel to Port Arthur, Beaumont, and Orange. Sediment dredged from the western margin of the Lake to form the waterway was placed in disposal areas to protect the channel from waves and to reduce maintenance dredging that is periodically required to remove shoals. Some of the dredged material was used to create made land at Port Arthur that is used for wharves and other docking facilities. Most of the western (Texas) shore of Sabine Lake has been artificially hardened and consists of rock revetments constructed to contain the dredged material and protect it from erosion. Before it was artificially stabilized, the western shore of Sabine Lake was being eroded by waves generated by the predominant southeastern winds. This erosion made the Lake wider than its original valley width. Unprotected delta plain, coastal marsh, and chenier plain shores of southwestern Louisiana continue to retreat as a result of frequent storm waves and inadequate sediment supply.

Water depths in Sabine Lake generally range from 3 to 8 ft. Greatest depths occupy the eastern two-thirds of the open lake, which generally coincides with the axis of the drowned valley. The shallower platform that occupies the western third of the open lake was formed by wave erosion. Natural shoals are also located near the mouths of the rivers and along the channel flanking the chenier plain that connects Sabine Lake with Sabine Pass.

Dredging of Sabine Pass began in 1875 when the natural water depth over the outer bar was about 7 ft (U.S. Army Corps of Engineers, 1877). Projects designed to deepen the entrance to Sabine Lake, construct a stable navigation channel, and reduce channel shoaling by construction of jetties were intermittent throughout the late 1800s and early 1900s. The channel was progressively deepened and the jetties lengthened and currently the jetties extend nearly four miles into the Gulf of Mexico; the authorized project depth of the entrance channel is 42 ft.

Sabine Lake forms a trap for sediments transported by the Sabine and Neches Rivers, therefore the floor of the Lake is composed primarily of mud, sandy mud, and muddy sand (White, et al., 1987). Mixtures of mud, sand, and shell occur in the southern part of the Lake in the vicinity of oyster reefs, along mounds of reworked dredged material, and where the beach ridges in southwestern Louisiana are being eroded. High concentrations of sand are restricted to areas surrounding the mouths of the Sabine and Neches Rivers. Bottom sediment textures are slightly coarser on the Texas side of the Lake. This asymmetrical pattern generally reflects the regional coastal processes as well as the relationship between grain size and water depth. The finest sediments (muds) tend to be concentrated in the deepest parts of the Lake, whereas slightly coarser sediments are deposited along the western margin in shallow water where the fetch is

greatest and highest waves impinge on the shore. Concentrations of metals (iron, lead, copper, zinc, chromium) in the surface sediments display patterns that are similar to the distribution of sediment textures (White, et al., 1987). Highest concentrations of metals generally are associated with the muddy sediments whereas concentrations of metals tend to be lower where sediments are coarser. Some high concentrations of metals in the sediments were taken from the ship channel, which suggests an anthropogenic contribution related to industrial or municipal waste water discharged along the channel.

The physical processes that continue to influence Sabine Lake and the lower reaches of the Sabine and Neches Rivers are reduced peak river discharge and sediment influx, frequent intense winter storms and tropical cyclones, and a relative rise in sea level. The relative rise in sea level in the Sabine Lake region is caused primarily by land surface subsidence (Swanson and Thurlow, 1973). Some of the subsidence is related to natural (geological) compaction of sediments in the basin and some is locally caused by extraction of subsurface fluids, principally oil, gas, and associated formation water. Man-induced subsidence near oil and gas fields may occur across the entire area of production or it may be concentrated along faults activated by the fluid withdrawal. Although the tide gauge record at Sabine Pass is incomplete, the historical trend of sea level is similar to that recorded at Galveston where the rate of relative sea-level rise is about 2.6 ft every hundred years (Lyles et al., 1988).

The sediments beneath Sabine Lake record a rich history of climatic changes and sea-level fluctuations that altered the natural ecosystems and required environmental adjustments to rapidly changing conditions over thousands of years. Some of the older historical ecological changes may be preserved at the surface in shell middens at archeological sites along the waterways. Detailed examination of shell midden strata may reveal how the estuarine organisms responded to changing salinity, water depth, and sediment type caused by regional variations in rainfall and sea level position.

REFERENCES

Anderson, J. B. Siringan, F. P., Taviani, M., and Lawrence, J., 1991, Origin and evolution of Sabine Lake, Texas-Louisiana: Gulf Coast Association of Geological Societies Transactions, v. 41, p. 12-16.

Bernard, H. A., 1950, Quaternary geology of southeast Texas: Unpub. Ph.D. dissertation, Louisiana State University, Baton Rouge, Louisiana, 164 p.

Gould, H. R., and McFarlan, E., Jr., 1959, Geologic history of the chenier plain, southwestern Louisiana: Gulf Coast Association of Geological Societies Transactions, v. 9, p. 261-270.

Kane, H. E., 1959, Late Quaternary geology of Sabine Lake and vicinity, Texas and Louisiana: Gulf Coast Association of Geological Societies Transactions, v. 9, p. 225-235.

Lyles, S. D., Hickman L. E., Jr., Debaugh, H. A., Jr., 1988, Sea-level variations for the United States 1855-1986: U.S. Department of Commerce, NOAA-NOS, Rockville Md., 182 p.

Morton, R. A., W. A. White, J. C. Gibeaut, R. Gutierrez, and J. G. Paine, 1995, East Texas and Western Louisiana Coastal Erosion Study Annual Report, Year 4: University of Texas at Austin, Bureau of Economic Geology, contract report prepared for the U.S. Department of Interior, Geological Survey Contract No. 14-08-0001-A0912, variously paginated.

Nelson, H. F., and E. E. Bray, 1970, Stratigraphy and history of the Holocene sediments in the Sabine-High Island area, Gulf of Mexico, *in* J. P. Morgan, and R. H. Shaver, eds., Deltaic sedimentation, modern and ancient: SEPM Special Publication No. 15, p. 48–77.

Swanson, R. L., and Thurlow, C. L., 1973, Recent subsidence rates along the Texas and Louisiana coasts as determined from tide measurements: Journal of Geophysical Research, v. 78, p. 2665–2671.

U.S. Army Corps of Engineers, 1877, Sabine Pass, Texas: Annual Report of the Chief of Engineers, part 1, p. 75.

U.S. Army Corps of Engineers, 1880, Survey of Sabine River, Texas from its mouth to East Hamilton: Annual Report of the Chief of Engineers, p. 1195-1204.

White, W. A., Calnan, T. R., Morton, R. A., Kimble, R. S., Littleton, T. G., McGowen, J. H., Nance, H. S., and Schmedes, K. E., 1987, Submerged lands of Texas, Beaumont-Port Arthur area: sediments, geochemistry, benthic macroinvertebrates, and associated wetlands: The University of Texas at Austin, Bureau of Economic Geology, 110 p.

RECENT WETLAND LOSSES AT THE GSU MARSH RESTORATION SITE, NECHES RIVER VALLEY

Final Report

by

William A. White, Robert A. Morton, and Thomas A. Tremblay

Bureau of Economic Geology
Noel Tyler, Director
The University of Texas at Austin
Austin, Texas 78713-8924

May 1996

CONTENTS

Figures

Table

INTRODUCTION

Texas Parks and Wildlife Department's (TPWD) plans to restore a marsh in the lower Neches River valley south of the Gulf States Utilities (GSU) power plant, an area of known historical marsh loss due partly to subsidence and faulting, emphasized the need to investigate potential long-term impacts of subsidence on the marsh site (fig. 1). Marsh restoration efforts could fail, however, if the area continues to subside at a rate that exceeds marsh vertical accretion. Determining whether the GSU area is subsiding at a rate higher than that of the surrounding landscape could be answered by benchmark releveling surveys across the area, but those surveys have been conducted only across regions more inland (Ratzlaff, 1980). Although site-specific releveling surveys would provide the most quantitative and reliable data regarding subsidence, lack of time and funding for establishing benchmarks and conducting releveling surveys over a sufficient period of time prevented such an approach. Consequently potential future marsh loss as a result of submergence had to be estimated by other means.

HISTORICAL CHANGES IN MARSHES

Delineation of wetlands on sequential aerial photographs allows researchers to document the magnitude and rate of marsh loss through time. By looking at rates of change, they can draw conclusions about the stability of the marsh system and expected future trends. Previous studies have indicated that subsidence and faulting are among factors contributing to the transformation of areas of emergent vegetation to open water (White and others, 1987; White and Tremblay, 1995; White and Morton, in press). Marsh losses documented by White and others (1987) covered the period from 1956 through 1978 (fig. 2). During that period, more than 9,400 acres of marsh loss occurred in the Neches River valley, mostly as a result of encroachment of open water into areas previously supporting emergent vegetation.

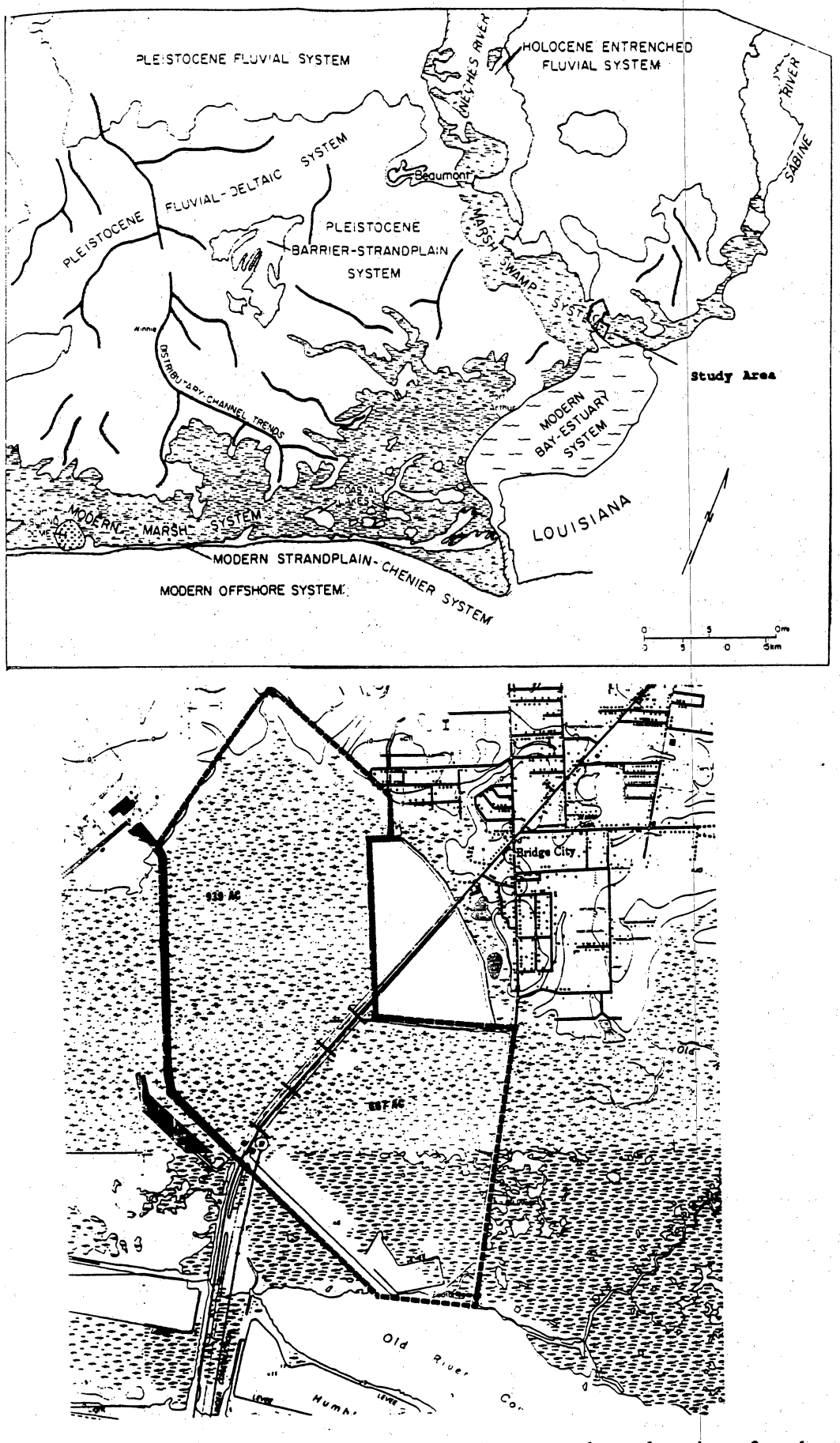

Figure 1. Index map showing location of study area. Map at top shows location of study area with respect to natural systems in the Beaumont–Port Arthur area (from Fisher and others, 1973); map at bottom shows study area in more detail (from E. J. Taylor, Texas Parks and Wildlife Department, personal communication, 1996).

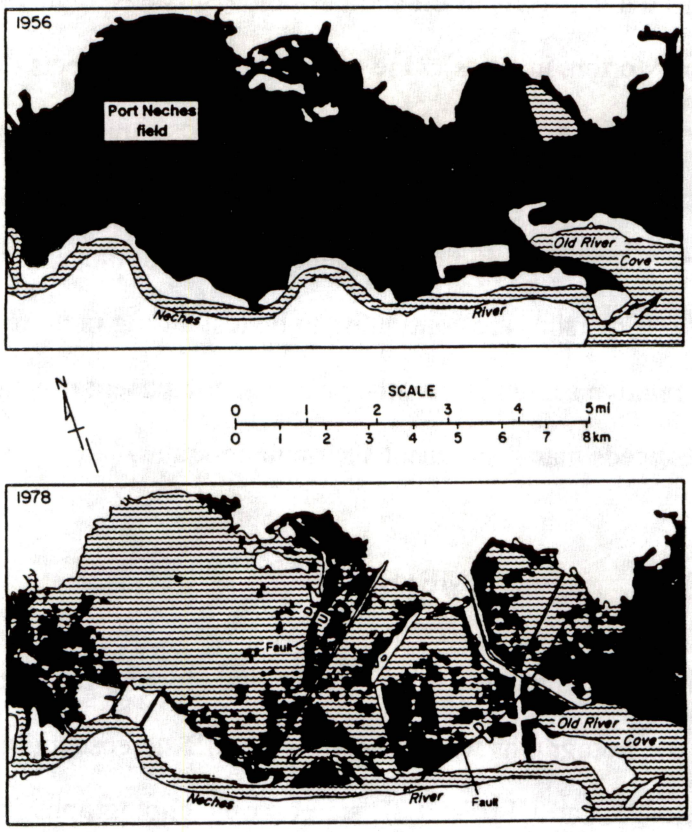

Map Unit	1956		1978		Net Change*	
	Acres	Hectares	Acres	Hectares	Acres	Hectares
Water	2,560	1,037	11,070	4,483	+8,510	+3,446
Marsh	15,740	6,375	6,330	2,564	−9,410	−3,811

* Loss of additional 900 acres (365 hectares) of marsh primarily due to spoil disposal.

QA3384c

Figure 2. Changes in the distribution of wetlands between 1956 and 1978 in the Neches River valley at the head of Sabine Lake. Differential subsidence along the faults crossing the valley has contributed to conversion of emergent vegetation to open water. D = downthrown side, U = upthrown side. From White and Morton (in press) as modified from White and others (1987).

The marsh system in the Neches River valley is intersected by two high-angle normal faults that are downthrown toward the Port Neches oil and gas field (Bessie Heights field) (White and Tremblay, 1995; White and Morton, in press). One of the faults that intersects the GSU marsh can be traced on aerial photographs for a distance of 5.5 km. Marsh loss in the GSU area is more extensive on the downthrown side of the fault. Documentation of wetland losses from 1978 through the 1990's provides more recent, indirect evidence about fault movement and associated subsidence in the GSU area. If marshes are continuing to be lost during more recent periods, one possible conclusion is that relative sea-level rise, the principal component of which is subsidence, is continuing at a rate that exceeds marsh sediment accumulation rates.

METHODS

The most recent available aerial photographs were obtained for analysis of marsh distribution and areal extent. Two sets of photographs were used: TPWD CIR stereoscopic photographs (scale 1:9,600) taken on July 11, 1995, and USFWS CIR stereoscopic photographs (scale 1:65,000) taken March 3, 1993. The TPWD photographs cover approximately 60 percent of the study area (south portion), and the USFWS photographs cover the entire area.

Areas of emergent vegetation, open water, and barren flat were interpreted and delineated optically at a common scale (approximately 1:22,500) for all photographs. Using a Zoom-Transfer-Scope, we transferred delineations to enlarged (10-percent enlargement) USGS 7.5-minute base maps. We checked marsh interpretations using a fixed mirror stereoscope that had 6× magnification. We then digitized wetlands and areas of open water and entered the data into the geographic information system (GIS) ARC/INFO. We followed these same procedures using NASA CIR stereoscopic photographs taken October 9, 1978 (scale enlarged to 1:21,800; original scale 1:65,000). We also delineated areas of open water and digitized them on black and white aerial photographic mosaics taken in September 1956 (scale 1:24,000).

The GIS data sets consist of digital overlays corresponding to mapped marsh and open water areas for 1978 and 1993–95 and open water for 1956. We plotted draft maps of each period at a

scale of 1:12,000 and checked them against aerial photographs for consistency and accuracy of delineations and to verify observed changes. We manipulated the final data sets as information overlays, from which we analyzed detailed spatial and temporal patterns to determine trends in habitat losses or gains. To develop trends, we compared the most recent data with habitat changes during earlier periods.

Because the major objective of the study was to determine the magnitude, location, and rate of marsh transformation to open water, we used fixed outer boundaries of the study area so that the total acreage would be equal for each year. Also, because some changes in marsh area were due to construction of the new State Highway 87 and disposal of dredged spoil from channels, we used the highway and dredged material areas as they were mapped on 1990 photographs for both time periods.

RESULTS

Analyses of marsh and open-water habitats on sequential aerial photographs show a net transformation of marsh to open water through time (table 1). In 1956, marsh/land covered an area of 1,496 ac and water, 70 ac. By 1978 (fig. 3), 892 ac of marsh/land and 674 ac of open water existed, and by 1993–95 (fig. 4), 815 ac of marsh/land and 751 ac of water.

Marsh loss has been continuous but not constant (fig. 5). In 1956, open water was 4 percent of the map area, by 1978, 43 percent, and by 1993–95, 48 percent of the area. The highest rate of change occurred during the period from 1956 through 1978, when 604 ac of marsh was converted to open water. The average rate of loss of marsh habitat during this 22-yr period was 27.5 ac/yr, and about 40 percent of the marsh was lost. The rate of marsh loss decreased from 1978 through 1993–95 (1994 was used to calculate rates), to 4.8 ac/yr—a reduction in rate of loss of about 5.7 times. During this period, 9 percent of the existing marsh was lost.

To go back farther in time, we reviewed vertical aerial photographs taken in 1938. Because open water was an insignificant part of the map area in 1938, we assumed that the study area consisted of all marsh/land habitat, or 1,566 ac. According to this figure, the amount of marsh loss

Table 1. Acreage of marsh and open water in the GSU map area, 1938 through 1993–95.

Year of aerial photograph	Area of marsh/land (ac)	Area of water (ac)
1938	1,566	0*
1956	1,496	70
1978	892	674
1993–95	815	751

*See text.

Figure 3. Distribution of marsh/land and open water in the study area in 1978. Green or black represents marsh/land areas and blue or white, open water. The red or black line in the south part of the study area represents trace of the easternmost fault shown in figure 2.

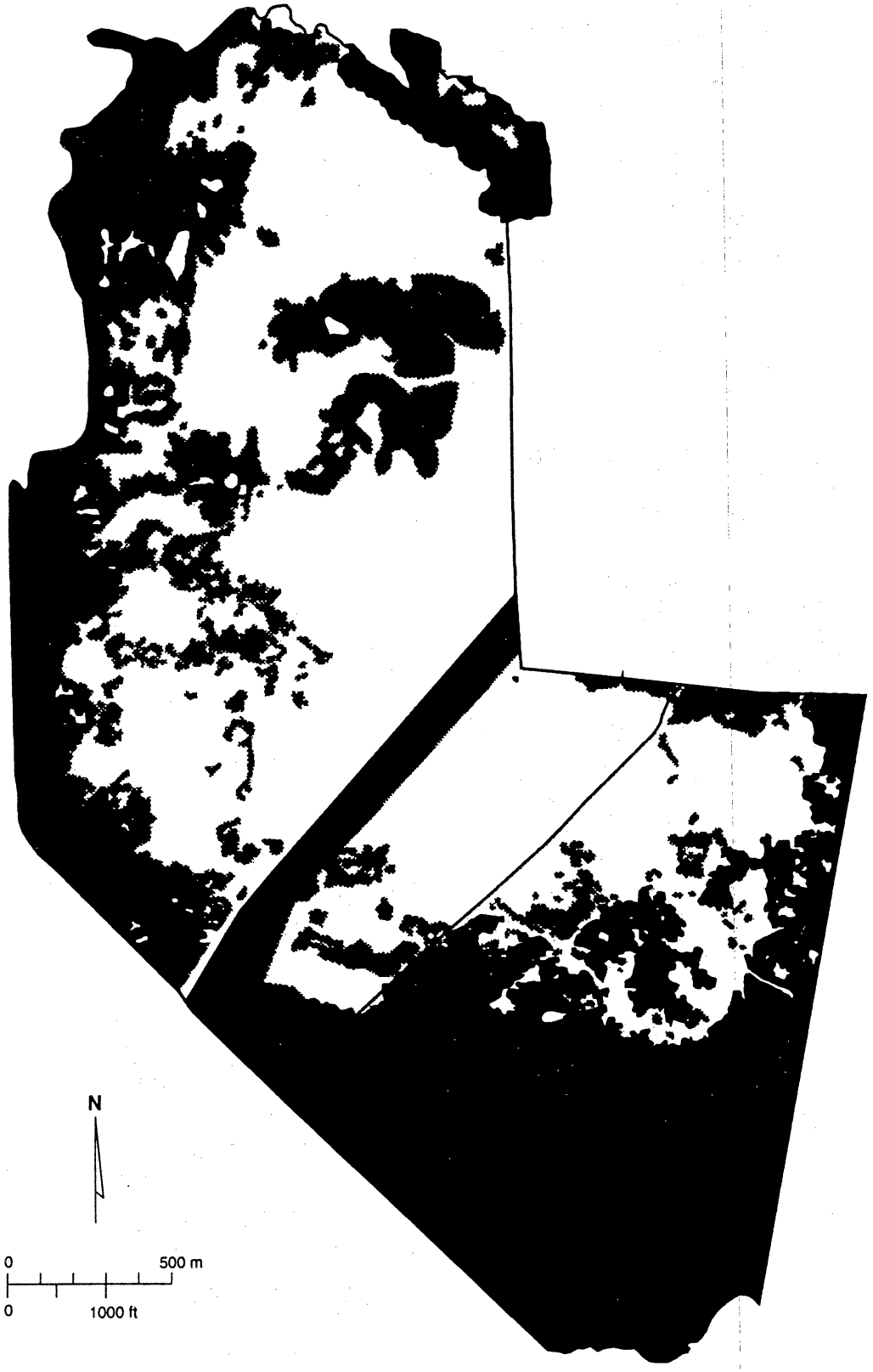

Figure 4. Distribution of marsh/land and open water in the study area in 1993–95. Green or black represents marsh/land areas and blue or white, open water. The red or black line in the south part of the study area represents trace of the easternmost fault shown in figure 2.

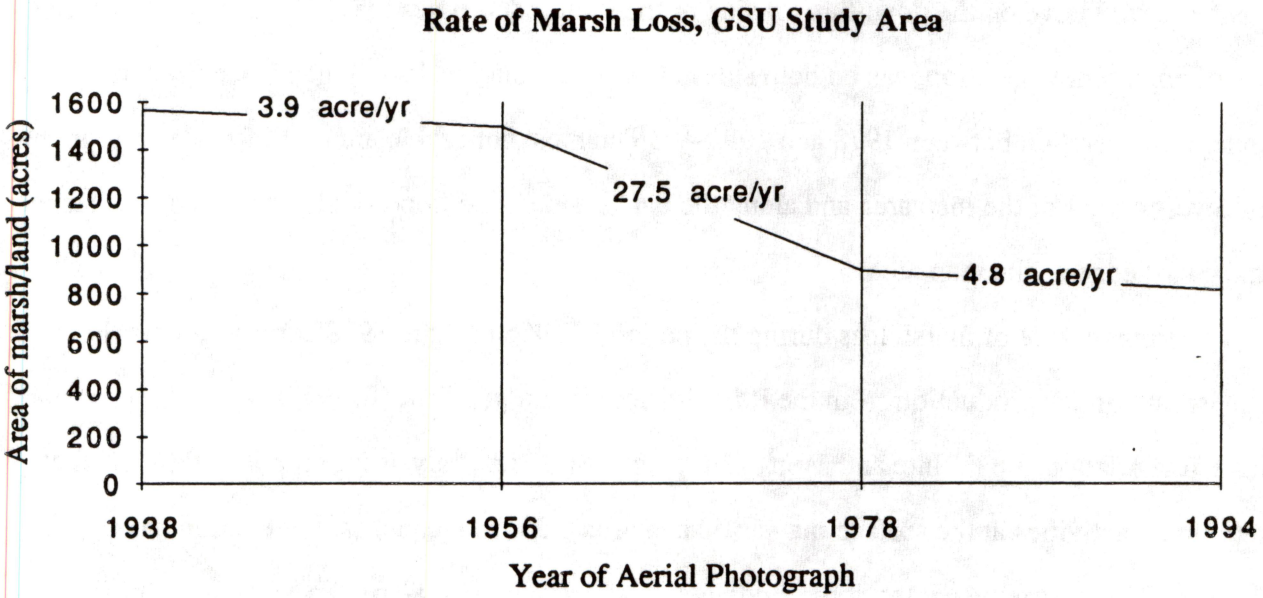

Figure 5. Approximate rates of marsh loss from 1938 through 1993–95.

between 1938 and 1956 was about 70 ac, yielding a rate of loss of 3.9 ac/yr for this 18-yr period, or slightly less than the rate of the most recent period, 1978 through 1993–95 (fig. 5). Approximately 4 percent of the marsh was lost during this early period. Interestingly the rate of loss for the midperiod (1956–1978) is about seven times higher than that of the early period.

Although marsh habitat was converted to open water throughout the map area, the conversion was more extensive on the downthrown side of the fault that crosses the study area (fig. 6). A net loss of emergent vegetation was on both sides of the fault, but local small gains occurred in emergent vegetation between 1978 and 1993–95. The most noticeable areas of increase were in the northwest corner of the map area and along the banks and on the flood-tidal delta of a tidal channel on the east edge of the map area.

The higher rate of marsh loss during the period of 1956 through 1978 correlates with the highest rate of gas production from the Port Neches oil and gas field (fig. 7), suggesting a cause-and-effect relationship (White and Morton, in press). Still, the analysis is complicated by the fact that human activities at the surface may also have affected marsh changes. For example, old Highway 87 through the center of the study area and a gravel road along the east margin of the study area were constructed before 1938. In addition, the GSU intake canal that borders the west side of the study area was dredged soon after 1956, and the GSU discharge canal was dredged southwest of the study area. Increases in aquatic habitat (open water) to the southwest were attributed to intrusion of water as a result of the canal being dredged through the marsh (Wiersema and others, 1973). Discharges are not made along the intake canal that borders the west side of the study area, however, and the impact of this canal on the marsh is different. The intake canal isolates or compartmentalizes the marsh and may have contributed to ponding of water as subsidence occurred. Transformation of the marsh to open water, however, had begun in 1956 before the canal was dredged. Other factors, such as disposal of dredged material and reductions in sediment supply, which may have contributed to marsh loss in the Neches River Valley, were reported by White and others, (1987).

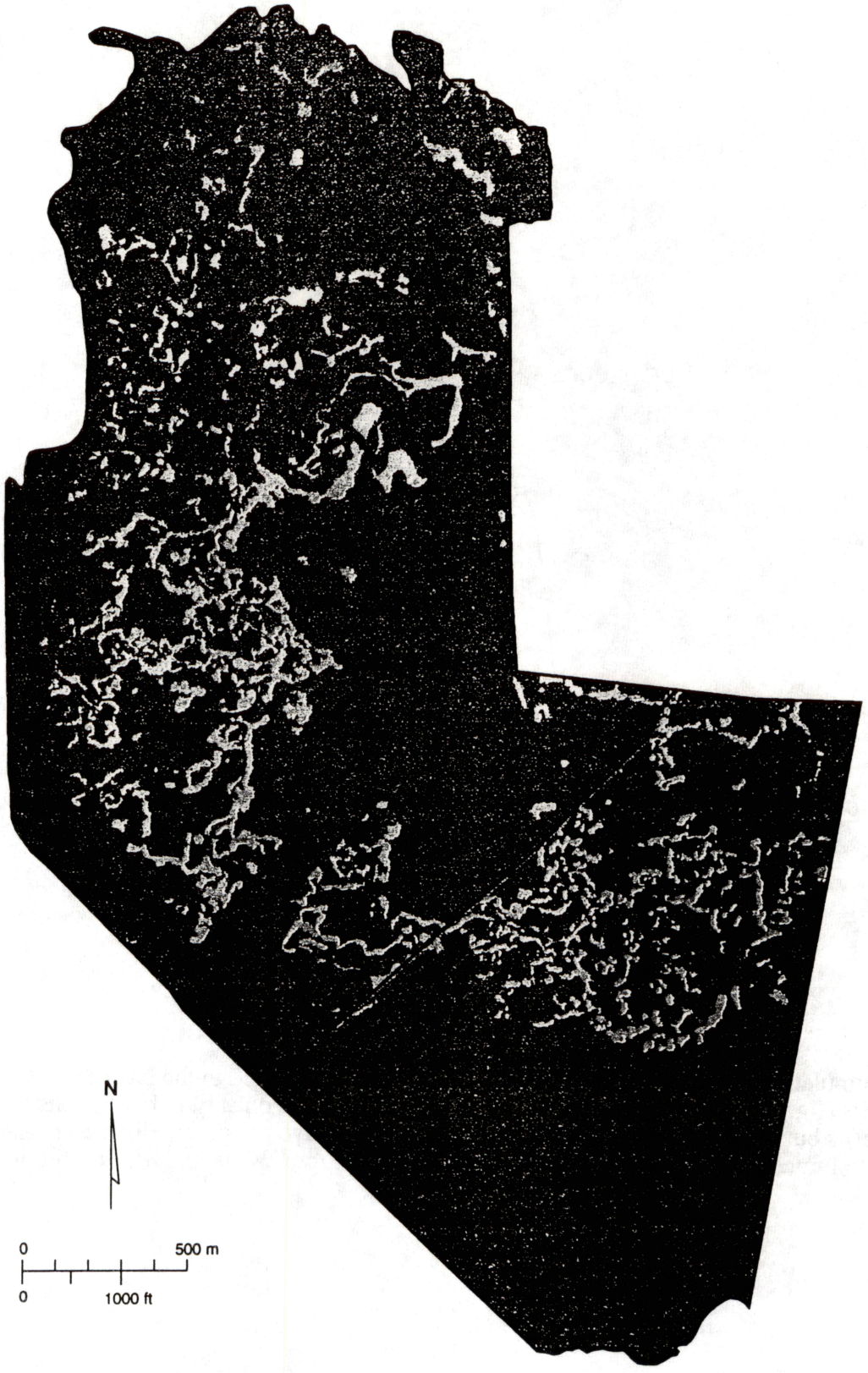

Figure 6. Distribution of marsh loss from 1978 through 1993–95. Lighter color represents areas of marsh that were converted to open water. The red or black line in the south part of the study area represents trace of the easternmost fault shown in figure 2. Note that losses were more extensive on the northwest, downthrown side of the fault.

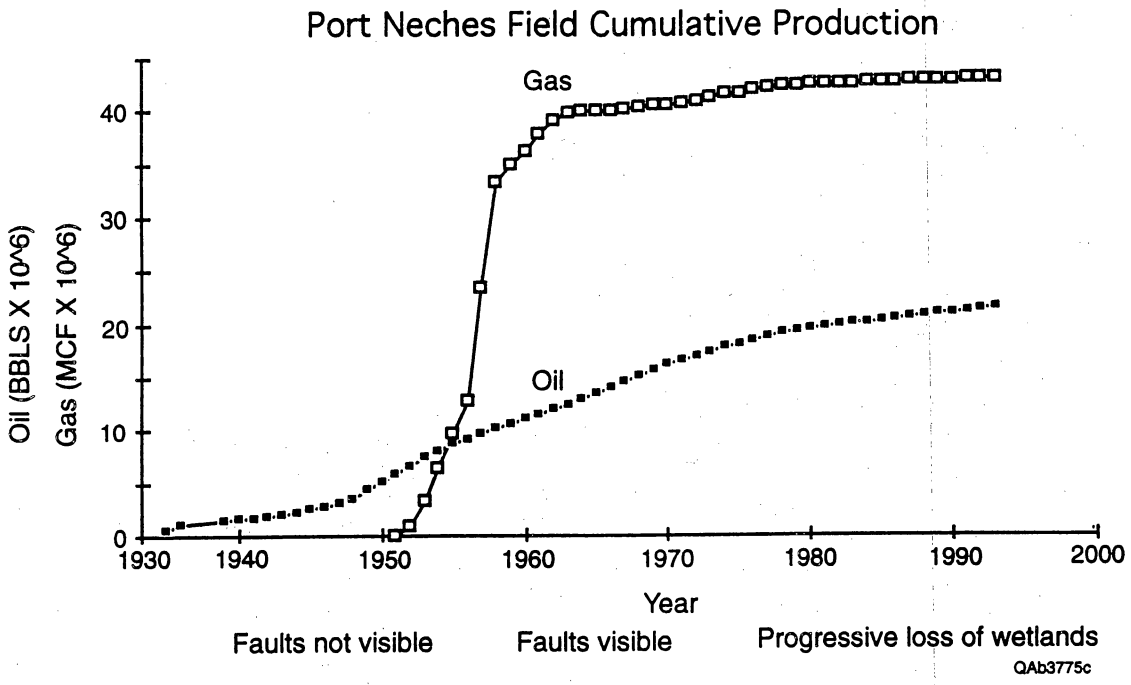

Figure 7. Cumulative production of oil and gas from Port Neches field in the Neches River valley. Surface faults (fig. 2) downthrown toward the field are not visible on aerial photographs taken in the mid-1950's but are visible by the mid-1960's after cumulative gas production had peaked. Production volumes from the Texas Railroad Commission. From White and Morton (in press).

CONCLUSIONS

Analysis of historical changes in marsh habitat provides indirect evidence that subsidence is contributing to loss of emergent vegetation. The more extensive losses of marsh have occurred on the downthrown side of a fault that crosses the marsh, a fact indicating that subsidence is occurring at a rate higher on the downthrown side than on the upthrown side. Similar observations have been made along other Gulf coast faults (White and Morton, in press).

The rate of marsh loss during the most recent period, from 1978 through 1993–95, was almost six times lower than the rate during the preceding period, 1956 through 1978. This decline in rate of marsh submergence appears to coincide with a 23-fold decrease in the rate of gas production in the Port Neches field. This lower rate of marsh loss suggests that the rate of subsidence (and fault movement) has declined.

Nevertheless, the conversion of marshes to open water has continued over the past 16 yr (although at a much slower rate) at about 4.8 ac/yr. If this rate continues, it will take approximately 170 yr for the 815 ac of marsh/land that existed in 1993–95 to be transformed to open water. Because part (185 ac) of the 815 ac includes upland areas, loss of existing marshes would occur over a somewhat shorter period.

Marsh restoration, if done properly, could reduce the rate of loss and extend the life of the marshes. Assuming that the principal cause of marsh loss is subsidence, which is a major factor contributing to a rise in relative sea-level, then trying to lower water levels and increase sediment deposition in marsh areas should help counter submergence of emergent vegetation and loss of marsh habitat.

ACKNOWLEDGMENTS

This investigation was funded by the Texas Parks and Wildlife Department. Supplementary funding was provided by the U.S. Geological Survey as part of a cooperative investigation on coastal erosion and land loss along the upper Texas coast. Susan Lloyd did word processing and pasteup. Lana Dieterich edited the report.

REFERENCES

Fisher, W. L., Brown, L. F., Jr., McGowen, J. H., and Groat, C. G., 1973. Environmental geologic atlas of the Texas Coastal Zone—Beaumont–Port Arthur area: The University of Texas at Austin, Bureau of Economic Geology, 93 p., 9 maps.

Ratzlaff, K. W., 1980, Land-surface subsidence in the Texas coastal region: U.S. Geological Survey Open File Report 80-969, 19 p.

White, W. A., Calnan, T. R., Morton, R. A., Kimble, R. S., Littleton, T. G., McGowen, J. H., and Nance, H. S., 1987, Submerged lands of Texas, Beaumont–Port Arthur area: sediments, geochemistry, benthic macroinvertebrates, and associated wetlands: The University of Texas at Austin, Bureau of Economic Geology, 138 p.

White, W. A., and Morton, R. A., in press, Wetland losses related to fault movement and hydrocarbon production, southeastern Texas Coast: Journal of Coastal Research.

White, W. A., and Tremblay, T. A., 1995, Submergence of wetlands as a result of human-induced subsidence and faulting along the upper Texas Gulf Coast: Journal of Coastal Research, v. 11, no. 3, p. 788–807.

Wiersema, J. M., Mitchell, R. P., and James, S. N., 1973, Sabine Power Station ecological program, v. 1, A. utilization of aquatic habitats in the GSU marsh; B. assessment of GSU thermal discharge on the biota of the Neches River: Austin, Texas, Tracor, Inc., document no. T73-AU-9507-U(R), submitted to Gulf States Utilities, 215 p.

Addendum 11

Requests for Project Data

Requests for Project Data

Agency	Data
Minerals Management Service	ARC-INFO layers of shoreline positions, Sabine Pass to Bolivar Roads
Minerals Management Service	62 shoreline history plots, Sabine Pass to Bolivar Roads
Texas A&M University Galveston	Beach and offshore profiles, Galveston Island beach nourishment area
Texas A&M University Corpus Christi	ARC-INFO layers of shoreline positions, Mustang Island and North and South Padre Island
Texas A&M University College Station	ARC-INFO layers of shoreline positions, Galveston Island
Texas A&M University College Station	Report on recent shoreline changes, southeastern Texas coast
Texas Department of Transportation	Report on recent shoreline changes, southeastern Texas coast
Pipeline Company	Report on recent shoreline changes, southeastern Texas coast
Texas General Land Office Coastal Division	Report on recent shoreline changes, southeastern Texas coast
Federal Emergency Management Agency	Report on recent shoreline changes, southeastern Texas coast
Texas General Land Office Coastal Division	GPS beach and dune surveys
Texas Parks and Wildlife Department	Wetlands maps, Galveston Bay
Galveston Bay National Estuarine Program	Wetlands maps, Galveston Bay
Texas General Land Office Oil Spill Division	ARC-INFO layers of Shoreline Types Maps
NOAA	ARC-INFO layers of Shoreline Types Maps
Minerals Management Service	ARC-INFO layers of Shoreline Types Maps